Study on accelerated exposure testing and thermal insulation for a Glass Fibre Reinforced Polymer in simulated Oil & Gas environment

Doctoral Dissertation
Doctoral Program in Material Science and Technology (31th Cycle)

Study on accelerated exposure testing and thermal insulation for a Glass Fibre Reinforced Polymer in simulated Oil & Gas environment

By

Matteo Cavasin

* * * * * *

Supervisors
Prof. Milena Salvo, Supervisor
Prof. Marco Sangermano, Co-Supervisor

Doctoral Examination Committee:

1. Prof. Emiliano Bilotti, Queen Mary University of London, United Kingdom
2. Prof. Valentina Casalegno, Politecnico di Torino, Italia
3. Prof. Alberto Frache, Politecnico di Torino, Italia
4. Prof. Andrea Lazzeri, Università di Pisa, Italia
5. Dr. Anthony Maxwell, National Physical Laboratory, United Kingdom

Politecnico di Torino
September 5th, 2019

I hereby declare that, the contents and organisation of this dissertation constitute my own original work and does not compromise in any way the rights of third parties, including those relating to the security of personal data.

Matteo Cavasin
Turin, September 5th, 2019

* This dissertation is presented in partial fulfilment of the requirements forPh.D. degree in the Graduate School of Politecnico di Torino (ScuDo).

Summary

Polymer Matrix Composites (PMCs) are becoming widespread in the Oil & Gas industry. Their outstanding mechanical properties, along with their improved resistance to the corrosion compared to metals makes them a suitable candidate to overcome the physical limitations of traditional structural alloys, in particular for production pipelines and submerged structures in the offshore extraction of fossil fuels.

Oil & Gas industry is interested in employing PMCs as the structural material to make the exploitation of eXtreme High-Pressure High-Temperature (XHPHT) offshore reservoirs viable. There is not a single definition for XHPHT, but it refers to scenarios where materials will experience temperatures up to 200 °C and pressures reaching 140 MPa. These are very demanding conditions for polymer composite materials. These materials are expected to survive 25+ years in a harsh operative environment. PMCs are known to be affected by the seawater as the permeable polymer matrix undergoes plasticisation. Other ageing phenomena can be caused by the biological activity in the marine environment (biofouling), as well as chemical degradation due to the presence of CO_2 and H_2S in so-called "sour" reservoir or to the production chemical additives for boosting the *Enhanced Oil Recovery* (EOR). There is limited experience with composite materials in such specific applications, in particular for long term exposures. It is pivotal to gain enough understanding of how the material will age to judge if it is fit for purpose and economically sound. For most of the PMC composites, there is not enough confidence in how they would endure in those particular environments.

In this project, the focus was on mapping the evolution of the physical and mechanical properties of a Glass Fibre Reinforced Polymer (GFRP) composite, in relation to the progress of the absorption of fluids. The performance of the material was monitored while it was exposed to a basic simulated offshore Oil & Gas environment. The aim was to characterise how the properties of the materials evolve due to the fluid permeation at different temperatures, to evaluate the accelerated ageing effect. An extensive parallel testing campaign was carried out on both the epoxy matrix and the GFRP composite separately at increasing ageing stages.

Gravimetric measurements were performed to calculate the diffusion coefficients when the composite is exposed to the seawater and an aromatic hydrocarbon mixture, to simulate production fluids. At the same time, Dynamic Mechanical Analysis (DMA) was used to measure the shift in the Glass Transition temperature.

Using an Arrhenius plot, the exponential relation between the seawater diffusivity coefficient and the exposure temperature was verified and the diffusivity coefficient values for the materials at a temperature of 4 °C, typical of offshore operative scenarios, were estimated at 0.23 and 0.05×10^{-13} m^2/s for the neat epoxy matrix and the GFRP composite, respectively.

To monitor the evolution of mechanical performance, tensile tests were performed on progressively aged material. The materials appeared less prone to absorb the oil mixture and the effect on the mechanical performance on the epoxy matrix was limited. From the seawater exposure results, instead, it was possible to linearly correlate the loss in the GFRP tensile strength with the weight fraction of water absorbed. Time-Shift Factors were calculated with partial success, in order to estimate the accelerating effect of the higher temperature exposures on performance degradation.

Improved thermal insulation is beneficial towards the flow assurance of hot fossil fuel in offshore pipelines. Polymer foams are known for their low thermal conductivity, which is related to their apparent density. The foam density is controlled during the foaming process, depending on the technology employed: usually, these foams are less dense than water. The possibility of adding a buoyant core to a pipeline structure, made by the polymer foam, would significantly reduce the structural loads at the top section due to the weight of the structure, thanks to the hydrostatic thrust.

Utilizing a *Chemical Foaming Agent* (CFA), an epoxy foam was successfully synthesised and tested for its mechanical properties, thermal conductivity and stability. An apparent density of 0.4 g/cm^3 and conductivity of 0.06÷0.07 W/(m·K) were obtained which are competitive with other commercial insulation systems A composite sandwich was prepared to evaluate its adhesion to a GFRP substrate. In this configuration, it can be used as thermal insulation for offshore composite pipes.

Acknowledgements

First and foremost, I would like to express my gratitude to my supervisors Prof Milena Salvo and Prof Marco Sangermano for their support and guidance during these three intense years of my PhD experience. They trusted in my abilities and gave me the freedom to design and execute my research plan while being truly supportive when I needed some more experienced advice.

This research project was carried out within the framework of the project "CoACH" European Training Network (Grant Agreement no. 642557), funded under the Marie Sklodowska-Curie Action of the EU funding program for research and innovation "Horizon 2020". I am grateful for the financial support received and the great opportunity for the personal and professional growth that this fellowship offered me.

I am grateful to my industrial supervisor Dr Barry Thomson, for supporting my research activities and offering scientific advice in the last year and a half while I was working at the Element Hitchin facility.

I offer my sincere gratitude to my former industrial supervisor Dr Stefanos Giannis, whose efforts went well beyond his professional duty. If I made it to the conclusion of this PhD, it is in a good deal thanks to his expertise, his complete confidence in my capabilities and his relentless encouragement.

A special thanks go to Silviu Ivan, for his friendship and day to day technical support in the Element laboratory. He is a truly dedicated engineer; it has been a pleasure working with him along these years.

Many thanks to the staff of the Element Hitchin laboratory but in particular the Composite Testing team: Sabina, Amir, Dave, Sandra, Choothum, Valentina, Joanna and Tasos. They have been genuinely supportive of me and been more than just colleagues during these years abroad.

Thanks to Element Materials Technology Ltd. for offering me the opportunity to work in their lab and benefit of their advanced testing facilities.

Thanks to my ESR fellows in the CoACH project, aka "Coachitos". This experience was way improved by meeting all of them, and I am proud to be part of this group of brilliant young scientists. A special mention goes to Cristian Marro

Bellot, whose never-ending positive mood helped me through some difficult times and cheered up during brighter ones. Also, a sincere thanks to Nicoletta Toniolo e Alex Persico, long-time friends, companions of past ventures and, I am sure, many more in the future.

I'd like to thank also some more people from Politecnico di Torino for both the research support offered or the valuable contribution to organising the many activities related to the CoACH project: Valentina Casalegno, Monica Ferraris, Cristina Balagna, Cristiana Contardi. A special thanks to Lorenzo Costantino for his tireless mentoring and for explaining to me how to eat a whole elephant.

Thanks to my friends and folks back in Italy. Three years abroad went pretty fast, but I really missed many of them all the same. Sincere thanks to Nicolò Pasini and Giacomo Principe for the real help in the last sprint for finishing this thesis. I doubt it would have been completed without their final push.

This work is dedicated to my family: Alessandra, Marco e Paola. I could not accomplish this without their unconditioned support and love. It has been quite an eventful ride: now, in the end, we know that it was worth it.

Matteo Cavasin

Table of contents

List of Tables

List of Figures

Chapter 1 Introduction

1.1 Motivation

Polymer Composite Materials (PMCs) are largely successful in engineering applications thanks to the variety of properties they offer. Thanks to their lightness and stiffness, they are particularly appreciated in the aerospace industry, where they are well-established as structural materials.

Nowadays, polymer composites account for up to 50 % of the structural weight in the last generation of civil airliners. Newer designs are continuously developed as more performing materials are introduced [1].

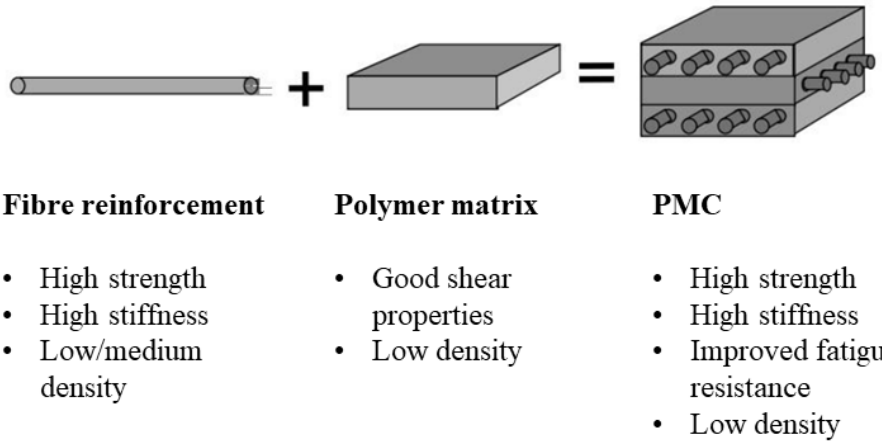

Figure 1-1: the basic morphology of a fibre-reinforced polymer matrix composite. Adapted from [1]**.**

Another market interested in the potential of PMCs is the renewable energy one. There is a push from public institutions, in particular in developed industrialised countries, to improve the production of energy using alternative sources rather than fossil fuels. The wind is already widely exploited to power "turbine farms" in areas where there are steady currents. The blades can span for several tens of meters and are built of long-fibre reinforced laminated composite, with the addition of composite sandwich elements to add stiffness to the section. This demanding design would not be possible using metal alloys due to their excessive weight. Mostly E-glass or carbon fibres are used, sometimes in hybrid design to tailor weight and stiffness [2].

Thanks to their superior durability to environmental exposure, PMCs are pivotal for more efficient exploitation of renewable resources as they offer the possibility to build structures with an extended operative lifetime compared to the metal alloys. They are promising for marine applications, such as submerges tidal

turbines, as they are more resistant to the corrosion action caused by the seawater and they can withstand dynamic and cyclic loading, typical in a scenario characterised by waves and tidal currents.

Due to the remote location of offshore turbines (both wind and tidal type), the maintenance requirement needs to be kept to a minimum, lest to incur in significantly higher operational costs, which are one of the main drawbacks for renewables, besides the lack of steady power output [3].

There is a need to ensure the durability of structures and components before the commercialisation of these power generating devices. This is closely related to the capability of foreseeing the evolution of the structural material's performance for a time-span of 20-30 years in advance. PMCs are demonstrating to fulfil these requirements, and presently, many ongoing studies are aiming to collect experimental data about their degradation in the marine environment.

Oil & Gas industry, even if not focusing on renewables, shares a common interest in PMCs. They are a solid candidate as the structural material to make the exploitation of eXtreme High-Pressure High-Temperature (XHPHT) offshore reservoirs viable. There is not a single definition for XHPHT, but it refers to scenarios where materials will experience temperatures up to 200 ℃ and pressures reaching 140 MPa. These are very demanding conditions for polymer composite materials. Also, this environment can be made harsher due to the sourness of the reservoir or the injection of CO_2 and H_2S to boost the *Enhanced Oil Recovery* [4].

These reservoirs are mostly located in the Atlantic Ocean (Mexican Gulf or off Brasil's coast) at a depth of 2000 m or more. It is expected that 40 % of the future oil offshore supply will come from water depths between 1500 and 3000 m. The critical technology to reach these very high depths are the risers pipelines, as they serve for the transportation of the fossil fuels from the seafloor wellhead to the drilling and production facility at the surface [5]. Steel catenary pipes have been progressively substituted with unbonded flexible pipes which have the advantage that they do not need to be assembled from short pipe sections, so the installation is much quicker, and they can adapt to the movements of the floating surface structures. This kind of pipes comprises a multi-layered design of several metallic carcass and armours alternated with polymer liners and an external sheath. The limitation of this design is that it would fail under its weight for the very high drop in depth needed to reach the seafloor, due to the tensile stresses generated in the top section.

Polymer Matrix Composites have demonstrated to be an alternative to substitute partially or entirely the metal alloys, thanks to their higher specific mechanical properties (e.g. their tensile strength to density ratio). However, the Oil & Gas industry has not built yet the same confidence on PMCs as other industries, and they are usually employed in non-structural applications. There is not enough knowledge about how this material would behave in the long term at deepwater conditions. The combination of mechanical loads, pressure, temperatures and

chemical exposure is unique to this kind of applications, and it has no similar scenario in other industry where the proven experience with composites can be drawn on. The components for offshore oil recovery have to comply with very high safety standards, considering the hazard posed by a pipeline failure to the working personnel and the environment contaminated by the ensuing spillage.

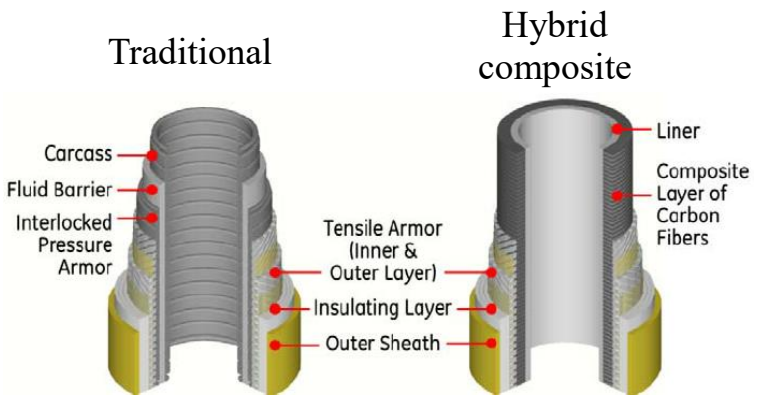

Figure 1-2: comparison between a traditional riser design and a hybrid one combining metal and fibre-reinforced composite. Adapted from [6]**.**

On top of these, deepwater installations are requested to endure an operative lifetime of about 20-25 years, with minimised maintenance operations due to the very limited capability of access to the pipeline at such depths. Only unmanned devices would be capable of operating in that environment, with very high costs related to it, or, if it is not possible to repair it, the substitution of the entire pipe could be necessary.

PMCs are progressively introduced in more demanding Oil & Gas applications. Nevertheless, the material needs to be fully qualified in advance in order to select the best option, based on its properties, for a tailored design. The long-term degradation of its performance must be addressed by accurate modelling to assure the reliability of the component in a harsh environment for the whole duration of the planned operative lifetime.

1.2 Objectives

The project was divided into two main research branches. The first one was related to the study of the ageing effect due to fluid diffusion in Glass Fibre Reinforced Polymer (GFRP) composites. The second involved the development of a polymer foam with low thermal conductivity to be applied on composite substrates.

1.2.1 Ageing of GFRP composite

The objective of the first topic of the project is to improve the understanding of how experimental parameters such as the specimen's geometry or the exposure temperature influences the performance degradation of the material over time. As composite materials in submarine structures are expected to have a long operative

life with the minimum required maintenance, it is critical to forecasting how the material will degrade in advance. There is a vast literature regarding the current evaluation methods, but the ageing processes are complex and usually interacting among them. It is challenging to design an experimental method which can realistically simulate the marine environment, particularly the high depths the offshore extraction pipelines have to reach. Factors as hydrostatic pressure, ocean currents and waves, mechanical loadings or biological action, require all an increasingly sophisticated experimental design to account for.

At the same time, measuring the relevant physical and mechanical properties of inhomogeneous materials as PMCs is not trivial. Several mechanical parameters have to be evaluated for a standard composite laminate to gain a full understanding of its mechanical state. Most of these parameters are then strongly influenced by the loading mode, the intensity, the frequency and the temperature at which the load state is applied.

The other critical factor is time, or rather the relationship between the length in time the material has been exposed to the environment (i.e. how long it has aged) and the level of degradation in the performance (i.e. how much it has aged). Most of these physical properties cannot be continuously evaluated as it would add significantly to the complexity of the experiment, but at the same time, it is difficult to establish the optimal frequency for the measurements due to the limited knowledge about these ageing mechanisms. The increased amount of experimental data produced will not provide a better insight into the phenomena evolution in proportion to the resources needed to measure them in a continuous way. Moreover, most of the traditional mechanical tests are destructive; hence, several runs of the same test at different ageing intervals are required to describe the said evolution.

In our project, we tried to maintain the experimental design as lean as possible, in order to keep it mostly manageable by a single person and without requiring intense data post-processing, in terms of modelling or statistical analysis. This approach is commonly employed in the industrial material qualification: the test design is based on requirements sourced from test standards issued by international standardisation bodies (such as ISO and ASTM).

A standard Glass Fibre Reinforced Polymer with epoxy matrix was selected as the material to investigate the ageing effect of the exposure to the simulated environment. Such material is widely described in the literature for its properties, and it is suitable for the manufacturing of pipelines because of its minor cost compared to carbon fibre composites.

It was decided to focus on the following experimental factors from the simulated exposure to the operative environment:

a) Specimen's material
b) Specimen's geometry (and reinforcement orientation for the GFRP)
c) Fluid
d) Temperature
e) Time

Regarding the material, both the neat polymer matrix and the GFRP composite were separately investigated, as the matrix is expected to be more sensitive to the fluid conditioning. The specimen's geometry was also tested to evaluate how shape and scale factors could affect the evolution of the fluid permeation.

The exposure fluids, i.e. the fluids which the materials soaked in, were seawater and a mixture of mineral hydrocarbons in order to simulate the operative scenario in Oil & Gas applications.

The temperature of the exposure was a critical factor as it is known to control the kinetics of many physical and chemical transformation. It can be used as leverage to accelerate the ageing process, but this necessarily involves the other main physical parameter, the exposure time length. It is known that polymer material's response is a combined function of temperature and time: this is the basic principle for the Time-Temperature SuperPosition (TTSP) model used to describe linear viscoelasticity [7]. Also, air exposures were set to evaluate the thermal effect alone as a benchmark.

The material properties were evaluated by means of the gravimetric test, Dynamic Mechanical Analysis and unidirectional tensile testing. The objective of this study is to define the relationships between the performance loss and the exposure conditions, comparing the results from these tests, to describe the ageing process happening in the materials.

Another objective is to use the experimental data to estimate Time-shift Factors in order to quantify the accelerating effect of the temperature on the ageing process.

1.2.2 Epoxy foam

The second topic of the project is related to the development of a thermal insulation material to be applied on a composite substrate. *Flow assurance* is the technical term referring to the design and operative strategies to ensure an effective hydrocarbon stream from the reservoir to the surface production facility.

Passive thermal insulation can be highly beneficial to maintain the upstream fuel flow at the proper temperature in order to prevent the clogging of the pipeline [8]. Solid gas hydrates or denser phases (e.g., asphalts, waxes) can appear in the oil flowing inside the pipeline in particular condition of temperature and pressure and deposit over time on the internal surfaces, leading to a complete interruption of the production. Thermal insulation layers are employed to limit the heat exchange with the colder ocean water during the journey from the subsea wellhead to the surface production facilities. Insulation materials as Polypropylene (PP) and Polyurethane (PU) are commonly used. When higher mechanical performances are required, *syntactic foams* are available with a variety of polymer matrix, but the addition of hollow spheres (usually glass or ceramic made) keeps their density to above 0.6 g/cm^3 and their thermal conductivity above 0.14 W/(m·K) [9].

In our project, we aimed to develop a cellular material using the same epoxy matrix as the GFRP substrate to which it is meant to be applied. The foaming is obtained by the addition of a *Chemical Foaming Agent* (CFA) which is not resin

specific, following a formulation by Stefani *et al.* [10]. The foam was characterised for its mechanical and thermal properties. Another objective is the manufacturing of a composite sandwich using the foam as a core to evaluate the strength of the adhesive bonding with the composite facings.

1.3 Thesis outline

The thesis structure is outlined following.

In Chapter 2, a brief literature review is presented about the theory and modelling related to phenomena such as fluid diffusion, ageing and thermal conductivity in Polymer Matrix Composites. An overview of the Oil &Gas market demand is also presented.

In Chapter 3, the materials preparation and the testing methodologies are presented in detail.

In Chapter 4, the results concerning the parallel testing performed on the epoxy matrix and GFRP composite while being exposed to the simulated environment are discussed.

Chapter 5 describes the preparation process and the testing results related to the epoxy foam and the composite sandwich preparation.

Chapter 6 includes general conclusions, a summary of the main achievements and suggestions for further investigations.

Chapter 2 Composite materials in the marine environment

2.1 Polymer Composite materials in Oil&Gas industry

2.1.1 Fossil fuels global demand

Metal alloys have been the prime structural material in the Oil & Gas industry throughout its history. Steel alloys have found countless applications thanks to their competitive cost and excellent mechanical properties. The advantage of using metal alloys was also to hold a thorough knowledge of their long-term performance, hence making possible to design reliable components with confidence, even if they have to operate for decades ahead [11].

The demand for fossil fuels has been steadily increasing since the second half of the XX century, and there is no sign of a reduction in the near future, despite the diffusion of renewable energy sources [12]. Recent forecasts expect fossil fuel to remain the primary source of energy for at least the next 20 years. Worldwide consumption of liquid fuel is expected to increase to 97 million barrels per day by 2020 and to reach 115 million barrels per day by 2040 [5,13].

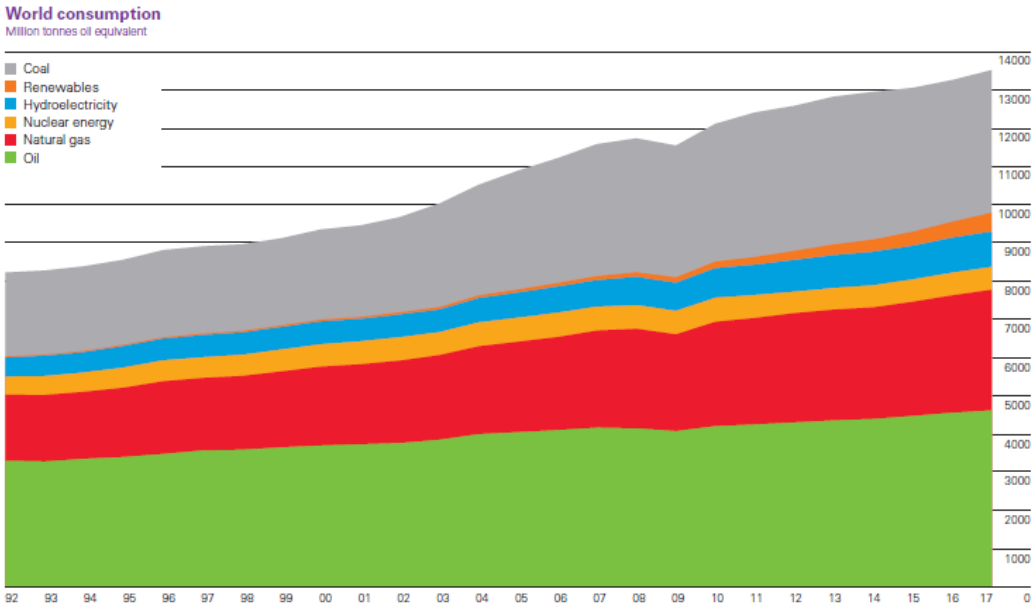

Figure 2-1: yearly energy world demand, divided by sources (in million tonnes oil equivalent), adapted from [12]

The exploitation of traditional fossil fuels reservoirs is becoming more expensive due to their limited productivity or the cost for revamping outdated

extraction technologies. Oil & Gas industry puts a significant amount of effort to discover new and more productive reservoirs [14]. Most the time, these unexploited reservoirs are progressively harder to access, both from a logistical and technical point of view. A significant share of the newly discovered reservoirs is deep-water offshore ones. They are mostly located in the Atlantic Ocean, in the areas of the Mexican Gulf, the Guinea Gulf and off the Brazilian coast. Operators are looking to exploit reserves that are located underneath the seabed at over 2000 m in depth and which are characterised by high acidic content [9,15]. This operative scenario poses a dual challenge to the steel alloys traditionally employed for the construction of pipelines and recovery rigs:

a) Standard carbon steel alloys are sensitive to the marine environment as they significantly suffer from electrochemical corrosion;
b) The depths to be reached at the bottom of ocean seabed is so deep that they are pushing the steel alloys to their physical limits.

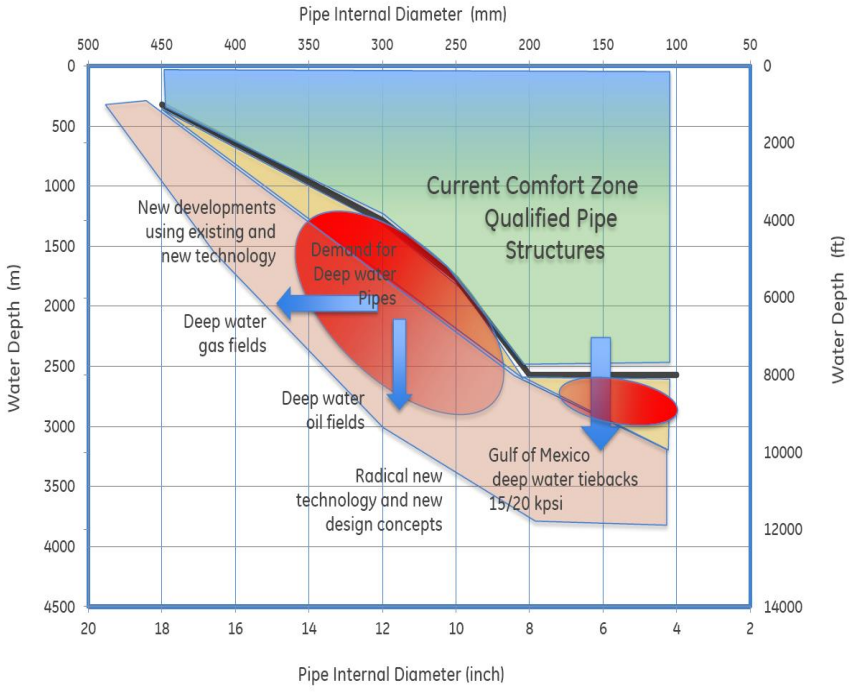

Figure 2-2: trade-off between operative depth and internal diameter for commercially available pipeline technology. Adapted from [16]**.**

In the last decades, Polymer Matrix Composite (PMC) materials have been investigated as an interesting alternative. They show higher specific mechanical properties, which allows designing lighter structures, which in turn can reach higher depth. They are intrinsically resistant to the corrosion thanks to their dielectric nature [9]. Some studies indicate that galvanic corrosion is possible when the composite is in contact with the metal substrate, in particular when are reinforced with carbon fibres, which have a limited conductivity [17].

Although the initial investment for adopting a composite component can be significantly higher than their steel counterpart, the improvement in performance and the allowed production depths can justify the transition [11,18].

However, the introduction of innovative materials for critical structural applications requires careful preventive investigations. PMCs are widely used in the aerospace industry, even in primary structural components, but specific material grades have been developed over decades, and the designers gained an in-depth knowledge of the material performance before entrusting it with safety-critical functions. Oil and Gas industry is more conservative and risk-averse by necessity. There is little willingness to accept components fabricated from composite materials in high-risk applications. An exception is technologies for fire and blast protection, but these are considered auxiliary systems [11,18].

The marine environment is aggressive in several ways, due to physical, chemical and even biological factors. Even if from a theoretical point of view, PMCs can withstand such factors individually, it is very difficult to predict how they could interact in the actual scenario. Moreover, the significant mechanical loads and chemical substances expected to be met by the material in fuel recovery applications make the operative conditions even more demanding. Oil & Gas operators aim to develop technology able to continuously work in eXtreme High Pressure High Temperature conditions, where downhole temperatures exceed 180 °C, and hydrostatic pressures can surpass the 700 bar [4,19]. The high temperatures in operation already disqualify most of the conventional engineering polymers: only advanced high-performance thermoplastics (PEEK, POM and PPS) or thermosets such as bismaleimides and high-temperature epoxies can be used as matrices for the composite to operate in such conditions.

One of the main drawbacks of using PMC in the marine environment is that they are prone to adsorb water (while metals are known to be impermeable), in particular if polar groups are present in the polymer structure. It is extensively reported in the literature that water has a significative effect on the composite physical properties [20,21]. In particular, the absorption of water is associated with a decrease of the polymer's *glass transition temperature* (Tg), which is usually regarded as an upper limit to the maximum service temperature for the composite material [22].

The other critical factor is time. Oil & Gas components are expected to operate for tens of years to be economically viable. The maintenance required should be kept at a minimum, either because of the cost related or the difficulties to access and operate on the structures in depth. At the same time is much complex, if not even not feasible, to predict how the material's properties will evolve during such a long operative lifespan. In an analogy to the biological systems, the degradation of the performance of a material over a long period is generally addressed in a broad sense as "ageing". Ageing can have different causes and control factor; it can affect

only some physical or chemical properties of the material; it can be reversible to some extent [23].

It is pivotal to gain enough understanding of how the material will age to judge if it is fit for purpose and economically sound. For most of the PMC composite, there is not enough confidence and experience on how they would fare in those very specific environments [8]. In order to promote confidence in composites, accelerated ageing tests could shorten the process of evaluating the long term degradation that occurs term in natural conditions after years in operation [11,24].

The incomplete knowledge about the ageing process of PMC, and hence their long-term durability, in the specific marine environment, is one of the main limitations to a further introduction of these materials for offshore fuel production in the Oil & Gas industry. Another important barrier is the lack of cheap and reliable in-service integrity monitoring testing, which would allow assessing the structural integrity condition of the material during its operative life [18].

2.1.2 Other applications of composites in the marine environment

Polymer Matrix Composites are employed for other applications in the marine environment. Wind turbine requires constant wind flow and a significant clear surrounding area to operate safely. Hence, they are not suitable for urban or rural areas. Installation at sea can address some of these issues. Large wind turbine farms are nowadays common in shallow coastal areas, where they can exploit the steady sea breezes without subtracting productive land to other activities. Their blades, which can span up to 80 m in length, are mostly built by glass- and carbon- fibre reinforced polymer [3].

Their use is more favoured when it involves the design of structures that go directly in contact with the seawater, thanks to their corrosion resistance. From boat and ships hulls to submarine hulls, to tidal turbine blades or more general submerged structures, these all application that involve or could benefit the use of PMC [7]. These structures are often subjected to significant dynamic loads; the improved fatigue resistance that is offered by the composites is highly beneficial to extend their operative lifespan.

2.2 Diffusion kinetics in polymers and PMCs

In the last decades, significant efforts have been driven towards improving the understanding of fluid diffusion in PMCs. It is fundamental to have a complete understanding of the diffusion mechanism to be able to predict how the fluid diffuses in the material

The mass transport of a fluid that permeates a polymer medium is commonly explained as a diffusion process occurring by a random walk of the diffusant molecules through the so-called *free volume* [20,25]. The free volume is the sum of the micro-volumes available (non-sterically hindered) distributed across the

polymer network. It is a function of the polymeric configuration, hence depending on temperature and pressure primarily.

The most common description of the classical diffusion kinetics is based on the one-dimensional Fick's laws. In literature, there is an ongoing debate discussing if the Fickian model is accurate enough to describe the diffusion process in a solid medium, and there is experimental evidence that for many polymer systems there are significant deviations from such model [17,26]. Still, for historical relevance and ease of application, it is the foundation of the majority of more advanced models. Beside some applied geometrical corrections, this is the primary model used for the calculations performed in Chapter 4. Advanced models will be briefly described here for comparison.

2.2.1 Fick's model

The first Fick's law states that the diffusing flux is proportional to the concentration gradient of the chemical species *i* [27]:

$$J_i = -D_{z,i}\frac{\partial n_i}{\partial z} \qquad \text{Eq. 2-1}$$

The proportional coefficient D_i is called the *diffusion coefficient*. In the fickian description, it is independent of the species concentration.

The second law correlates the rate of change over time with the second spatial derivative of the concentration:

$$\frac{\partial n_i}{\partial t} = D_{z,i}\frac{\partial^2 n_i}{\partial z^2} \qquad \text{Eq. 2-2}$$

In a commonly cited scenario, the Fickian model is employed to describe the fluid diffusion as a unidirectional mass transport through a semi-infinite plate with a stationary fluid concentration as boundary conditions. The semi-infinite condition of the plate means that its thickness is much smaller than the other dimensions: it is necessary to justify that the diffusion process happens uniformly only in the direction of "least resistance", hence through the thickness of the plate. To solve the differential equation, boundary and initial conditions state that at the beginning (t=0) of the diffusion process, the concentration within the plate is null while at its boundary is equal and constant to the equilibrium concentration M_∞. Standard solutions to this mathematical problem are presented in the literature [27]. By integrating the fluid concentration profile over the diffusion domain, the mass gain function for the unidirectional Fickian diffusion is calculated:

$$M_{1D}(t) = M_\infty\left(1 - \frac{8}{\pi^2}\sum_{j=0}^{\infty}\frac{1}{(2j+1)^2}\cdot\exp\left(-\frac{(2j+1)^2\pi^2}{h^2}D_z t\right)\right) \qquad \text{Eq. 2-3}$$

where *h* is the thickness of the specimen in the z-direction (see Figure 2-3).

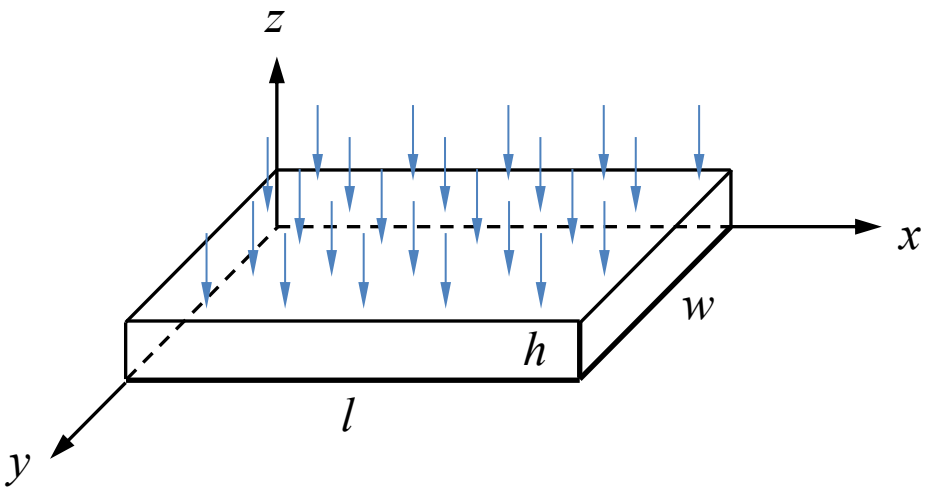

Figure 2-3: diffusion domain orientation and dimensions. All the following equations presented refer to this reference system.

This solution has an immediate experimental relevance, as it allows to correlate the data from a gravimetric test with the parameters of the diffusion kinetics. The gravimetric test consists of the repeated weighing of material samples exposed to a fluid to measure their change in weight due to the fluid absorption. The solution proposed is not a closed-form equation, hence making its evaluation computationally expensive. In particular, the recovery of the diffusion coefficient is possible only through an optimal fitting algorithm. Hence, simplified versions are proposed.

An approximated closed solution is often reported [28] is:

$$M_{1D}(t) = M_{\infty}\left[1 - exp\left(-7.3\left(\frac{D_z t}{h^2}\right)^{0.75}\right)\right] \qquad \text{Eq. 2-4}$$

From an analysis of the Eq. 2-3, at the initial stage of diffusion ($M(t) < 0.6M_{\infty}$) the weigh uptake is linear to the square root of exposure time $\sqrt{t}$ [29]; D_z can be calculated as [30]:

$$D_z = \pi\left(\frac{h}{4M_{\infty}}\right)^2\left(\frac{dM}{d\sqrt{t}}\right)^2 \qquad \text{Eq. 2-5}$$

2.2.2 Time-Varying diffusion model

The deviation of experimental data from the Fickian model raised the need for proposing alternative models. While considering the diffusion as a unidirectional process in the semi-infinite plate scenario for ease the mathematical description, these models suppose that the polymer is not just an inert medium which the fluid diffuses through without any interaction.

Weitsman postulates that the visco-elastic response of the polymer generates time-dependent boundary conditions, which in turns reflects on a time-varying

diffusivity in the polymer [31]. The diffusion coefficient has to be expressed in terms of a Prony series [32]:

$$D(t) = D_o + \sum_{r=1}^{R} D_r \left(1 - e^{-\frac{t}{\tau_r}}\right) \quad \text{Eq. 2-6}$$

Where τ_r are parameters related to the polymer relaxation times. This expression of the diffusivity has to be introduced in Fick's governing equation (Eq. 2-2), which in turns return a different integral solution for the mass gain function the visco-elastic polymer behaviour influences the fluid absorption.

2.2.3 Dual-diffusivity model

A dual-diffusivity model assumes that there are two phases of the polymer matrix which different densities or hydrophilic properties, hence different diffusion behaviour, both for absorption rates and concentration at equilibrium (i.e. saturation). This condition can be found when polymer blends are realised, such as when a plasticiser or a toughening phase is added [33].

$$M(t) = V_{phase\,1} \cdot M_{phase\,1}(t) + (1 - V_{phase\,1}) \cdot M_{phase\,2}(t) \quad \text{Eq. 2-7}$$

The weight gain function becomes the linear combination of two independent diffusion process, each weighted by the volumetric fraction of the respective phase. This model seems to provide an accurate description for the experimental data only if there is no strong interaction between the diffusing fluid and the polymer: this is not the case when polar moieties are present in the polymer structure.

2.2.4 Langmuir-type diffusion model

An alternative to the diffusion in two phases with different properties is the diffusion in a single phase where the transport of the fluid molecule shows two different kinetics. The first one follows a fickian model, characterised by random molecular motions. The second kinetic is determined by the weak chemical interactions between the diffusing molecule and the polymer structure, usually hydrogen bonds or attraction between polar groups.
This dual-mode model is named "Langmuir-type" diffusion as first proposed by Carter and Kibler [34] and has been applied to several polymer and composites systems [17]. It refers mostly to water molecule diffusion, and it classifies the water molecules as mobile or strongly bound types, as proposed in the Langmuir's theory of adsorption isotherms.

The model is essentially the unidirectional isotropic linear diffusion to which a term is added to account for possible sources or sinks of the diffusion molecules. The coupled governing equations are:

$$D_z \frac{\partial^2 n}{\partial z^2} = \frac{\partial n}{\partial t} + \frac{\partial N}{\partial t} \quad \text{Eq. 2-8}$$

$$\frac{\partial N}{\partial t} = \gamma n - \beta N \quad \text{Eq. 2-9}$$

Where *n* and *N* represent the respective concentrations for mobile (or free) and bound molecules, γ [1/s] is the probability for a mobile molecule to become bound per unit time, while β is the probability for a bound molecule to become mobile. The diffusion equilibrium is reached when the following condition is satisfied: $\gamma n = \beta N$

It is possible to calculate a solution for this system of equation starting from the same boundary conditions as the Fickian model, using a Laplace transform. The solution is a fairly complex series equation that can be found in the literature [35].

If the condition: $k = \frac{\pi^2 D_z}{h^2} \gg \gamma, \beta$ is verified, which is practically always true for polymer mediums, the integral mass weight function can be expressed as:

$$\frac{M_{1D}(t)}{M_\infty} = \frac{\beta}{\gamma+\beta}\left(1 - \frac{8}{\pi^2}\sum_{j=0}^{\infty}\frac{1}{(2j+1)^2}\cdot\exp\left(-\frac{(2j+1)^2\pi^2}{h^2}D_z t\right)\right) + \left(1 - \frac{\gamma}{\gamma+\beta}e^{-\beta t} - \frac{\beta}{\gamma+\beta}\right) \quad \text{Eq. 2-10}$$

Which is analogous to the fickian solution except for the multiplication factor and the second addend which accounts for the "sink and sources" contributions.

2.2.5 Other models and transport phenomena

The literature about fluid diffusion, with a significant focus on water solutions, in polymer or composite material, is very broad and diversified. Other models have been proposed with various degrees of complexity; some can be demonstrated to be mathematically equivalent to those cited here. Our review does not pretend to be completely exhaustive, but the briefly presented ones and the relative literature covers the most popular models applied to the diffusion phenomena of fluid in engineering polymers and their composites.

In general, other physical phenomena can affect or interact with the fluid diffusion. Some consideration can be done about the time-scales [20]:

a) Temperature diffusivity is about six orders of magnitude greater than mass one, so the two processes are decoupled (even if diffusivity *D* is temperature dependent)
b) Capillary transport is about six orders of magnitude faster than diffusion; they can be decoupled.
c) Wicking along fibre interphases is about ten times faster, so there is a weak coupling.
d) Relaxation and creep phenomena happen at about the same time scale, so they are usually coupled.

More information can be found at the following sources: Weitsman's [20] and Davies's [7] books, Bond and Smith review [21].

2.2.6 Effect of dimensionality and anisotropy

Most of Fickian or relaxation derived analytical models assumes that the diffusion transport happens mainly along one direction of the absorbing material. This is a reasonable assumption for a plane geometry, in which one of the dimensions is significantly smaller than the other: the shortest path for the diffusing species is through the thickness. Hence it will have the steepest concentration gradient and the highest thrust to diffuse in such direction. But not all the geometries can justify this assumption (e.g., beams, ties, structural joints).

Things get even more complex for PMCs. Composites are not only anisotropic from a mechanical point of view: the presence of long oriented reinforcement fibres introduce anisotropy for several physical properties, such as thermal [36], electrical and diffusivity as well [37,38]. Significant differences arise in the diffusion kinetics if it is assumed that the diffusion happens actually along all the three spatial directions [35].

Considering the governing equation for the fickian model, the anisotropic three-dimensional form is:

$$\frac{\partial n}{\partial t} = D_x \frac{\partial^2 n}{\partial x^2} + D_y \frac{\partial^2 n}{\partial y^2} + D_z \frac{\partial^2 n}{\partial z^2} \qquad \text{Eq. 2-11}$$

Where D_x, D_y and D_z are the diffusion coefficients along the spatial directions. The solution of such an equation quickly escalates to a level of mathematics difficult to treat without solid calculus knowledge and computational power to support, and somewhat out of the scope for our purposes. Just for reference, the mass gain function, as calculated by Aktas *et al.* [39], is:

$$M_{3D}(t) = M_\infty \left(1 - \frac{512}{\pi^6} \sum_{i=0}^{\infty} \sum_{j=0}^{\infty} \sum_{k=0}^{\infty} \frac{1}{(2i+1)^2 (2j+1)^2 (2k+1)^2} \cdot \exp\left[-\pi^2 t \left(\frac{(2i+1)^2 D_x}{l^2} + \frac{(2j+1)^2 D_y}{w^2} + \frac{(2k+1)^2 D_z}{h^2} \right) \right] \right) \qquad \text{Eq. 2-12}$$

It can be noted that the diffusion along the three directions does sum up in the exponential argument and each contribution is proportional to the diffusion coefficient, and it is inversely proportional to the square of the geometric dimension in each direction (the diffusion domain is considered to have a parallelepiped shape). For components which geometry is not planar, deviations from the one-dimensional fickian solutions can be accounted for the diffusion through other dimensions.

An alternative solution to address the deviation of the diffusion process from the ideal one-dimensional Fickian model is to calculate some correction factors which take into account the geometry of the diffusion domain, or even the anisotropy of the particular material. This approach does not help to gain a better understanding of the diffusion kinetics but keeps the calculations complexity to a

minimum. For certain applications, the Fickian model can still be a reasonable trade-off between accuracy and ease of use.

In literature, there are examples regarding the evaluation of these correction factors [38]. The underlying assumption is that the degree of saturation for the unidirectional diffusion, defined as:

$$G_{1D} = \frac{M(t)}{M_\infty} \cong \frac{4}{h}\sqrt{\frac{D_z t}{\pi}} \qquad \text{Eq. 2-13}$$

is a linear function of the square root of time $\sqrt{t}$ (compare with Eq. 2-4), for $G < 0.6$. This stage is indeed called of *linear diffusion*, and from the slope of the G_{1D} vs $\sqrt{t}$, it is possible to calculate the diffusion coefficient. This linearity assumption holds true in good approximation for the three-dimensional scenario, and from the gravimetric plot is possible to calculate an "apparent" diffusion coefficient D_{eff} using the same equation for the unidirectional case.

Limited to the linear region, a correction factor *f* can be defined as:

$$G_{3D} = f \cdot G_{1D} \qquad \text{Eq. 2-14}$$

and hence, applying it to the diffusion coefficients:

$$D_{corr} = f^{-2} D_{eff} \qquad \text{Eq. 2-15}$$

where D_{corr} is the corrected diffusivity coefficient for diffusion through the free edges and $D_{eff.}$ is the diffusivity coefficient measured from the gravimetric experiments.

Shen and Springer [29] and Starink, Starink and Chambers [37] have derived correction factors that are used in this paper to correct the diffusivity coefficients:

[29] $$f_{S\&S} = 1 + \frac{h}{w} + \frac{h}{l} \qquad \text{Eq. 2-16}$$

[37] $$f_{SSC} = 1 + 0.54\frac{h}{w} + 0.54\frac{h}{l} + 0.33\frac{h^2}{wl} \qquad \text{Eq. 2-17}$$

The correction factor proposed by Starink returns more consistent values of diffusivity when applied on experimental data from the gravimetric test. The diffusion coefficients calculated through f_{SSC} are closer to the value returned from the quasi unidirectional diffusion and are less sensitive to experimental samples geometry.

In the analysis of the experimental data produced within this research project, we mostly relied on the corrected coefficients using the Starink's factor.

2.2.7 Effect of temperature on diffusivity

As for most of the physical and chemical processes, temperature plays a pivotal role in influencing the kinetics of diffusion process. The temperature directly influences the mobility of chemical species, control the activation of vibration/rotation in polymer groups and, at the macroscopic level, their relaxation time. From experimental data, a strong correlation can be found between the mass transport rate and the temperature which it occurs.

From a theoretical point of view, diffusion follows the activate transition state theory. For most diffusion mechanisms, the diffusion coefficient increment with the temperature is represented by the classical Arrhenius relationship [21]:

$$D = D_0 exp\left(\frac{E_a}{RT}\right) \quad \text{Eq. 2-18}$$

Where E_a is the diffusion activation energy, R is the universal ideal gas constant, and D_0 is typical of the diffusant/diffusing medium system. Typical activation energies in polymer materials are in the 35÷50 kJ/mol range. In polymer composites, different activation energies can be found, depending on which additional transport mechanism is enabled, but the exponential relationship does usually match the experimental trend.

2.2.8 Effects of water on polymer composites

As previously stated, PMCs tend to absorb water, either from the atmospheric moisture or when they are in direct contact with it, as in marine applications. There is an extensive literature about the effect of the water interaction on the physical properties, for the polymer matrix in particular. Commonly, the inorganic reinforcement fibres are considered impermeable and relatively inert to water, while organic and biological fibres are significantly affected by it.

Due to the great variety of composition and configurations of composites, there is not always complete agreement on the effects reported or coherence in the analysis of the mechanism. There is a variety of different properties or loading condition that could be tested to this aim: tensile, compression, interlaminar, under fatigue or creep loading, relaxation times [40].

Usually, a decrease in mechanical performance is reported, both with thermoplastic and thermosetting composites [17]. Some authors aim to relate with the length of the exposure to water; others prefer to relate the change in properties to the saturation degree of the material, as well as the environment temperature.

At the molecular level, the degradation of the mechanical strength is related to the disruption of the hydrogen bonds of the polar groups of the polymer due to the interference of the water molecules. This loosening of the bond can be involved even in a reduced capability of the matrix to transfer loads to the fibre by a weakening of the fibre-matrix interphase cohesion [41].

2.3 Ageing

The process of performance degradation in material over a long time is generally referred to as *ageing*. It can be broadly characterised by three primary typologies: chemical, physical and mechanical. The possible interactions are highly dependent on the material characteristic and the environment the material is exposed to [42].

Typical kinds of ageing mechanism that can be found in offshore operations are thermal degradation, due to the contact with the hot extraction fluids, which usually causes embrittlement of the material. It can be particularly aggressive if combined with the presence of environmental oxygen. The process is autocatalytic and generates peroxide radicals, which can attach and degrade the polymer chain in a severe way [43]. However, the oxygen concentration in water is relatively low, in particular at increasing depth, so the radical formation is prevented.

Hydrolytic degradation also occurs, following the water diffusion in the polymer matrix: the plasticisation effect is an early symptom, but it can be followed by a decrease of the mechanical properties due to chemical aggression on the polymer. This is linked with an increase of microcracks density, which usually brings a reduction of fracture toughness [30,44,45].

Another common ageing effect is ultraviolet radiation degradation. From the solar radiation, UV rays in the 290-400 nm wavelength range reach earth surface, which can be absorbed by the polymer molecules and lead to photochemical reactions, with dissociations of the covalent bonds of the carbon backbone or release of free radicals. UV exposure can be highly detrimental to the polymer mechanical properties. Usually, protective coating/paints can be used to shield the polymer from the radiation [46,47]. In case of submerged structures, the radiation is completely absorbed in the first tens of meter of seawater, so it represents a minor threat for most applications.

Accelerated ageing is defined as the process required to boost a specific critical degradation mechanism in comparison with the ordinary ageing conditions: during it, the material reaches the same aged end-state but in a significantly shorter time. Being material testing an expensive activity, accelerated ageing can help to shortlist possible candidates for a specific ageing condition or may help to determine the residual service life of existing structures [42,48].

To develop an accelerated testing program, it is important that the ageing mechanism does replicate the real-time, long-term environment effect. This would imply a thorough understanding of all the possible concurring mechanisms, which in most cases would be beyond the experimental scope. It is preferred to devise a simple way to measure the main degradation mechanism progression, identifying direct or indirect material properties which are easy to measure. Nominally, these could be the weight, as in gravimetric testing, the *glass transition temperature* (Tg),

crack density or mechanical performance, to evaluate the damage state. The change of these properties should be measured at a reasonable number of intervals and tracked against a baseline of the same property measured in the material not exposed to the ageing conditions. The final and not trivial aim is to correlate the data from the accelerated ageing with the real-time ones. An acceleration factor should be found as a function of the controlled ageing parameters [42].

2.4 Thermal insulation of composites

Offshore installations are expected to endure for an operative lifetime of 20 ÷ 25 years to be economically viable, with a minimum amount of maintenance. Composite materials are attractive as they are almost inert to the marine environment, hence solving most of the corrosion issue typical of metal alloys [9].

Besides their improved durability, PMCs are interesting for other physical properties:

a) Their densities are significantly lower than steel alloys (a 7:1 ratio in favour of composite relatively to the water density);
b) Their lower thermal conductivity compared to any metal alloys.

One of the issues affecting offshore oil recovery is the need to keep the extracted crude in a fluid state to avoid clogging or solid-phases precipitation, despite the low temperature of ocean water (4 °C on average, can be even lower in particular conditions). There are different techniques to maintain the fluid at the optimal condition, but passive thermal insulation (applied to the pipelines) is one of the most convenient. Thermal insulation is not only a technical requirement but can profoundly affect the energy efficiency of the extraction process [8].

Their insulation performance can be further improved by the addition of polymer foam liners to the layered pipe structure. Several thermoplastic polymers have been developed in the format of low-density foams, from basic polystyrene and polyurethane, up to high-performance polymers like poly(vinylidene fluoride) and are already used in commercial products. The drawback of using these foams is that they usually have poor adhesion properties to thermoset matrix composite substrates unless advanced adhesive techniques or surface treatment are involved [49].

The development of foams obtained from thermosetting epoxy resins has followed different routes due to their different processability. For this class of polymer, there has been a significant development of syntactic foams, which can be considered a sort of particulate composite, where hollow spheres are introduced in the resin before curing in order to generate controlled porosity distribution [50].

Epoxy foams are interesting for composite structural application as they have the attitude to adhere effectively to many substrates, show excellent mechanical properties and are thermally and chemically stable [10].

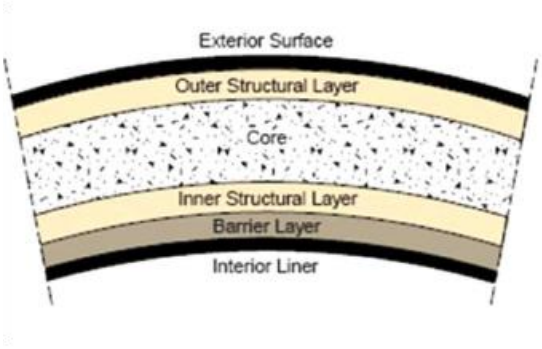

Figure 2-4: a schematic of a composite sandwich pipe wall construction. Adapted from [51]

Another positive feature of the introduction of foam in the pipe structure is that it does reduce the overall density of the structure. This can play an important role in an offshore riser system, which often has to withstand high structural tensile loads and needs additional external buoyancy to achieve a steady structure. The possibility to design the foam layer to be introduced, to achieve a buoyant indifferent pipeline, would greatly ease the designer work, relieving critical stresses to the components and materials involved, and increasing the versatility of these pipeline systems. For reference, the main design constraints required to an insulating material for a component such as an offshore deep-water riser for oil recovery are a wide operative temperature range (exceeding 100 °C), a compressive strength able to withstand the high hydrostatic pressure and a very low thermal conductivity (below 0.2 $Wm^{-1}K^{-1}$), as reported in literature [52]. Other sectors of interest for the polymer insulating materials are the maritime industry in general, the military for submarine vehicles and the oceanographic one for deep-water explorations.

The industry is interested in developing systems where the foaming agent does not involve the use of hazardous chemicals and requires only to introduce simple alteration to the resin curing routine. There are reports in the literature where the foaming agent for epoxy is introduced as an additive in the resin formulation and releases a blowing gas simultaneously with the curing reaction, exploiting the same curing agent, and polymerisation heat generated [10,53]. An advantage over the syntactic foams is that it is possible to obtain lower foam densities. By adjusting the resin formulations and the curing parameters, it is possible to obtain foams of different morphologies, with low apparent density.

The foaming process is more sensitive to the curing route and needs to be precisely controlled to optimise the foam morphology. The porosity distribution is highly dependent on the timely release of the foaming gas when the resin viscosity has reached an optimal value: if the resin is too fluid, the small bubbles will coalesce

and generate a much inhomogeneous morphology; whereas when the resin gets too thick, the pores won't develop in a sufficient number and size. It has been shown that the most favourable time for pore development is around the resin gel point when the viscosity rapidly change in a short time interval [54,55].

Further development is needed to fully characterise the mechanical and thermal properties of this class of foams, in particular regarding:

a) Mechanical strength
b) Adhesion strength
c) Permeability
d) Thermal stability
e) Thermal conductivity

Ideally, the foam can be combined to a fibre-reinforced composite substrate to form a sandwich composite, which would allow to tailor the mechanical properties and adding significantly improved thermal insulation, so beneficial for offshore applications [56]. The sandwich geometry could be implemented in continuous pipeline manufacturing with a dedicated design. Manufacturers are already introducing innovative technologies to produce multi-layered pipe combining pultrusion, fibre winding, braiding and Automated Fibre Placement in complex manufacturing lines [15].

Chapter 3 Experimental methodology

3.1 Aim of the testing

This work was started with the intent of investigating how the properties of composite material evolve when exposed to harsh marine environment typically found in the offshore Oil & Gas industry. There is a growing interest to introduce composite materials in structural applications for offshore extraction rigs and underwater pipelines. The gap of experience with these materials needs to be bridged. A better understanding of the performance's evolution and the ageing process in Polymer Matrix Composites (PMCs) is required to enable designers to forecast the durability of components made of composite material. Only if a competitive gain in durability per unit of cost against the use of standard building materials is demonstrated, the choice will be for the PMC option.

Our aim is not intended in characterising the properties of this particular material grade but rather to identify a good practice about the design and to perform of the exposure testing, which allows investigating the behaviour of the tested material when exposed to an environment simulating the foreseen one of the operative scenarios. The understanding of how the material performance changes over time allows designing with reasonable confidence of components which are supposed to last for decades.

3.2 Accelerated fluid exposure

3.2.1 Experimental approach

The experiment consists in exposing (being liquid formulations, soaking) samples of the interest materials to a simulated environment as much representative as possible of the real operative scenario. Oil & gas application is where we focused our attention, in particular to the offshore marine applications. In such a scenario, those components are in continuous contact with seawater and a range of mixtures of fossil fuels. The materials' specimens, named coupons in the literature [7,20], are manufactured in-house, in the attempt to have the best consistency on the material and sample quality.

As discussed in the previous chapter, Polymer Matrix Composites (PMCs) show appealing properties for the marine applications, in particular, their resistance to electrochemical corrosion. Glass Fibre Reinforced Polymer (GFRP) composites have the advantage to be cheaper in comparison to Carbon fibre reinforced ones. Due to the very different physical nature of the matrix and the reinforcement, we

deemed useful to split the exposure experiment into two subsequent stages: in the first one, we used coupons made of the thermoset polymer, an amine-cured epoxy, which is used as the matrix in the composite when infused. We also postulated that the effect of the diffusing fluid was negligible on the glass fibres, which are theoretically impermeable to fluids. It is known that the fibres are subjected to surface aggression, in particular by water, but this is highly dependent to the interface condition [57], which cannot be recreated without the infusion in the epoxy matrix. The whole composite coupons, with unidirectional fibre reinforcement, were introduced in the later stage, a repetition of the gravimetric experiment. In such a way, we attempted to separate the effect of the ageing on the matrix and the composite, to independently understand the degradation mechanisms.

Fluid permeation is a complex phenomenon: it is influenced by physical variables, chemical interaction, mechanical loads and the conditions of the material. There is no direct practical measurement to evaluate how a fluid permeates a solid medium. The most popular is gravimetric testing, which is basically to weigh the coupons to record the change in their mass: the increase of weight is indicative of the fluid diffusion and allows to evaluate the diffusion kinetics.

In order to investigate the effect of fluid diffusion on material performance, analytical and mechanical testing needs to be performed. The tests allow monitoring the change in the material properties as the exposure is ongoing. The Dynamic Mechanical Analysis (DMA) is an established technique to evaluate the shift in the glass transition temperature of the material. Tensile testing is the most reliable destructive mechanical testing to directly measure the mechanical performances, which are of prime importance to the designers.

Alongside with these techniques, we employed some other analytical testing to a smaller extent: Thermal Gravimetric Analysis (TGA) provided some further information about how the materials desorb absorbed fluids and its thermal degradation limits.

3.2.2 Materials and manufacturing

Specimens are obtained directly from the machining of the material of interest. The manufacturing process should provide a representative material as the one suitable to be used for the foreseen application. It was decided to manufacture the materials in house, which will provide better control on the quality of the product from batch to batch. At the same time, the more advanced composite manufacturing technologies were not available in our laboratories, so we employed some more traditional one such as compression moulding and vacuum bag infusion, which can provide good quality materials if performed correctly. The materials used for the investigations do not aim to reproduce any specific available commercial-grade but rather a quality-controlled material representing an ideal reference PMC.

Squared specimens, commonly named *coupons* are manufactured by machining a plate of pristine material. The coupons can have different geometries, in particular if mechanical testing will follow the exposure.

In practice, test specimens can be obtained by cutting full-scale components, but usually, this makes the dimensional control more difficult, considering that most surfaces are curved.

3.2.3 Ampreg 26 epoxy

A standard representative polymer matrix was chosen. A commercial epoxy thermoset, *Ampreg 26*, distributed by Gurit (UK) was selected, using the s*low hardener* provided with the resin. This material is suitable for vacuum assisted infusion. The epoxy resin consists of a blend of bisphenol A, bisphenol F and 1,6 hexanedioldiglycidylether, while the hardener is a blend of amines (polyoxyalkyleneamine, 2,2'-dimethyl-4,4'methylenebis (cyclohexylamine), 4,4'-methylenebis (cyclohexylamine) and 2,2'iminodiethylamine). It is recommended for high-performance structures and actively used in the manufacturing of racing and military boats [58].

A compression moulding technique [59] was selected to manufacture the plates which the test specimens were cut from. Two different steel moulds were used. The smaller mould had an internal cavity of 200×200 mm^2 area, and it was a straight plunger mould type, so the height of the cavity could be varied. The mould assembly comprised the actual two halves of the closed mould, a pair of 2 mm thick PTFE sheets, which were placed to avoid the epoxy to sticks to the surfaces; additionally, a 2 mm thick Viton rubber rim was placed in the middle to frame the mould cavity. This rim allows the mould to adjust while maintaining the needed thickness of the produced plate; at the same time, it allows the air and excessive adhesive to escape through the runners, reducing the trapped porosity in the cured plate [60].

The second larger mould was simply a pair of flat plates (runner grooves were cut along the sides), which external dimension were 300×300 mm^2; side metal guides and an adjustable hinge kept them in place. A set of metal frames were inserted to obtain the desired cavity height (1,2 or 3mm). Similarly, a rubber rim was added to contain the spreading resin while allowing the air or excess resin to flash out. The available cavity surface was 225×225 mm^2, as limited by the presence of the metal frame and rubber rim.

At the beginning of the experimental design, a thickness of 2 mm was decided to be the best trade-off to have reasonable short diffusion times and specimens resistant to handling, hence this was the constant nominal thickness. Due to the presence of the rubber rim, the available internal cavity of the moulds had the following nominal dimensions:

Mould	l (mm)	w (mm)	t (mm)	V (cm^3)
small	165	165	2	54.5
large	205	205	2	84.1

The dimensions of the internal cavity were needed to calculate the amount of resin to be mixed. The (epoxy resin + slow hardener) mixture density was 1.112 g/cm^3) [58]. This way, it was possible to calculate the amount of resin needed to fill up the mould cavity. An extra 20 %wt was added to account for the losses (remaining in the beaker or spilling out of the mould).

Mould	Net mass (g)	Gross mass (g)
small	60.6	72.7
large	112.6	135.1

From these quantities, it was straightforward to calculate the amount of resin and hardener to be mixed in 3:1 *m/m* ratio. A precise mixing and degassing procedure were followed (see § 3.2.3.1) in order to reduce the number of porosity introduced and to get a good homogeneity in the material.

Once, the resin was approaching the gel point (around 4 h at RT after hardener mixing), it was ready to be poured in the prepared mould. One of the issues faced during the epoxy preparation was the *thermal runaway* that could happen while the resin was setting. It seemed the resin was susceptible to changes in temperature and ambient moisture. Even the amount of mixed resin was critical, being its thermal conductivity very low. Some batches were lost as they set abruptly due to uncontrolled heating up, known as thermal runaway, typical when curing thermosets. To mitigate this phenomenon, the amount of mixed resin per beaker was not larger than 60 g, and it was kept inside a desiccator in a temperature-controlled room in order to keep under control these operational parameters.

The mould's metal surfaces were wet with a release agent, Loctite Frekote 700 NC [61], and let it dry, to ensure the epoxy does not glue it together, in particular for the large mould, where no PTFE sheet was used. Once the resin was poured, the mould was closed and proceeded to the compression stage straight away.

Two hydraulic presses were used for the compression moulding. A pressure of about 2 MPa (around 8 metric tonnes for the small mould and 18 tonnes for the larger one) were applied to optimise the air and excess resin removal, to minimise the number of voids in the cured plate. A curing routine of 24 h at room temperature (RT) followed by a post-cure of 5 h at 80 °C was used, as prescribed by the manufacturer and verified in another study [62]. Heating elements were installed in the press plates and were regulated by closed-loop temperature control. An independent thermocouple was also recording the internal cavity temperature to ensure accurate and repeatable post-cure. The heating elements were set to maintain the required temperature with a ±1 °C variance.

Figure 3-1: the open small mould (the PTFE cover sheets and rubber rim are visible), on the left, and the hydraulic press used for the compression moulding, right.

Once the curing was completed, and the mould cooled down overnight, the cured plated was removed from the mould and checked for compliance. If there was no relevant porosity and the plate thickness was uniform all around, the batch was suitable to manufacture samples. A common issue in several batches obtained with the smaller mould was the poor planarity of the neat epoxy plates and hence the non-uniform thickness. This defect was sometimes due to not sufficient amount of resin poured in the mould or excessive flashing out of its gap while still too runny. However, the primary reason was found in a non-perfect alignment of the press surfaces which applied a skewed angle to the mould at compression. The planarity was improved by retightening the nuts visible on the connecting rods. Still, plates with evident resin starvation or had an overall thickness difference more than 0.5 mm were discarded. Even finished specimens with a difference in thickness for more than the 10 % nominal thickness (i.e. 0.2 mm) were rejected in order to preserve test repeatability.

From each cured batch, a piece of epoxy was sampled in order to verify by Differential Scanning Calorimetry the degree of curing and the consistency of the process. The machining of the experimental specimens was performed either using computer numerical controlled (CNC) drill machining or waterjet cutting (this last performed by external contractors).

3.2.3.1 Ampreg 26 compression moulding procedure

a) Mix the two components resin/hardener in a 3:1 ratio. Do not exceed the 60-70 g of mixed resin per beaker, to avoid thermal runaway during the curing due to poor thermal conductivity.
b) Degas the mixed resin for about 2 h. Repeat the vacuum after the first hour: the abrupt compression helps to burst and remove some of the superficial bubbles in the mixture.
c) Once the degassing is performed, keep the beakers in a desiccator to maintain a dry atmosphere for the remaining waiting time.

d) Meanwhile, prepare the mould by cleaning it and applying the release agent. Once dried, introduce any PTFE sheets at-need and the rubber rim (use release agent on it as well).
e) Pour the resin, starting from the centre of the cavity and moving the flow around in expanding circles, try to maintain a whole lump of gelling resin. If any superficial skin is present, remove it before pouring. Avoid pouring impurities or bubbles in the resin. If present, pour them in the outer region. Leave the remaining resin in the beaker to be cleaned off, do not force it down with the spatula or other means.
f) Close the mould and insert it in the press. The temperature controller is set at 25 °C. Apply the required pressure in incremental steps. Check the alignment is correct and that the resin outflow is not excessive. Leave the resin to cure for 24 h.
g) After the RT curing, increase the temperature to 80 °C. Check if the applied pressure is still at the required level. Control it does not overshoot and start the post-cure timing when the thermocouple records the proper temperature.
h) After 5 h, switch off the heaters and let the press cool down naturally (usually overnight). When cool, release the pressure, remove the mould and open it to check the batch quality. Remove the cured plate gently from the mould, as it is relatively brittle.

3.2.3.2 Ampreg 26 machining

Epoxies at temperatures below their glass transition are known to be naturally brittle unless some toughening agent is added (rubber phase, nanoparticles) [63]. The Ampreg 26 has no toughening agent added To manufacture the experimental specimen, no chopping or cutting with blades can be used, they give no control on the shapes and damage the material. The only viable option was machining. Due to the complexity of some of the shapes (dumbbell specimens) and the higher dimensional control, a CNC milling machine was used. Standard *high-speed steel* (HSS) drill bits were used, without any lubrification lest to contaminate the material. Low feed rates were used in order to avoid any overheating or burnt off the cut edges.

3.2.4 GFRP composite

To manufacture the Glass Fibre Reinforced Polymer composite, it was decided to use the same Ampreg 26 epoxy as matrix and long glass fibres as reinforcement. Unidirectional fibre reinforcement configuration was used, like in a single composite lamina, to simplify the determination of the physical properties and the fluid diffusion kinetics, in other words, to remove the fibre orientation from the experimental variables. The stitched unidirectional glass fibre fabric (1200 g/m2, from Gamma Tensor, SPA) was selected. It comprises 3B Advantex® SE 2020 Direct Roving made of boron free E-CR glass, which are specifically designed for

the production of non-crimped fabrics and have a proprietary sizing specifically designed for excellent adhesion with epoxy resin systems. To reach a similar thickness as the epoxy samples, 2 overlaid layers of fabric were stacked to get a nominal thickness of 1.7 mm, close enough to the 2 mm target.

The vacuum bag infusion technique was chosen to manufacture the GFRP composite plates. A carbon steel plate was used as stiff support, which surface was ground to give the best smoothness to the composite. A standard infusion setup was purchased from Easy Composites (UK), providing the bagging material, other consumables and a positive displacement vacuum pump.

Although the vacuum bag technique allows much more versatility in the geometry of the infused plate, it was decided to manufacture always 350×350 mm plates. In this way, the infusion procedure and resin quantity were kept the same, and the composite plate could fit in ovens for post-cure. To perform the infusion, two layers of GF fabric were cut and overlapped on the metal plate. A release peel and a breathing mesh were added on top of them. Then the vacuum bag was prepared, the edge sealed with dedicated sealant rubber and the rig was checked for vacuum tightness. The vacuum also helped to compact the glass fibres. Once the resin was mixed and degassed, it could be infused in the bag while it still was at a very low viscosity. It had to be checked that the fibres were completely wet and in a homogenous way. Once the bag was completely filled, the inlets were sealed, checking again for any leak: the vacuum pressure ensured proper compaction while the resin was hardening.

The curing routine was 24 h at room temperature, same as for the neat epoxy; then the composite plate was removed from the bag and post-cured for 5 h at 80 °C in forced ventilation electric oven. Some warping was induced by thermal stresses, possibly caused by a non-perfect symmetry in the reinforcement distribution.

Due to the higher hardness of the glass fibres, most of the plates were machined by waterjet cutting. From straight cuts, in house diamond-blade

3.2.4.1 GFRP infusion procedure

a) The glass fibre fabric is cut in the required shape and laid as the prescribed orientation.
b) The required amount of resin is mixed and degassed.
c) In the meantime, the vacuum bag is prepared and checked for leaks.
d) When the resin is adequately degassed, it can be infused in the bag. The proper fibres wetting needs to be checked.
e) Once the infusion is complete, the vacuum can be sealed. If it is vacuum-tight, leave the resin to cure for 24 h at RT.
f) Remove the solidified plate from the bag, and post-cure the plate for 5 h at 80 °C. Place it on an even horizontal surface to avoid any unwanted bending.
g) When the plate is properly cured, it can proceed to the specimens cutting.

3.2.4.2 GFRP machining

GFRP composite is known to be difficult to machine. It is very abrasive due to the presence of the hard glass fibres [64]. Instead of drilling it, it is more convenient to use abrasion techniques, such as a diamond-coated blade (Struers) aided by liquid lubricant and water-jet abrasion (performed at a contractor). These techniques guarantee a smooth cut edge and reduce the damage to the fibres and interfaces.

3.2.4.3 Evaluation of the fibre volume fraction

A calcination method was used to estimate the GFRP composite fibre volume fraction as prescribed by the ISO 1172 standard [65]. The test was subcontracted to the National Physical Laboratory, in Teddington (UK).

GFRP samples (dimensions: 20×20×1.8 mm) were dried at first to remove any possible residual moisture. Then they were weighed, and their volume measured by immersion in a liquid at 23 °C using a pycnometer: in this way it was possible to calculate the composite's apparent density. The apparent density of the epoxy was previously calculated measuring weight and volume of the gravimetric coupons: it was 1.158 g/cm^3. The density of the Advantex glass-fibres was provided with the technical datasheet, and it was equal to 2.620 g/cm^3.

To determine the fibre volume fraction, the burn-off Method A prescribed by the standard was used. Specimens were placed in dried crucibles and heated to 650 °C in a muffle furnace for 60 mins in order to remove the polymer matrix phase. The mass of the remaining reinforcing fibres was subsequently measured, and the fibre and resin densities used to calculate the fibre volume fraction.

The density and fibre volume fraction determined for each specimen is provided in Table 2, alongside relevant statistics. An average fibre volume fraction of 56 vol% was measured.

Table 3-1: Apparent density and fibre volume fraction of GFRP samples.

Sample no.	***Density (g/cm^3)***	***Fibre volume fraction (%)***
1	1.973	55.2
2	2.004	57.1
3	1.984	55.7
4	1.962	54.3
5	1.993	56.4
Mean	**1.983**	**55.7**
SD	**0.016**	**1.1**
CV (%)	**0.8**	**2.0**

3.2.5 Gravimetric test design

A gravimetric test is a test where the weight of material specimens, usually named coupons, are weighted at selected intervals to record possible changes in their mass. As reported in the extensive literature [7,20,35], gravimetric is still a widespread test to investigate the diffusion kinetics of fluid permeating a polymer or a polymer composite. The debate is still very open about what is the most suitable theoretical model to describe mass transport through a polymer medium, but there is a good agreement about how a gravimetric test is fundamentally performed. The tested coupons are obtained from the material of interest and cut in rectangular specimens which have one of the geometric dimensions much smaller than the other two: in this way, the diffusion process happens mainly through this only direction, making the data analysis less computationally expensive. The main ASTM standards (D570 [66] and D5229 [67]) prescribe dimensions ranges for the coupons, but there is not complete agreement in literature, both because of manufacturing limitations and experimental needs [68,69]. For our testing, as mentioned before, we selected a nominal thickness of 2 mm as a reasonable trade-off between the minimum mechanical strength of the materials and keeping the diffusion process as quick as possible. In particular at low temperatures, the fluid diffusion process is quite slow, in the order of months to get to saturation in dense material like epoxy.

The ASTM standards require for the coupons to maintain a minimum thickness to length ratio of 1:100 to ensure the diffusion transport happens almost exclusive in the direction orthogonal to the main dimension. The thickness being the minimum geometrical dimension by far, it is the shortest path for the fluid to diffuse. In literature, it is not fully agreed if such an assumption is sufficient [70]. There are numerical or approximation methods that try to address the influence of a non-perfectly unidimensional diffusion, as opposed to what the fickian model states [38,71]. In order to evaluate the "edge effect", the diffusion in other direction rather than the through-thickness one, different geometries were selected, both for the neat epoxy and the GFRP. The other dimensions were calculated, keeping the specimen thickness fixed, in order to have some significant difference in their side to thickness ratio. From the paper from Starink et al.[37], they proposed a correction factor to account for the non-1D diffusion:

$$f_{SSC} = 1 + 0.54\frac{h}{w} + 0.54\frac{h}{l} + 0.33\frac{h^2}{wl} \qquad \text{Eq. 3-1}$$

According to this equation, the nominal specimen dimensions were calculated:

Table 3-2: coupons geometries used in the gravimetric testing.

Specimen	length (mm)	width (mm)	thickness (mm)	f_{ssc}	$1/(f_{ssc})^2$
alpha	19	19	2	1.117	0.80
beta	40	40	2	1.055	0.90
gamma	100	100	2	1.022	0.96
delta	100	10	2	1.120	0.80
epsilon	10	100	2	1.120	0.80

Three replicas for each specimen geometry will be introduced in any experimental condition to ensure the statistical significance of the measurements.

In order to investigate the evolution of the properties of the material when exposed, a number of soaking conditions were planned at the beginning of the experiment.

Three different soaking fluid were planned for exposure:

a) Substitute (or synthetic) seawater, compliant with ASTM D1141;
b) An aromatic oil mixture, as for standard Norsok M-710, shorten as *Norsok oil;*
c) Dry air.

Indoor moisture measurements were continuously recorded by lab environmental logger and RH levels were kept between 40% and 60%. Inside the heated ovens, RH below 10 % was measured using a portable hygrometer, but it was not continuously recorded, and there is no data log.

The substitute (or synthetic) seawater composition is described by the ASTM D1141 standard [72] and purchased by ReAgent, UK, in order to simulate the marine environment.

Table 3-3: standard substitute seawater as per ASTM D1141

Compound	*Concentration, g/L*
$NaCl$	24.53
$MgCl_2$	5.20
Na_2SO_4	4.09
$CaCl_2$	1.16
KCl	0.695
$NaHCO_3$	0.201
KBr	0.101
H_3BO_3	0.027
$SrCl_2$	0.025
NaF	0.003
Other metal nitrates/nitrites	< 0.1 mg/L
H_2O	balance

The aromatic oil was prepared following the recipe prescribed by the NORSOK M-710 standard [73], used for the qualification of polymer materials when they exposed to harsh fossil fuel mixtures, typical of offshore Oil & Gas operations. It comprised three hydrocarbon compounds with the following composition:

Table 3-4: hydrocarbon mix composition

Hydrocarbon compound	*Volume fraction*	*Boiling point*
n-heptane	70 vol%	98 °C
cyclohexane	20 vol%	80.7 °C
toluene	10 vol%	110 °C

To evaluate the effect of temperature in the conditioning of the material, three exposure temperature were selected, namely 25, 55 and 80 °C. Such temperatures were chosen to span over the range from room temperature to the glass transition in similar steps. The temperature was controlled by placing the containers in forced ventilation electric ovens. The internal temperature was monitor and logged by calibrated thermocouples. The liquid used for the diffusion guarantees to keep a good thermal equilibrium thanks to its thermal inertia (particularly true for the seawater).

The containers chosen for the seawater were food-grade polypropylene buckets, as they can withstand temperatures up to 100 °C and they are inert to water. Their dimensions were 138 mm in height and 200 mm in diameter, with a capacity of about 3 dm^3.

Figure 3-2: experimental setup for the accelerated exposures in electric oven.

For the Norsok oil, pressure-tight stainless-steel vessels were employed, because the solvent chemical present in the mixture would degrade most of the thermoplastic polymers. Also, the oil vapours, the toluene's in particular, are toxic to breathe. Considering the high volatility of the compounds, there was the need to minimise their evaporation. These vessels are named "vapour-pressure cells" as the vapours would build up inside them until the vapour pressure at the given

temperature is reached inside. These cells have an internal diameter of 120 mm and are 250 mm tall; their capacity is about 2.8 dm^3. The top rim featured a groove designed to host a nitrile butadiene rubber (NBR) seal, against which the lid rested. This kind of rubber was chosen due to its excellent resistance to solvent vapours, but more performing rubbers, such as HNBR or fluorinated ones (Viton) are available for more demanding conditions. Eight bolts fix the lid to the vessel body. On the lid is present a high-pressure access port, to allow installing internal monitor thermocouple and a pressure release scream. The cells are rated up to 50 bar of internal pressure. A drawing of a vessel is reported in Figure 3-3:

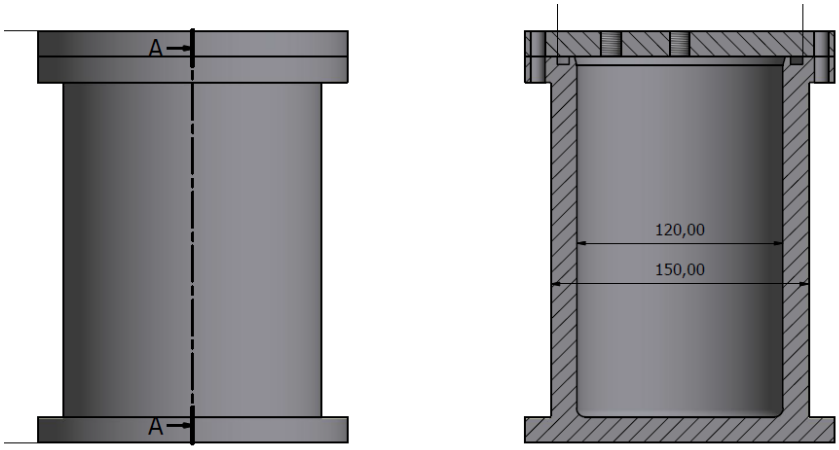

Figure 3-3: a blueprint of a vapour-pressure cell. Dimensions are in mm.

For the Norsok exposure of neat epoxy at RT, there was an exception as a PET bottle was used as the container, for ease of handling. PET has good compatibility with all the Norsok components [74]. Viton rubber was applied in the inside of the bottle cap to improve the sealing.

For the dry-air conditioning, steel cans with sealed tops were used to store the coupons in a controlled atmosphere. Silica gel bags were added to capture any residual moisture at the conditioning beginning.

The different exposure conditions were coded as the following scheme:

Table 3-5: Description of the exposure conditions and relative coding.

Conditions	*Seawater*	*Dry air*	*Norsok oil*
25 °C	A	F	M
55 °C	B	G	N
80 °C	C	H	O

Additionally, the condition *P* identified samples which are in their original *pristine* state, to serve as a benchmark for the properties of the material in the aged conditions.

To provide some numbers, just the gravimetric coupons for the seawater and Norsok oil exposures account for:

$$3\ replicas \times 3\ Temp. \times 2\ fluids \times 4\ geometries = 72\ coupons$$

For the dry air exposures, only the alpha or beta geometry samples were added, as the shape factor would not influence the ageing process. At least 10 more delta or epsilon samples were added to each exposure condition to be used as DMA specimen at the selected intervals.

3.2.6 Gravimetric testing procedure

At the beginning of the experiment, all the coupons were randomly assigned uniquely coded in order to be able to identify them and connected to the origin batch, the coupon type and the exposure condition they were intended for. To ensure to recall them correctly, they were marked with permanent ink and superficially engraved with the unique coding, as the ink could disappear over time, particularly when in contact with solvents. Other means to ease the identification were specific marking on the sides or corners, again following a specific scheme.

As described in the previous paragraph, the simulated environments consist of containers or vessels of sufficient dimensions to contain the samples and exposure fluid without interacting with them. The amount of fluid should be large enough to avoid an excessive concentration of the leaked or reaction products, not to alter excessively the simulation environment.

The experimental setup comprised a set of 2 precision scales:

Scale	*Weight capacity (g)*	*Weight resolution (g)*
Reflex HP 220 Avery Weigh-Tronix	0.001÷220	0.0001
SD-200L Alfa Mirage	0.01÷200	0.0001

The second was the scale of a densimeter. Using two different scales could add some experimental error. The choice to use two different scales was taken because the plate of HP 220 was returning not precise weight when measuring *gamma* coupons. The scale plate smaller than these coupons and placing them in correspondence of the geometric centre was not straightforward. This probably led to out of balance momentum to the place, causing the measurement error. The larger plate available with SD-200L ensured better repeatability in the measurement with ease of operation, so it was decided to use it for weighing the *gamma* coupons.

The exposed samples were pre-conditioned beforehand, to reduce any possible influence of the prior history and remove residual moisture. Minimum 2 weeks in forced ventilation oven at 50 °C were necessary to reach the weigh equilibrium in the completely dried coupons. Few randomly chosen “traveller” coupons were used to monitor the change in weight. The D5229 standard defines the effective equilibrium as a change in weight by less than 0.020 wt% over each of two consecutive reference periods. The reference period is set for a week when the diffusivity of a material is not known.

When the coupons were completely dried, hence their moisture content was close to zero beyond experimental sensibility, the exposure to the fluids can start. The coupons were weighed again to measure their initial dry weight. This measure was critical, as it defined the reference value against any further weight was compared when the testing was ongoing.

The exposure containers/vessels were introduced in the ovens in advance to reach the temperature equilibrium. When the planned temperature was reached, the coupons were introduced in an ordered way and trying to avoid them to pile at the bottom of the vessel: stainless steel supports, Pyrex beakers and small plastic cups can help to organise the smaller coupons. The time of introduction was the one recorded as the beginning of the exposure.

3.2.6.1 Weighing operations

From the exposure start, the coupons were periodically extracted from the conditioning environment and weighed at the precision scale following this procedure:

a) The extracted coupons were re-immersed straight-away in a "transfer" container of the same liquid as the exposure one, to lower their temperature and to protect them from the atmosphere. The removal time was recorded to calculate the length of the elapsed time.
b) The *vapour cells* for the Norsok oil needed to be cooled down entirely as it was not safe to open them at high temperature, risking hot burns and hazardous vapour pressure built-up. The oil vessels were always to be operated under a fume-hood or in a protected atmosphere.
c) At the scale, the coupons were taken out of the liquid in reasonably small groups and carefully wiped to remove the remaining liquid on the surface. Only the absorbed liquid is of interest, not the one wetting the surfaces. When weighed, the single coupons were plunged back into the transfer container.
d) The gamma coupons needed to be weighed twice in quick succession at the densimeter to reduce the experimental error further.
e) Once the weighing was complete, the coupons were returned to their conditioning. The time they were reintroduced was recorded as the new start for the exposure time. In the case of the vapour cells, the time was recorded when the monitor temperature was 5 °C below than the planned one.

The planning of the weighing intervals was critical to capture the key features in the weight uptake curves, such as the linear diffusion and the fickian saturation plateau. For the exposure at higher temperatures in particular, more than a single weighing for the very first days was needed to properly populate the curve with enough experimental points.

At the end of the conditioning, usually one year after the start, the coupons were removed from the exposure and started the re-drying process. Similarly, this conditioning was now aimed to remove as much absorbed fluid as possible from the materials, to evaluate the reversibility of the process. Due to limited capacity, the re-drying was performed at 50 °C for all the conditioned coupons.

Once the drying was completed, the coupons were stored in vacuum-tight bags for the records.

3.2.6.2 Saturation criteria

The recorded data were collected in spreadsheets, divided by exposure conditions. Here the weight uptake was automatically calculated, and the curves were plotted. When the coupons reached effective equilibrium, considered as fickian saturation, the diffusivity factors were calculated as well.

A pivotal feature is the saturation criteria used, which should be a numerical one, and it relies on the convergence of the weight of the coupons as they approach a steady saturated state. From the continuous weight measurements, when the relative change in per cent weight gain decreases, below a certain threshold, the material can be deemed as in *effective equilibrium*. The ASTM D5229 requires a change in weight *by less than 0.020 wt% over each of two consecutive reference periods, and examination of the weight gain versus (time)$^{1/2}$ plot*. This criterion is stricter for the composite material because they are less prone to absorb fluid as inorganic fibres are considered inert.

$$\left|\frac{W_n - W_{n-1}}{W_0}\right| \times 100 < 0.02\% \; for \; 2 \; consecutive \; reference \; time \; span \quad \text{Eq. 3-2}$$

This approach has its limitations. In particular, it does not consider the actual saturation level of the material. Hence polymers with low saturation level or with very low diffusivity can be evaluated as saturated too early, while others which are more prone to absorb or to show secondary stages could eventually never reach proper saturation. From experimental practice, this criterion is not good enough to capture the time to saturation, but it highly relies on the subjective evaluation of the operator.

In this work, a slightly different saturation criterion is proposed by evaluating the partial increase over consecutive measurements and dividing this against the overall weight gain to that point. In this way, small changes are more relevant to low diffusing materials compared to more permeable ones. A more robust numerical saturation criterion is defined:

$$\left|\frac{W_n - W_{n-1}}{W_n - W_0}\right| < [threshold \; value] \; for \; [n] consecutive \; reference \; time \; spans \quad \text{Eq. 3-3}$$

Even this criterion is susceptible to the selection of an appropriate threshold value. From our analysis, it was found that a value of 0.02 (in other words, less than 1/50 of the overall weight gain) allows individuating the saturation point with good

consistency, even when the fluid uptake is very slow, i.e. ambient temperature conditions.

In order to improve the reliability of a numerical criterion for the identification of the effective equilibrium, the results obtained using different criteria are compared in Table A1 (see Appendix A).

From the values reported, it can be highlighted that the criterion prescribed by the ASTM D5229M is the less precise and reliable, with a large scatter in the values obtained for each specimen geometry at any temperature. The proposed method appears to be more consistent, yet it is susceptible to noisy measurement and still requires a comparison of the M_t vs $\sqrt{t}$ plot. Between the two different threshold values proposed, the 0.02 is to be preferred as it captures the effective equilibrium at 25 °C in a more accurate way. For these reasons, for the rest of this study we refer to the effective equilibrium as defined by the *residual increment Criterion A*.

3.2.7 Calculations of the diffusion coefficients

3.2.7.1 The diffusion coefficient for an isotropic homogeneous material

The moisture content in the isotropic ($D_x = D_y = D_z = D$) rectanguloid of Figure 3-4 is given by the following integral solution to Fick's equation for one-dimensional diffusion [27]:

$$\frac{M_t}{M_\infty} = G_{1D} = 1 - \frac{8}{\pi^2}\sum_{j=0}^{\infty}(2j+1)^{-2}\exp\left[-\frac{(2j+1)^2\pi^2 Dt}{h^2}\right] \quad \text{Eq. 3-4}$$

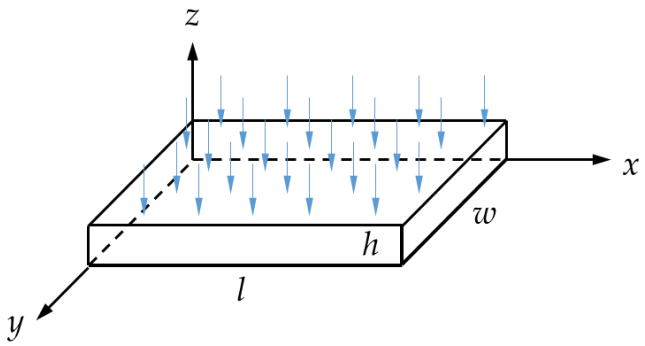

Figure 3-4: directions and dimensions of parallelepiped isotropic material specimen.

To calculate the diffusivity coefficient, D, a simplified version of the above equation was considered:

$$\frac{M_t}{M_\infty} = G_{1D} = \frac{4}{h}\sqrt{D/\pi}\cdot\sqrt{t} \quad \text{Eq. 3-5}$$

where, M_t is the moisture content at time t, M_∞ is the moisture content at the Fickian saturation (effective equilibrium) and h is the thickness of the specimen. The slope of the M_t vs $\sqrt{t}$ for $M_t < 0.6\,M_\infty$ (linear diffusion) is equal to:

$$Slope = \frac{4M_\infty}{h}\sqrt{D/\pi} \quad \text{Eq. 3-6}$$

The main reason for this choice is the saving in computational power by dealing with a simple closed solution, compared to more accurate ones but requiring advanced calculus capabilities. The above equations are not taking into account any diffusion happening from the free edges of the specimens. To account for that, the three-dimensional problem of diffusion in a parallelepiped needs to be considered and solved. Apart from being very computationally expensive, this has the additional drawback that the diffusivity is not easily determined from the initial linear slope of the M_t vs $\sqrt{t}$ graph. For this reason, the introduction of a correction factor can be considered so:

$$G_{3D} = fG_{1D} \quad \text{Eq. 3-7}$$

moreover,

$$D_{corr} = f^{-2}D_{eff} \quad \text{Eq. 3-8}$$

where D_{corr} is the corrected diffusivity coefficient for diffusion through the free edges and $D_{eff.}$ is the diffusivity coefficient measured from the gravimetric experiments.

Shen and Springer [29] and Starink, Starink and Chambers [37] have derived correction factors that are used in this paper to correct the diffusivity coefficients:

Shen and Springer: $$f_{S\&S} = 1 + \frac{h}{w} + \frac{h}{l} \quad \text{Eq. 3-9}$$

Starink, Starink and Chambers: $$f_{SSC} = 1 + 0.54\frac{h}{w} + 0.54\frac{h}{l} + 0.33\frac{h^2}{wl} \quad \text{Eq. 3-10}$$

These are the correction factors that were applied for the correction of the experimental values obtained from the gravimetric test.

3.2.7.2 The diffusion coefficient for an anisotropic material

As with the isotropic case for the neat polymer, a correction for the diffusion through the free edges needs to be evaluated for the composite material, in addition to considering the anisotropic nature of the diffusion process.

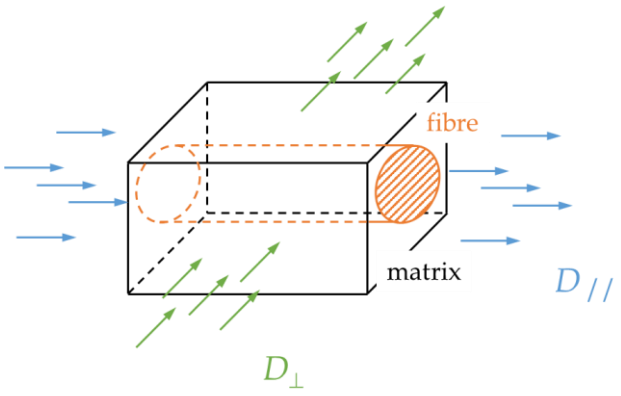

Figure 3-5: Simplified geometry of unidirectional composite for diffusion parallel and transverse to the fibres.

Starink, Starink and Chambers [37] have presented a modified treatment of diffusion in unidirectional composites assuming that the fibres do not take any moisture where the diffusivity parallel ($D_{\parallel}$) and transverse ($D_{\perp}$) to the fibres in Figure 3-5 is given by:

$$D_{\parallel} = D_r \qquad \text{Eq. 3-11}$$

$$D_{\perp} = \frac{\left(1 - 2\sqrt{\frac{v_f}{\pi}}\right)}{1 - v_f} D_r = g^2 \cdot D_r \qquad \text{Eq. 3-12}$$

where v_f if the fibre volume fraction of the composite and D_r is the diffusivity coefficient of the neat resin. The *fibre hindrance* factor g is the expression of the reduced free path for the diffusion species to follow due to the volume fraction taken by the inert inorganic fibres. It does not take into account any possible contribution due to the possible different chemical activity of the fibre-matrix interphase.

For the unidirectional composite in Figure 3-6 the diffusivity coefficients are:

$$D_x = D_{\parallel} \qquad D_y = D_z = D_{\perp} \qquad \text{Eq. 3-13}$$

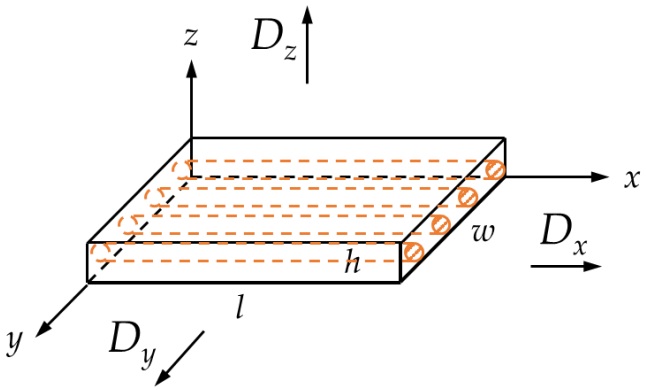

Figure 3-6: Schematic of rectanguloid anisotropic material specimen.

Similar to the isotropic case, Starink *et al.* have proposed a correction factor for an orthotropic medium, ignoring second-order edge effects:

$$f_{ortho} = 1 + 0.54\frac{h}{w}\sqrt{\frac{D_y}{D_z}} + 0.54\frac{h}{l}\sqrt{\frac{D_x}{D_z}} \qquad \text{Eq. 3-14}$$

By a combination of Eq. 3-14 with Eq. 3-11 to Eq. 3-13, it can be found that for the unidirectional composite the correction factor is only a function of the geometry of the specimen, considering along which main direction the diffusion is favoured (usually the shortest), and the fibre volume fraction. For the fibres aligned along the x-axis as in Figure 3-6, this results in two possible scenarios:

$$f_{ortho,\perp} = 1 + 0.54\left(\frac{h}{w} + \frac{h}{l}\frac{1}{g}\right) \qquad f_{ortho,\parallel} = 1 + 0.54\left(\frac{h}{w} + \frac{h}{l}\right)g \qquad \text{Eq. 3-15}$$

(a) diffusion mainly $\perp$ to the fibres (b) diffusion mainly $\parallel$ to the fibres

Therefore, the effective diffusivity for the composite transverse and perpendicular to the fibre direction can be estimated as:

$$D_{eff.\perp} \cong f_{ortho,\perp}^2 D_\perp = f_{ortho,\perp}^2 \cdot g^2 \cdot D_r \quad D_{eff.\parallel} \cong f_{ortho,||}^2 D_\parallel = f_{ortho,||}^2 \cdot D_r \qquad \text{Eq. 3-16}$$

(a) (b)

The above relationships are plotted in Figure 3-7 in function of the fibre volume fraction in the composite material. It is apparent that the 100 × 100 specimen geometry is closer to the infinite plate solution than any other geometry hence providing the most accurate geometry for the measurement of the diffusivity.

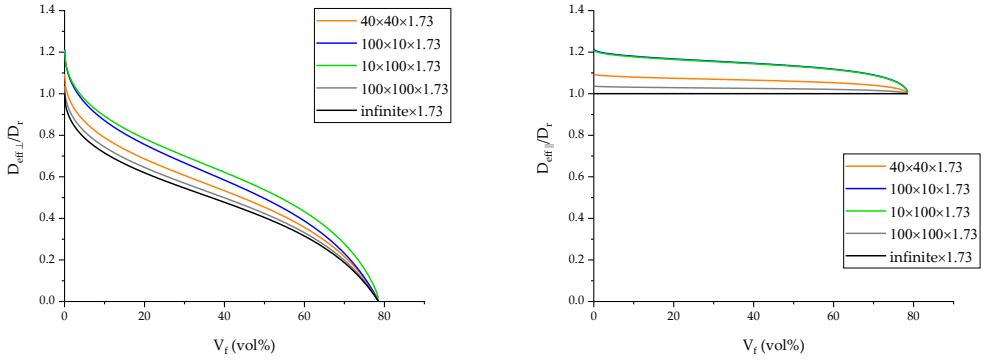

Figure 3-7: (a) $D_{eff.\perp}$ / D_r and (b) $D_{eff.||}$ / D_r versus fibre volume fraction for the different shape specimens used in the study.

3.3 Epoxy foam synthesis and preparation

A polymeric foam was prepared using the same epoxy resin chosen for the preparation of the composite material. Ideally, the epoxy foam would be applied to an epoxy/composite substrate to improve the thermal insulation of it. It is known from the literature that porous medium has lower thermal conductivity due to the low conductivity of the air, which composes the foam in high percentage [10,75]. It is possible to define the non-linear relationship between the conductivity and weight fractions down to around 20÷30% of relative density compared to the bulk material. Then, other heat transfer mechanisms come to play, rather than conduction (i.e. convection if an open cell structure, radiation at higher temperatures), or the material gets too weak for practical use: hence, usually, it makes no use to further decrease the foam density.

To prepare the said foam, we started by a formulation by Stefani *et al.* [10]. They proposed to add tetramethyl disiloxane to an amine-cured epoxy system. The reaction between the methyl groups and the amine groups leads to the formation of gaseous hydrogen, which can form bubbles within the resin. This kind of reaction involving a chemical dissociation was called chemical foaming. Hence the disiloxane was defined as *Chemical Foaming Agent* (CFA).

The characterisation of the foaming process was done mainly through curing trials. Small silicone elastomer moulds were used to cure the resin/foam. The first trial consisted of simply mixing the CFA in different weight fractions, up to 5 %wt., to the Ampreg 26 epoxy system to evaluate the compatibility with it. It was decided not to exceed this amount as:

i. the disiloxane was not readily mixed to the resin; it required some prolonged stirring to obtain a homogeneous mixture (it turns opaque). The higher the amount of CFA added, the longer the mixing;
ii. not to alter the stoichiometry of the epoxy reaction significantly, as the CFA would partially react with the hardening agent.

Moreover, with the first trial, it was found that adding the CFA straight away caused some steady bubble formation while the resin was still very runny. These bubbles were quickly emerging and evaporating, so they did not contribute to the proper foaming of the resin. Several attempts with different combinations (time, amount, mixing) were performed, but they were all quite unsuccessful as the foam obtained was very coarse, with relatively big bubbles and poor dispersion. Some of the results can be seen below:

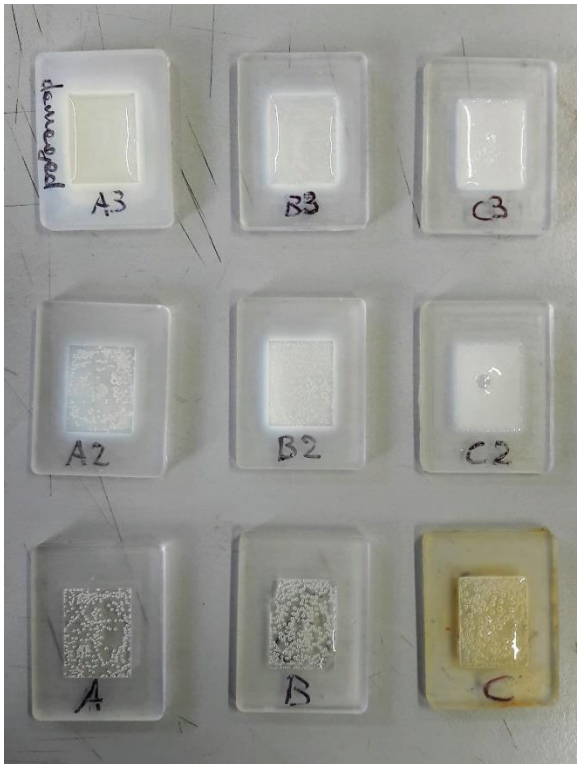

Figure 3-8: some example of early batches of A26 foam trials. Either the bubbles are not properly developed, or they have grown in a non-uniform way.

It was noticed how the addition of the CFA was significantly slowing down the resin curing. The standard gelling point for the neat Ampreg 26 at about 4 h since the addition of the hardener, while the disiloxane worked as “solvent” due to its low molecular weight, and pushed it even beyond the 8 hours.

There was an improvement when we decided to add the CFA in a later stage, about 2 hours after the hardener was mixed. This brought a dual improvement:

i. the resin was allowed to start the curing without any hinder the presence of CFA.
ii. The high activity of the hardener as soon as it was mixed was partially reduced after the first stage of curing, so the reaction with the CFA was at the slower rate, minimising the release of the gaseous hydrogen at the introduction.

The further step was to evaluate the interval at which the viscosity of the resin was optimal to induce the proper foaming reaction. It was noted that simple mechanical stirring could induce the nucleation of many bubbles in the resin, shifting from transparent to white cloudy. Similarly to the neat epoxy, the resin seems to be highly sensitive to the internal temperature and prone to thermal runaways, making it more complicated to make an evaluation. After several attempts, it was agreed that the most suitable moment to induce the foaming was at about the gel point of the resin. The sharp increase of the viscosity was pivotal: on one side, at lower viscosity, the bubble generated easily coalesce and quickly climb to the surface, escaping from the resin. On the other, at a higher one, it would be impossible to mix the resin thoroughly and obtaining a homogeneous pores distribution, or rather no bubble nucleation at all. If the suitable morphology was obtained, it was defined as a *pre-foam* because the resin matrix was not completely cured yet and subjected to possible further alterations.

As the pre-foam was produced, it was promptly transferred to a mould for the curing, before it got too viscous to pour. The mould had an open structure and it was built by an interlocking rectangular frame of polytetrafluoroethylene (PTFE) bars, to minimise the adhesion. The bars had a squared cross-section, 19×19 mm^2. The dimensions of the internal cavity where 150×125 mm^2. The bottom of the mould was initially closed by an aluminium plate, wet by Frekote to prevent the foam from sticking to it. The first batches produced had some large irregular bubbles in the lower part. It was suspected the impermeable plate would not let any gas excess to escape. It was decided to substitute the plate with a transpiring fabric, which it was the peel ply used for the vacuum bag infusion. The fabric lets any released gas to escape while retaining the viscous resin, a minimum amount soaking into it and, at the same time, was easy to remove at the end of the curing. The fabric was sustained by a stiff perforated steel plate to maintain planarity. It was coated in Frekote, to prevent sticking to the mould bottom.

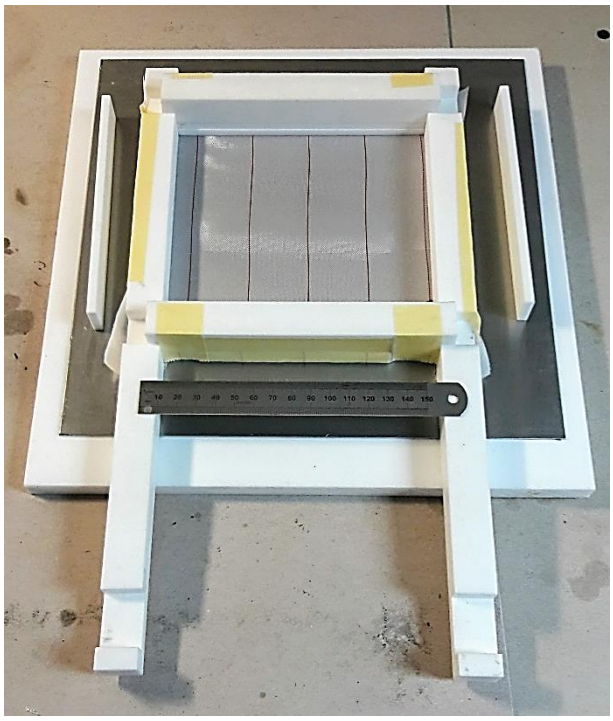

Figure 3-9: the assembled PTFE mould with the peel-ply bottom used to manufacture the foam slabs.

If proceeded with the post-cure of the pre-foam straight-away, the fine porous morphology would have been quickly lost. Indeed, it was found that, if external heating was applied, such pre-foam could either continue foaming or rather degrade and release most of the gases trapped in the pores, the latter option, in particular, was not desirable. This is due to the reduction of viscosity in thermosetting resin at higher temperature while they have not reticulated yet, just as it happens for the thermoplastic polymers: the viscous flow is thermally activated, so there is an initial drop in their viscosity with the increasing temperature before the sudden and irreversible increase due to the curing.

In order not to undo the foaming progress, the pre-foam was let rest for 1 to 2 hours at room temperature, to allow it to set further. When it got to complete gelification, it was ready to undergo the post-cure. Following a similar curing route as the neat epoxy, the mould was introduced in an electric oven already warmed at 80 °C. Thanks to the increased temperature and heat provided, the foaming process could continue, leading to an increase in the pre-foam volume up to 100%. The viscoelastic behaviour of the not completely cured epoxy allowed for the pore to expand. For the foaming at higher temperature and post-cure, a natural convection oven was preferred. The forced convention causes to transfer heat at a significantly higher rate, inducing a more sustained foaming compared to natural convection. However, considering the low thermal conductivity of epoxy and PTFE (mould's elements), this quicker heat transfer promoted the development of excessive foaming on the upper surface and pass-through bubbles, generated at the bottom of the slab and progressively climbed in the foam by coalescence with smaller bubbles. Hence, the forced convection was found to promote an inhomogeneous development of the porosity because of the poor heat conductivity of the materials:

the bubbles on the top layer in particular, the more exposed to the heat flux, grew excessively, making the material very weak from a mechanical point of view. The slower heating rate provided by natural convection was more apt to warm up the batch homogenously, resulting in a suitable texture of small bubbles (0.1÷0.3 mm) uniformly distributed across the thickness. The foaming process was complete approximately in the first hour; by then, the foam was totally solidified. The overall post-cure duration was 5 hours, to guarantee a good epoxy conversion, as for the bulk cured resin.

Once the curing was complete, the foam batch, now in the format of a small slab, approximately of the dimension of 125 × 150 mm^2 with a variable thickness between 15 to 30 mm, could be removed from the mould. The obtained slab needed to be checked for defects such as non-foamed regions or big holes/pores. It was performed visually, with the assistance of visible or UV-light torches, or strategically cutting the slab in the region to be investigated. Most of the major defects could be removed by precise manufacturing of the test specimens. The foam slab was initially squared by a band saw and cut in pieces approximately of the dimension of the specimens. If the geometry was relatively simple, the specimen could be finished at the linish grinder by accurate grinding down to the required dimensions. In case of more complex geometries, like cylinders for compression testing, the CNC milling machine was used to obtain better dimensional control.

The foam was evaluated in respect to its density, thermal properties and stability and mechanical performance.

3.3.1.1 The indicative timescale for the preparation of the Ampreg 26 epoxy foam

Operation	*Time (h)*	*Temp. (°C)*	*Actions*
Mixing	0	25	Mix slow hardener to Ampreg 26 resin, 3:1 wt./wt.
CFA addition	2	25	Add 5 %wt. of disiloxane to the epoxy resin
Pre-foaming	4	25	Mechanically stir to induce bubble nucleation, pour in the mould.
Post-cure	~5	80	Introduce the mould in a preheated oven.
End of curing	10		Stop the heating, leave cooling down naturally.

3.4 Preparation of the epoxy foam sandwich

A further step in the development of the epoxy foam was the investigation in using it as a structural core for a composite sandwich. Sandwiches are widely employed in structural applications where weight saving is critical as high flexural stiffness and strength are required [56]. The sandwich structure is used in wings or large panels subjected to flexural loads. The advantage is that the external

composite skins can carry very high tensile/compression loads, while the weaker core has to carry minor shear loads but dramatically increases the bending (2nd order) momentum of the resistant section without adding consistently to the structure weight thanks to their low density. In our specific case, the core can add thermal insulation properties if the material used has sufficient low thermal conductivity.

The first step in the sandwich preparation was the evaluation of the adhesion of the foam to the GFRP composite material. Thanks to the same nature of the matrix of the two materials and the excellent adhesion properties of the epoxy, there were good reasons to expect an excellent mechanical bond between the materials. The trials were qualitative. The epoxy foam was "foamed" directly on the GFRP substrate instead that in a mould. At first, only small composite square samples (approximately 25×25 mm^2) were employed. Flexible silicone frames were laid on top of the samples to contain the still runny pre-foam, then the standard foaming process followed. The foaming was good, and the adhesion interface was invisible, even by means of microscopy analysis.

At a later stage, the manufacture of proper sandwich samples was designed. It was decided to use the same open PTFE frame to confine the pre-foam on the sides, while the GFRP skins would be placed at the top and the bottom, kept in place by adhesive paper tape. The pre-foam was poured in the mould, and subsequently, the top skin would be fixed. The mould would still be partially open, to allow the foam to expand, if in excess. The bottom side was "sealed" with the peel-ply fabric as usual.

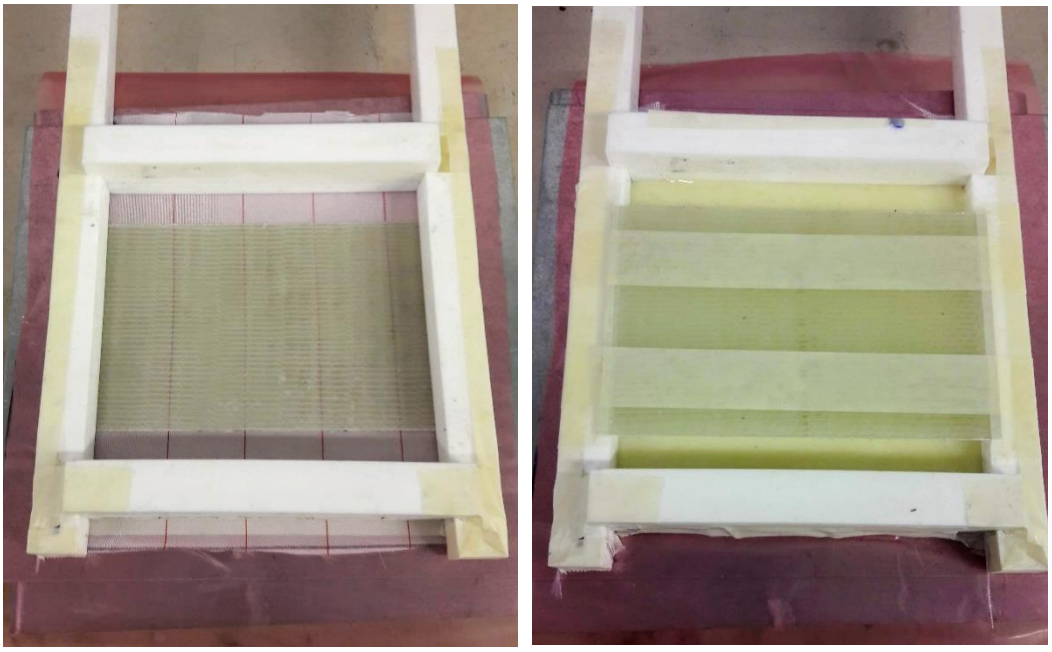

(a) (b)

Figure 3-10: the assembled PTFE mould before (a) and after the pouring of the pre-foam and the application of the top GFRP skin (b).

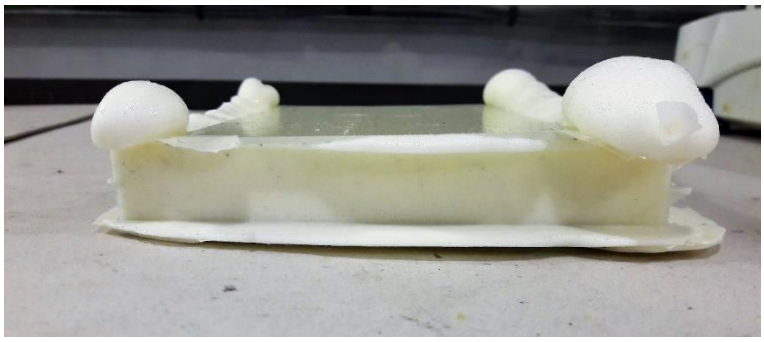

Figure 3-11: the composite sandwich slab obtained by the foaming during the high-temperature post-cure, once removed from the mould.

The adhesion of the foam to the GFRP skin is influenced by the roughness of the composite surface. The GFRP was very smooth on the lower surface, the one in contact with the steel plate during the vacuum bag infusion. The upper surface had a rougher texture, due to the intrinsic waviness of the glass-fibre fabric and the presence of the peel-ply at the top of the infusion stack. Better adhesion was obtained by placing the upper surfaces inward to face the expanding foam, as confirmed by the mechanical testing on the material. To further improve the adhesion bond, a light sanding was performed on the inside of the skins to provide a rougher surface for the foam to attach to.

Once the post-cure was complete, the sandwich plates were cut down to the regular specimens' dimensions. The foam surplus was removed, and the cuts were performed in order to use as much available material as possible. A circular saw with a diamond-coated blade was used as it could easily cut through both the foam and GFRP composite. The edges were cleaned by resin flashes and fibre splinters to ensure safe handling.

The specimens were then ready to undergo mechanical testing. Beforehand, they were weighed and measured to evaluate the material apparent density.

3.5 Analytical testing

3.5.1 Dynamic Mechanical Analysis (DMA)

Dynamic Mechanical Analysis allows determining the viscoelastic properties of a polymer material. One of the typical applications is in the detection of the *glass transition temperature* (Tg) for a polymer. The tests were performed according to ASTM standards D7028 [76] and E1640 [77].

The nominal specimen dimension were 33×10×2 mm^3. They were usually obtained by cutting an end from the delta coupons for the neat epoxy and the epsilon coupons for the GFRP composite. The delta ones for the composite, which had the fibres aligned in the longitudinal direction, were found to return not accurate values, probably due to the high bending stiffness.

3.5.1.1 Testing setup

The testing machine used was an RSA III Analyzer, from TA Instruments. The instrument was mainly composed by a forced convection oven, a direct drive linear motor and a force transducer and could perform measurements in several different modes. The stress or strain applied can be transient or dynamic oscillatory (sinusoidal). The machine, designed for polymer and polymer composites, can be used to evaluate the modulus transitions, stress relaxation or the properties can be investigated through Time-Temperature Superposition. Different clamping rigs were available, allowing different loading modes (tension, compression, flexure).

For the specific purpose of localising the *glass transition temperature* (Tg), the 3-point bending configuration with a 25 mm span was chosen. Minimal sinusoidal strain, 0.02÷0.04 % mm/mm, was applied. The values were selected after performing the strain sweep at different dynamic strain values and was found to fall within the linear elastic field of the material sampled. Being a 3-point bending configuration, the corresponding deformation at the mid-span can be calculated with the following equation:

$$\Delta = \frac{\varepsilon}{K_\varepsilon} = \frac{\varepsilon L^2}{6T} = \frac{0.0002 \cdot 25^2}{6 \cdot 2} = 0.01\ mm = 10\ \mu m \qquad \text{Eq. 3-17}$$

Where the ε = 0.02 % is the maximum dynamic strain, L = 25 mm is the bending span and T = 2 mm is the nominal specimen thickness. This deformation is small enough to be fully reversible (at least until the glass transition point) but it does apply a sufficient strain to the resistant cross-section in order to obtain a good quality output signal. Usually, this deformation was slightly increased for the GFRP (up to ε = 0.04 %), in order to obtain a smoother transition at the Tg: the intrinsic inhomogeneous structure of the composite did not return a linear elastic response for very small strain, in the same order of magnitude of a single fibre.

There is a relationship between the frequency of the applied sinusoidal strain and the viscoelastic behaviour of the polymer, shifting the glass transition. To

compare runs from different samples, the frequency needs to be kept constant. It was set at 1 Hz, a standard value for a DMA test, as the machine motor can easily apply it. A static load was applied during the run, superimposed to the dynamic one, to ensure that the sample is never completely unloaded, even at the minimum of the loading cycle. In the 3PB configuration, a null load at the midspan would mean that the loading tip is not entirely in contact with the specimen, and this would generate unwanted noisy output. A recommended static to max sinusoidal load ratio is 1.2. The machine had a feedback control able to adjust both static and dynamic load as the material elastic modulus changed during the transition maintaining the dynamic strain at the required level.

While dynamic strain was applied, the temperature was ramped from 25 to 150 °C at 5 °C/min, to capture the transition of the modulus from a purely elastic to a viscoelastic behaviour. Usually, slower heating rates (~3 °C/min) are recommended in order to ensure the proper thermal equilibrium in a sample which has not good thermal diffusivity properties. It was preferred to accelerate a bit the heating stage in order not to let evaporate a significant amount of the absorbed liquid from the tested exposed sample, otherwise not being truly representative of the soaked material. Platinum Resistance Thermocouples (PRTs) where present in the conditioning chamber to record the temperature. They were calibrated with a piecewise linear correction interpolation against the melting point of some low-T melting pure metals (In, Zn, Pb).

The samples were taken from the same exposure tests as the gravimetric coupons. Additional *delta* coupons for the Ampreg 26 epoxy and *epsilon* ones for the GFRP were added specifically for the DMA runs. The epsilon coupons, having the reinforcement in the transverse direction, were preferred as the Tg is a matrix dominated property. Usually, the sampling was determined by the trend of the gravimetric test for the specific exposure condition: when the material was showing to be at the end of the linear uptake, approaching the saturation or longer ageing state, a coupon was extracted from the exposure to undergo the DMA test. Once removed it was kept in a container, usually a small bottle, in the same liquid not to alter its condition before the test. It was then weighed, to evaluate the fluid absorption, cut to required measure and measured to input the geometric dimensions as test parameters (i.e. width and thickness to calculate the cross-section area). Then the specimen was placed on the support span in the heating chamber, and the run started.

The remaining portion of the coupon was re-dried in an oven for the following 1-2 weeks, and follow-up DMA runs were performed to evaluate if the effects of the absorbed liquid were reversible.

3.5.1.2 Data analysis

Once the run was concluded, the *storage* and *loss* modulus curves were plotted against the temperature at the measured point, along with the *tanδ* ratio, known to

be an indicator of the viscoelastic behaviour. From the three curves, the main features were calculated:

i. The onset (located as the intersection of the tangents originated from the E' curve before the glass transition and at the curve inflexion) of the drop of the storage modulus, which it was deemed to be the primary indication of the glass transition happening.
ii. The peaks of the loss modulus and in particular of the *tanδ*, which can provide a further assessment on the transition. Sometimes double or overlapping peaks were individuated, suggesting some concurring physical transformation.

The software controlling the DMA tester (Orchestrator) was equipped with tools to analyse the raw data. At the beginning of the testing, it was decided the storage modulus onset (intersection) to be taken as the glass transition point, to be very conservative from a design point of view. As soon as a structural material stiffness change in an abrupt way, it is no more suitable for stable applications.

The whole glass transition points calculated were stored and plot against the exposure time for the specimen, in order to evaluate the shift of the Tg for increasing soaking times and temperatures.

3.5.2 Thermal Gravimetric Analysis

Thermal Gravimetric Analysis is a precise measurement of the mass change in a material specimen at the change of its temperature. It allows calculating phase composition or thermal degradation using very accurate mass measurement. In our work, it was mainly used to evaluate the epoxy and its hybrid pyrolysis temperature and to evaluate the carb residuals.

The specimens were obtained directly from the material of interest, by cutting or punching through. The typical sample mass 10÷20 mg. Unlike DSC, this technique does not use an empty pan to compare the signals; hence it can be critical to calibrate the test heating ramp to adjust for possible weight changes in the pan weight or heating delays due to thermal inertia. This is particularly true when tiny changes in weight are expected, in the order of few per cent weight as when desorbing liquids from a polymer.

The tests were performed on a TG 209 F1 *Libra* (Netzsch, Germany) capable of temperatures as high as 1100 °C, still maintaining very close temperature control, and has an internal scale as sensitive as down to 0.1 μg, to record the slightest change in sample mass. Standard aluminium pans were used, so the maximum temperature was limited 600 °C lest to approach the metal melting point too close: the temperature range was enough to investigate our material, as above 500 °C most of the polymer phase was carbonised.

The output of the test was a thermogravimetric curve, a plot of the per cent mass change against temperature (or time if isothermal steps are included in the testing routine). The curve allowed to evaluate up to which temperature the material

was stable, or it otherwise it started to degrade and to calculate the carb residual, indicative of the presence of inorganic phases/elements, such as fillers or reinforcement fibres.

3.5.3 Thermal conductivity measurement

Thermal conductivity is a critical parameter for materials that are involved in heat transfer applications by conduction, being heat sinks rather than insulating layers. The linear thermal conductivity λ is defined by the Fourier's equation of steady-state heat conduction as the proportional coefficient between the heat flux and the spatial temperature gradient that generates it:

$$Q = -\lambda \cdot A \cdot \frac{\partial T}{\partial x} \qquad \text{Eq. 3-18}$$

Where Q is the heat power transferred and A is the area of the surface the heat is flowing through.

To measure it in a material, both steady-state and transient techniques are available. In a steady-state measurement, a sample of it is subjected to a steady temperature gradient generated by two heat sources, until the equilibrium is reached. The conductive heat flux through it is measured, and the coefficient is recovered by the inverse equation. The techniques differ mainly in the way such heat flux is evaluated.

In our project, two different experimental setups were used, depending on the available test machines: the *guarded-hot-plate* (GHP) and the *heat-flow meter* (HFM). The guarded hot plate provides a direct electric power measurement of the heat flux, returning an absolute value of it, and it is described by the ASTM C177 standard [78]. On the other side, the heat flow meter needs to have its heat transducers calibrated against one or more reference materials, whose conductivity values are known, to be able to convert the output electric signal in an accurate value of the heat flow. It is described by the ASTM C518 [79].

The testing apparatuses were commercially available machines:

i. A TPS 2500 (Hot Disk AB, Sweden) for the GHP;
ii. A Fox 50 (TA Instruments, USA) for the HFM. Three reference materials were used for the calibration: Pyrex glass, Pyroceram and Vespel 1.

The main interest within our project was to measure the thermal conductivity of the epoxy foam (see Chapter 5), to evaluate how the foaming was improving the insulation performance of the materials.

The preliminary tests were performed on the different foam formulations to evaluate the effect of the increasing amount of the foaming agent on the obtained relative density. The test specimens for the GHP comprised a couple of foam samples, as it was needed that they were placed on both surfaces of the flat sensor, which works as a heat source at the same time. The foam samples were rectangular, had nominal surface dimensions of 15*20 mm^2, with a thickness between 6 and 13 mm.

The HFM was employed at a later stage to confirm the value of the conductivity and to check the quality of the foam batches prepared. The test specimen was a straight cylinder, with a diameter up to 60 mm. The cylinder was placed between two heat sources which generated the temperature gradient, measuring the heat flux at the same time; a pneumatic system kept the heating plates in contact with the specimen.

The thickness ranged from 5 up to 25 to evaluate if there was any influence on the test results. It has been suggested that the use of a two-thickness analysis allows calculating the contribution of the specimen contact thermal resistance from the material conductivity value The contact resistance is generated by discontinuity at the interface between the material specimen and the heat source [80]. As the HFM can measure only the total thermal resistance of the system, it turns out:

$$R_{total} = R_{sample} + 2R_{thermal\ contct} = \frac{\Delta x}{\lambda} + 2R_{thermal\ contct} = \frac{\Delta T}{Q} \quad \text{Eq. 3-19}$$

Where R is the resistances, Δx the specimen thickness.

The ratio between the temperature difference at the sources and the heat flux measured by the instrument is the definition of the thermal resistance. The total resistance is a linear function of the sample thickness: by plotting test results at least two different thicknesses, it is possible to extrapolate the resulting contact resistance at null Δx. From the linear slope, instead, it is possible to calculate the value of the actual thermal conductivity of the material.

An important feature in the specimens' preparation was to shape them with good surface planarity; otherwise, they would not make good contact with the heat sources. This "apparent" surface resistance of the specimen could alter the test result, as the air has very low thermal conductivity. In order to improve the dimensional control, the HFM specimens were manufactured by CNC machining.

The HFM was also used to evaluate the influence of the environment temperature to the thermal conductivity. This was possible by increasing the temperature of the heat sources step by step, while maintaining the same temperature gradient, and repeating the conductivity measurement every time at a different average temperature.

3.6 Mechanical testing

3.6.1 Tensile test

The quasi-static tensile test is one of the most popular destructive mechanical testings to evaluate basic mechanical properties in a material, such as Young's modulus (or elastic modulus) and tensile strength.

International standards thoroughly describe the test. It was performed following the ASTM D638 standard for the neat epoxy and ASTM D3039 for the GFRP material.

3.6.1.1 Test planning

The test was performed on both pristine and aged samples in order to monitor the evolution of the material's mechanical properties. It is known from the literature how polymers are prone to absorb fluids and it can significantly alter their strength and durability. In our investigation, we tried to gain a better understanding about how epoxy-GFRP composite performance can be altered by the exposures to fluids typical of the offshore operation, and how main physical factor as the soaking temperature and length influence such ageing process. The aim is to find some correlation between the degree of ageing at the mechanical performance.

To optimise the monitor of the changing properties, some critical points have to be chosen along with the progress of the adsorption curve. Being a destructive test, a limited number of sampling moments has to be chosen. The best options were:

i. Before the start of the exposure as Pristine material, named as Cond P. It will serve as a benchmark to compare the performance of aged materials
ii. End of linear uptake
iii. Fickian saturation, as defined by the effective equilibrium criterion
iv. Later aged stages at 3, 6 or 12 months.

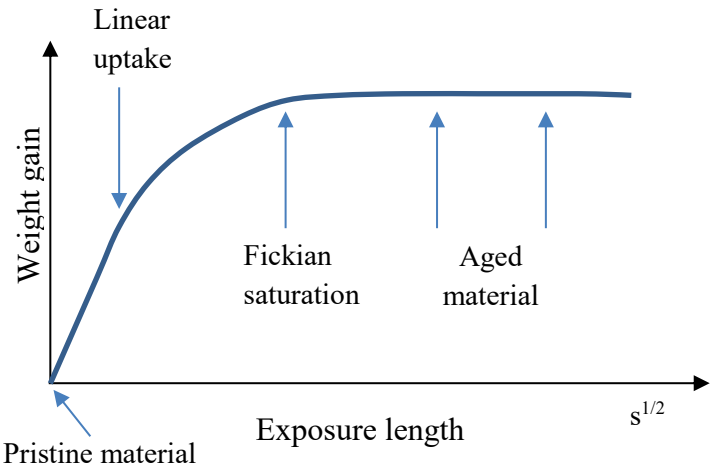

Figure 3-12: a sketch of the selection of the tensile test sampling time from the gravimetric curve.

The test campaign was closely linked with the gravimetric fluid exposures in order to compare the results from the different tests. The very same exposures conditions, fluids and temperature, were naturally chosen but the specimens were added at a later stage, as they were manufactured while the exposures had already started. From the gravimetric testing, it was evident that the neat epoxy was little absorbing the Norsok oil, and likely the same behaviour was expected for the composite material. It was hence decided to concentrate the GFRP specimens in the seawater and dry air exposures, as the manufacturing of further GFRP specimens was calculated to be excessively time consuming and could not fit the long testing schedule.

Table 3-6: kind of mechanical specimens introduced to the exposure conditions.

	25 °C	55 °C	80 °C
Seawater	Cond. A ▪ A26 ▪ GFRP 0 deg. ▪ GFRP 90 deg.	Cond. B ▪ A26 ▪ GFRP 0 deg. ▪ GFRP 90 deg.	Cond. C ▪ A26 ▪ GFRP 0 deg. ▪ GFRP 90 deg.
Norsok oil	Cond. M ▪ A26	Cond. N ▪ A26	Cond. O ▪ A26
Dry air	Cond. F **omitted**	Cond. G ▪ A26 ▪ GFRP 0 deg.	Cond H ▪ A26 ▪ GFRP 0 deg.

Note:

i. GFRP 0 deg: composite specimen with longitudinally oriented fibres;
ii. GFRP 90 deg: composite specimen with transversely oriented fibres.

The vessels used were the same: polypropylene buckets for the seawater, stainless steel vapour pressure cells for the aromatic Norsok oil. In the case the longer tensile specimens could not fit the available vessels, 300 mm copper pipes with brass end fittings were used as containers: this was the case for the seawater and dry air conditioning.

There was no specimen exposed at room temperature exposure to dry air as such an environment was not considered to alter the mechanical properties of the materials in a significant way.

3.6.1.2 Specimens preparation

The tensile specimens were prepared accordingly to the related ASTM standards. For the neat epoxy, the relevant standard is the ASTM D638-14 [81]. The type I dumbbell geometry was chosen but scaled-down of 5%, to ease the manufacturing from the epoxy plate, which would not be long enough otherwise. Specimens were machined directly from epoxy plates using a CNC milling machine.

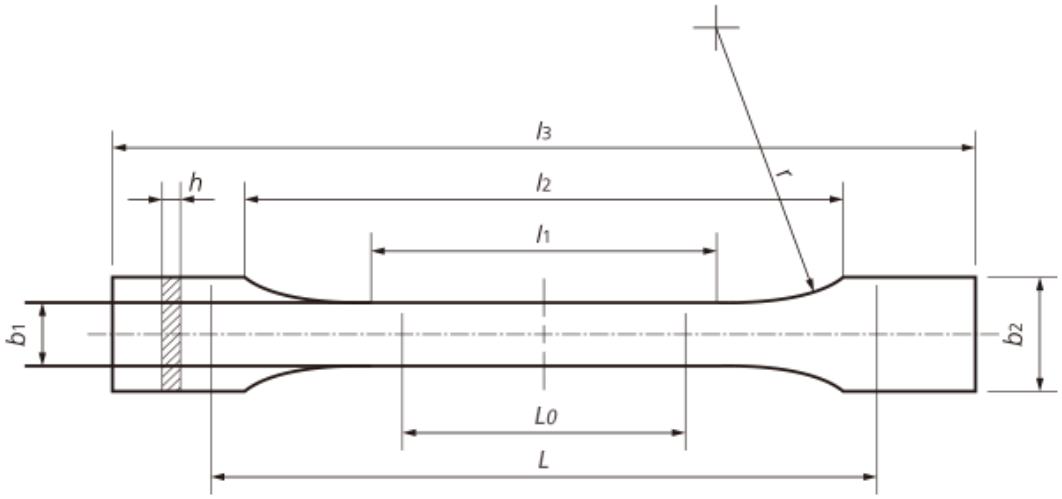

Figure 3-13: type I tensile specimen geometry. Adapted from [81]

Type I	*Size [mm]*
Full length, l_3	160
Parallel length, l_2	57
Gauge length, l_1	50
Parallel section width, b_1	12.5
Thickness, h	2 (nominal)
Grip section width, b_2	19
Distance between grips, L	115

The GFRP composite tensile specimens were of 2 different type, due to fibre orientation. The material has unidirectional reinforcement, so both the longitudinal and the transverse directions have to be characterised. The longitudinal specimen shows mostly the contribution of the glass fibres while the transverse properties are matrix dominated, providing information about the fibre-matrix interphase. The dimensions of the specimens are reported:

Size [mm]	*0° unidirectional*	*90° unidirectional*
Width	15	25
Overall length	250	175
Thickness	1.7 (nominal)	1.7 (nominal)
Tab length	56	N/A
Tab thickness	1.5	N/A

3.6.1.3 Sample preparation/tabbing

The longitudinally oriented fibre specimen usually reaches a very high level of the load before failure. The geometry does not allow a stress distribution as in the case of the polymer dumbbell: if the composite surfaces at the specimen's ends do not grant enough grip, the risk of slippage during the test is realistic. A common practice in order to limit such an issue is to apply laminated composite tabs, with sanded surfaces to increase the roughness, at the specimen's ends using structural adhesive, usually 2-part epoxies. It provides a dual benefit: it protects the specimen from the

direct pressure of the metal grips to it, reducing the probability of a failure happening in the gripping area and it provides a better surface to grip the specimen, in order to avoid any unwanted slippage. Another approach, but complementary, is to wrap the specimen ends in a sandpaper layer to gain a similar improvement.

The test machine was a Zwick Roell (Germany) Z50 universal testing machine, controlled by the proprietary software TestXpert. The load cell was the original one provided with the machine, capable of measuring loads up to 50 kN. The grips were chosen depending on the material strength, either for nominal load up to 5 kN (for the neat epoxy or the GFRP transverse specimens) or up to 50 kN (for the GFRP longitudinal oriented fibres).

3.6.2 Compression test

The compression test is a destructive mechanical test that consists in the application of a unidirectional compressive loading on a material specimen with a uniform cross-section, trying to squeeze and flatten it. The test is commonly used on brittle building material such as concrete or ceramics. These materials are sensitive to pre-existing defects, and due to their little ductility, they return very scattered results if tested in tension. In the compression test, these cracks are not activated as long as the stress state is of unidirectional compression. But for higher strain, due to the Poisson's effect and usually exacerbated by the friction of the contact faces with the loading plates, the specimen tends to expand around its middle section, in a process called barrelling [82], which induces a three-dimensional stress state in that region, which usually lead to ultimate failure due to critical shear stresses. This failure is commonly named crushing.

There is an alternate failure mode: if the specimens are lean, meaning that their length to thickness (actually the radius of gyration) ratio is high, then the specimens will experience an elastic instability, a condition in which more than one static configuration is possible. Either the specimen continues to deform in uniaxial compression, or it bends sideways, depending on its cross-section shape. Moreover, it is likely that the compressive load is not perfectly axial to the sample, generating some bending momentum, or rather the sample itself is not perfectly homogeneous or regular in shape. The critical buckling load is given by the simplified equation:

$$\sigma_{crit} = \frac{\pi^2 E}{\left(l/r\right)^2} \qquad \text{Eq. 3-20}$$

Where E is the materials Young's modulus, r is the radius of gyration of the cross-section and l is the specimen length.

If the critical buckling load is lower than the compressive strength of the material, the specimen will buckle, because the bend configuration is more stable than the compressed one. This is not desirable as the failure ultimately will be in bending, not providing relevant data for the compression behaviour. Hence, it is

crucial to prepare a compression specimen short enough compared to its cross-section to avoid buckling.

The test was performed on both the foamed and the neat epoxy to compare how the foaming process affected the mechanical properties. The neat epoxy was tested following the ASTM D695, which prescribes two specimen geometries: one for the strength measurement, a cylinder of 12.7 mm in diameter and 25.4mm in height, and another for the elastic modulus measurement, a cylinder with 12.7 mm in diameter and 50.8 mm in height.

The foam instead was tested following the ASTM D1621 standard: the nominal specimen prescribed was a cylinder high 25.4 mm and the cross-section diameter of 58 mm.

The test machine was a Zwick Roell (Germany) Z50 universal testing machine, the same used for the tensile testing.

3.6.3 Flexural test

The flexural test is a destructive mechanical test that is performed by bending a bar-shaped specimen of the materialalong its main dimension. The most common loading point configuration is the three-point bending, where the specimen is loaded in a single point at the midspan while freely supported at both ends, and the four-point bending, where it is loaded in 2 points symmetrically from the midspan.

It has the advantage of requiring very little specimen preparation, just to be machined in the required dimensions. Also, there is no need for gripping the specimen, which is usually critical for brittle materials, as they tend to fail because of the local stress contraptions at the grips.

In particular, for the three-point bending, the drawback is that the stress state induced is non-uniform along the span of the specimens, but it maximises at the midspan where the maximum bending momentum is reached. At the midspan cross-section, there is a linear trend of the axial stress across the thickness: the maximum compression is experienced in contact with the loading point on the upper surface, while the maximum tensile stress is generated at the lower surface, as the specimen is bending downward.

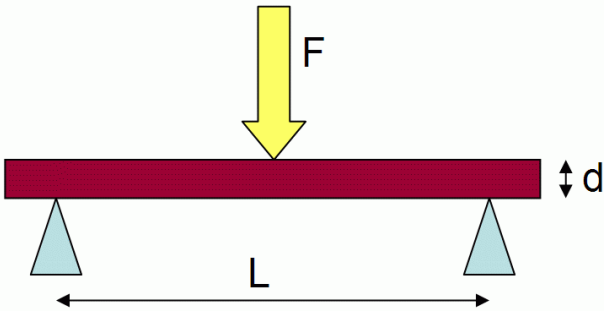

Figure 3-14: the three-point bending test configuration.

The test runs were performed following relevant standards: the ASTM D790 for the neat epoxy as bulk, and the ISO 1209 for the epoxy foam (as it was not possible to find a specific ASTM standard relating to cellular polymer material).

A requirement for the specimen dimensioning is the span-to-thickness ratio to be at least 16 or 32:1, to ensure that the shear loads generated are minimised. The failure happens in the proximity of the midspan unless some critical flaws occur somewhere else in the specimen.

The maximum axial flexural stress experienced at the midspan is:

$$\sigma_f = \frac{3FL}{2wd^2} \qquad \text{Eq. 3-21}$$

Where F is the applied load, L is the support span length (not the specimen length), w the width and d the specimen's thickness. The absolute value in compression and tension in equal in isotropic homogeneous materials, to ensure the system equilibrium.

The flexural strain at the midspan is:

$$\varepsilon_f = \frac{6Dd}{L^2} \qquad \text{Eq. 3-22}$$

where D is the vertical displacement experienced at the midspan.

The test was performed both on the GFRP composite and the sandwich material, to understand the sandwich bending properties.

Chapter 4 Accelerated exposure to harsh environments – Results and Discussion

The results and discussion on the diffusion coefficients and Glass Transition shift (§4.1 to 4.2) have been published in the *Materials* (MDPI) journal, they have been adapted from the paper: Cavasin *et al*., *Materials* ***2019****, 12, 807* [83]

Fibre-reinforced Polymer Matrix Composites (PMC) have been employed for over 50 years in structural components, e.g., the hull of boats, and they consistently demonstrated to be mechanically efficient and more durable than traditional materials, namely wood. In more recent time, the developing off-shore energy industry, from fossil fuels extraction to the exploitation of tidal and wave energy as renewable resources, can highly benefit from the application of such high performing materials. Despite their remarkable properties, the design constraints in terms of long-term ageing and fatigue resistance require for specific qualifications programme, as there is no consolidated experience about how the material would behave in the operative scenario [7,84].

Despite their attractive specific properties, the deep-sea use of polymers and composites offshore is still limited, so there is little in-service data and experience to validate design predictions. It is necessary, therefore, to resort to accelerated testing, to evaluate the long-term durability of these materials. Ageing can be accelerated in the simulated exposure by increasing the severity of environmental conditions (temperature, humidity) or mechanical loading (applied stress, hydrostatic pressure). However, it is essential to ensure that the acceleration does not trigger degradation mechanisms which will not be faced under operative conditions, and this is not a trivial task [8].

In our experimental work, we aimed to investigate the effect of the exposure of PMC to the fluids which simulate two of those encountered in Oil & Gas offshore operations: seawater and aromatic hydrocarbon. The accelerating factor was chosen to be the exposure temperature, known to control the rate of most physical and chemical transformation [8]. Polymers are known to be permeable to fluids: a gravimetric test was designed to monitor the diffusion progress in the different exposure conditions. Two parallel campaign of Dynamic Mechanical Analysis (DMA) and tensile testing on progressively aged material were performed to record the changes in the glass transition temperature (Tg) and mechanical performance.

The data were compared to the results of material aged in dry air or reconditioned at the end of exposure by drying the absorbed fluid, in order to evaluate if the ageing process was reversible.

4.1 Gravimetric results and diffusion coefficients

As described in Chapter 3, several different exposures conditions were devised to characterise how the materials will respond. For ease of understanding, the conditions were referred to using a letter coding as follows (compare with Table 3-5):

Temperature\Fluid	*Seawater*	*Norsok oil*	*Dry air*
25 °C	A	M	F
55 °C	B	N	G
80 °C	C	O	H

The gravimetric coupons are classified by their nominal dimension, which are:

Specimen	**fibre orientation**	**length** (mm)	**width** (mm)	**thickness** (mm)
alpha	indifferent	19	19	2
beta	indifferent	40	40	2
gamma	indifferent	100	100	2
delta	longitudinal	100	10	2
epsilon	transverse	10	100	2

It will be used in the following paragraph to refer to the corresponding exposure conditions.

Except for the DMA results and where indicated otherwise, the results presented and point plot on charts are representative of an average of the results obtained by performing the test on three sample replicas, calculated as the arithmetic mean:

$$\bar{x} = \frac{1}{n}\sum_{i=1}^{n} x_n,\ n = 3 \qquad \text{Eq. 4-1}$$

The error bars presented in the charts are always indicating the standard deviation of the set of 3 (or more for some of the mechanical tensile test) specimens tested. The sample's standard deviation is calculated as:

$$s = \sqrt{\frac{1}{n-1}\sum_{i=1}^{n}(x - \bar{x})^2} \qquad \text{Eq. 4-2}$$

4.1.1 Preconditioning

To make sure the specimens are effectively dry at the start of the exposure test, they had to be dried in advance, to eliminate any possible residual moisture from the manufacturing or other volatile by-products. The weight of some sample coupons was monitored on a daily basis until no further detectable change is recorded: it has reached effective equilibrium and hence is ready for starting the exposure.
After roughly two and half weeks of preconditioning of the coupons in the forced ventilation oven at 50 °C, the average weight loss was about 0.3 %wt.

4.1.2 Seawater exposures

The gravimetric coupons were all weighted to record their dry weight (w_{dry} or w_0). Then they were periodically weighted to monitor how they changed their mass over time. Being completely dried beforehand and then kept immersed in seawater, it can be reasonably assumed that the change in their weight is due to the absorption of the seawater.

The plots of the weight gain versus the exposure length are reported following, listed by the coupon's geometry. The exposure length is reported both as the square root of a second, to highlight the linear uptake in the initial stage of diffusion, and in days, for ease of understanding.

4.1.2.1 Neat epoxy coupons

As widely reported in the literature, the neat epoxy is expected to be prone to adsorb the seawater [7,23]. The exposure temperature influences primarily the absorption rates: as it can be seen in Figure 4-1 and following, while for the exposures at 80 °C the fickian saturation happened after only about a week, the weight uptake at the lower temperature continued with no clear inflexion point for more than 400 days. Moreover, while weight uptake tops the 3 wt%, the coupons at the lower temperature did not even reach the 2.5 wt%.

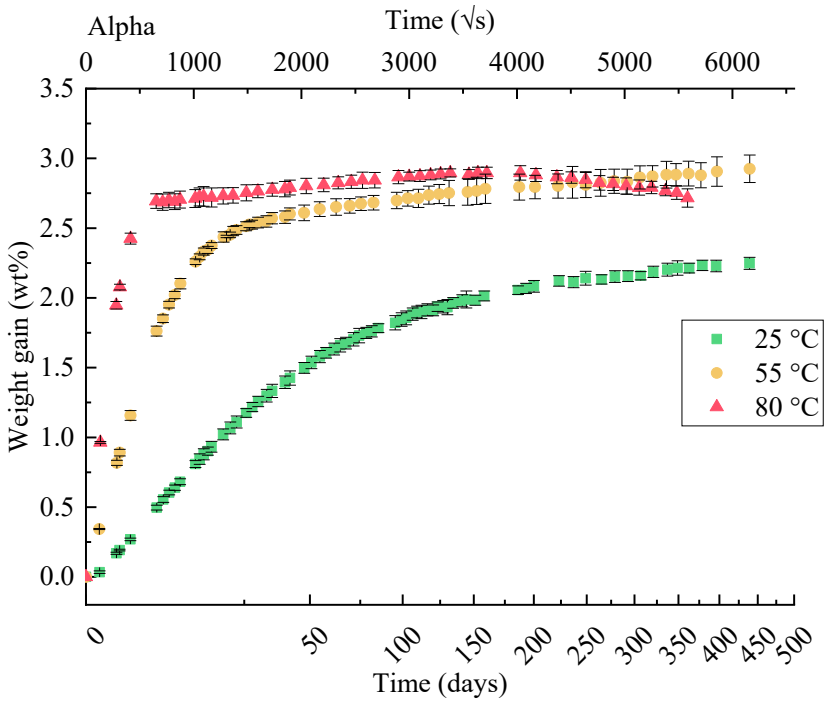

Figure 4-1: gravimetric measurements on epoxy Alpha coupons in seawater exposure

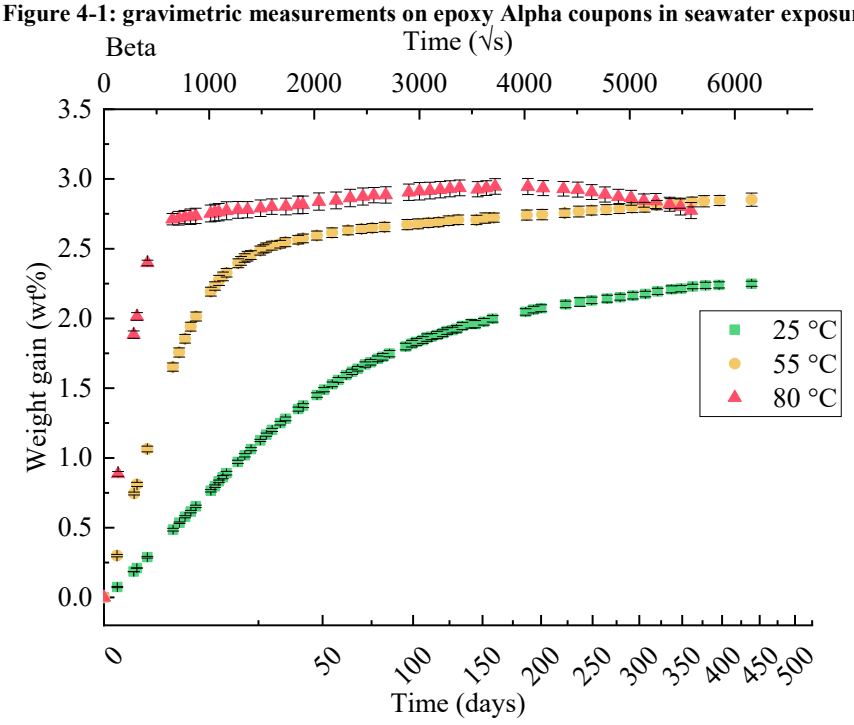

Figure 4-2: gravimetric measurements on epoxy Beta coupons in seawater exposure.

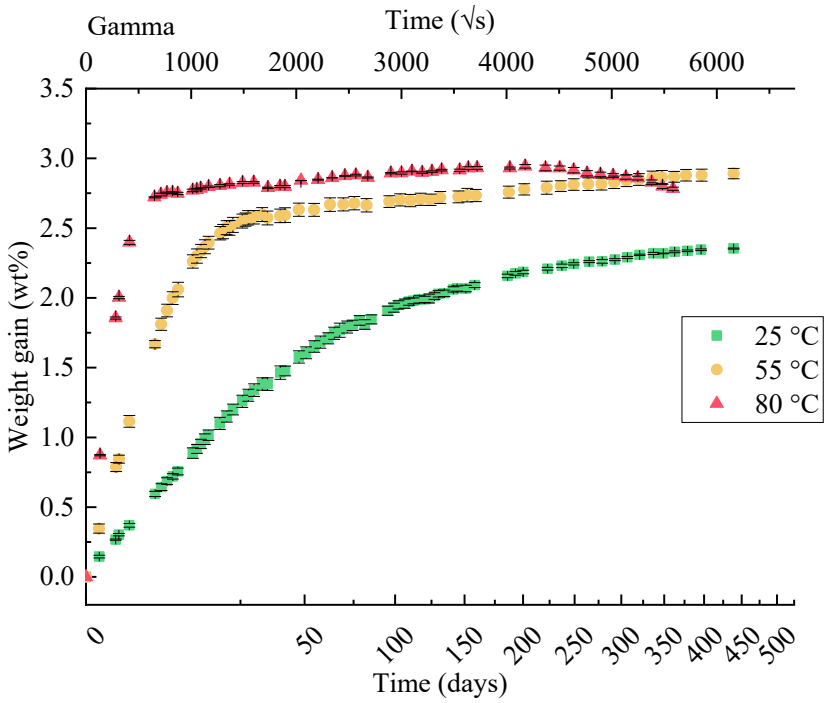

Figure 4-3: gravimetric measurements on epoxy Gamma coupons in seawater exposure.

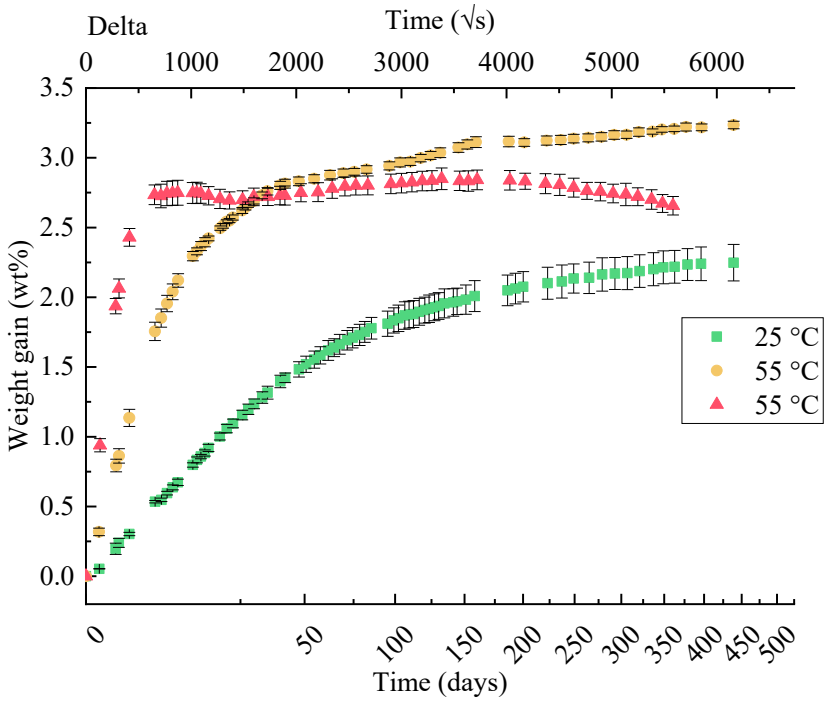

Figure 4-4: gravimetric measurements on epoxy Delta coupons in seawater exposure.

There is a good agreement on the weight uptake among the coupon replicas of the same geometry and the curves from the different geometries. The only clear deviation regards the *delta* geometry (see Figure 4-4): the curve for the exposure at 55 °C climbs to a significantly higher value compared to other geometries, while those for the other temperatures have a higher measurement scatter, in particular at later stages. It is not clear what this anomalous behaviour is due to, but some white

residual precipitate was found on the edges of the aged *delta* coupons, in particular from the 55 °C exposure, not found on other coupons. Being the weight difference after the fickian saturation in the order of the mg, these precipitates could have affected the measurements.

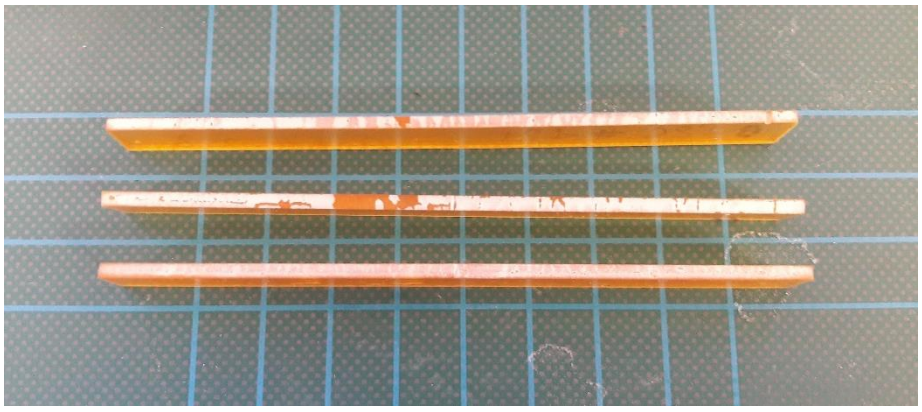

Figure 4-5: neat epoxy delta coupons from the 55 °C seawater exposure. White precipitate residual is present on the samples' edges.

It can be noted that for all the coupons exposed at 80 °C, after saturation, there is a progressive reduction in weight, which is likely a sign of the beginning of the epoxy physical degradation with the destruction of the epoxy network and leaching in the seawater [85,86].

A summary of the seawater exposure test main features is reported in the following table. The saturation points were evaluated using the effective equilibrium criterion described in § 3.2.6.2.

Table 4-1: Saturation levels and times for neat Ampreg 26 epoxy in seawater.

Temp. (°C)	**Specimen**	**h × w × l** (mm × mm × mm)	**Slope** ($\times 10^{-4}$ %/√s)	M_∞ (%)	t_∞ (days)
25	alpha	2.09×18.86×19.15	8.8	1.94	113
	beta	2.18×40.00×40.08	7.9	1.90	107
	gamma	2.04×100.04×100.07	8.4	2.01	110
	delta	2.15×10.08×100.03	8.2	1.91	107
55	alpha	2.11×18.96×19.05	28.4	2.69	55
	beta	2.16×40.03×39.99	26.6	2.60	33
	gamma	2.12×100.05×100.05	26.6	2.63	33
	delta	2.07×10.06×100.05	28.4	2.91	48
80	alpha	2.15×19.31×19.14	71.7	2.77	16
	beta	2.15×39.96×40.03	65.9	2.77	9
	gamma	2.13×100.03×100.05	64.9	2.79	9
	delta	2.12×10.05×99.97	69.9	2.73	9

4.1.2.2 GFRP composite coupons

The GFRP coupons were exposed to identical soaking conditions to evaluate the effect of the seawater conditioning on the composite material. The trends (see **Figure 4-6** and following) were similar to those found for the neat epoxy, with a very rapid saturation (after about a week) at the 80 °C, while it seems just to have reached equilibrium after more than one year at the 25 °C exposure. The scatter of the measurements was generally higher compared to the neat epoxy curves. This could be due to either the intrinsic higher inhomogeneity in the composite material or to the smaller amount of water absorbed by the composite in general, in the order of few mg or less between measurements, approaching close the balance sensitivity (of 0.1 mg), hence generating "noisier" measurements.

Again, it can be found a significative difference between the saturation values between the exposure at 25 °C, which did not reach the 0.5 wt%, and those at higher temperatures which exceeded the 0.6 wt%. Moreover, at 80 °C exposure, it seems there was a second-stage diffusion happening after the fickian saturation, in a more evident fashion than on the neat epoxy.

The last pair of measurements on the coupons exposed at high temperature showed a sharp decrease in weight, which could hint to a severe material degradation after about one-year-long exposure. Leakage of material from the composite as an effect of high-temperature network degradation is reported in the literature by Grammatikos [86] and Bond [21].

The gravimetric plots are reported in Figure 4-6 and the following:

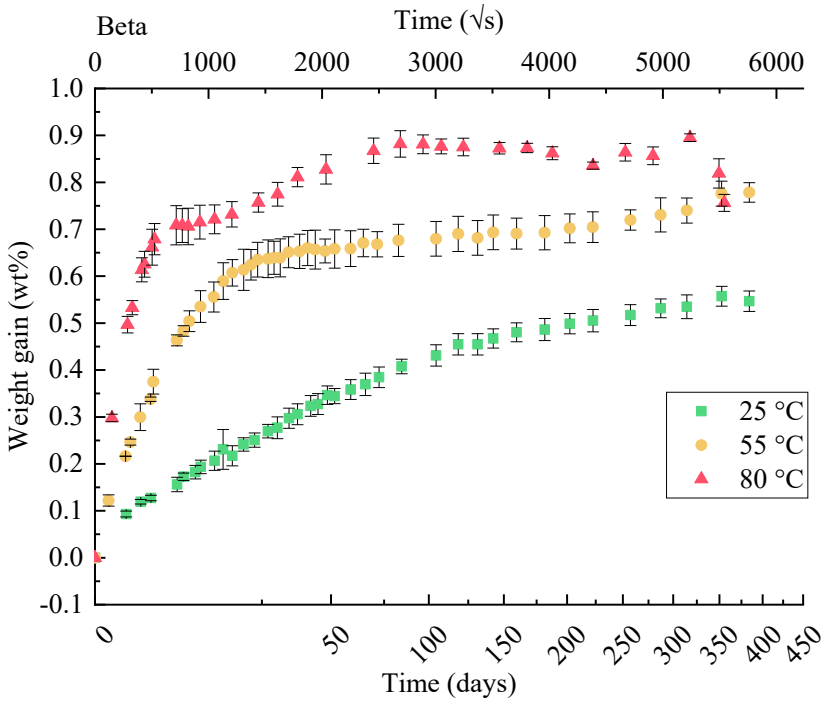

Figure 4-6: gravimetric measurements on GFRP Beta coupons in seawater exposure.

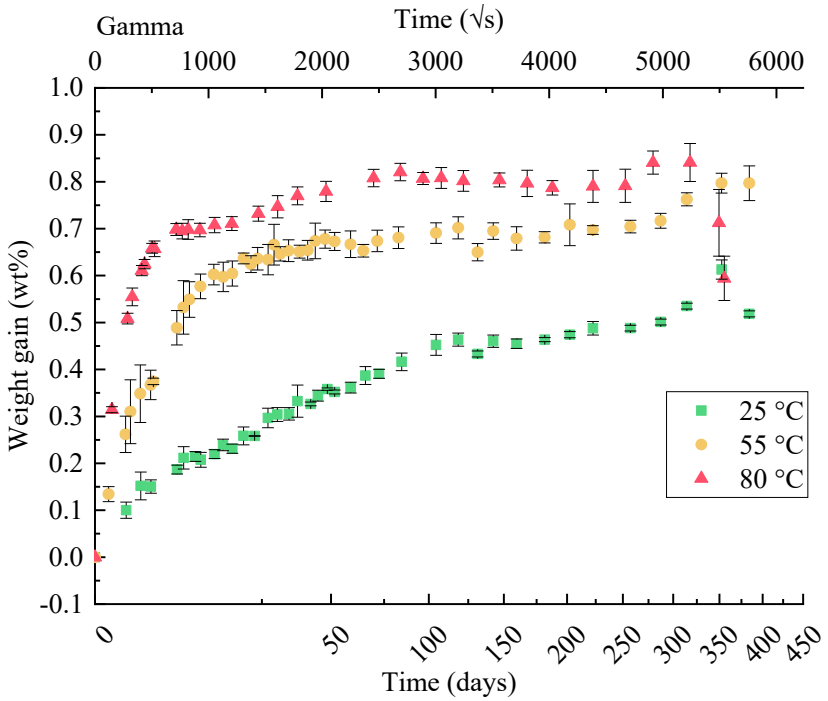

Figure 4-7: gravimetric measurements on GFRP Gamma coupons in seawater exposure.

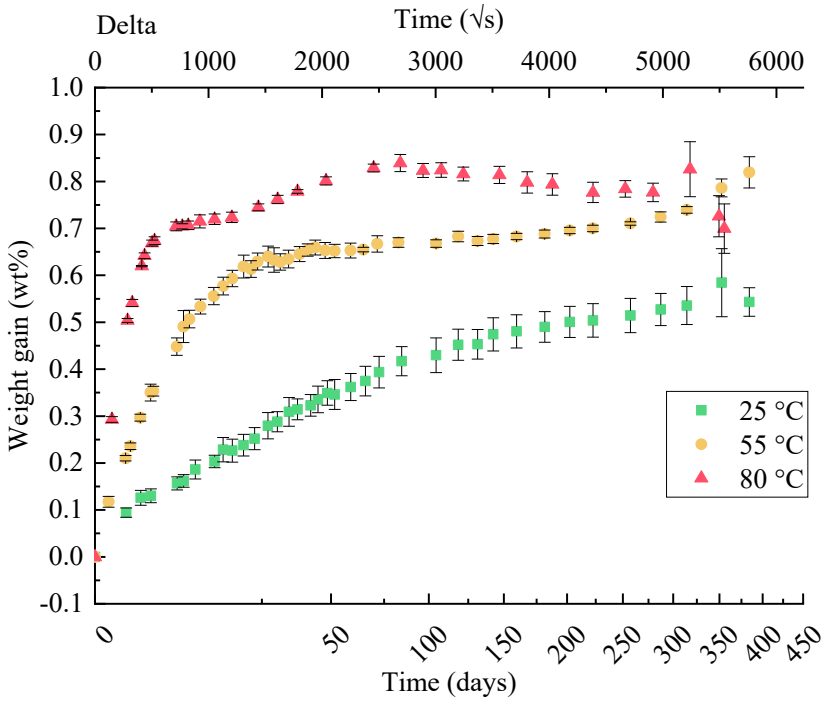

Figure 4-8: gravimetric measurements on GFRP Delta coupons in seawater exposure.

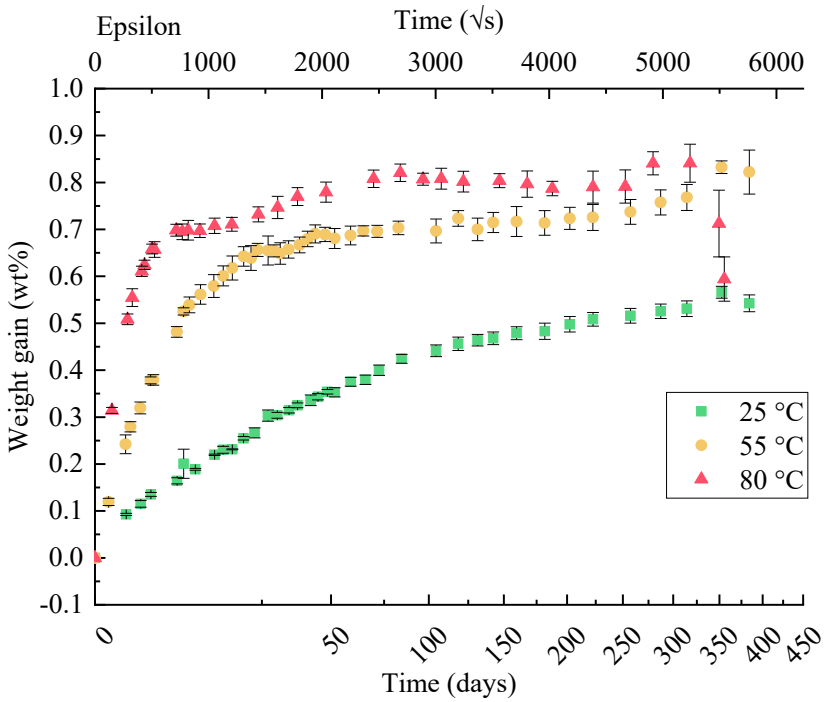

Figure 4-9: gravimetric measurements on GFRP Epsilon coupons in seawater exposure.

A summary of the seawater exposures main features for the GFRP composite is reported in the following table:

Table 4-2: Saturation levels and times for the GFRP composite in seawater

Temp. (°C)	Specimen	h × w × l (mm × mm × mm)	Slope ($\times 10^{-4}$ %/√s)	$M\infty$ (%)	$t\infty$ (days)
25	beta	1.72×39.99×40.00	1.4	0.48	143
	gamma	1.70×99.84×99.73	1.3	0.46	132
	delta	1.72×9.99×99.96	1.4	0.51	182
	epsilon	1.70×99.90×10.03	1.5	0.47	119
55	beta	1.73×40.00×40.04	6.2	0.65	29
	gamma	1.70×99.91×99.98	5.9	0.67	41
	delta	1.73×9.95×99.98	6.1	0.64	31
	epsilon	1.72×99.93×9.99	6.6	0.66	29
80	beta	1.73×39.99×39.99	20.0	0.72	8
	gamma	1.76×99.12×99.75	20.0	0.82	24
	delta	1.71×10.00×100.03	19.6	0.75	17
	epsilon	1.74×99.93×10.01	21.1	0.80	70

4.1.3 Exposures in Norsok oil

The little data available in the literature [4,11,87], could not provide much insight about the possible outcome of the exposure of the epoxy thermoset to the aromatic

oil mixture, briefly called *Norsok oil*. Even if not extensively investigated, the interaction of the epoxy matrix with hydrocarbons is pivotal for a comprehension of the concurring ageing mechanisms in a fossil fuel production scenario.

The exposure to the Norsok oil resulted in a minor absorption of the oil by the neat epoxy compared to the seawater. Except for the exposure at 80 °C, no significant weight uptake was recorded. For this reason, it was decided to extend the exposure to the GFRP composite only at a later stage, for 6 months only. Considering the lesser permeability of the composite, the balance was barely able to record a slight increase of weight at the lower temperatures. Moreover, no tensile test GFRP specimens were added for the ageing For further insight, check the following paragraphs about Tg measurements (see §4.2.3.1) and the mechanical properties (see §4.3.4).

4.1.3.1 Neat epoxy coupons

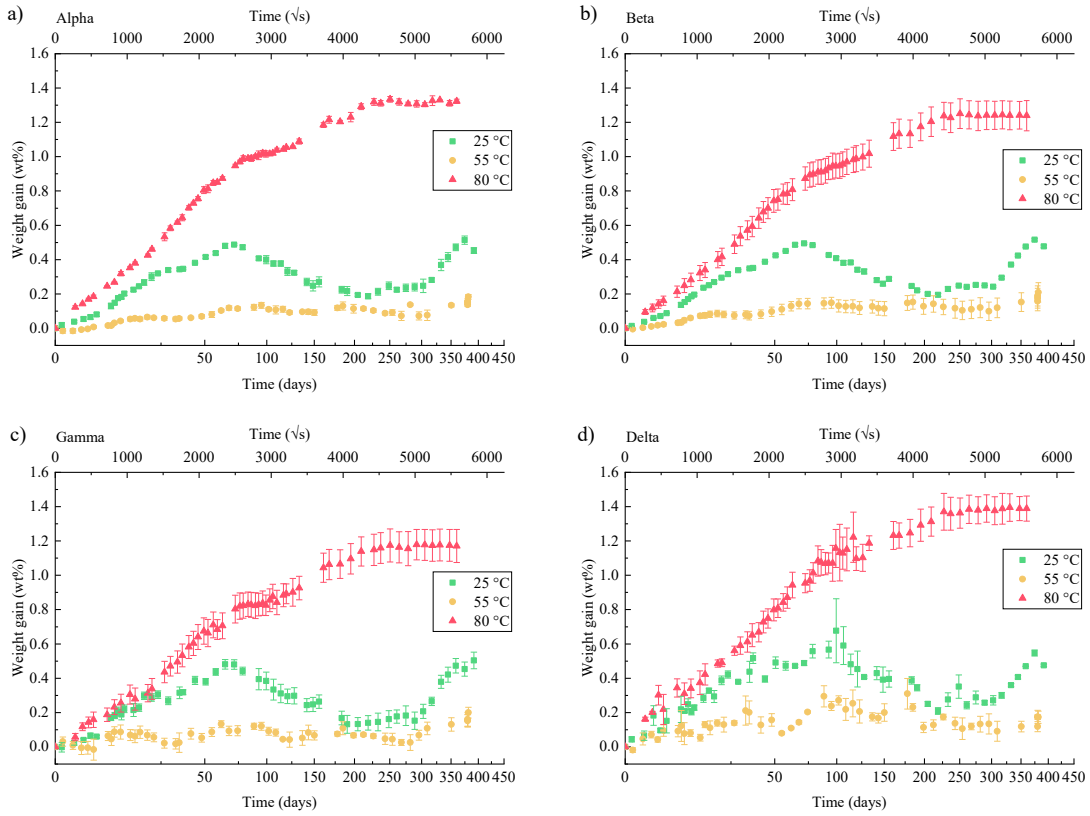

Figure 4-10: gravimetric measurements on epoxy coupons in aromatic Norsok oil exposure. Geometry: (a) alpha, (b) beta, (c) gamma, (d) delta.

The coupons geometry was the same as for seawater exposure. The trends for the absorption of Norsok oil (presented in Figure 4-10) are not fully understood, but it seems the fluid is not following a Fickian behaviour at lower temperatures. A steady fluid absorption happens only at the 80 °C.

It is not evident how the absorption is more dynamic at the 25 °C, even if the trend is alternate in time: it almost appears to follow a seasonal trend (exposures

started in June), with maximum peaks at 0.5 ÷ 0.6 wt%. At 50 °C there is a very little change in the coupons' mass, irrespective of the shape factors, with a maximum gain of 0.2 wt%. The unusual behaviour of the aged material found correspondence in the shifts of the Tg (compare the results in § 4.2.3).

Table 4-3: Saturation levels and times for the epoxy in oil at 80 °C

Temp. (°C)	Specimen	h × w × l (mm × mm × mm)	Slope ($\times 10^{-4}$ %/√s)	M_∞ (%)	t_∞ (days)
80	alpha	2.10×19.01×19.11	3.2	1.32	237
	beta	2.12×40.00×40.00	3.0	1.22	182
	gamma	2.15×99.96×100.06	2.7	1.14	182
	delta	2.04×10.03×100.03	3.3	1.33	168

Only the specific values for the exposure at 80 °C are reported for later calculation. The saturation criterion fails to locate a unique saturation time.

4.1.3.2 GFRP composite coupons

The GFRP coupons were added at a later stage, and the exposures lasted only 6 months. Due to the lesser activity found in the neat epoxy, fewer measurements were performed. The gravimetric data are presented in Figure 4-11 and following.

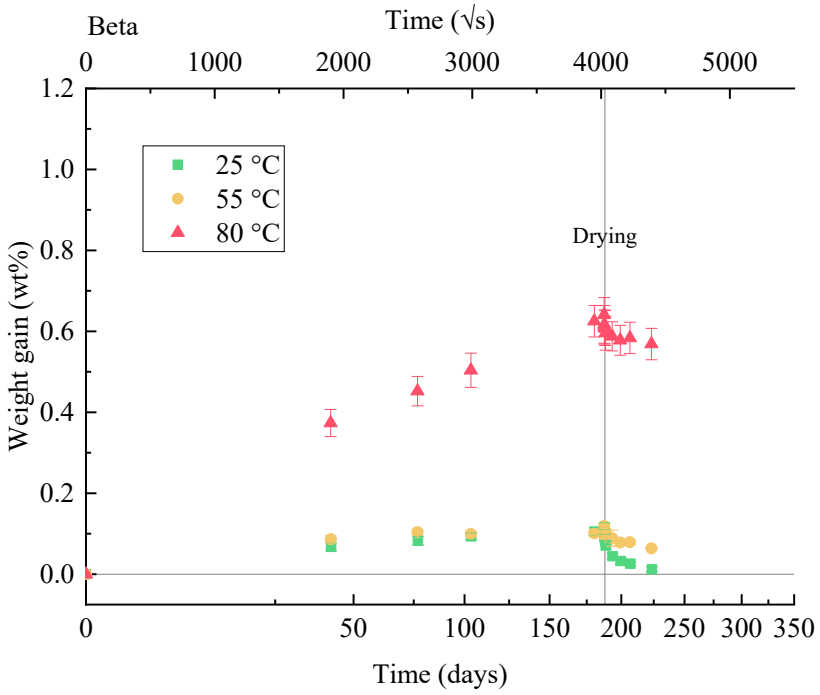

Figure 4-11: gravimetric measurements on GFRP Beta coupons in aromatic Norsok oil exposure.

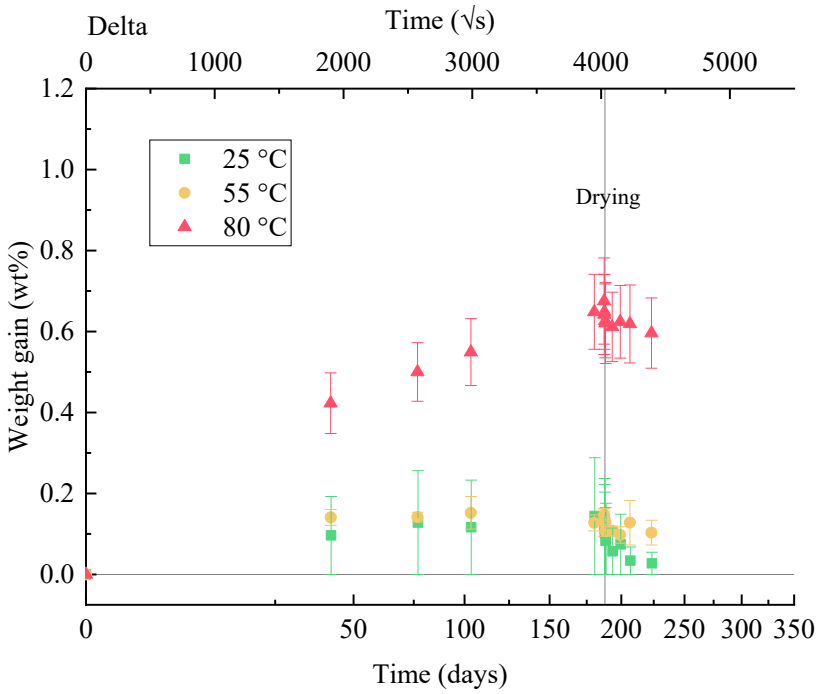

Figure 4-12: gravimetric measurements on GFRP Delta coupons in aromatic Norsok oil exposure.

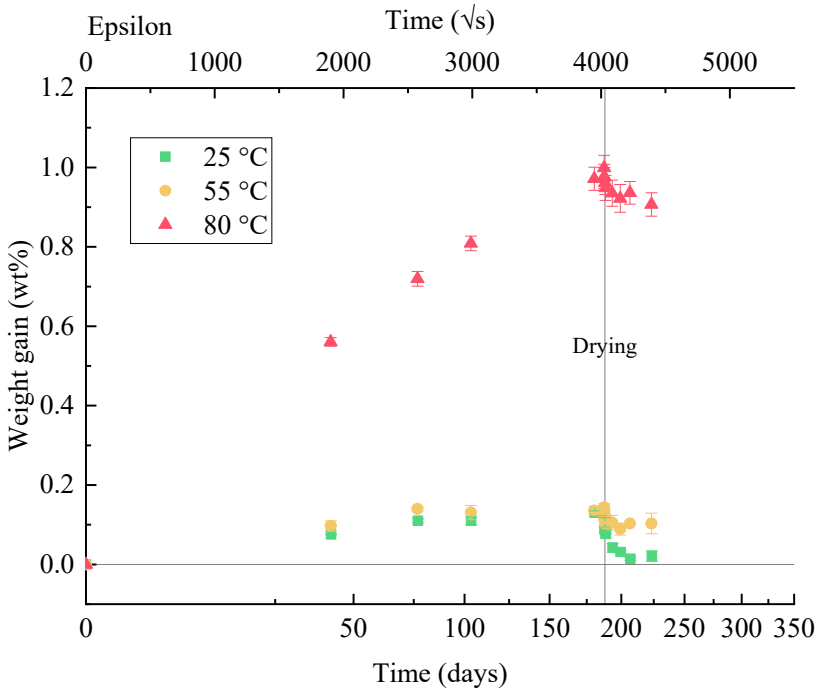

Figure 4-13: gravimetric measurements on GFRP Epsilon coupons in aromatic Norsok oil exposure.

In the same fashion as the neat epoxy, the GFRP coupons absorbed a very little amount of the Norsok oil, except for the exposure at the 80 °C. It shows how the approach to the epoxy Tg can deeply alter the permeability of these materials. After 6 months, the weight gain was of 0.6 wt% for the *beta* and *delta* coupons. The *epsilon* even reached 1 wt% uptake. Likely, they would continue to absorb oil if left for longer exposure time (the test has to be stopped due to the approaching project

deadline). Even if the rate of diffusion is much slower, the partial saturation value is not far from those found for the seawater exposure at 80 °C.

The *epsilon* coupons absorbed a higher fraction of oil: this can be partially explained with the higher surface of the fibre-matrix interface exposed on their sides, as the fibres are oriented transversely to the longer dimension (while in *deltas*, the fibres are aligned longitudinally). There could be preferential paths for the oil to diffuse. Overall, it seems that the composite structure is more prone to absorb the oil mixture at temperatures close to the matrix Tg (check § 4.2). The main values for the exposure at 80 °C are reported in the following table for later calculation:

Table 4-4: Maximum absorption levels for the GFRP in oil at 80 °C

Temp. (°C)	**Specimen**	**h × w × l** (mm × mm × mm)	**Slope** ($\times 10^{-4}$ %/√s)	M_{max} (%)	t_{max} (days)	M_{dry} (%)
80	beta	1.72×40.03×40.03	1.6	0.64	188	0.58
	delta	1.68×9.99×99.99	1.7	0.68	188	0.61
	epsilon	1.85×99.82×9.99	2.5	1.00	188	0.92

After 188 days of conditioning, the coupons were removed from the oil bath and introduced in a forced ventilation oven to be dried at 50 °C for all the conditions, well below the boiling points for the components of the oil (compare with Table 3-4). It is interesting that while the coupons from the lower temperature exposures seem to progressively release the little amount they absorbed, it appears that the oil did not evaporate from the coupons extracted from the 80 °C exposure, while the oil components are expected to evaporate completely even at RT when left in contact with the atmosphere. It can be somehow related to the steric encumbrance of the larger oil molecules in comparison with the change in the average dimension of the *free volume* in the epoxy when approaching the glass transition [21]. The larger available intermolecular spaces at 80 °C could favour the diffusion of the oil molecules, which in contrast is not the case for the lower temperatures. When the coupons were removed from the oil bath and placed at 50 °C for the drying, the oil molecules were "trapped" in the tighter epoxy network, except for the free surfaces where the escape path was significantly shorter, and a small fraction of the oil managed to evaporate. We did not perform further conditioning testing to investigate the reason for this different behaviour.

4.1.4 Exposures in dry air

4.1.4.1 Neat epoxy coupons

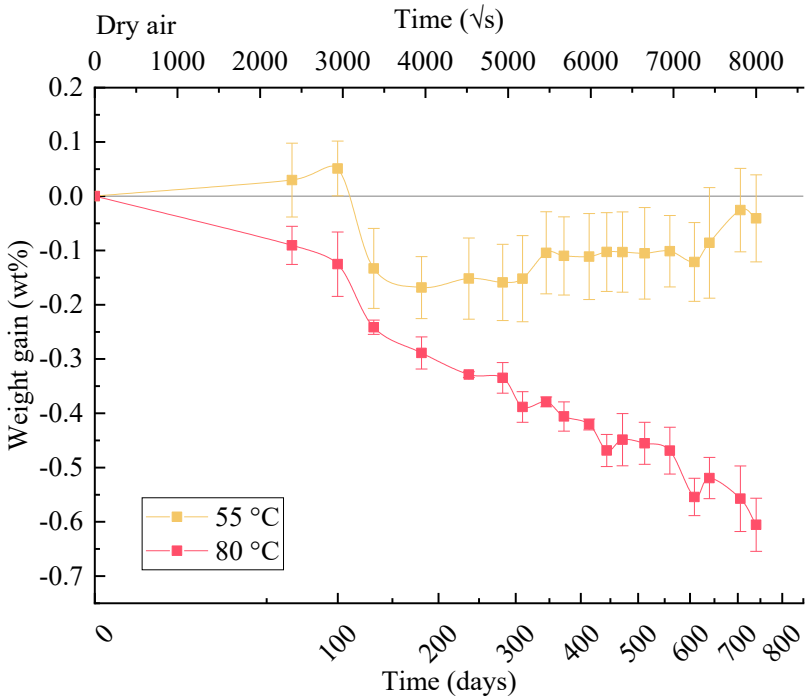

Figure 4-14: gravimetric measurements on epoxy Alpha coupons in dry air exposure.

The dry-air exposures were set to play as the control ones, in order to separate the fluid effects from the temperature ones. Only *alpha* coupons were used for the gravimetric measurements, as the geometry influence was expected to be negligible for this exposure (*delta* coupons were added as well to provide the DMA specimens). There was no exposure set at 25 °C, as it was supposed that no significant ageing happened at room temperature. Coupons were left to age up to two years continuously.

To support this hypothesis, no particular weight change was measured at 55 °C as shown in Figure 4-14: besides a 0.1 wt% drop after 100 days of conditioning, the coupons' mass was stable. Instead, a linear decrease in weight was measured at the 80 °C exposure, considering the square root of the conditioning length. It can be evidence of thermal ageing.

From the literature, the presence of oxygen even at relatively low temperatures can lead to oxidation of the polymer. No practical way of controlling the oxygen level in the experimental atmosphere was available; the oxygen partial pressure was the standard atmospheric one. Simar *et al.* [43] usually associated the oxidative process to it an increase of weight in time and a differential darkening in the sample cross-section, due to the oxidation/diffusion competitive kinetics. A homogenous colouring was found in all the sample, depending on at the exposure temperature, with slight hue variation depending on the fluid present, as presented in § 4.1.5. No colour gradient was observed in cross-section of the aged samples when cutting to size to perform the DMA runs.

Flore *et al.* [88], on the other side, associate the oxidative process with a loss in weight, even if related to higher exposure temperature. At the same time, they assess that most of the weight loss is related to the thermal ageing independent from oxygen reaction, as residual volatiles or fleeting reaction of chain scissions products. Hence, we ruled out oxidation as the primary ageing mechanism in dry air. For the scope of our work, the ageing will be considered only in function of the exposure temperature, considering the air as an inert fluid.

4.1.4.2 GFRP composite coupons

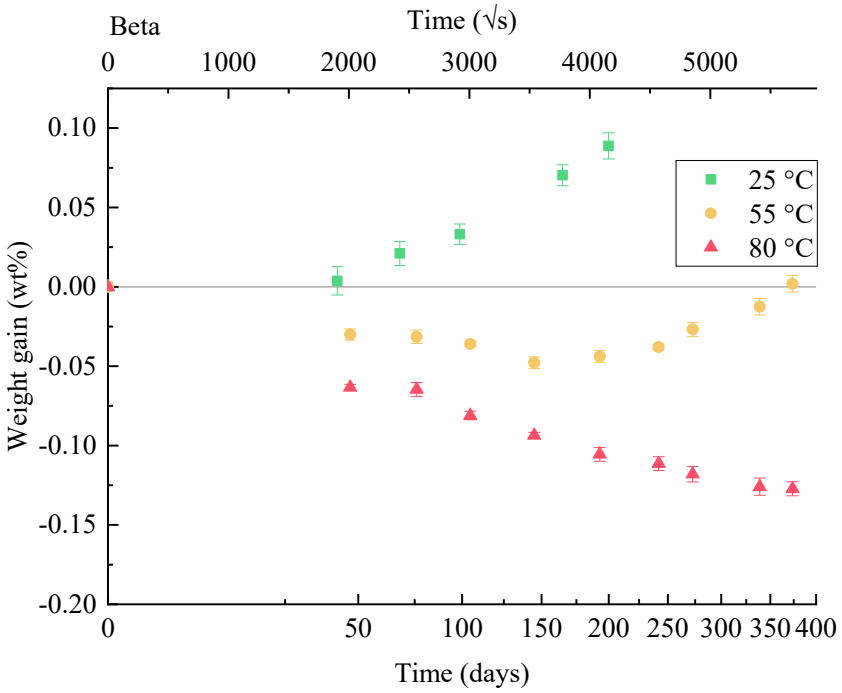

Figure 4-15: gravimetric measurements on GFRP Beta coupons in dry air exposure.

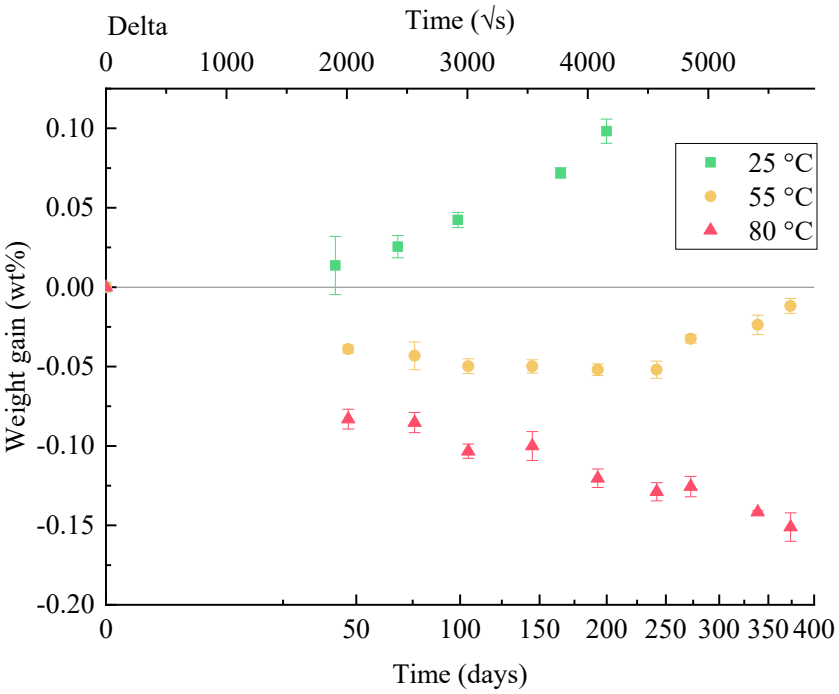

Figure 4-16: gravimetric measurements on GFRP Delta coupons in dry air exposure.

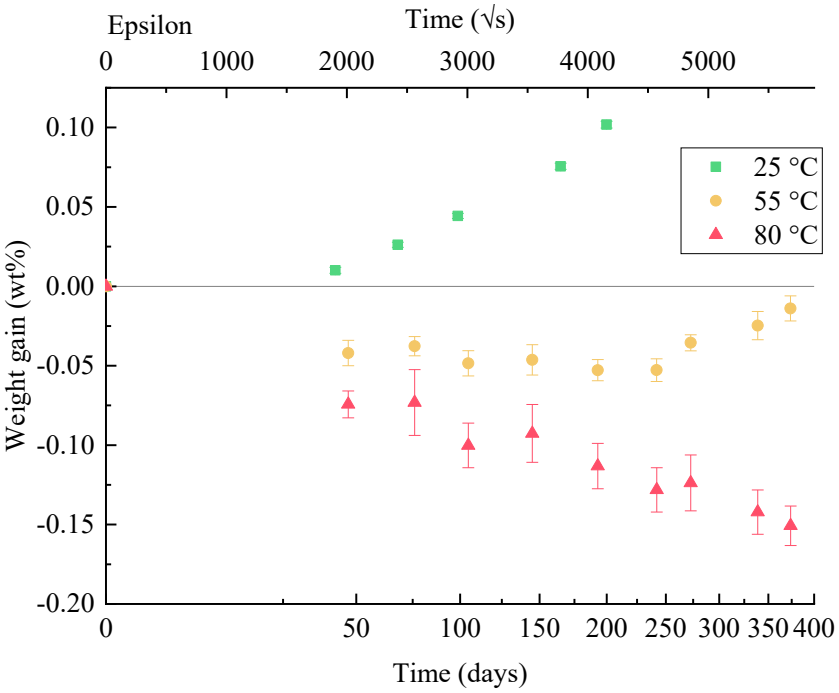

Figure 4-17: gravimetric measurements on GFRP Epsilon coupons in dry air exposure.

For the dry air conditioning on the GFRP, *beta*, *delta* and *epsilon* coupons were exposed up to one year, as shown in Figure 4-15, Figure 4-16 and Figure 4-17 respectively: as supposed, no significant difference was found in the weight trend among the sample geometries.

Similarly to the results from the neat epoxy, the change in weight is very limited compared to the fluid exposures. As expected, the reactivity with the air at these

temperatures is limited. It is possible to highlight a trend among the different exposure temperatures:

i. At 25 °C there is a progressive increase of the weight: possibly some atmospheric moisture penetrated the exposure container when it was opened for the coupons weighing. Then the moisture was progressively absorbed by the coupons.
ii. At 50 °C the weight is very steady, no immediate explanation for the slight decrease in mass after 50 days, later recovered.
iii. At 80 °C there is a progressive decrease in the weight. It could be justified either the release of some volatile resin by-products or residual absorbed moisture. We tend to exclude the oxidation reaction because the colouring of the aged cross-section appeared uniform, and the weight was decreasing. We had no mean of confuting which ageing mechanism was acting on the coupons.

4.1.5 Aged coupons appearance

A partial collection of pictures of aged gravimetric coupons is presented in Figure 4-18 and following. As mentioned before, the appearance of the aged coupons was characterised by increasing darker colour with the exposure temperature. The samples conditioned at room temperature do not show any significant change in their appearance. The aged coupons at 80 °C turn into a very dark brown hue, in particular those exposed to seawater. For these, signs of physical degradation were present at the later stages.

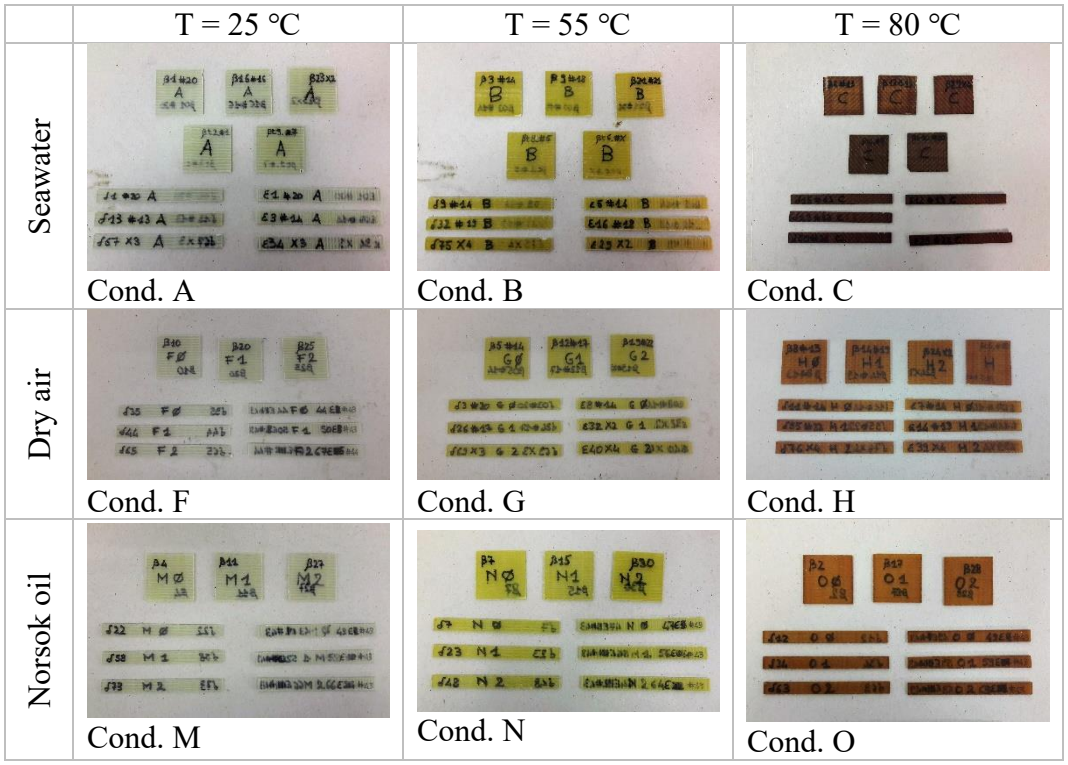

Figure 4-18: colour comparison of the aged GFRP gravimetric coupons.

T = 25 °C	T = 55 °C	T = 80 °C
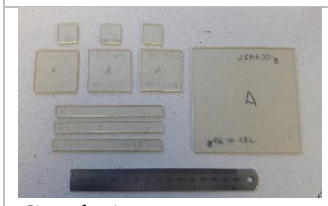	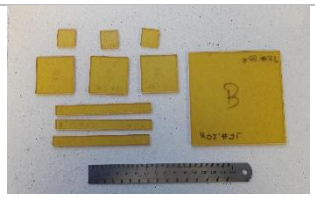	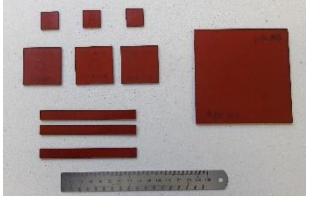
Cond. A	Cond. B	Cond. O

Figure 4-19: colour comparison of aged epoxy gravimetric coupons.

4.1.6 Effect of coupon's dimensions on diffusivity

4.1.6.1 Seawater diffusivity in the neat epoxy

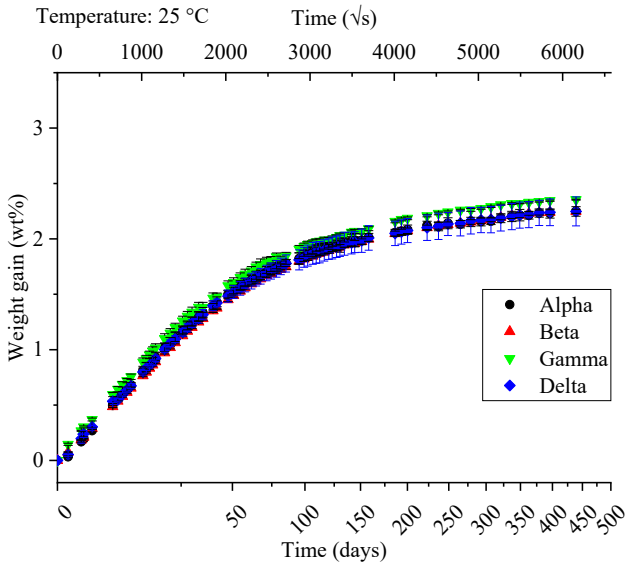

Figure 4-20: gravimetric measurements on epoxy coupons in seawater exposure at 25 °C.

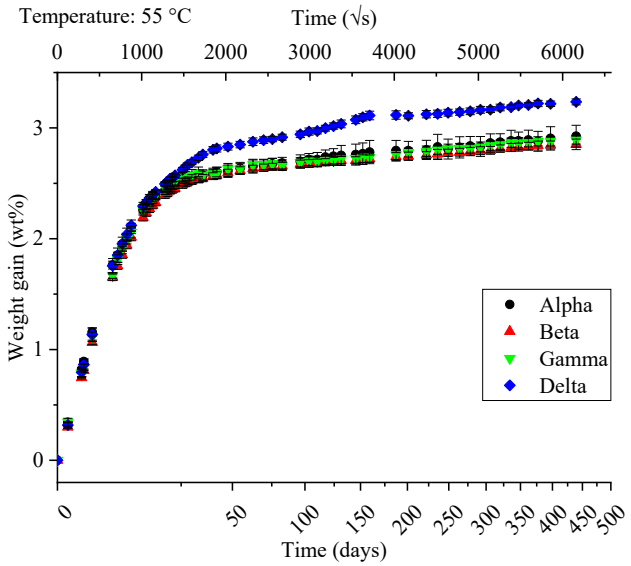

Figure 4-21: gravimetric measurements on epoxy coupons in seawater exposure at 55 °C.

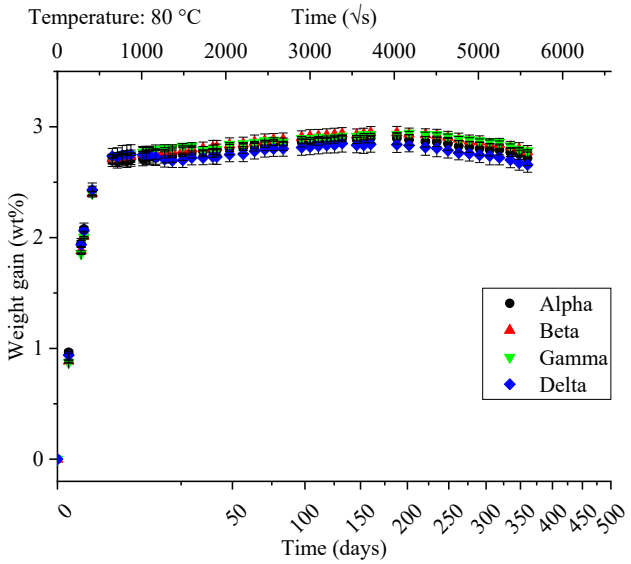

Figure 4-22: gravimetric measurements on epoxy coupons in seawater exposure at 80 °C.

From a graphical point of view, it is difficult to tell the differences between the absorption trend of the coupon geometries exposed to seawater. There is an apparent deviation only for the Delta coupons from the Cond. B (55 °C) exposure: as mentioned before (see §4.1.2.1) for this particular set, some white precipitate (likely could be the salt present in the seawater) was found at the sample edges, probably causing in this way the mass deviation.

However, from the analytical calculations, it is more evident that there are significant deviations from the ideal case of a semi-infinite plate that can affect the calculated diffusivity. As discussed in § 2.2.6, the coupon geometry can affect the diffusion kinetics as if its thickness is not small enough compared to the other geometrical direction, a significant contribution of the weight gain could come from the diffusion of the fluid from the side edges. Hence, the diffusion is not completely unidirectional as assumed by the standard fickian solution, and a more accurate three-dimensional solution can be used, as widely described by Grace *et al.* [17,70].

The diffusion coefficients calculated using the slope of the linear section of the weight gain plot result higher due to the contribution of an effectively three-dimensional diffusion process. The three-dimensional solution makes the analytical recovery of the diffusion coefficient way more computationally expensive. An alternative option is the use of the correction factors proposed by Shen and Springer [29] and Starink *et al.* [37] more recently, which amends the apparent diffusion coefficient obtained from the simplified Fickian solution. These correction factors account for the geometry of the experimental gravimetric coupon and return a value of the diffusion coefficient, which would be the one obtained in the ideal unidirectional diffusion scenario. A thorough description of the derivation of these correction factors was given at § 3.2.7. The value of such corrected diffusion coefficient should be geometry-independent, hence representing the actual material property sought.

The results for the neat Ampreg 26 epoxy are presented in Table 4-5, for the various temperatures and specimen shapes: the results reported are the average value obtained from the three coupon replicas for each exposure condition.

The diffusion coefficients are corrected as:

$$D_{corr} = f^{-2} D_r \qquad \text{Eq. 4-3}$$

Table 4-5: Diffusivity coefficients for neat epoxy at various exposure temperatures and coupon's geometry.

Temp. (°C)	Geometry	h × w × l (mm × mm × mm)	$f_{S\&S}$	f_{SSC}	D_r	$D_{r,\,S\&S}$	$D_{r,\,SSC}$
						($\times 10^{-13}$ m^2/s)	
25	alpha	2.09×18.86×19.15	1.22	1.12	1.74	1.17	1.38
	beta	2.18×40.00×40.08	1.11	1.06	1.59	1.29	1.41
	gamma	2.04×100.04×100.07	1.04	1.02	1.40	1.29	1.34
	delta	2.15×10.08×100.03	1.24	1.13	1.67	1.09	1.31
55	alpha	2.09×18.86×19.15	1.22	1.12	9.57	6.43	7.59
	beta	2.16×40.03×39.99	1.11	1.06	9.57	7.80	8.53
	gamma	2.12×100.05×100.05	1.04	1.02	9.03	8.31	8.63
	delta	2.07×10.06×100.05	1.23	1.12	8.02	5.33	9.01
80	alpha	2.15×19.31×19.14	1.22	1.13	61.09	40.80	48.27
	beta	2.15×39.96×40.03	1.11	1.06	51.01	41.60	45.49
	gamma	2.13×100.03×100.05	1.04	1.02	48.13	44.28	45.98
	delta	2.12×10.05×99.97	1.23	1.13	58.21	38.32	45.83

Note: the subscript S&S refers to the correction proposed by Shen and Springer [29], while the SSC refers to the one proposed by Starink *et al.* [37].

The *gamma* geometry can be referred to as the *quasi-infinite* coupon size because the thickness is much larger than the other main directions. Hence the contribution from the side edges to the diffusion is very limited, as in the original Fick's description. Indeed, the two correction factors converge to the unit for this geometry, and therefore, the corrected diffusivities are in a better agreement and close to the apparent ones measured from the experimental curves. For smaller coupon geometry, and especially for the tiny *alphas* and the narrow *deltas*, the correction factors diverge from each other, showing a broad range of diffusion coefficients. If all results are compared to the quasi-infinite coupons (*gamma* geometry), the $f_{S\&S}$ underestimates the diffusivity values, so the f_{SSC} is considered as more accurate and applicable. This is in agreement with the results presented in [37,38].

The present analysis demonstrates that quasi-infinite coupons are necessary to obtain accurate diffusivity values and, in the case that these aren't available due to manufacturing issues (i.e., extracting coupons from a small slab of material), the f_{SSC} correction factor should definitely be considered to avoid errors even up to 30% compared to the coefficient obtained from the ideal quasi-infinite coupons.

4.1.6.2 Oil diffusivity in the neat epoxy

Regarding the diffusivity of the aromatic Norsok oil in the epoxy thermoset, only the exposure at 80 °C showed a trend which could be assessed using the Fickian solution. Hence the diffusion factors were calculated only for the Cond. O; the results are presented in the following table:

Table 4-6: Diffusivity coefficients for neat epoxy in Norsok oil at 80 °C

Temp. (°C)	Geometry	h × w × l (mm × mm × mm)	$f_{S\&S}$	f_{SSC}	D_r	$D_{r,S\&S}$	$D_{r,SSC}$
					($\times 10^{-13}$ m^2/s)		
80	alpha	2.10×19.01×19.11	1.22	1.12	0.54	0.36	0.42
	beta	2.12×40.00×40.00	1.11	1.06	0.55	0.45	0.49
	gamma	2.15×99.96×100.06	1.04	1.02	0.51	0.47	0.49
	delta	2.04×10.03×100.03	1.22	1.12	0.49	0.33	0.39

There is some scattering in the diffusivity values, and the average value is about $4 \div 5 \cdot 10^{-14}$ m^2/s. This diffusion coefficient is about two orders of magnitude smaller than the one for the seawater at the same temperature, highlighting the much slower rate at which oil diffused. While the $f_{S\&S}$ yet underestimates the diffusion coefficient, both the correction fails to reduce the geometry effect, and the uncorrected coefficient D_r seems to be the most consistent. As the correction factors are uniquely based on geometrical consideration, their performance should be independent of the diffusing fluid: we are not able to explain as they seem ineffective in adjusting the diffusivity for the oil.

4.1.6.3 Diffusivity in the GFRP composite

Similarly to the neat epoxy, the diffusion coefficient was calculated from the weight gain first and then adjusted for the geometry of the coupons, to correct the contribution from the side edges. The GFRP composite under investigation was found to have a fibre volume fraction of 56 vol% (see at § 3.2.4.3). For this V_f value, the g^2 calculated was 0.3536. These values were used in the calculation of the correction factors.

In Table 4-7, the correction factors and diffusivity coefficients for the composite material are listed. The value of the diffusivity calculated from the experimental weight gain test curves following the Fickian approach is denoted as D_c. The corrected values $D_{c,S\&S}$ and $D_{c,SSC}$ were calculated from Eq. 3-8 combined with Eq. Eq. 3-9&10 and Eq. 3-15(a), respectively. Also, the effective diffusivity transverse (⊥) and parallel (||) to the fibres was calculated from Eq. 3-16 and presented for comparison. The corrected diffusivity of the neat epoxy at the respective temperatures was used in the prediction of the effective anisotropic diffusivity.

Table 4-7: Diffusivity coefficient for GFRP at various exposure temperatures and coupon's geometry.

Temp. (°C)	Geometry	h × w × l (mm × mm × mm)	$f_{S\&S}$	$f_{ortho,\perp}$	$f_{ortho,\parallel}$	D_c	$D_{c,S\&S}$	$D_{c,SSC}$	$D_{eff,\perp}$	$D_{eff,\parallel}$
						($\times 10^{-13}$ m^2/s)				
25	beta	1.72×39.99×40.00	1.09	1.06	1.03	0.51	0.43	0.45	0.56	1.49
	gamma	1.70×99.84×99.73	1.03	1.02	1.01	0.49	0.46	0.47	0.50	1.37
	delta	1.72×9.99×99.96	1.19	1.11	1.06	0.45	0.31	0.37	0.57	1.47
	epsilon	1.70×99.90×10.03	1.19	1.16	1.06	0.60	0.43	0.44	0.63	1.47
55	beta	1.73×40.00×40.04	1.09	1.06	1.03	5.40	4.58	4.78	3.40	9.01
	gamma	1.70×99.91×99.98	1.03	1.02	1.01	4.46	4.17	4.25	3.20	8.82
	delta	1.73×9.95×99.98	1.19	1.11	1.06	5.37	3.78	4.36	3.92	10.15
	epsilon	1.72×99.93×9.99	1.19	1.17	1.06	5.75	4.06	4.23	4.33	10.14
80	beta	1.73×39.99×39.99	1.09	1.06	1.03	45.81	38.80	40.57	18.17	48.06
	gamma	1.76×99.12×99.75	1.04	1.03	1.01	36.29	33.85	34.50	17.10	47.03
	delta	1.71×10.00×100.03	1.19	1.11	1.06	39.91	28.27	32.52	19.89	51.53
	epsilon	1.74×99.93×10.01	1.19	1.17	1.06	40.94	28.84	30.05	22.08	51.63

Note: the subscript S&S refers to the correction proposed by Shen and Springer [29], while the SSC refers to the one proposed by Starink *et al.* [37].

In all cases the least correction is required for the *gamma* geometry coupons, confirming the convergence to the infinite specimen ideal scenario. In analogy with the neat epoxy case, it is evident that the correction proposed by Shen & Springer seems to underestimate the material's diffusivity (i.e., highest values of the correction factor). The one proposed by Starink *et al.* is more consistent and converge the corrected diffusivity values towards the experimental of the *gamma* geometry (100 × 100 mm) coupon, which is the closest representative to the ideal one-dimensional diffusion case.

The results in Table 4-7, also plotted in Figure 4-23 as a function of the diffusivity of the resin, suggest that:

a) the effective diffusivity transverse to the fibre direction ($D_{eff,\perp}$) is approximately half that of the resin while the diffusivity along the fibres ($D_{eff,\parallel}$) is slightly higher than that of the resin;
b) there is a satisfactory agreement for the values of the GFRP diffusivity at 25 °C to $D_{eff,\perp}$ but it progressively deviates at higher temperatures towards $D_{eff,\parallel}$. This is an indication that while at ambient temperature diffusion is occurring mainly through the thickness of the specimen, as the temperature increases there is significantly more seawater travelling through the edges of the specimens and along the fibres, which in turn suggests a possible weakening of the fibre-matrix interface providing an easy pathway for the diffusing liquid.

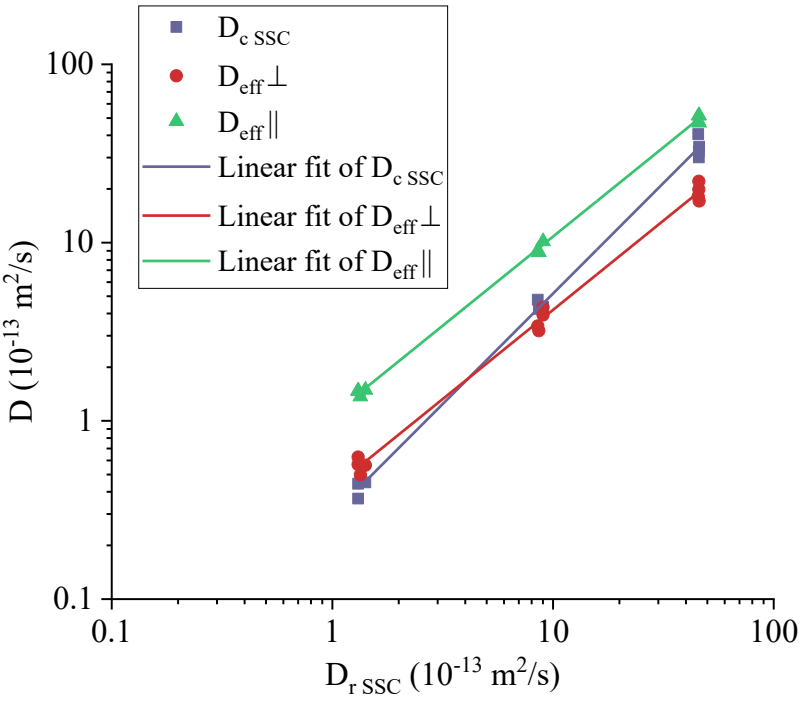

Figure 4-23: Plot of the effective and measured diffusivity coefficient for the GFRP composites against that of the corrected epoxy matrix. Note that all temperatures and specimen sizes were considered.

Regarding the diffusivity of the aromatic Norsok oil in the GFRP, only the exposure at 80 °C showed a trend which could be assessed using the Fickian solution. The exposure test had to be stopped before the effective equilibrium could be reached. Hence the diffusion factors here calculated are only an estimation from the partial gravimetric curves, to provide an order of magnitude of the diffusivity in the composite material. The correction factors were not applied as they would be affected by a significant experimental error and not contributing to the analysis.

Table 4-8: Diffusivity coefficients for the GFRP in Norsok oil at 80 °C

Temp. (°C)	Geometry	h × w × l (mm × mm × mm)	D_c (×10^{-13} m^2/s)
80	beta	1.72×40.03×40.03	0.36
	delta	1.68×9.99×99.99	0.34
	epsilon	1.85×99.82×9.99	0.42

From this approximate calculation, it can be noted how the diffusivity of the oil is about two orders of magnitude smaller than the seawater at the same temperature, similarly to the coefficients for the epoxy. It seems evident that in case of the exposure of the material to both water and oil, the most active diffusant species will be the water by far and, hence, the primary external agent to influence the ageing process.

4.1.7 Diffusivity relation with exposure temperature

From literature sources [8,21], it is stated that in general, the diffusivity dependence on temperature follows the Arrhenius equation:

$$D(T) = Ae^{\frac{-E_a}{RT}} \qquad \text{Eq. 4-4}$$

where A is a pre-exponential factor, a constant for each diffusion system, T is the absolute temperature in Kelvin, E_a the activation energy for the diffusion mechanism and R is the universal gas constant equal to 8.13446 J/(mol·K).

To explore this assumption for the materials under investigation an Arrhenius plot (lnD vs $(1/T)$) was constructed for the diffusivity values obtained from the *gamma* geometry (100×100 mm) coupons (see Figure 4-24), which are considered the ones providing the most accurate values. The values obtained by linear interpolation of the available experimental data has given the two relationships:

Epoxy: $$D_{r,SSC} = 7.74 \cdot 10^{-4} \cdot exp\left(-\frac{54629}{R}\frac{1}{T}\right) \qquad \text{Eq. 4-5}$$

GFRP $$D_{c,SSC} = 3.34 \cdot 10^{-2} \cdot exp\left(-\frac{66380}{R}\frac{1}{T}\right) \qquad \text{Eq. 4-6}$$

The higher exposure temperature (80 °C) was very close to the glass transition temperature of the dry materials (about 86 °C), and in the literature some authors suggest not to expose the material to accelerated hygro-thermal ageing condition to not more than 20 °C below the glass transition [86].

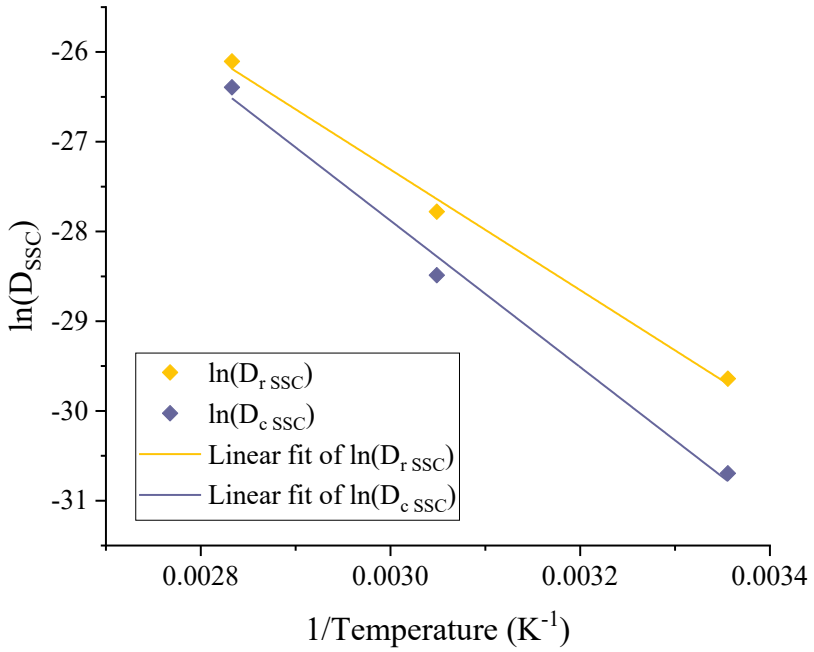

Figure 4-24: Arrhenius plot of diffusivities for the neat Ampreg 26 and GFRP materials. Note that only gamma specimens (quasi-infinite) diffusivities values are considered.

Despite this, it appears that the Arrhenius relationship holds for the range of temperatures investigated, and extrapolation can be safely made to lower temperatures (Figure 4-25). Considering the calculated activation energies of 54.6 kJ/mol and 66.4 kJ/mol for the neat Ampreg 26 and the GFRP, respectively, the diffusivity at a temperature of 4 °C, representing realistic deep-water applications, was evaluated to be 0.23 and 0.05×10^{-13} m^2/s.

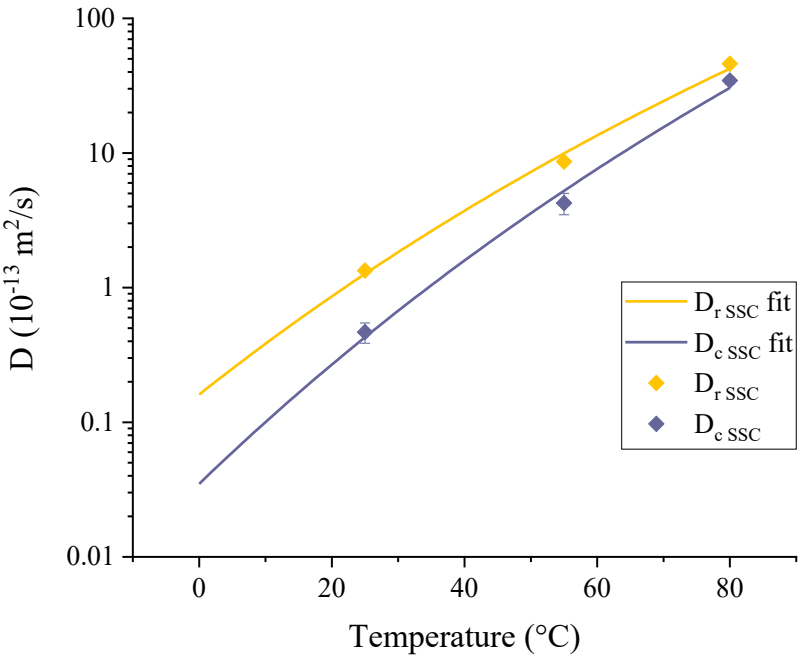

Figure 4-25: predicted diffusivities for the neat Ampreg 26 and GFRP (some error bars are not visible due to very small standard deviation associated).

This is a result of prime utility for the characterisation of the diffusion behaviour of this polymer composite system, as it allows to evaluate the diffusivity trend for a significant range of temperature only by measuring a few experimental points.

4.2 Physical Properties – Glass Transition Temperature

The critical effect of the long-term exposure to the simulated working environment on the material is the change of its physical and mechanical properties. A vast literature reports the hygrothermal ageing of different kind of water (sweet and seawater, distilled, saline solutions) on polymer composite material [9,30]. In smaller extent, other fluids were investigated about their effect on PMC, strong acid and alkaline solutions, solvent and organic fluids, which mostly are employed in industrial applications [42,89].

Generally, the exposure to these chemical agents usually induces a degradation in the composite properties, which is proportional to the duration of the contact with the fluids. The effects can be reversible or not, and other physical factors (temperature, hydrostatic pressure, mechanical loads) strongly influence the overall loss of performance, most of the times in a highly non-linear way. The whole phenomena can be improperly addressed as *ageing*, as it results in a weakening of the material over time. There is no universal agreement about how to describe analytically these phenomena that can vary substantially in their nature [7,20].

In our project, we decided to monitor the evolution of some of the basic properties of the material:

i. Glass transition temperature (Tg);
ii. Young's (or elastic) modulus (E);
iii. Mechanical strength as Ultimate Tensile Strength (UTS).

The reason for choosing these properties is that they are widely used to describe a polymer composite's performance. The material properties are of prime utility for design purposes as they can support an initial estimation about the suitability for a possible application, depending on the temperature range experienced or the structural loads involved.

Another reason for the popularity of these materials properties is that they can be measured by well-established laboratory testing: Tg is measured by Dynamic Mechanical Analysis, elastic modulus and UTS by means of a destructive tensile test. While the tensile test is strictly regulated by technical standards released by international bodies such as ASTM and ISO, the debate on how performing DMA and in particular how to calibrate the temperature sensors of the testing machine is still open to debate [90]; anyhow, standards such as ASTM D7028 [76] and E1640 [77] are widely employed for performing the DMA on polymer composite materials.

Things get possibly even more open to interpretation when it comes to performing a test on aged material, as the specimen preparation and the exposure methodology are very little standardised and usually highly dependent on the specific application or conditioning fluid. Water, due to its everywhere presence and notable chemical reactivity is an exception, as the standards ASTM D570 [66] and D5229 [67] describe in detail how to perform the polymer materials conditioning to water, but it concerns mainly how to perform gravimetric testing

(as seen in the previous paragraph) while not much is stated about how to proceed with other follow-up tests.

Anyhow, DMA and tensile testing are standard practises when it comes to evaluating the performance at the material level, both in academia and industry. These tests find application when new material grades are investigated and are versatile resources when quality has to be assured in a production line.

To study the viscoelastic behaviour of polymers (and composites) from a mechanical point of view, a DMA test is an immediate choice, in particular to evaluate the glass transition. The results of a DMA run test is the typical set of curves which describe the change of the storage and loss moduli in relation to the temperature. They are expressions of the viscoelastic nature of the polymer. Considering a simple Kelvin-Voigt model for the viscoelastic material, the *storage modulus E*' is linked with the elastic response of the polymer, while the *loss modulus E"* is related to the inner viscous dissipation due to molecular movements/rotations. A useful parameter is the tangent of the phase angle δ between stress and strain in a sinusoidal deformation. It is usually shortened in *tanδ* or *tanD*. From a simple trigonometric relation, it can be demonstrated that:

$$tan(\delta) = \frac{loss\ modulus}{storage\ modulus} = \frac{E''}{E'} \qquad \text{Eq. 4-7}$$

Hence, *tanδ* is a useful indicator of the glass transition happening as soon as it starts growing, to approach or even exceed values of 1 at its peak in polymer materials.

For our analysis, we chose the onset of the drop in the storage modulus (E') as point estimator of the glass transition temperature. It is a bit more complicated to calculate, compared to the identification of the *tanδ* peak, often used in literature: the tester software provides a tool for the calculation of it. From an engineering point of view, the onset of the E'drop is more conservative for structural application, as it identifies the temperature at which the material starts to lose its stiffness in an abrupt and significative way. For this reason, the Tg is often used as the upper-temperature limit for mechanical applications.

From each sample removed from the exposure, two or three specimens were obtained by cutting it along its length. The first specimen was tested straight away to measure the Tg of the material as it absorbed the exposure fluid (commonly known as "wet" Tg) at the given time. The remaining specimens were dried in an oven at 50 °C for 1-2 weeks, and then the test repeated in order to evaluate if the process was reversible. The points plotted in the charts of the following paragraphs are representative of the calculated Tg for a single run. Hence no statistical error can be associated with it. The reason for such an approach was due to the high number of experimental points to be measured as is (well over 300 runs).

4.2.1 Seawater exposure

An important feature was to determine the Tg of the pristine material. Several runs were performed on unaged samples, both for the neat resin and the GFRP. The results were very consistent for the neat epoxy, which has an original Tg of about 86 °C after the standard post-cure.
Calculating the Tg for the GFRP was more complicated because the measurement was influenced by the fibre orientation in the test. Both *delta*, with the fibres oriented in the longitudinal direction and *epsilon* coupons, which fibres were oriented in the transverse direction, were tested. Usually, the runs on Delta specimens returned a higher value of the Tg. Possibly, the higher stiffness of the glass fibres somehow hindered the abrupt E' drop, until the epoxy matric reached a complete rubbery state. It was preferred to use the Tg values from the runs on Epsilon specimens. The transverse direction of the fibres allowed to stress the epoxy matrix directly in the 3-point bending configuration, returning a more accurate value of the Tg. The test results for the different exposure conditions are reported following, for the neat epoxy first, then the composite material.

4.2.1.1 Neat epoxy coupons

(a)

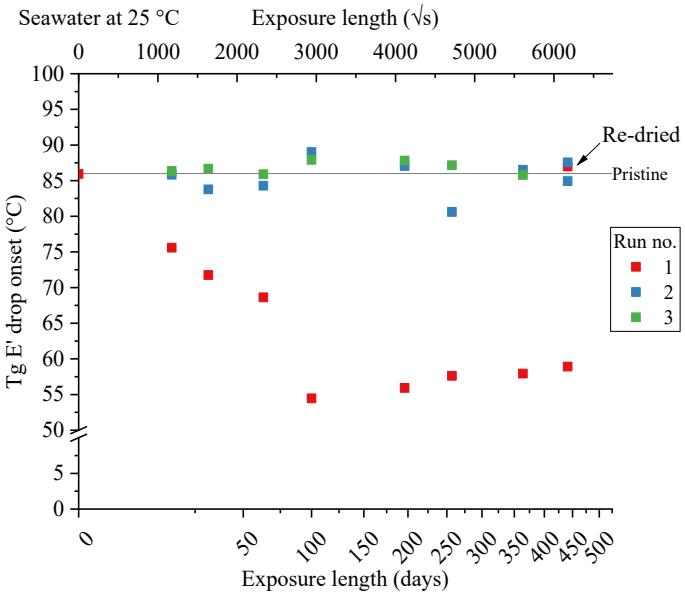

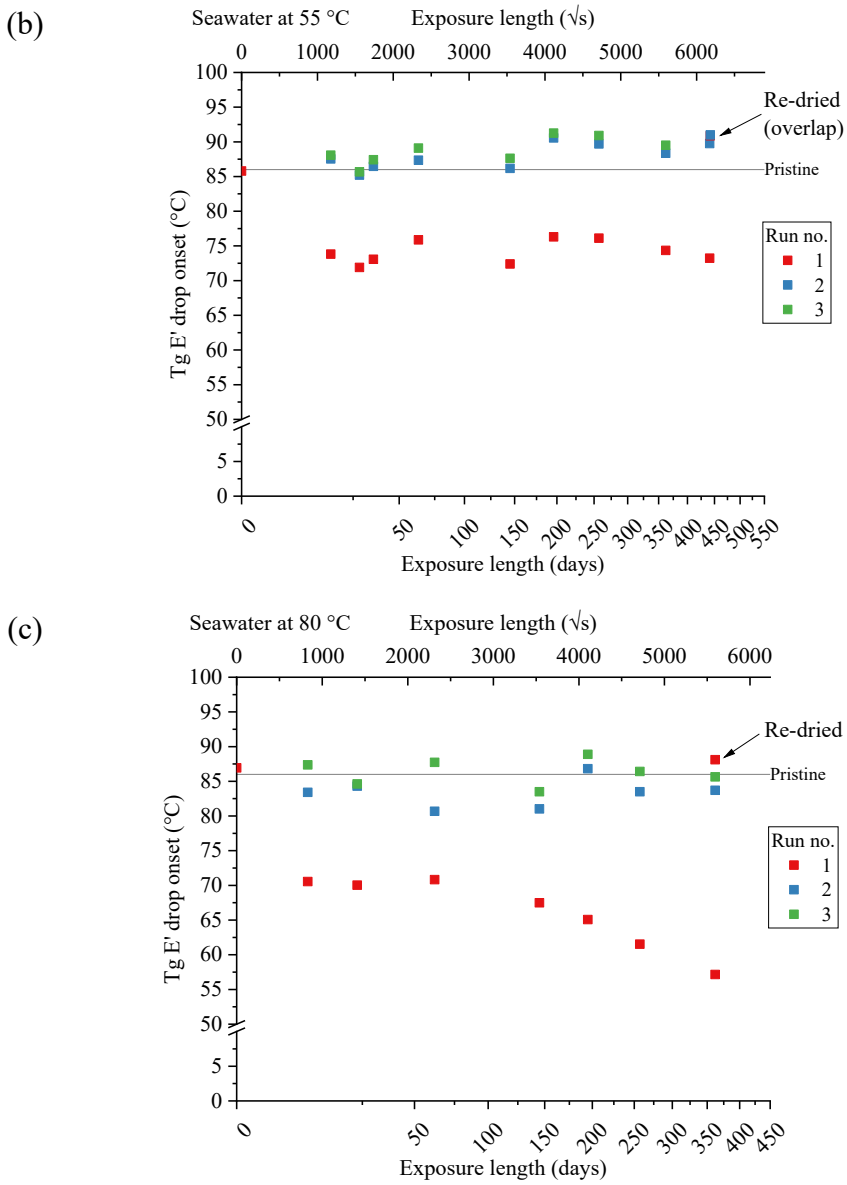

Figure 4-26: results of DMA runs on epoxy samples from seawater exposures at different ageing times. Exposure temperatures were: a) 25, b) 55, c) 80 °C.

The results from the exposures (see Figure 4-26) show how seawater significantly affects the Tg of the epoxy. The higher loss is for the exposure at 25 °C, in which the decrease of the Tg dropped below 55 °C at after 100 days of exposure, then to slight recover over time. For the exposure at 55°C, there is an initial drop at 74 °C after 16 days of exposure, and then the value of the "wet" Tg swung around the 75 °C for the whole duration of the exposure. In the exposure at 80 °C, there was a quick decrease of the wet Tg to 70 °C after only 8 days. Then it stayed relatively constant up to about 150 days of exposure. After that, it slowly started to progressively decrease down to 57 °C after 1 year soaking in seawater. It is interesting to see how the Tg is practically completely recovered at any stage of the exposure upon drying of the specimens, even samples been exposed for more than 1-year result to regain the same Tg as the pristine material. This suggests that

the plasticization effect due to the diffusion of seawater is completely reversible [91].

Considering the trends of the Tg in relation to the exposure temperatures presented in Figure 4-27, it appears that the exposure at the lower temperature is the one showing the most significant drop, at least for the time-span we investigated. This behaviour is not fully understood, but it can be explained with the different interaction of the water molecules with the epoxy network. As proposed by Zhou and Lucas [92], two kinds of water-epoxy bond can be formed, and they have a counteracting effect on the network mobility. If the water molecule substitutes itself to some hydrogen bond between the epoxy chains (Type I bond), the result is indeed a plasticization effect which induces a reduction of Tg. On the other side, if the molecule acts to form new inter-chain hydrogen bonds (Type II bond), this counters the plasticisation effect and partially recover the Tg to higher values. This could partially explain the more sustained drop for exposure conditions at the lower temperature (comparing 25 to 55 °C exposures), while at the higher exposure temperatures Type II bond is favoured due to the higher activation energy required to form it [93]. The Tg appears to gradually decrease at 80 °C for exposures longer than 100 days, which can be indicative of some further ageing phenomena severely degrading the polymer structure.

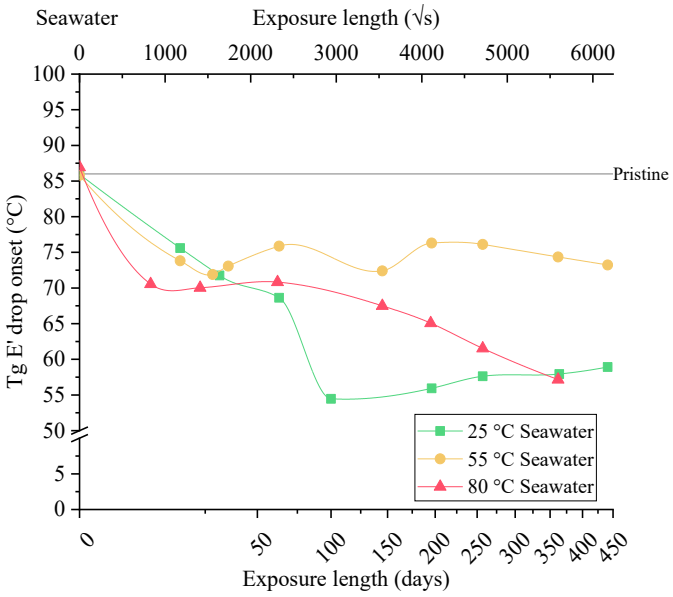

Figure 4-27: the shift of the "wet" Tg in the epoxy during the exposure in seawater.

4.2.1.2 GFRP composite coupons

(a)

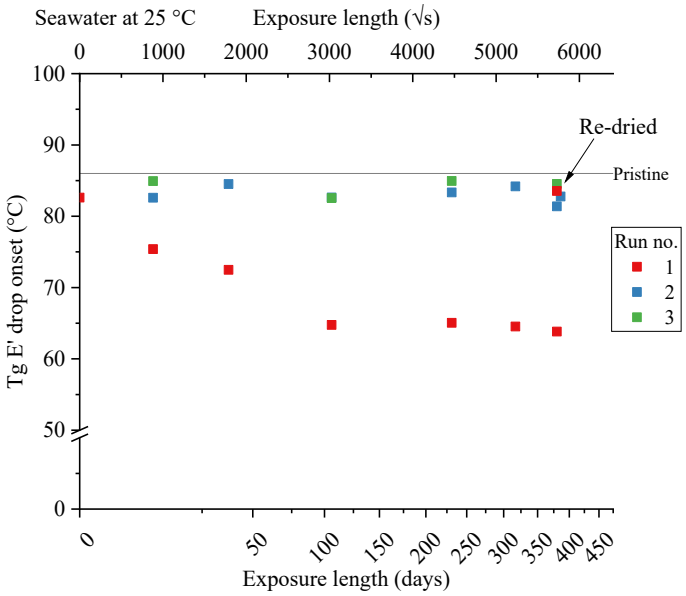

(b)

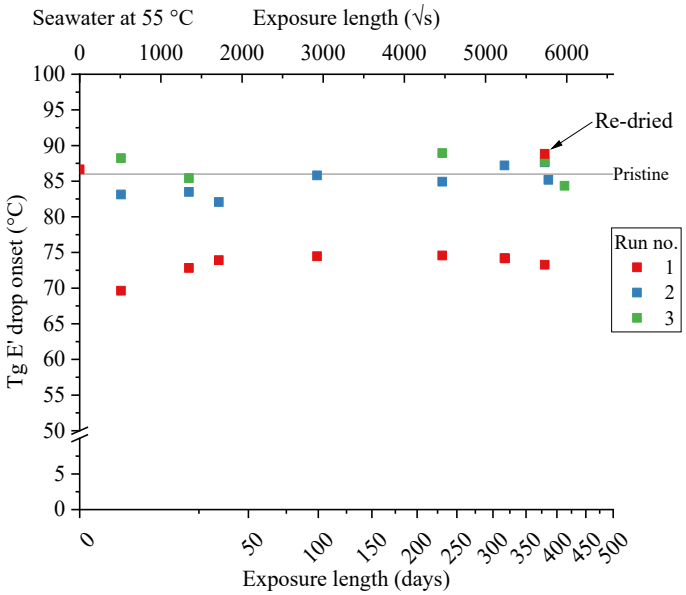

(c)

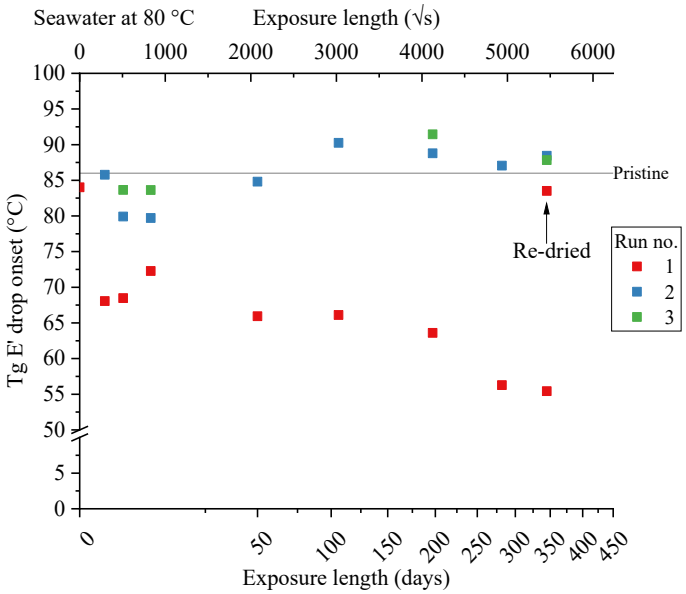

Figure 4-28: results of DMA runs on GFRP samples from seawater exposures at different ageing times. Exposure temperatures were: a) 25, b) 55, c) 80 °C.

The wet Tg evolution for the GFRP is presented in Figure 4-28. From an immediate analysis of the test results, the trends are similar to the neat epoxy runs. It is confirmed that the drop in Tg due to water absorption is mostly reversible at any stage of the exposure, even up to one solar year.

While a similar trend is observed in the wet Tg at different exposure temperatures in comparison with the neat epoxy, there is a clear difference in the value for the lower limit for the drop of the Tg a for the samples from the 25 °C seawater exposure (Cond. A), which sits around 65 °C, well above the 55 °C found for the neat epoxy.

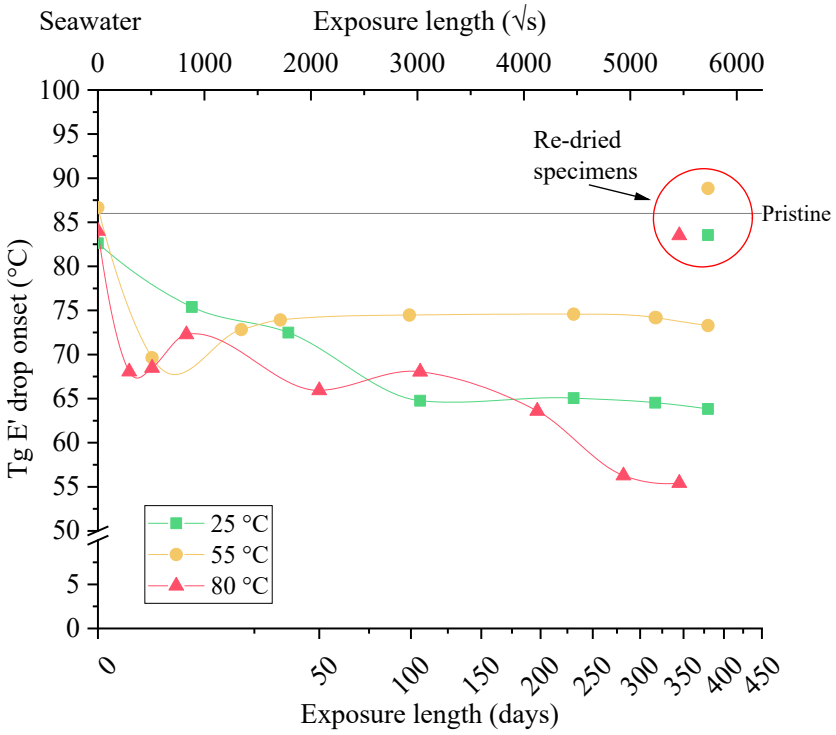

Figure 4-29: the shift of the "wet" Tg in the GFRP along with the length of the exposure in seawater.

4.2.2 Dry air exposure

4.2.2.1 Neat epoxy coupons

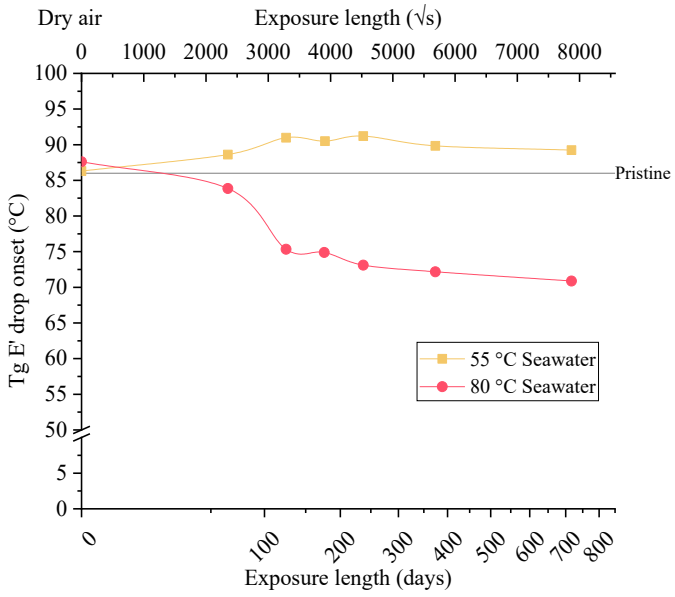

Figure 4-30: evolution of the Tg in epoxy when exposed to dry air.

The exposure at 25 °C was not performed, as it is not plausible a significant change in the Tg of the epoxy when kept at room temperature in dry conditions. The exposure at 55 °C shows a slight increase in the Tg, but it stabilises at about 90 °C. The samples from the 80 °C exposure show a significant drop in Tg around 100 days, down to 75 °C and decreasing, may be indicative of some irreversible ageing

happening; differently from the seawater exposures, this decrease in Tg is not reversible. Even if the run was repeated after some re-conditioning in the oven at a lower temperature (50 °C), there was no significant recovery in the measured Tg. Likely, some form of oxidation is happening due to the high temperature of exposure (indeed there is no sign of Tg drop for the 55 °C exposure). This phenomenon can happen at relatively low temperatures as reported by Gigliotti et al. [43], in particular when approaching the material's glass transition.

4.2.2.2 GFRP composite coupons

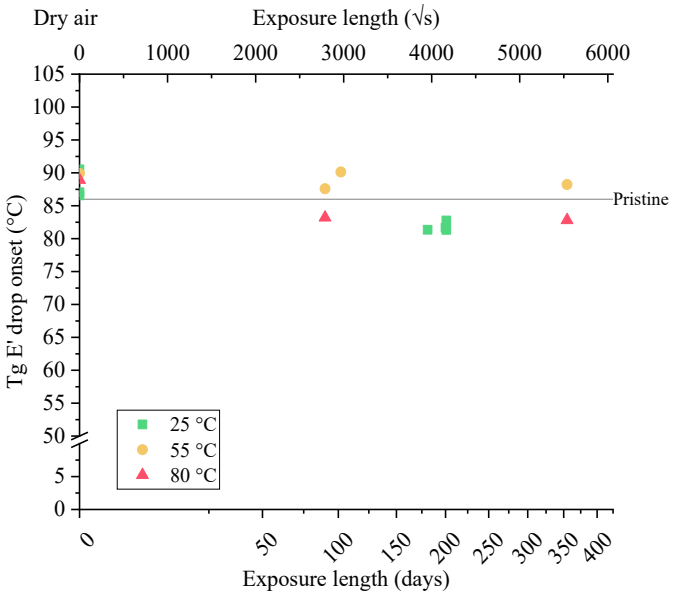

Figure 4-31: evolution of the Tg in the GFRP when exposed to dry air.

DMA runs on composite samples were performed in a smaller number. The test confirmed a fairly steady glass transition for the GFRP, not showing any significant deviations from the values of the original pristine material.

4.2.3 Norsok oil exposure

4.2.3.1 Neat epoxy coupons

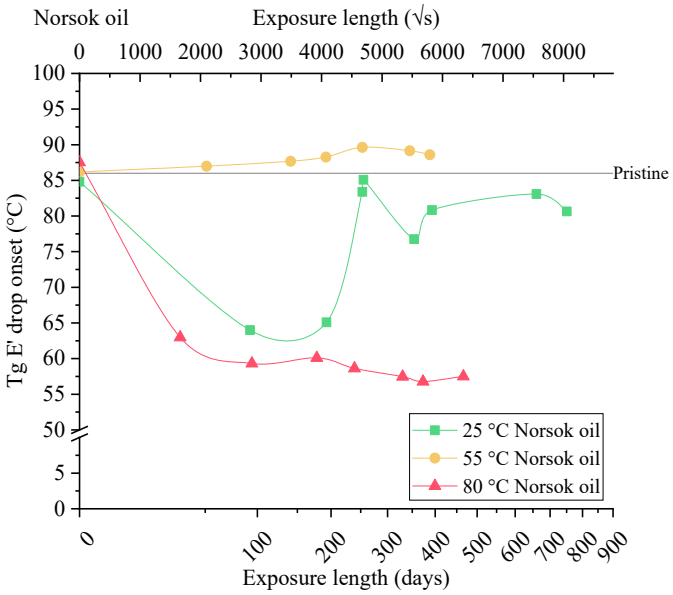

Figure 4-32: evolution of the Tg in epoxy when exposed to Norsok oil.

The exposure of the neat epoxy to the aromatic Norsok oil returned a completely different pattern than what seen with the other exposure conditions, as shown in Figure 4-32. The exposure at 55 °C showed little change at all in the glass transition temperature, as it appeared to absorb a very little amount of oil from the gravimetric testing.

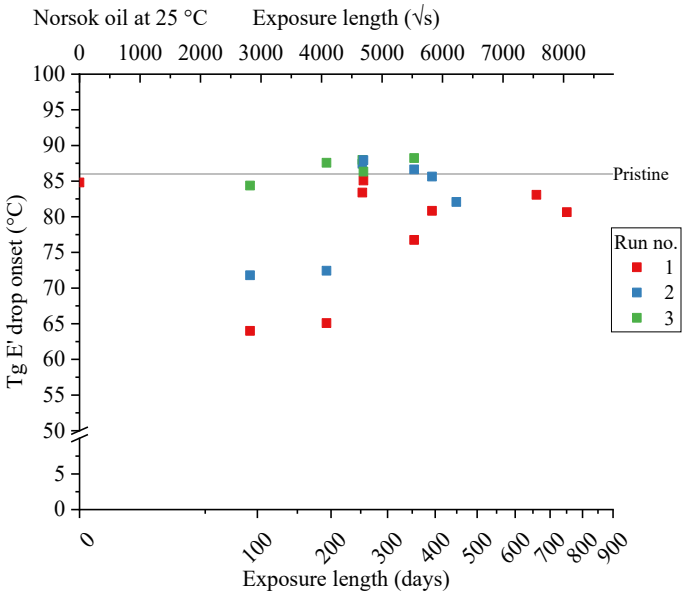

Figure 4-33: evolution of the Tg in epoxy when exposed to Norsok oil at 25 °C.

The samples from the exposure at 25 °C instead, had an alternated trend with an initial significant decrease in the Tg, which was later recovered after about 250 days. Then it continued to fluctuate at temperatures around the 80 °C for longer

exposure times. Even here there is symmetry on the behaviour found in the gravimetric curves, which is not fully understood. Even more, from the repeated runs after the reconditioning in an oven at 50 °C, there is a significant recovery to the pristine Tg (see Figure 4-33). Probably, whatever oil absorbed was evaporated, and the material returned to the original conditions.

This behaviour is opposite to the one found for the epoxy when exposed to the oil at 80 °C. In this case, the Tg decreased down to values below the 60 °C, in parallel with the absorption of the oil recorded in the gravimetric test. If the material was then re-dried in air at 50 °C, little or no recovery happened to the Tg. Similarly to what was found for the gravimetric measurements (compare to § 4.1.3), which showed no evaporation of the oil upon drying in the oven.

4.2.3.2 GFRP composite coupons

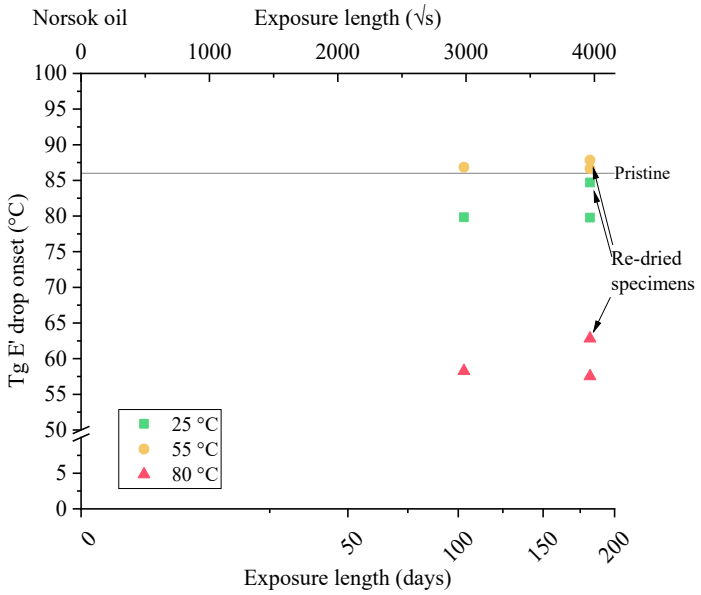

Figure 4-34: evolution of the Tg in the GFRP when exposed to Norsok oil.

Even if measured in a significantly smaller number of tests, the results from the GFRP specimens exposed to the Norsok oil provided a scenario in fair agreement with the results on the neat epoxy. The Tg of the specimens exposed to the oil at 25 °C is slightly reduced, as for the later stage in the neat epoxy. For the condition at 55 °C, the glass transition in the material seems quite unaffected. The specimens exposed at the 80 °C had their Tg reduced below the 60 °C and seemingly there was no recovery even after 2 weeks drying in dry ait at 50 °C.

Together with the more extensive results from the epoxy, all the data suggest that absorption of the oil is a non-reversible process when it happens at a higher temperature.

4.3 Mechanical properties: Tensile testing

Unidirectional tensile tests were performed on the pristine and progressively aged materials due to the exposures. The aim is to compare how the material mechanical performance evolved over time under the influence of different factors such as the exposure fluid and temperature. Both tensile specimens made of neat thermoset and GFRP composite were tested, to evaluate separately how their mechanical properties would degrade over time.
Tensile testing is the prime and most common experimental technique to qualify structural materials, and most of the times, it is the only one accepted to measure the material properties for design purpose. The testing procedure was described in detail in § 3.6.1.

4.3.1 Failure criterion

The tensile test is fairly straightforward when it comes to determining the point of break of a specimen, as a sudden and irreversible decrease of tensile load is recorded, and the specimen is clearly broken, leaving an open gap at the break location. It often happens with an explosive failure (usually of limited intensity when polymers or PMCs are involved), due to the abrupt release of elastic energy.

This is one of the reasons for the ease of performing this test and it holds true for basically all the homogenous materials. When it comes to composites, the joint presence of two genuinely heterogeneous materials with very different mechanical performance usually leads to a more complex scenario. Considering only composite with unidirectional long-fibre reinforcement, we can usually have two alternative situations: with brittle matrices, the matrix is the first one to give up, leaving the fibre to break in quick sequence when they are not able to distribute the load anymore. When the matrix is more ductile, the very stiff fibres break first at relatively small strain, leaving the matrix to significantly deform in a plastic way, not able to sustain significant loads, before the complete failure.

Without examining all the possible outcome, we had to select some robust criterion to determine the break in our tested material univocally. The break-point on the stress-strain curve was determined as:

Material:	*Break criterion*
neat epoxy	The break is brittle or, if yield point is reached, it happens after limited plastic deformation. No necking visible. Very sudden and complete loss of load, easily identified.
GFRP with longitudinal fibres	Brittle failure with an almost simultaneous break in both fibres and matrix (impossible to say in real-time). Different degree of explosivity, more clean fracture surface in aged samples. On the curve, the first point where the load does not increase is taken for the break-point.

GFRP with transverse fibres	Brittle failure with debonding of the fibres from the matrix. The break would be neat, but the orthogonal fibre stitches played as structural ligament able to sustain high loads. The break-point is set where there is a clear deviation from the elastic linearity, as an indication of the compromised structural integrity of the specimen. Usually, the final break happens at higher loads when the stitches finally fail.

4.3.2 Exposure/ageing duration

The drawback of most mechanical test is that they are destructive. They are aimed to push the tested material beyond its mechanical capabilities to find out at what load level it will fail, not able of deforming under stress any further. That means that for each test run, a new specimen is necessary. Moreover, like any experimental technique, it is affected by some degree of statistical dispersion of the results due to either random errors introduced by the performing of the test itself (e.g. incorrect measurements of specimen dimensions) or by defects/alterations in the material of the specimen, which affect its mechanical response.

To reduce the influence of these deviations, more test runs were performed at the same ageing stage. The minimum number of specimens recommended by the testing standards is 3 for a homogeneous material as the epoxy and 5 for the composite material. This makes the whole testing plan requiring a significantly large number of replicas to start with: due to the limited availability of GFRP material, for most of the sampling point for the test only 3 (or more) specimens were tested

In order to optimise the use of the limited number of specimens, the sampling times were planned in advance. The properties for the material in pristine conditions were measured once and used as starting values for all the exposures on it. As the aim is trying to correlate the effect of fluid diffusion on the mechanical properties, the exposure lengths were decided in relation to the gravimetric patterns:

a) For seawater exposures, as mentioned in § 3.6.1, the sampling moments were spread along the sampling curve, trying to test the material at the relevant point of the absorption curve.
b) For the Norsok oil and the dry air, at the gravimetric curves did not show the same degree of weight change to highlight specific moments, the sampling was done at 3 and 6 months of exposure.

Due to limited availability of the material, a reduced number of specimens were introduced to the oil and dry exposures, as they were expected to show a limited reaction to such ageing condition, while the focus was placed mostly on the seawater ones. In particular, only the neat epoxy specimens were exposed to the Norsok oil, and only the longitudinal specimens for the GFRP were used in the dry-air conditioning.

4.3.3 Tensile tests on neat epoxy from seawater exposure

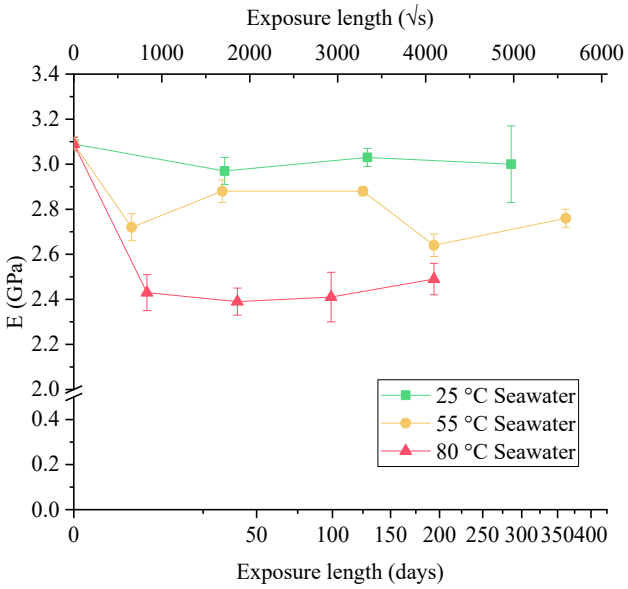

Figure 4-35: the shift of the epoxy Young's modulus for seawater exposures over time.

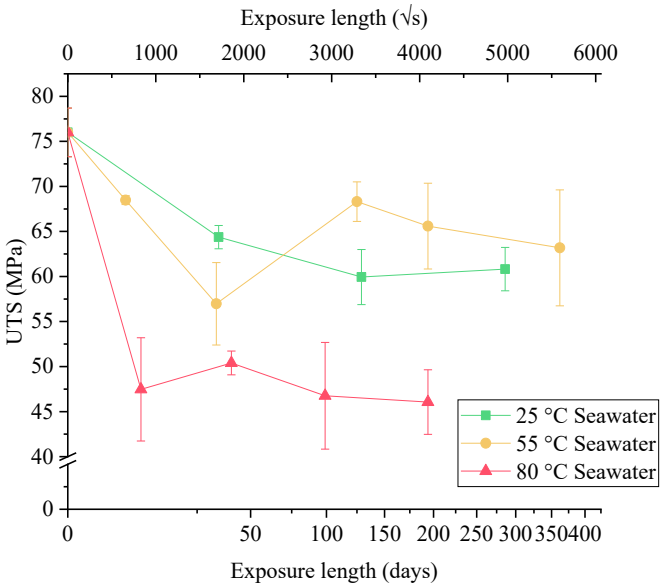

Figure 4-36: the shift of the tensile strength in the epoxy for seawater exposures over time.

The effects of the seawater permeation are quite visible in a progressive weakening of the epoxy over time. The higher the exposure temperature, the more significant the loss in performance. It is also correlated with the degree of saturation of the material, even if is not as well mapped as in the other testing (far fewer experimental data points, as said due to the destructive nature of the test).

The result from the specimens conditioned at 55 °C do not have a monotonic trend and for the tensile strength, in particular, the epoxy seems to regain over 65 MPa after 125 days, at a higher level than the results from the 25 °C exposure. This trend could be partially explained by the fact that the plasticization induced by the seawater allowed for more samples to yield rather than break in a brittle way before

reaching the yield point [7]. A relaxation of curing residual stresses could have favoured the better elasticity of the epoxy [94]. It can be highlighted by the comparison of the strain at maximum stress for the specimens from different exposure temperature (see Figure 4-37). The strains for the specimen at the higher temperatures are in large majority higher than those aged at room temperature. This is an explicit confirmation of the plasticising effect of the water. However, while the strength is significantly affected at the 80 °C, which cannot sustain more than 50 MPa, it results partly beneficial for the specimens from Cond. B. The plasticization effect makes the epoxy less sensitive to internal defects and allows to carry loads all the way up to the yielding point, which can be considered the best tensile performance the material can provide in its condition.

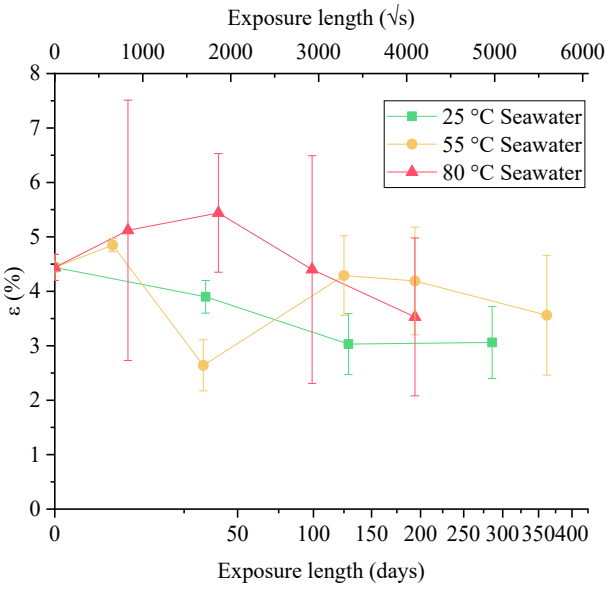

Figure 4-37: the shift of the measured strain at maximum stress for the specimen tested from seawater exposures at different temperature.

The large scatter of the strain for the specimens from Cond. C is indicative of progressive degradation of the epoxy though: it is more acute at a higher exposure temperature. Due to the brittle nature of the epoxy, the strain at maximum stress is not a consistent measurement to monitor the evolution of the material performance.

4.3.4 Tensile tests on neat epoxy from Norsok oil exposure

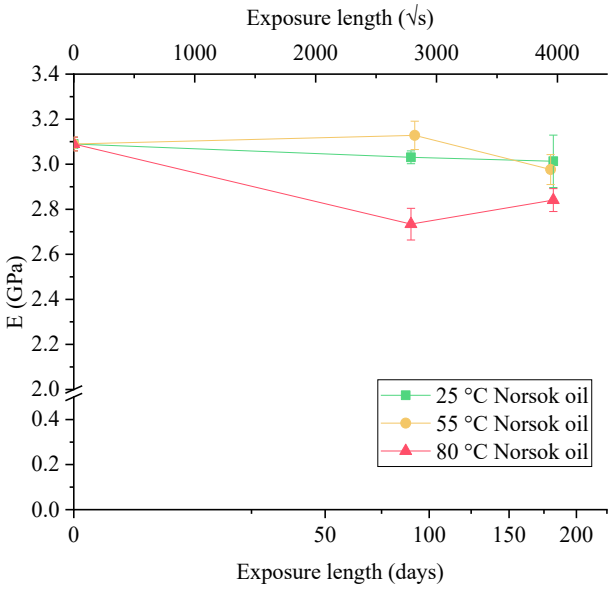

Figure 4-38: shift of Young's modulus in the epoxy in relation to the exposure in Norsok oil.

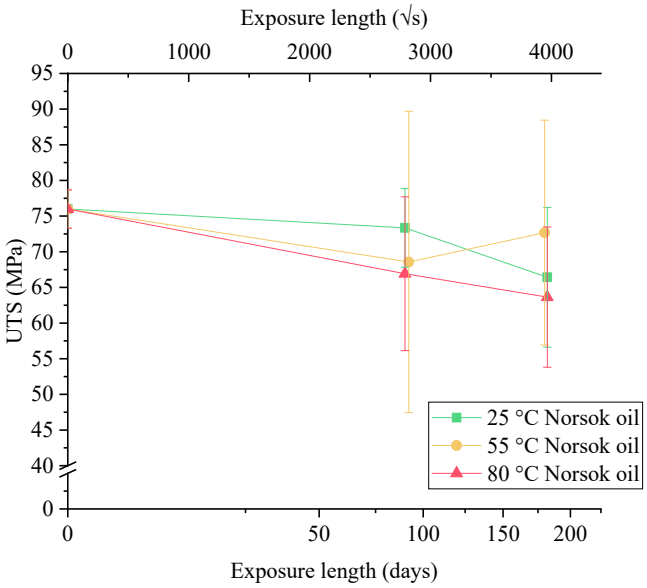

Figure 4-39: shift of the tensile strength in the epoxy in relation to the exposure in Norsok oil.

In agreement with the results from the gravimetric and DMA testing, the Norsok oil seems to have a lesser effect on the mechanical properties. After 3 months of exposure, there is a drop in Young's modulus of the specimens from Cond. O, down to 2.8 GPa, which is slightly recovered after 3 further months, possibly due to some epoxy embrittlement due to thermal ageing [95]. The tensile strength appears to lower below the 70 MPa on average, but there is a large dispersion of values: the difference between the results from different exposure temperatures is not statistically significant.

4.3.5 Tensile test on GFRP from seawater exposure

4.3.5.1 Longitudinal fibre reinforcement

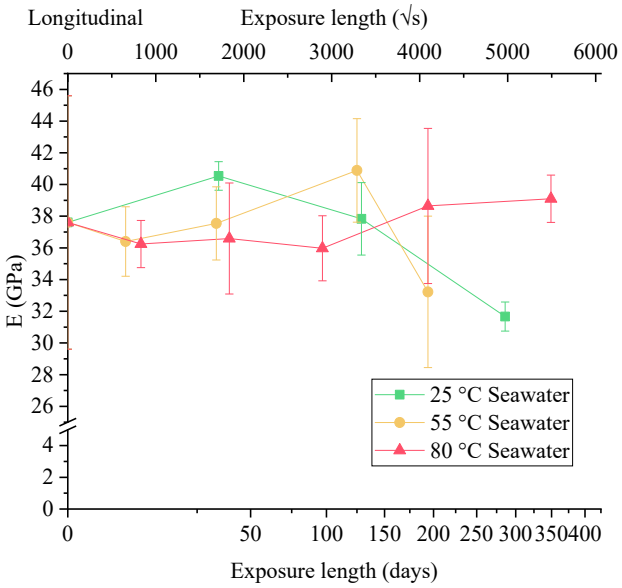

Figure 4-40: shift of Young's modulus of the GFRP in the longitudinal direction of the reinforcement in relation to the exposure in seawater.

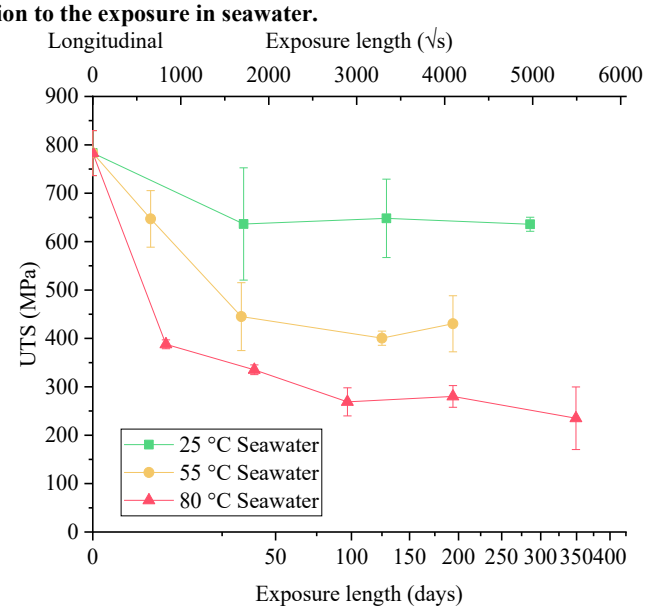

Figure 4-41: shift of the tensile strength of the GFRP in the longitudinal direction of the reinforcement in relation to the exposure in seawater.

The effect of the seawater on the GFRP composite in the direction of the reinforcement fibres is dual. The elastic modulus does not show a clear trend at any temperature, even for exposure up to one year of duration. This suggests that the seawater does not affect the stiffness of the glass fibre, which provides the main contribution to the composite's elastic modulus.

The tensile strength on the other side is greatly affected by the permeation of water: it progressively decreases both due to the exposure temperature and duration. It is likely that the weakening of the matrix, as verified by the tensile test on the

neat epoxy, does primarily affect the way that subcritical defects propagate until the final failure. When pristine, the composite fails with a very energetic and explosive break, the fracture surface is very irregular and usually interest the whole gauge length of the specimen. Along with the progression of the ageing in the material, the failure becomes progressively neater, with an orthogonal sharp main crack (see Figure 4-42). Due to the harshness of the conditioning at the higher temperatures, we cannot exclude completely direct damage to the fibres themselves.

Figure 4-42: picture of broken tensile specimens from Cond B. (a): tested after 5 days; (b): after 6 months of exposure.

4.3.5.2 Transverse fibre reinforcement

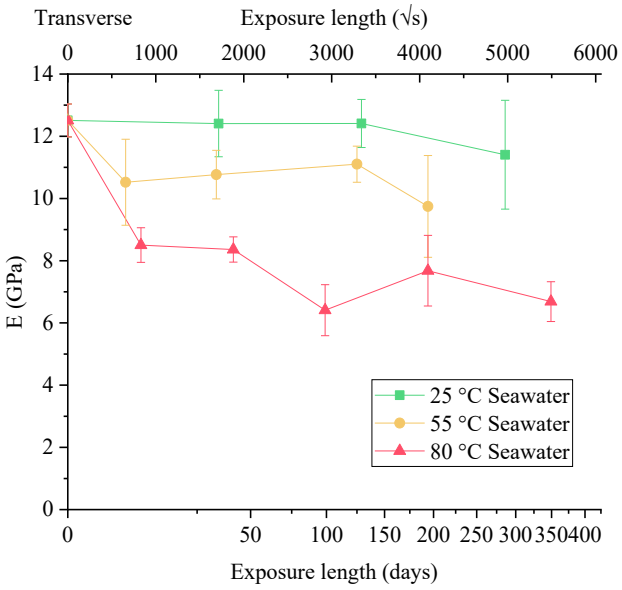

Figure 4-43: shift of Young's modulus of the GFRP in the transverse direction of the reinforcement in relation to the exposure in seawater.

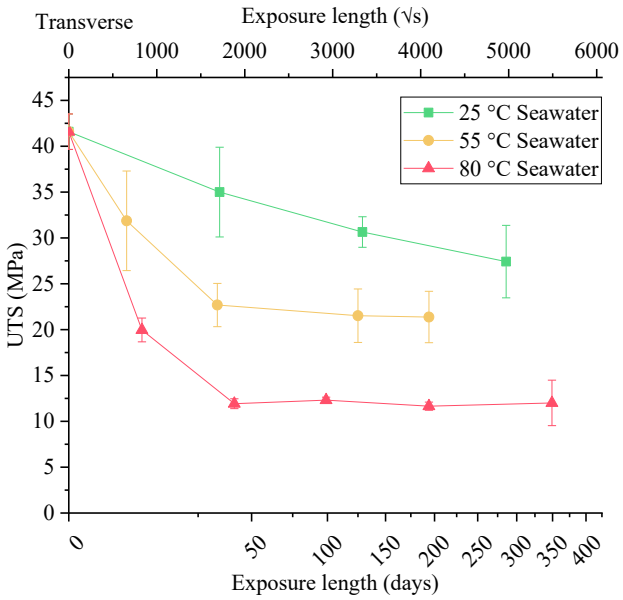

Figure 4-44: shift of the tensile strength of the GFRP in the transverse direction of the reinforcement in relation to the exposure in seawater.

The tests on the transverse direction of the fibre reinforcement brought results much closer to those found for the neat epoxy. For a unidirectional composite, the transverse properties are strictly matrix dominated. Apparently, the drop in the elastic modulus is mainly related to the exposure temperature, rather than the exposure duration. The modulus is lowered to the deficit "wet" value after a few days of exposure, and then it remains relatively unchanged for exposure times up to one year.

The decrease in the strength seems to be more progressive before stabilising at a minimum value. For Cond. B, it seems to settle at about 22 MPa at the same time as the material saturates with water. For Cond C, it took up to a further month after saturation in order to stabilise at 12 MPa. The strength of the samples in Cond A went progressively reducing down to 30 MPa after 286 days, and it would likely continue to reduce if let continue to age.

From the results of the tensile testing, it appears that the main reason for the degradation of the GFRP composite properties is to be ascribed to the weakening of the matrix. Even the loss in strength for the longitudinal direction can be due to different interaction of the fibre-matrix interface, leading to an early fracture of the fibre and eventually of the whole composite.

4.4 Correlation of fluid diffusion and mechanical performance

The results from the gravimetric measurements and the tensile tests were compared in order to understand if there is any correlation between the two phenomena. Young's modulus and tensile strength are plotted against the mass change of the gravimetric coupons, calculated as an average among all the coupons exposed to the same ageing conditions.

The focus was on the seawater exposures, as the mechanical performance appeared to be most affected by it.

4.4.1 Neat epoxy in seawater

(a)

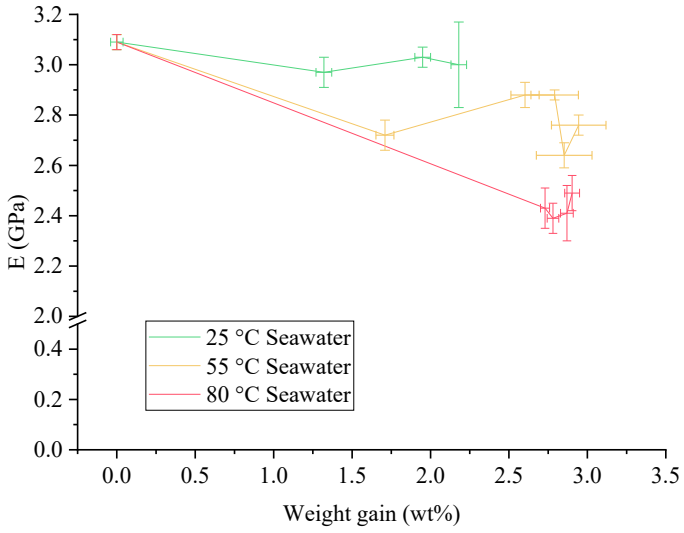

(b)

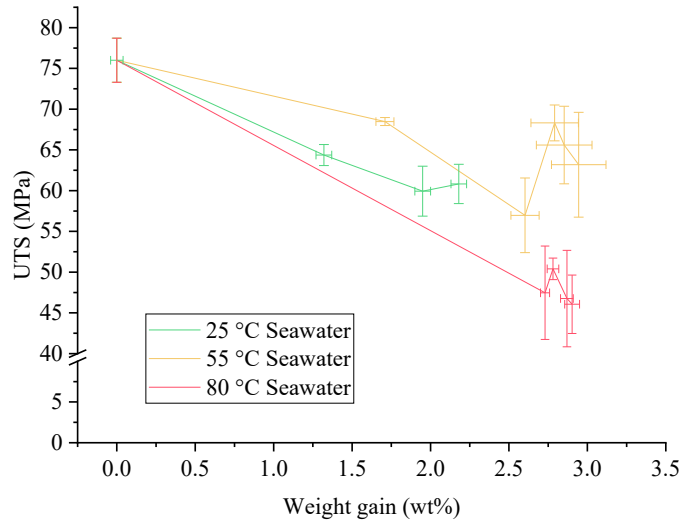

Figure 4-45: mechanical properties in relation to the weight gain for the epoxy exposed to the seawater. (a): Young's modulus; (b): Ultimate Tensile Strength.

From the comparison of the results obtained from the neat epoxy, Young's modulus shows different trends, depending on the exposure temperature. It appears to stabilise at different levels after an initial drop, most likely due to a plasticisation effect of the seawater. However, the degree of plasticisation is mainly determined by the temperature.

The most critical decrease in the mechanical performance happened for the 80 °C exposure, with a drop of elastic modulus to 2.4 GPa and in strength below 50 MPa. As all the test were performed when the epoxy had already saturated (after just 8 days), there are no data for intermediate moisture content.

The results from lower temperature exposures show a more progressive degradation along with the moisture absorption, and they seem to stabilise at higher values than the Cond. C (seawater at 80 °C) scenario. The Young's modulus for the Cond. A appears to be only slightly affected.

The evolution of the tensile strength is less straightforward. The epoxy appears to decrease its strength for increasing values of the seawater absorbed but the exposure at 55 °C shows signs of recovering in strength at a later stage, in contradiction with the other exposure conditions.

4.4.2 GFRP in seawater

(a)

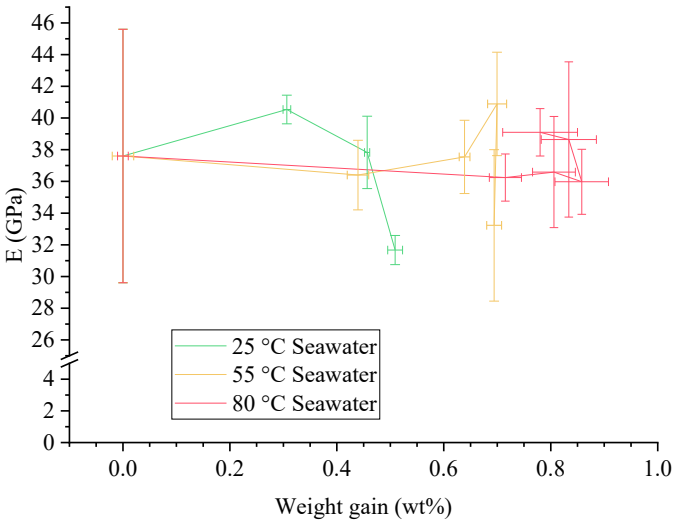

(b)

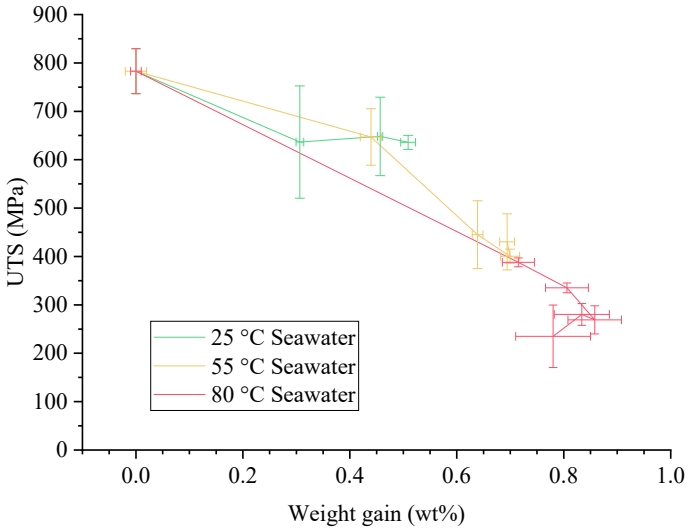

Figure 4-46: GFRP mechanical properties in relation to the weight gain in seawater. In the longitudinal direction of the fibre, (a): Young's modulus; (b): Ultimate Tensile Strength.

The unidirectional composite material was tested both in the longitudinal and transverse direction of the long fibre reinforcement.

For the longitudinal direction (see Figure 4-46), the modulus of elasticity seems to remain almost unchanged, sitting around a value of 37 GPa on average for all the measurement (the initial measurements on the pristine material returned a particularly high standard deviation, probably a higher number of runs would have been required to reduce such value). Despite the large statistical dispersion, this trend is not unreasonable as the material stiffness is mainly dominated by the glass fibres, which are impermeable to water.

The tensile strength, on the other side, appears to follow a decreasing trend as it progressively absorbed more seawater, dropping from 780 MPa down to 235 MPa for the most degraded condition at 80 °C after about one year of exposure.

(a)

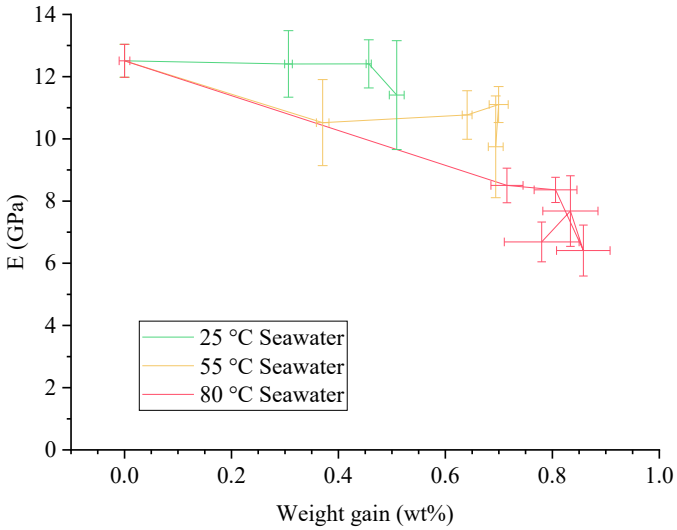

(b)

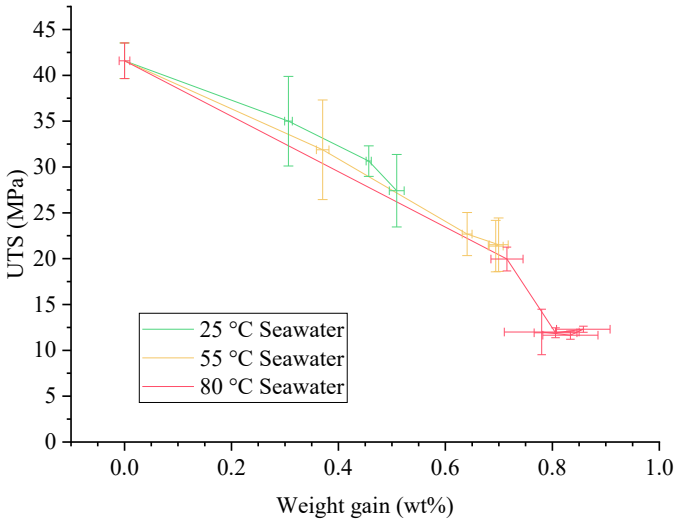

Figure 4-47: GFRP mechanical properties in relation to the weight gain in seawater. In the transverse direction of the fibre, (a): Young's modulus; (b): Ultimate Tensile Strength.

The test on the transverse direction of the composite (Figure 4-47) returned a different trend regarding Young's modulus, closer to what was found for the neat epoxy, with a more severe loss in stiffness at the increase of the exposure temperature. This is consistent as the epoxy matrix dominates the elastic response in the transverse direction for a unidirectional laminate.

The loss in tensile strength, instead, seems to follow the linear trend as for the longitudinal direction: for a level of moisture uptake of 0.8 wt%, the UTS drops just to 12 MPa. It seems that the moisture induces some severe degradation of the matrix and fibre-matrix interface, causing an ineffective load transfer and consequent strength degradation. We cannot exclude some severe degradation of the fibres themselves: they were corrosion resistance grade (E-CR), but the conditioning at the higher temperature is a very demanding scenario even for them [96].

We attempted a basic linear fitting of the UTS of the GFRP in function of the weight gain, for both fibre orientation, in order to quantify the seawater degradation: it is an approximated estimation, but it gives a sense about how the moisture ingress has a detrimental effect on the composite performance.

The relations obtained from the fitting are:

Longitudinal: $$UTS_{long.} = 826 - 606\, wt\% \quad \text{Eq. 4-8}$$

Transverse: $$UTS_{trans.} = 43 - 35\, wt\% \quad \text{Eq. 4-9}$$

(a)

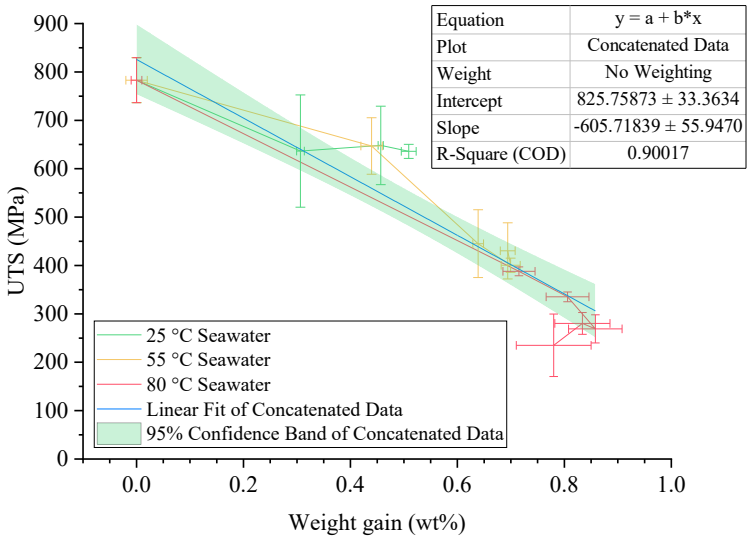

(b)

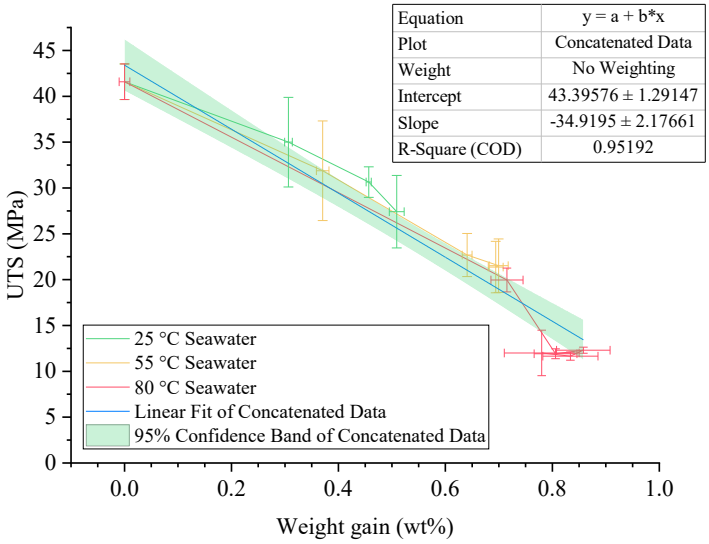

Figure 4-48: linear interpolation of the UTS of the GFRP in relation to the weight uptake, with a 95% confidence interval. (a) longitudinal, (b) transverse direction.

4.5 Mechanical performance prediction

Based on the results from the tensile tests, the calculations of the Time-shift factors was performed, based on the procedure from Silva *et al.* [48]. Comparing the results obtained from the tensile testing, the UTS from the seawater exposures was selected as performance index because it is the one showing the best trends to be used to measure the ageing as it progresses. As later shown, this method seems to work only in the case of the transverse direction of the fibre in the GFRP.

4.5.1 GFRP in the transverse direction

The UTS for the GFRP with the fibre oriented in the transverse direction was plot as the percentage of the Residual Strength (RS) retained by the material at different exposure times, in comparison to the pristine condition:

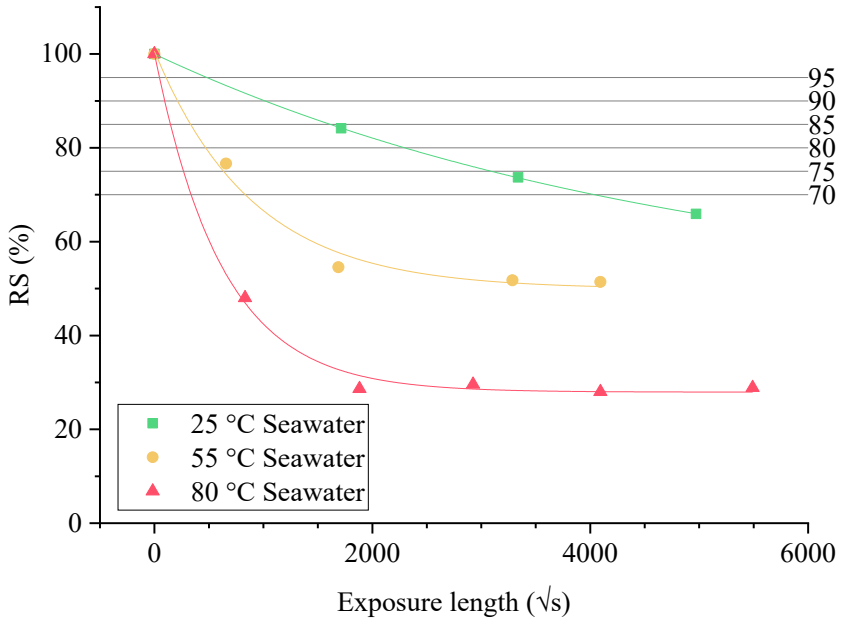

Figure 4-49: Residual Strength in transverse direction for the GFRP exposed to seawater. Different levels of performance drop are highlighted by reference lines.

Only the mean values were taken into account. For each of the exposure conditions, an exponential decay function was evaluated. The fitting was performed using Origin Lab 2019. The iteration algorithm was a Levenberg-Marquardt type. The parameters of the fitting curves are reported in Table 4-9. An exponential decay equation was chosen as able to fit the data in the time-scale of the square root of seconds correctly. It was favoured to the logarithmic relation proposed in [48], which diverges for the exposure time approaching to zero.

Table 4-9: exponential fitting parameter for the RS

Model	*ExpDec1*		
Eq.	y = A1*exp(-x/t1)+y0		
Plot	RS 25 °C	RS 55 °C	RS 80 °C
y0	46.63±0.99	49.90±2.43	27.93±1.09
A1	53.35±0.96	50.74±3.52	72.21±2.16
t1	4895±144	900±169	623±53
R-Square (COD)	0.99	0.99	0.99

For each curve the time to lose a given amount in strength (progressively at 5 % loss), was inversely calculated:

Table 4-10: times to drop at different RS level (in $s^{1/2}$ and s)

RS	25 °C	55 °C	80 °C	25 °C	55 °C	80 °C
%	$s^{1/2}$	$s^{1/2}$	$s^{1/2}$	s	s	s
70	4041.6	834.0	336.8	16334472.0	695504.7	113457.9
75	3092.3	633.9	266.8	9562313.4	401859.7	71199.2
80	2297.5	470.3	203.9	5278721.7	221221.5	41576.4
85	1614.0	332.0	146.7	2604973.8	110195.8	21535.2
90	1014.3	212.0	94.4	1028816.9	44958.6	8911.0
95	480.1	106.2	46.1	230531.7	11283.0	2125.7

If the reference temperature is set at 25 °C, the relative Time Shift Factors are calculated as:

$$TSF = \frac{t_{RS\%}(25\ °C)}{t_{RS\%}(T\ °C)} \qquad \text{Eq. 4-10}$$

The TSF found from the experimental drop times (in seconds) are:

Table 4-11: TSF calculated from the drop times at different exposure temperatures.

RS	25 C	55 C	80 C
%			
70	1.00	23.49	143.97
75	1.00	23.80	134.30
80	1.00	23.86	126.96
85	1.00	23.64	120.96
90	1.00	22.88	115.45
95	1.00	20.43	108.45
Avg.	**1.00**	**23.02**	**125.02**
SD	0.00	1.31	12.90

It appears that the TSFs are reasonably constant down to a 70% RS level. For lower levels, it is not possible to find a corresponding time for the 25 °C exposure without extrapolating outside the experimental data range. If the average TSF are plotted in an Arrhenius chart, we obtain:

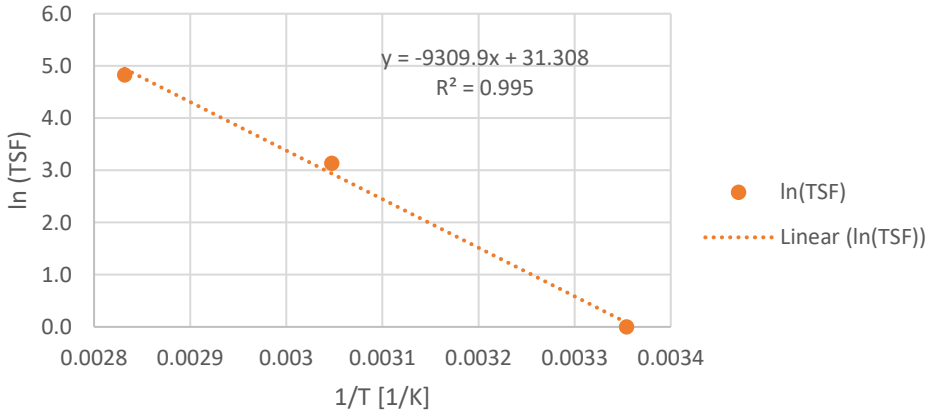

Figure 4-50: Arrhenius plot for the TSF obtained for UTS of the GFRP in the transverse direction.

Hence, an estimated relation of TSF in function of the exposure temperature in relation to the reference temperature of 25 °C (considering that TSF(25 °C) =1) is:

$$\ln(TFS) = \left(-\frac{E_a}{R}\right)\frac{1}{T} + \ln(A) = -9309.9\frac{1}{T[K]} + 31.3 \qquad \text{Eq. 4-11}$$

This allows to estimate the TSF for the whole temperature range and extend it for lower temperatures with reasonable confidence, while it is not reliable to extended to a higher temperature, as the kinetics of the ageing could be affected by other degradation mechanism and further accelerated.

The value of the Arrhenius plot slope is almost double the one reported in the literature (~ 5300 K) [48]. It appears that in our experiment, the degradation rate is significantly higher. There are many factors that can influence this value (harshness of the conditioning, the resistance of matrix, fibre layout). Hence they are not directly comparable, even if it still confirms the order of magnitude of the performance degradation process.

The value of the TSF in absolute is not particularly useful, while more interesting is the relation between two different temperature. From the Arrhenius relation definition, this can be evaluated as:

$$TSF = \frac{t_{T1}}{t_{T2}} = exp\left[-\frac{E_a}{R}\left(\frac{1}{T_2} - \frac{1}{T_1}\right)\right] \qquad \text{Eq. 4-12}$$

So, to evaluate the decrease in the tensile strength in the transverse direction for the GFRP material at a temperature of 4 °C (typical for ocean water), the ageing process can be accelerated through exposure at 50 °C. The corresponding Time-Shift Factor is:

$$TSF = \frac{t_{4\,°C}}{t_{50\,°C}} = exp\left[-9309.9\left(\frac{1}{323} - \frac{1}{277}\right)\right] = 119.9 \qquad \text{Eq. 4-13}$$

This means that the exposure of a month length in seawater at 50 °C induced a loss in mechanical strength of the material equivalent to almost 10 years of operative conditions at 4 °C. This assumption is made without taking into account other environmental factors except for the temperature and the absorption of seawater to which the GFRP is exposed.

4.5.2 Other materials properties prediction

Unfortunately, this approach seems not possible to be applied to the other strength comparative test as the data cannot be properly fitted with the same type of exponential curve which worked on the GFRP in transverse direction:

- For the neat Ampreg 26 (see Figure 4-36), there is an unexplained cross-over of the curves representing the 25 and 50 °C, which makes not possible to determine the average TSF at the different degradation extent.
- For the GFRP in the longitudinal direction (see Figure 4-41), the attempt to fit with the same exponential function (as for the GFRP in the transverse direction), returns a very skewed curve which again makes impossible to calculate TSF proportional to the exposure temperature.

An improved fitting could be obtained by using a bilinear function, but it seemed to overfit (having only 4 points to be connected by 2 segments, there will almost always be a proper way to match all of them as long as they follow a progressive trend). The other issue about using a linear relationship is that the proportionality of the TSF is trivial, and more related to the fitting rather than the material's property.

It appears that with the current set of experimental data, this prediction methodology fails to provide consistently the shift factors in order to evaluate the accelerating action of the exposure on the properties of the materials.

4.6 Considerations on the accelerated ageing and conclusions

An extensive accelerated exposure campaign on neat epoxy and GFRP composite material was conducted in the framework of our research project on the ageing of composite exposed to the simulated marine environment.

The results from the seawater exposures show that:

- Coupons dimensions and orientations have a significant effect on the evaluation of the diffusion coefficient of the materials. This must be taken into account when applying a linear Fickian solution for the recovery of the diffusivity factor: coupons with an elevated side-to-thickness ratio return more reliable gravimetric data. Correction factors, in particular the one suggested by Starink *et al.* [37], help to reduce the influence of the coupons geometry.
- Diffusivity should not be treated as isotropic mass transport. A more refined modelling is required to fully evaluate the influence of fibre orientation and the possible contribution of the fibre-matrix interphase. An improved three-dimensional model of the diffusion kinetics can provide further insight into the analysis of the gravimetric data, but they are more computationally expensive [38,71]. Different fibre type/quality, volume fractions and stacking sequences shall require performing dedicated experimental exposures to provide the basic diffusion parameters and validate any numerical modelling results.
- Temperature is the primary accelerating factor in the diffusion kinetics and degradation of mechanical properties in all scenarios. An Arrhenius relationship was used to describe the degradation rates at different temperatures (see § 4.1.7).
- Seawater showed to be an active diffusant in the polymer. The Fick model was used to calculate all the diffusion coefficients, even though there is evidence of "Langmuir-type" dual diffusion kinetic, in particular at the higher temperatures.
- There is evidence of physical degradation for the material exposed at the higher temperature (80 °C): after more than 6 months in the neat epoxy and about 10 months in the GFRP, a clear weight decrease is identified.
- The shifts in the glass transition temperature for the different exposure conditions show that the initial local minimum happens at about the same time as the material saturates. The data were analysed in light of the findings reported by Zhou and Lucas [92,93] about the two types of bonding of water molecules with the epoxy network. The different bonding can either increase chain mobility or induce secondary cross-linking, hence altering the materials' *Tg*. Higher temperatures and longer

exposures time favour Type II bond, hence an increase in Tg. Moreover, for the GFRP composite, the fibre-matrix interphase seems to play a role in the plasticization effect due to water absorption. When the specimens are re-dried after exposure, the recovery of *Tg* is almost complete, so the process seems to be mostly reversible.

- Finally, the results confirm the feasibility of accelerating the diffusion of seawater in polymer and polymer composites as a reliable way to recover the diffusivity factors at different temperatures and to estimate them for temperatures well below the glass transition of the polymer. The evolution of the glass transition temperature (*Tg*) is more complex to describe due to the concurring mechanism interacting with the polymer matrix.

The aromatic Norsok Oil appears to be absorbed significantly only at the higher temperature of 80 °C for both epoxy and GFRP. The absorption behaviour in not Fickian. The DMA results are not conclusive. The only solid conclusion is that once the oil is adsorbed at high temperature, it cannot be removed by drying at a lower temperature (50 °C) in dry air; on the contrary, the seawater uptake was reversible.

Regarding the tensile tests:

- Mechanical properties are affected by exposure to the seawater. In all of the cases, the matrix dominated performance showed to be the most affected, as expected. The temperature seems to have a stronger influence rather than the moisture ingress.
- The maximum degree of performance loss is achieved at 80 °C exposure. It did not seem to occur with the same extent for the lower temperature ones, even for longer times. Being the exposure temperature close to the Tg of the epoxy, the materials could be prone to an enhanced degradation caused by the viscoelastic nature of the polymer.
- It is our opinion that a safe-life approach must be employed when designing with composite materials. The more they are exposed to demanding conditions, the quicker they will degrade until they (or the components which are made of) will not be safe to operate any longer
- To reduce the experimental data scatter, it is necessary to test 5 or more specimens at any sampling point. It is also essential to take care that the manufacturing and the preparation of the samples are carefully controlled not to introduce any possible source of error, like defects or geometrical deviations. Composite materials are particularly subjected to change in their response if the infusion process or the fibre orientation is not consistent. An even larger number can be necessary to allow a statistical analysis of the performance, in particular regarding the fibre-dominated properties as the longitudinal tensile strength [97,98].

In conclusion, from our experimental data, it appears that:

a) the possibility of predicting the durability of the material is not always feasible and, even when Time Shift Factors are calculated, it is necessary to be cautious when extrapolating data to future timescale.
b) From all the exposures temperatures, it results that the stage at which the material strength is mostly affected is during the first month of the exposure. It is advisable to concentrate the sampling moments mostly during this time interval, hypothetically every 7 days of exposure, in order to add significant data points and obtain a more robust trend for the loss in tensile strength and Young's modulus.

Chapter 5 Epoxy foam and sandwich – Preparation, thermal and mechanical characterisation

The results and discussion on the foam synthesis and characterisation (§ 5.1 to 5.3) have been published in the *Journal of Applied Polymer Science*; they have been adapted from the paper: Cavasin *et al*., *J Appl Polym Sci* **2018**, *135*, 46864 [99]

5.1 Foam synthesis

Polymer foams are interesting from an engineering point of view for their very low density and low thermal conductivity [91,100]. These properties are promoted by the presence of porosities introduced in the polymer in a controlled manner. Different technologies are used to generate the bubbles of required dimensions and to have them distributed homogeneously. In a way, the epoxy foam can be considered as particle composite materials, where the secondary phase is represented by the porosities surrounded by the polymer matrix. The gas present in the pores, usually air, reduces the weight of the overall composites and provides the thermal insulation. They are also called cellular solids, in particular when referring to *syntactic* foams, where the material does not undergo a proper foaming process; instead, hollow spheres of required dimensions are mixed to a polymer matrix [101].

The foam preparation was based on the technique of adding a *Chemical Foaming Agent* (CFA). It follows a formulation presented in a paper by Stefani et al. [10,102], where a disiloxane was used to react with the amine hardener while the resin was still in an uncured state and produced gaseous hydrogen to act as the foaming agent.

5.1.1 Initial trials

The Chemical Foaming Agent (CFA) used was a 1,1,3,3-tetramethyl disiloxane purchased from Sigma Aldrich. It is a transparent, non-toxic and flammable liquid.

The first attempts were performed just by simple trial and errors approach. Using small batches of resin, different amounts of hardener were added at different stages of curing in order to understand the foaming effect better.

Even if the formulation was obtained from the literature, the detailed preparation routine needed to be optimised step by step (see Figure 5-1). At first, the CFA was added directly to the resin before the hardener and mixed until appeared homogeneous. Then the hardener followed. Some early bubbling was beginning since the hardener addition, but due to the low viscosity of the resin mix, the bubbles quickly escaped through the surface. The final result presented very poor foaming, with a few large bubbles distributed unevenly. Indeed, more than a foam it appeared to be an epoxy with some large porosity.

The early bubbling could be responsible in consuming a relevant amount of CFA without really contributing to the foaming process, as the gas would escape by nucleating in small bubbles, climbing upwards and evaporating at the surface.

A second option was to add the CFA after the hardener. Waiting for a pair of hours and leaving the resin at rest, it allowed the hardener to react primarily with the epoxy resin first and reduce its activity. While the viscosity of the resin was still relatively low, the CFA was added and mixed until homogeneity, trying to introduce as little external air as possible. Some bubbling happened at the mixing but in a minor extent compared when adding the CFA at the beginning of the curing. Significative nucleation of bubbles could be induced by a more intense mechanical stirring at this stage. However, the bubbles quickly tended to coalesce and eventually escape from the surface, resulting in poor porous samples. The viscosity of the resin was still not enough to retain most of the bubbles formed.

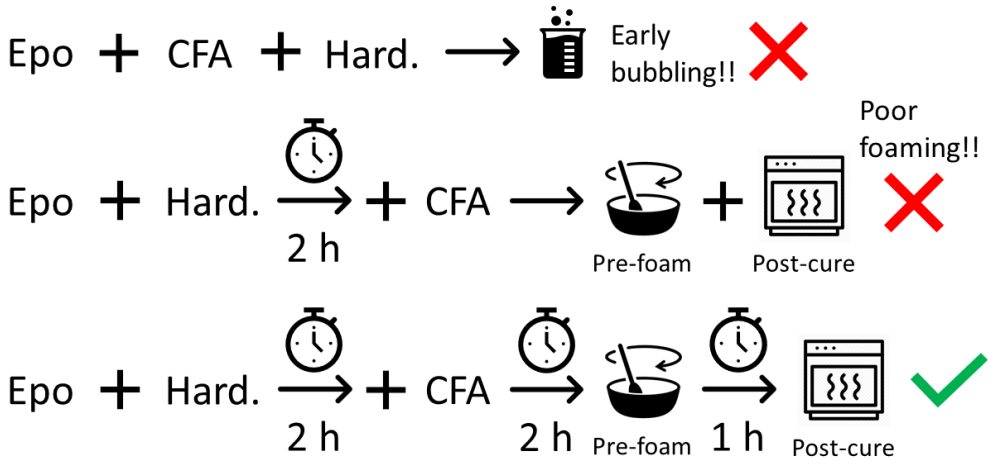

Figure 5-1: summary of the different trials to find a proper foaming routine.

The following trial stage was set to find a proper waiting time between the addition of the CFA and a proper mechanical stirring to stimulate the bubble nucleation, which is given the name of "pre-foaming". The trials showed that the more viscous was the epoxy resin at the time of pre-foaming, the better the bubbles retention and ultimately the foam quality.

Many factors contribute to the foaming reaction, the main ones are the temperature of the mixed resin, directly influenced by the curing heat released, and the amount of the CFA added. The viscosity of the resin is critical for the proper foaming mechanism, and the curing kinetics can abruptly trigger the gelification, which can happen in a matter of few minutes, posing a relevant processing difficulty. As reported in the literature [54,55], the optimal viscosity range to obtain a narrow pore size distribution is reached at the gel point. This leaves a very short window for processing the curing resin into the foam: a controlled pore size ensures consistent foam quality and improved mechanical properties.

Hence, the most suited time to proceed with the pre-foaming was as close as possible to the gel-point of the resin. The epoxy technical datasheet [58] indicates about 4 h to reach gel-point at room temperature. This was confirmed by the subsequent trials, with some deviation due to the amount of resin mixed. When larger amounts (> 50 g) were mixed, some significant thermal runaway could happen. These are localised hot-spots which can significantly accelerate the curing reaction of the epoxy: this triggers a chain reaction as more heat is realised and the curing rate is further accelerated. The thermal runaways caused abrupt and messy curing of the resin, without the possibility of obtaining a foam. This phenomenon can be controlled either by splitting the mixed batch into smaller amounts or preparing some water thermostat bath in order to remove the excessive curing heat. If the waiting time was set properly, the resin mix was pretty thick but workable. As the bubbles nucleated, it turned from a transparent gel to an opaque milky one. At this stage, it is still possible to pour it as a liquid, so it is the ideal time to transfer the mix to a mould of the desired shape.

Once the homogenous pre-foam is obtained, it would seem reasonable to start the high-temperature post-cure straight away, not to lose the metastable bubble distribution and possibly to further promote the foaming process. Since the very first attempts, it was ruled out as practise not to follow. Due to the typical initial reduction of viscosity in uncured thermoset at the temperature increase, after a few minutes of post-cure, the foam structure was completely lost, leaving the original neat epoxy.

Contrariwise, waiting for longer allowed the gelification process to continue until the pre-foam was almost solidified, showing very high viscosity. The high viscosity retained the bubbles and the porosity distribution did not change significantly. Such a semi-solid condition was achieved after about one hour since the pre-foam mixing. At that point, it was possible to perform the high-temperature post-cure without the destruction of the foam morphology.

Performing the proper heating process, the foam would further develop, growing in pore size and reducing density. Both forced and natural convection oven were used. Force ventilation was found to promote intense foaming but generated significant inhomogeneous bubble growth. Porosities on the upper surface grew significantly more than those in the core of the batch, as the open surface was

directly exposed to the hot airflow. Natural convection was found to allow for slower but more uniform heating; the foam growth was minor, but it produced a more refined bubble distribution.

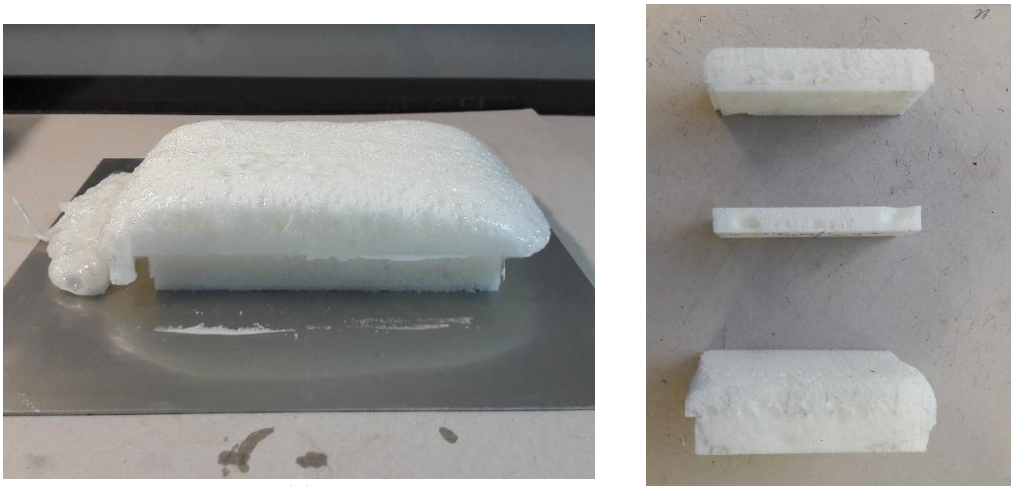

(a) (b)

Figure 5-2: main defects due to foaming in a forced ventilation oven (batch H#3). (a) excessive foam growth; (b) inhomogeneous morphology, large bottom bubbles and open porosities.

The formation of large porosity at the bottom area of the batches represented another issue, due to the coalescence of smaller bubbles caused mainly by an improper degree of viscosity. In order to mitigate the developing of such defects, the metal bottom of the mould was substituted with a transpiring peel ply (the same kind used for vacuum bag infusion). The mould was then laid on a steel grid to allow the excess gas to escape.

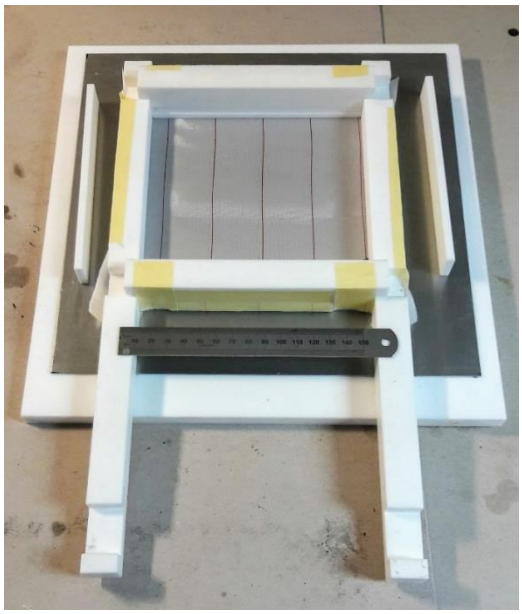

Figure 5-3: modified PTFE assembly mould with peel-ply as the transpiring bottom.

5.1.2 Effect of the CFA on foam density

Once a reliable foaming procedure was determined (see description in § 3.3), samples of the epoxy foams obtained with the addition of increasing siloxane content, from 1 to 5 wt% are shown in Figure 5-4.

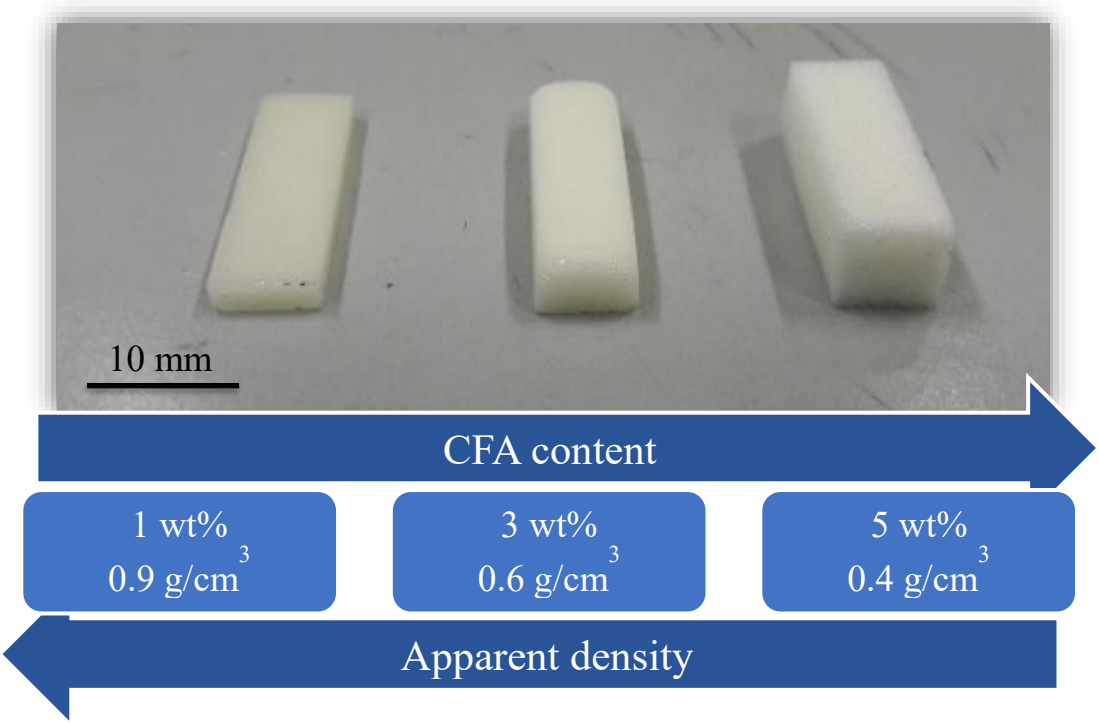

Figure 5-4: epoxy foams obtained by the addition of increasing content of the siloxane CFA.

In Figure 5-5, the foam density as a function of CFA content is reported. The apparent density was measured as the ratio of the sample mass and the external parallelepiped volume:

$$\rho_a = \frac{m}{V_{parallelepiped}} \qquad \text{Eq. 5-1}$$

As expected a significant decrease in the apparent density was achieved, from 1.2 g/cm^3 for the bulk epoxy material down to 0.4 g/cm^3 for the foam synthesized with the addition of 5 wt% of CFA. Few trials with a higher fraction of CFA, up to 7.5 wt%, were attempted but the foam produced did not show a significant further reduction in density. This may be due to the limited amount of CFA that could be dissolved in the resin: for fraction over the 3 wt% the disiloxane was progressively less prone to mix, floating at the top of it (0.76 for the CFA vs 1.11 g/cm^3 for the uncured epoxy) and longer mixing times were necessary to reach a good homogeneity. As the disiloxane has discrete volatility (vapour pressure of 150 hPa at 25 °C), it can likely be that the excess quantity over the 5 wt% evaporates and disperse before any reaction with the resin takes place.

The amount of CFA to be added was then set at 5 %wt. This fraction of foaming agent was found to be the most effective in returning a satisfactory development of

a uniform porous structure and allows a significant reduction of the bulk epoxy density.

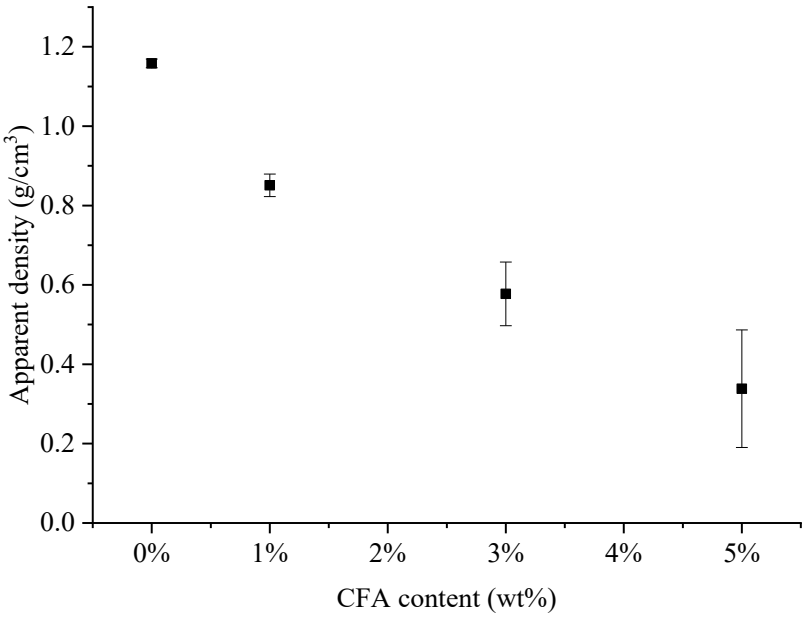

Figure 5-5: density of the crosslinked epoxy foam as a function of CFA content.

5.1.3 Influence of the CFA on curing

The foaming reaction is possible by the condensation of the amine groups of the hardener and the hydrogens of the disiloxane [10]. This could lead to a stoichiometry imbalance if there are too many amine groups reacting with the CFA rather than forming the polymer network with the epoxy.

To evaluate if the CFA had any detrimental effect on the curing of the epoxy resin, the glass transition temperature of the different formulations can provide information about the proper curing degree. Dynamic Mechanical Analysis was performed to evaluate if there was a significant influence of the foaming agent on the Tg. The glass transition was evaluated both at the drop onset of the storage modulus and at the tanδ peak.

Table 5-1: glass transition temperatures for the neat epoxy and epoxy foam at different CFA content (average ± standard deviation).

wt% CFA	*E' drop onset Tg*	*tanδ peak Tg*
	°C	°C
0%	86.4 ± 0.9	97.8 ± 0.9
1%	86.1 ± 2.3	96.7 ± 2.7
3%	83.0 ± 0.1	95.5 ± 3.5
5%	85.2 ± 2.5	96.8 ± 3.1

From the results, it can be seen that there is not a substantial deviation of the average values of the Tg for the increasing amount of CFA added. Only a drop of about 3 °C for the 3 wt% formulation which is partially recovered at the higher concentration. In general, there is an increase in the foam samples' Tg standard deviation: this may be due to the partially different room temperature curing time followed during the foam preparation, as for different amounts of CFA determined different gel-times.

In conclusion, the addition of the CFA has no major effect on the curing kinetics of the epoxy acting as foam matrix.

5.1.4 Degradation temperature

Another feature of the epoxy that could have been affected by the CFA introduction is its thermal stability. To evaluate it, Thermal Gravimetric Analysis (TGA) in an inert atmosphere was performed to evaluate at what temperature the organic polymer degrades by pyrolysis. In this process, the carbon backbone of the polymer is destroyed into its moieties, most of which are volatile and evaporates due to the high temperature. From the gravimetric curve recorded during the temperature ramp, it is possible to evaluate the onset of such degradations. The onset was measured as the temperature at which 5 wt% of the original mass is lost, named *T5%*. Considering that the samples were conditioned in the standard laboratory atmosphere, i.e. they were dry, such a mass loss was a clear indicator of significant matrix degradation.

Table 5-2: results from the TGA runs performed on the neat and foamed epoxy.

CFA content (wt%)	*T5% (°C)*	*Char residual (wt%)*
0	336.1	6.9
1	335.1	8.1
3	332.4	9.4
5	322.3	10.1

The gravimetric plots show a single clear transition for all the formulations, confirming no secondary reaction (decomposition, moisture evaporation, etc.) was taking place, beside the epoxy pyrolysis.

From the results, it turns out that for increasing amounts of CFA there is a progressive decrease of the T5%, which can be taken as the temperature at which the pyrolysis degradation starts to happen extensively in the material. The table also reports the char mass residual, which is increasing with the content of CFA added. The increment is due to the degraded remaining of the foaming agent, which transformed in some degenerate silicate, and it does not react with a maximum temperature of 450 °C [102].

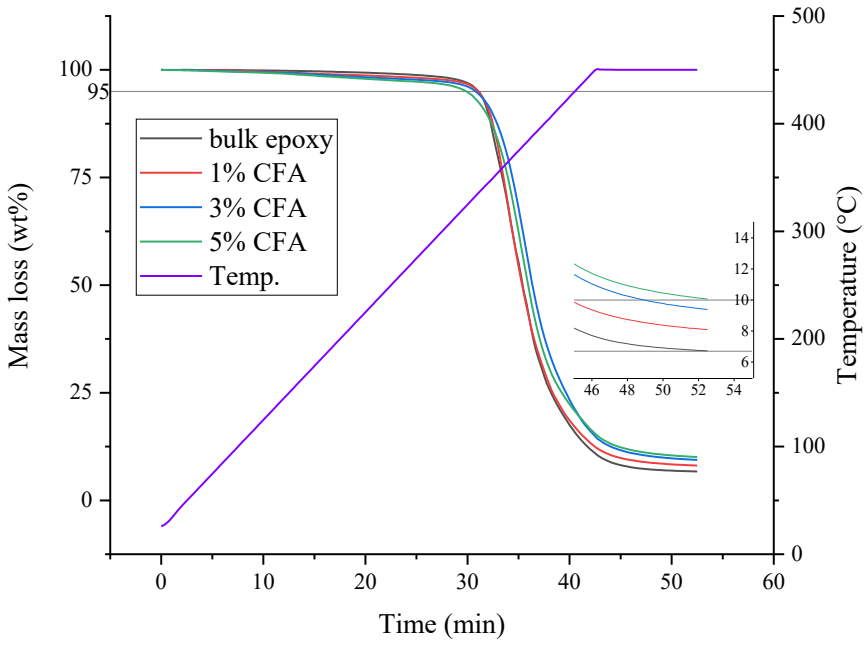

Figure 5-6: gravimetric curves for the TGA run on the different formulations of the epoxy foam.

5.2 Foam mechanical and thermal performance

The foam samples obtained were tested to evaluate the performance from a mechanical and thermal point of view. The 5 wt% CFA foam is the most promising formulation for the lower apparent density achievable, hence higher thermal insulation. For this reason, the mechanical characterisation focused on crosslinked epoxy foams obtained by this formulation. Since the sample preparation, the foam showed excellent elasticity and machinability, with no shattering even for thin section cut.

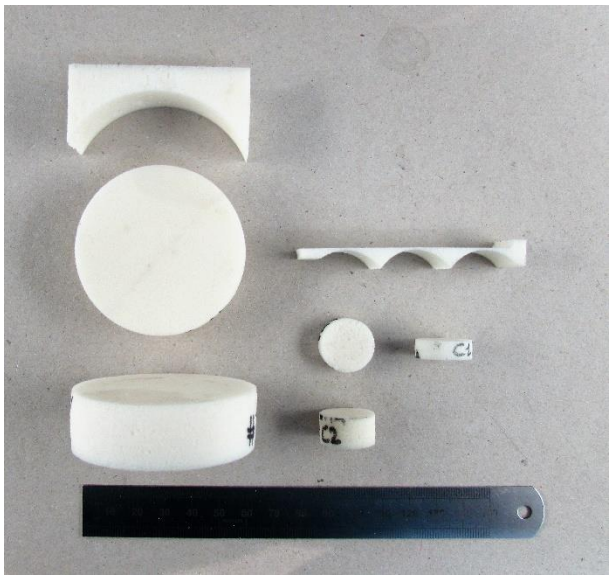

Figure 5-7: some example of samples and cut-offs obtained by the 5 wt% CFA foam formulation.

Quasi-static compression and 3-point bending mechanical tests were performed on foam specimens. To compare the performance, bulk epoxy specimens were tested in the same loading configurations. Characterising materials with such different morphologies is not a trivial task, as their mechanical properties can vary in a considerable extent and in this case the applicable test standards are different.

5.2.1 Compression test

Unidirectional compression is a common mechanical test to be performed on cellular materials. Foams are known not to be able to sustain high tensile stress. If the material, as this foam, is also brittle even gripping it to the clamps is not trivial in order not to affect the test results. Therefore, compression testing is recommended.

The foam test specimens were cylinders as defined by the ASTM D1621: their diameter was 58 mm, the height varied between 20÷30 mm, depending on the available thickness of the foam batch. The epoxy foam specimens were manufactured by CNC machining, to achieve good dimensional control on a shape like a cylinder. Only two test runs were performed per batch, due to the large dimensions of the specimens, which consumed a relevant amount of the foam slab. The crosshead displacement rate was 2 mm/min, about 10% of the specimen thickness per minute.

The neat epoxy cylinders instead were directly cast using some tubular mould with a diameter of 13.6 mm and a height of about 50 mm. The crosshead displacement rate was 1.3 mm/min, as prescribed by the applicable test standard ASTM D695.

The compressive stress was calculated as:

$$\sigma_{comp.} = \frac{F}{A} \qquad \text{Eq. 5-2}$$

where F is the measured force at the load cell and A is the cylinder cross-section area. The nominal compressive strain was measured as:

$$\varepsilon_{comp.} = \frac{\Delta h}{h_0} \qquad \text{Eq. 5-3}$$

where Δh is the deformation measured by the cross-head displacement and h_0 is the original height of the cylinder.

The elastic modulus was calculated from the slope of the linear interpolation of the steepest section of the stress-strain curve.

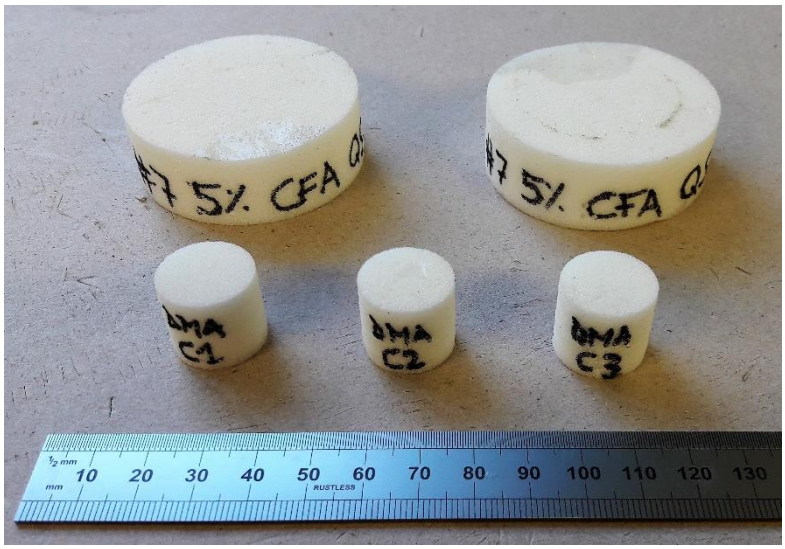

Figure 5-8: some of the epoxy foam specimens for the quasi-static compression and DMA tests.

During the compression test, none of the foam samples has failed (meaning as they did not crack or break in an explosive way), hence the run is ended at 25% of nominal strain. The deformation mainly happens by barrelling [82] and crushing of the porosity, with an increase of the apparent density. The bulk epoxy specimens tend to buckle instead, and the tests were interrupted after the maximum stress was reached, around 6% of strain.

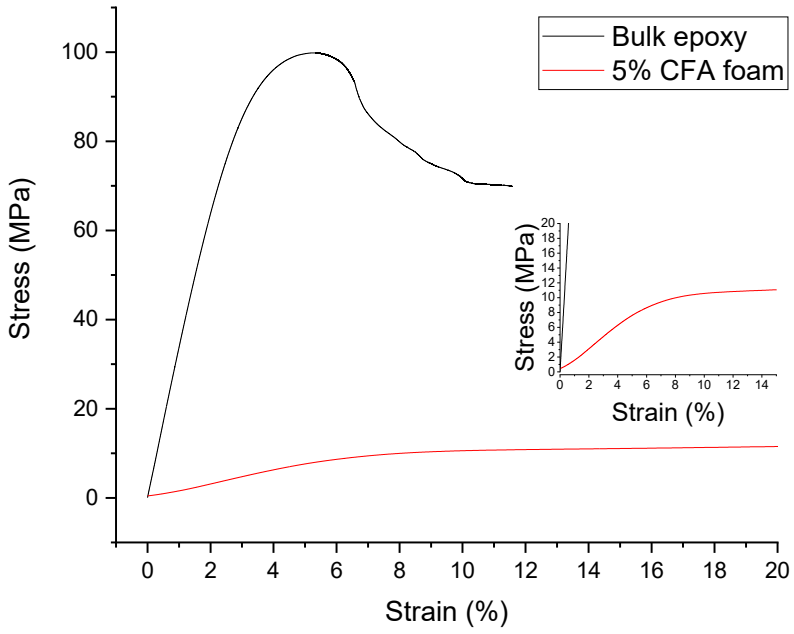

Figure 5-9: stress-strain curves for epoxy bulk and foam samples (two single runs) in compression. The inset magnified the stress level for the foam curve.

From an immediate analysis, the properties of the foam could appear to be poorly performing in comparison to the bulk material. This is due to the fact that the

geometric dimensions input to calculate the stress does not take into account the relevant reduction of the cross-section surface due to the presence of the porosity of the foam. The specific mechanical properties are more representative of the true performance: in general terms, these are the mechanical properties divided for the apparent density of the material itself. It is immediate that such parameters strongly favour the materials with a lower density. However, this is not a simple expedient to promote lighter materials. To compare the mechanical performance of different materials, it is useful to consider some of their physical properties, which become relevant for such design where the weight of the structure is a constraint. This is typical in aerospace and transport engineering design, but it can be relevant to other structural applications. The increase of a load to carry can be sustained by a proportional increase in the resisting cross-section, but the overall increase in the weight of the structure could make the design no more "sustainable". This is quite evident for lightweight structures such as wings, suspended structures, bridges [103].

Two typical density specific mechanical indices used are:

a) Specific modulus:

$$\frac{E}{\rho} = \frac{elastic\ modulus}{apparent\ density} \qquad \text{Eq. 5-4}$$

b) Specific strength:

$$\frac{\sigma}{\rho} = \frac{yield\ or\ tensile\ strength}{apparent\ density} \qquad \text{Eq. 5-5}$$

These metrics are immediate to calculate from the results of the compression test:

Table 5-3: comparison of the performances of bulk and foamed epoxy in compression.

Material	*ρ [kg/m³]*	*Comp. E [MPa]*	*Comp. E/ρ [MPa·m³/kg]*	*Comp. σ [MPa]*	*Comp. σ/ρ [kPa·m³/kg]*
Bulk epoxy	1150 ± 10	3330 ± 84	2.895	100.5 ± 1.1	87.4
5% CFA foam	400 ± 20	155 ± 3	0.386	10.4 ± 0.2	26.0

It is evident that in compression the bulk epoxy is still superior to the foam, both for stiffness and strength. For the same weight, the porous structure offers less resistance to the compressive loads.

5.2.2 Three-point bending test

The flexural test is common for evaluating the performance of polymer foam, in particular in the three-point bending configuration. The advantage of such a test is

the ease of the test specimen preparation and that it is not needed to grip the specimen.

The stress state applied to the specimen is not uniform, and usually, the break happens at the midpoint on the opposite side (also said the outer fibre) from which the load is applied, where the maximum tensile stress is generated.

The test runs were performed following relevant standards: the ASTM D790 for the neat epoxy as bulk, and the ISO 1209 for the epoxy foam (as it was not possible to find a specific ASTM standard relating to cellular polymer material).

The maximum flexural stress is calculated as:

$$\sigma_{flex} = \frac{3}{2} \times F \times \frac{L}{wt^2} \qquad \text{Eq. 5-6}$$

Where F is the force measured at the load cell, L is the bending span length, w is the width and the t is the thickness of the specimen cross-section.

The flexural strain is calculated as:

$$\varepsilon_{flexural} = \frac{6Dt}{L^2} \qquad \text{Eq. 5-7}$$

Where D is the displacement measured by the moving crosshead, t is the specimen thickness and L is the bending span.

The apparent flexural modulus was calculated using the slope of the steepest linear section of the stress-strain curve.

The epoxy foam specimen geometry had to be modified as it was not possible to manufacture samples of the required length (350 mm); it was scaled down, but the proportions were maintained. The thickness was chosen in order to be representative of the material, at least one order of magnitude larger of the characteristic dimensions of the pores. The epoxy foam specimens had the following nominal dimensions: an overall length of 120 mm, 17.6 mm wide and 4.6 mm thick. The span used was 72 mm long. The crosshead displacement rate was 20 mm/min.

For the bulk epoxy, the specimen nominal geometry was: length of 80 mm, 12.1 mm wide and 4.6 mm thick. The bending span was 48 mm long. The crosshead displacement rate was set at 12.8 mm/min, in order to obtain a strain rate of 0.1 min^{-1}.

In the flexural test, the epoxy foam showed a relatively brittle behaviour, failing just below 5% of flexural strain. The bulk epoxy well exceeded this value, allowing a good amount of plastic deformation before failure, which is remarkable for a relatively brittle material. The strength of the bulk epoxy was evaluated at 5% of strain, as prescribed by the relevant standard.

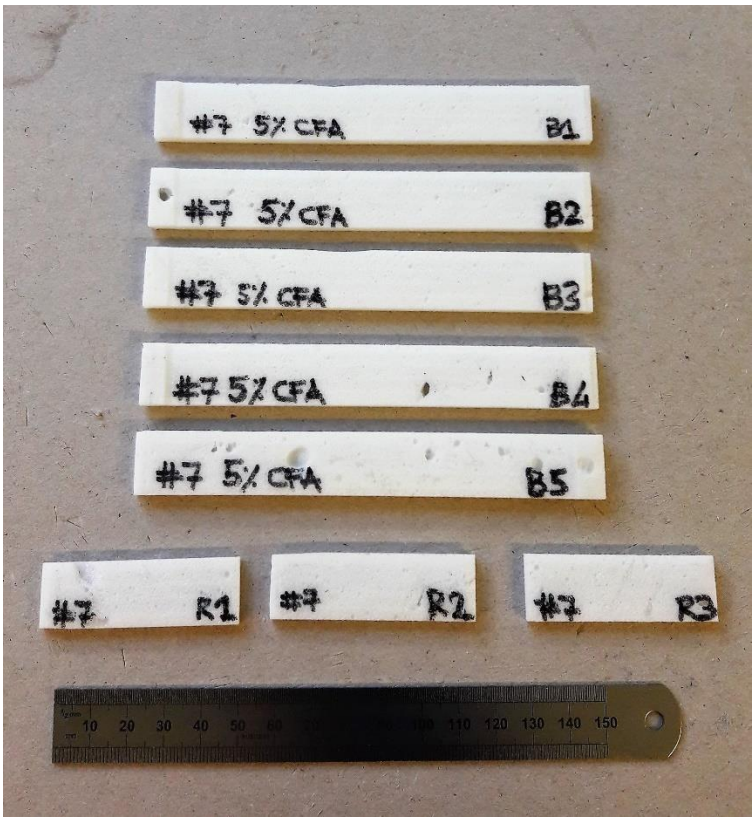

Figure 5-10: the epoxy foam specimens for the quasi-static three-point bending and DMA tests.

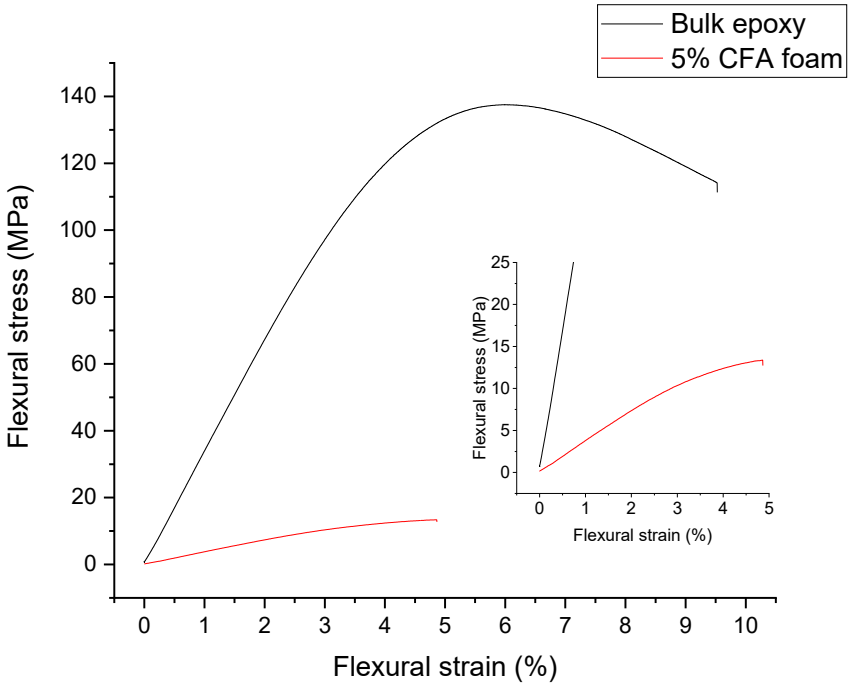

Figure 5-11: stress-strain curves for epoxy bulk and foam samples (two single runs) in bending. The inset magnified the stress level for the foam curve.

Similarly to the compressive loading, specific performance indices can be calculated. As the stress state is no more uniform across the cross-section, the distribution of the loads on the cross-section is no more simply determined by its area, but rather by the area moment of inertia relative to the bending plane [103]. Because of this and depending on how many degrees of freedom are allowed to the cross-section geometry, the specific performance indices are modified as follows:

Stiffness	$\frac{E^{1/2}}{\rho}$ for beams	$\frac{E^{1/3}}{\rho}$ for plates	Eq. 5-8
Strength	$\frac{\sigma^{2/3}}{\rho}$	$\frac{\sigma^{1/3}}{\rho}$	Eq. 5-9

The indices so calculated are the following:

Table 5-4: flexural elastic moduli and relative performance indices for bulk and foamed epoxy.

Material	*ρ [kg/cm³]*	*Flex E [MPa]*	*Flex E/ρ [MPa·m³/kg]*	*Flex $E^{1/2}$/ρ (beam)*	*Flex $E^{1/3}$/ρ (plate)*
Bulk epoxy	1150 ± 10	3404 ± 55	2.948	1.561	1.283
5% CFA foam	400 ± 20	378 ± 7	0.941	1.529	1.799

Table 5-5: flexural strength and relative performance indices for bulk and foamed epoxy.

Material	*ρ [kg/cm³]*	*Flex σ [MPa]*	*Flex σ/ρ [kPa·m³/kg]*	*Flex $\sigma^{2/3}$/ρ (beam)*	*Flex $\sigma^{1/2}$/ρ (plate)*
Bulk epoxy	1150 ± 10	132.3 ± 1.1	114.6	22.49	9.96
5% CFA foam	400 ± 20	12.6 ± 0.6	31.3	13.46	8.82

From these results, it is evident how the foam material is more efficient when subject to flexural loads. In particular for the plate configuration, i.e. when the thickness of the section can change only, the stiffness index is even higher than the bulk epoxy's. For this very reason, foams or cellular materials are usually employed as composite sandwich cores [103].

5.2.3 Thermal conductivity

The thermal conductivity was measured on samples of foam with different CFA content. As expected, the apparent density of the samples directly influences the heat transfer in the epoxy. The porosity distribution offers a much less direct path for the heat conduction, as the air that fills the voids provides a very good insulation effect. Other heat transfer mechanisms contribution can be neglected: convection is likely to be minimal in pores with a diameter of the fraction of a millimetre, while the radiation contribution at few tens of °C or lower is negligible.

The conductivity values from the Guarded Hot Plate (GHP) test are reported in Figure 5-12. As expected, an evident decrease of thermal conductivity is measured for the lighter foams, thanks to the increasing amount of CFA introduced in the formulation. The thermal conductivity decreased from 0.24 W/(m·K) for the bulk crosslinked epoxy resin down to 0.07 W/(m·K) for the crosslinked foams obtained adding 5 wt% of CFA. The substantial decrease of the thermal conductivity by decreasing polymer density can be addressed to the lower proportion of solid epoxy and the increased air volume fraction, which is characterized by a much lower thermal conductivity (0.026 W/(m·K)) compared to the epoxy polymer [104].

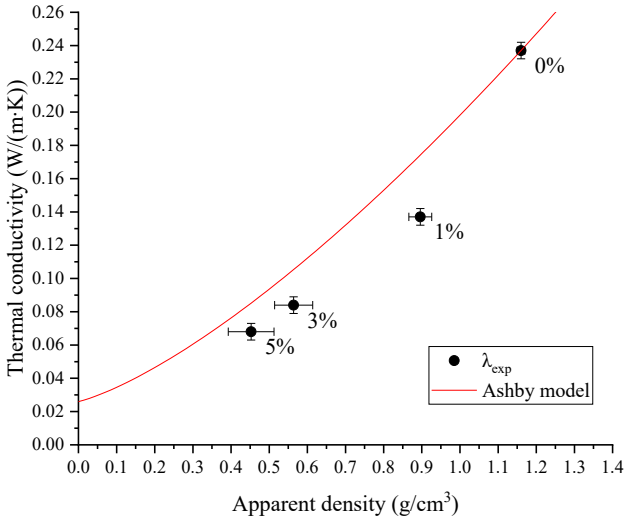

Figure 5-12: thermal conductivity of bulk epoxy and foams at 25 °C in relation to its apparent density. The percentages indicate the foaming agent wt% added to the relative foam formulation.

The increased apparent density leads to a decrease of 70% of the original bulk epoxy conductivity. Taking into account only the thermal conduction as heat transfer, Ashby proposed an analytical model for cellular materials [75]. It relates the thermal conductivity to the relative density (ρ_r), which is the ratio between the apparent density of the foam and the bulk polymer's, in the following equation:

$$\lambda_{foam} = \frac{1}{3}\left(\rho_r + 2{\rho_r}^{3/2}\right)\lambda_{epoxy} + (1 - \rho_r)\lambda_{air} \qquad \text{Eq. 5-10}$$

The model slightly overestimates the foam conductivity, but it predicts the same trend as shown by the experimental data. A conductivity value of 0.06÷0.07 W/(m·K) for the formulation at 5 wt% CFA content is competitive with other passive insulation materials [104].

This test was performed by Dr Samuele Colonna and Prof Alberto Fina from Politecnico di Torino, on a TPS 2500S (Hot Disk AB, Sweden) at the EMC laboratory, in Alessandria (ITA).

The thermal conductivity was also evaluated in function of the environment temperature. It was relevant to understand if there was any significant change in the heat conduction as the material could be employed from sub-zero up to a few tens of °C [8]. The higher limit is represented by the glass transition temperature (see § 5.1.3), at which the foam loses its mechanical stability and would collapse under any load. With this epoxy foam, it can be set at 70 °C, to keep a safe margin.

The test samples were obtained from batches of the 5 wt% CFA formulation. They were cut in disks of an approximate diameter of 56 mm and thickness of 5 and 10 mm. The test was performed using the TA Fox 50 Heat Flow Meter. The use of two-thickness analysis [80] allowed to reduce the error related to the contact resistance between the material and the heat sources: considering the low conductivity of the foam material, such an error is relatively low.

The test was run at different average temperatures (25, 45 and 65 °C). Higher temperatures caused the sample to be squeezed between the testing plates because of the approaching to the glass transition. The results show a progressive linear increment of the conductivity with temperature, but at a slope of $1 \cdot 10^{-4}$ W/(m·K^2), so for practical purposes, it can be considered as constant.

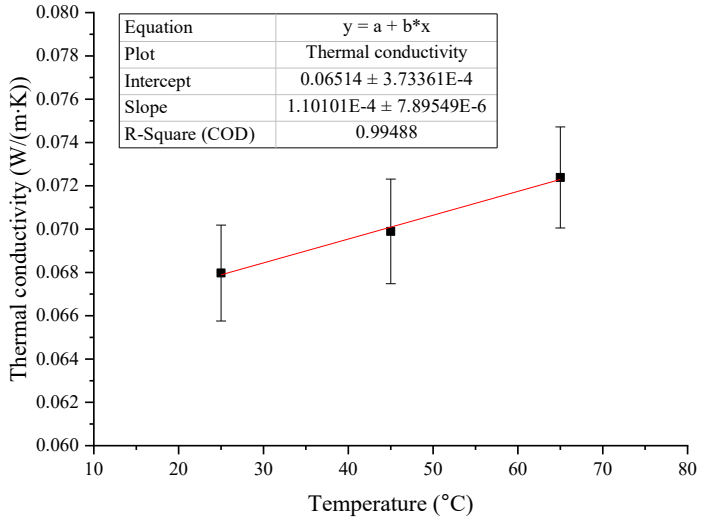

Figure 5-13: epoxy foam thermal conductivity vs the average environment temperature.

5.3 Morphology analysis

Micrographs were taken of the foam cross-section in order to investigate the foam morphology. A microtome was used to expose the cross-section surface of the foam. A Chromium coating (about 10 nm in thickness) was sputtered on the samples to make them conductive. The images were shot by field-emission SEM (FESEM SupraTM 40, Zeiss, Oberkochen, Germany) at an accelerating voltage of 15 kV.

(a)

(b)

(c)

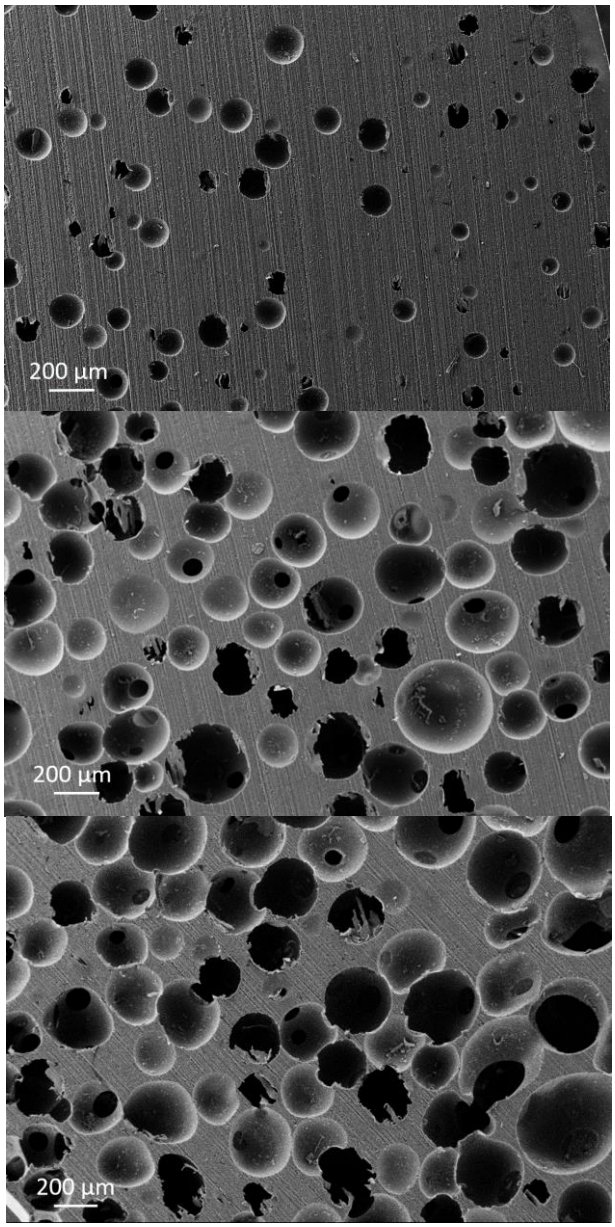

Figure 5-14: SEM micrographs of the epoxy foam. CFA content: (a) 1 wt%, (b) 3 wt%, (c) 5 wt%.

The samples preparation and SEM analysis were performed by Cristian Marro Bellot and Prof Valentina Casalegno from DISAT department in Politecnico di Torino.

The pore size dimensions were evaluated from the acquired cross-sectional images using the ImageJ image processing software [105]. Values obtained by image analysis were converted to three-dimensional values using the stereological equation $D_{pore} = D_{hole}/0.785$, in order to determine the actual pore size [106]. The increase in the amount of CFA added to the epoxy has a direct effect of the increase in the mean pore dimensions, as their number per unit volume, as it can be seen by the micrographs. Therefore, the apparent density of the foam results significantly reduced.

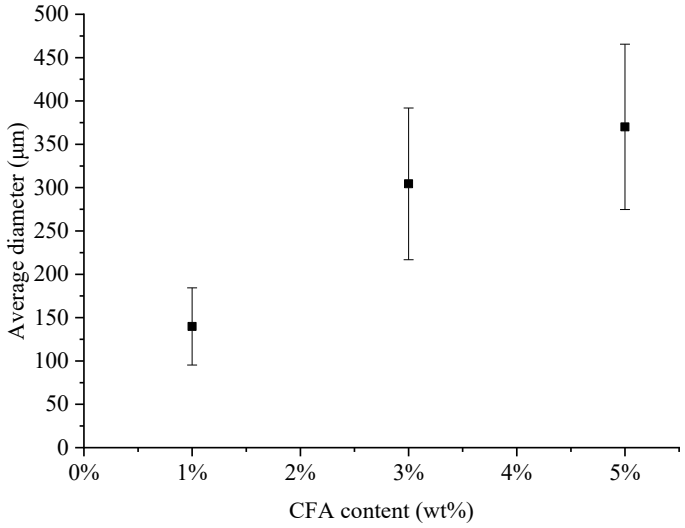

Figure 5-15: average pore diameter in the epoxy foam in relation with the CFA added to the uncured resin.

5.4 Sandwich preparation

5.4.1 First trials

Once the preparation and the properties of the epoxy foam have been assessed, the next development was to manufacture a polymer composite sandwich. Sandwiches are hybrid structures in which thin external facing (or skins) made of PMC laminates are joint by a much lighter thick core, usually made of cellular material: from balsa wood to honeycomb panels or polymer foams. The separation of the faces by the core highly increase the moment of inertia and the modulus of the section. Hence, the bending stiffness and the strength of the sandwich is highly improved compared to its single components, while not affecting the weight of the material in a sensible way [103].

In our project, we were already using GFRP unidirectional composite, which was a natural candidate to be introduced as outer facing. On, the other side, the epoxy foam is made of the very same Ampreg 26 resin as the GFRP matrix. Therefore it is was expected to provide excellent adhesion to the composite substrate.

The first adhesion trials were performed on small GFRP coupons. The pre-foam was poured directly on the top of the GFRP after it was carefully cleaned with isopropanol beforehand and let dry. A flexible silicone frame was employed to prevent the foam from spilling out before curing completely. The same curing cycle as for the standard foam was used, undergoing a high-temperature post-cure as soon as the pre-foam has reached a state of complete gelification. The composite coupons used as substrates were already regularly post-cured.

The first attempts were fairly successful. The foaming process seemed to be unaffected by the presence of the composite substrate. The adhesion strength was good. More careful analysis revealed the presence of defects. In particular, from a cross-section of the adhesion interface, it could be identified the presence of a layer of non-foamed epoxy in contact with the GFRP (see Figure 5-17). It is located at the bottom of the pre-foam lump, probably the bubbles migrated towards the upper surface, due to an insufficient viscosity when the pre-foam was produced. Another defect was found at the very centre of the 5 wt% CFA foam sample: a large bubble formed, likely during the first stages of the post-cure at high temperature. The temporary drop in viscosity at the temperature increase let smaller pores agglomerate and grow up to the size of a defect bubble.

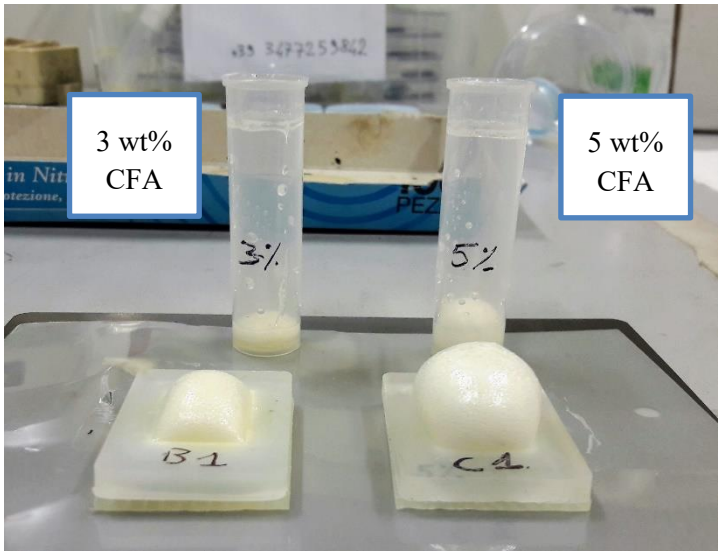

Figure 5-16: the first attempt to apply epoxy foam to the GFRP substrate by direct foaming. A modified silicone mould was used as a frame to confine the uncured pre-foam.

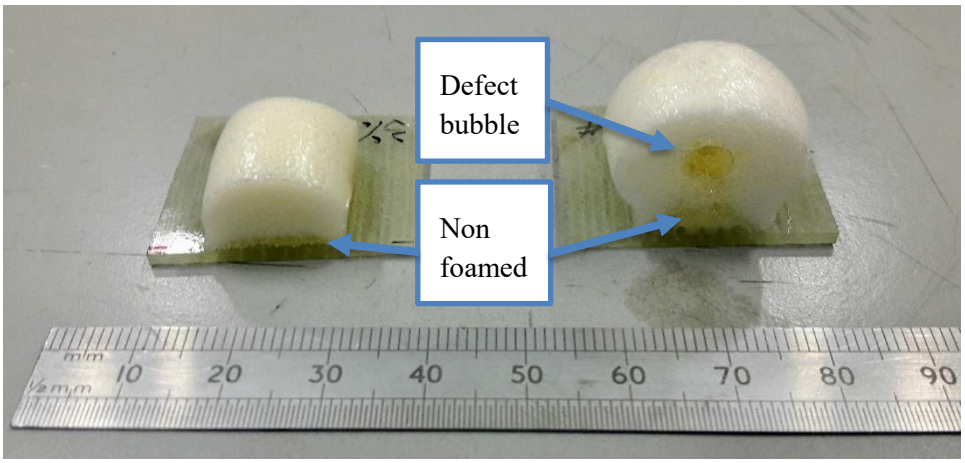

Figure 5-17: early issues with the foam on a composite substrate. In the sample on the right, there is a large defect porosity. In both samples, there is the formation of a non-foamed bottom layer sitting directly on the GFRP substrate.

From an SEM micrograph of the foam-GFRP joint interface, no major morphological differences were identified between the two materials. It was not possible to recognise where the epoxy matrix of the composite ended or where the foam began, and the interface could be identified only because of the transition from fibre bundles to porosities. This confirmed the proper adhesion of the foam to the composite substrate.

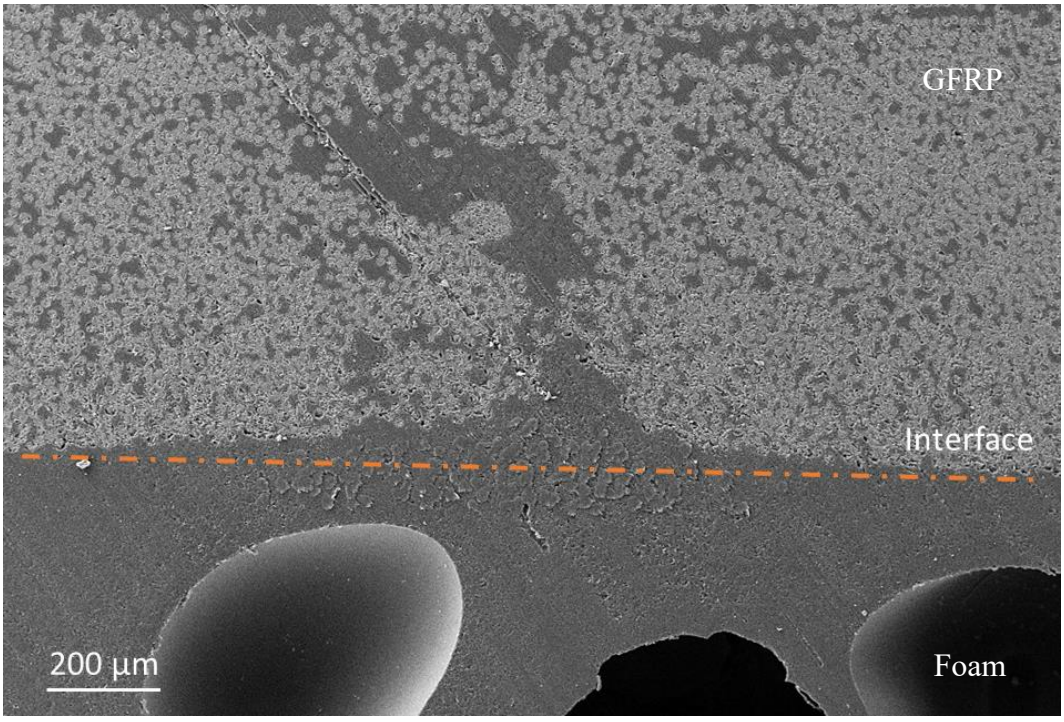

Figure 5-18: SEM micrography (secondary e^-) of the cross-section of the foam (bottom) to GFRP (top) interface.

Once the good quality of the bonding was assessed, the following stage was to scale-up to sandwich dimensions in order to be able to manufacture mechanical

specimens of required dimensions. Once again, the assembled PTFE mould was used for the purpose, as it could provide a sufficient volume (nominally 150×130×19 mm) to contain the sandwich core, which consisted of the epoxy foam. It was decided to let the resin foam directly between the composite faces, in order to achieve the bonding of the core during the expansion phase at the beginning of the post-cure of the foam. An alternative, which is used in particular with honeycomb or balsa wood, could have been to prepare the foam core separately, to cut it to the needed dimensions and then to glue it to the composite faces, ideally using the same Ampreg 26 epoxy as adhesive. This methodology was discarded as it made the preparation routine more complicated, time-consuming and did not guarantee a good core-to-facing adhesion, due to possible deviation from parallelism of the adhesion surfaces or not good wetting of the foam substrate.

On the other side, the risk of the chosen approach of direct foaming was that the foam expansion would be insufficient or not homogeneous, so the adhesion, in particular with the upper facing, would be poor. Indeed this was the case: in the first attempts, it happened that there was a just insufficient foam to fill the core gap. Besides a careful control of the foaming process, a proper calculation of the amount of epoxy resin to mix was critical to obtain a satisfactory filling. Knowing from the former foam batches the apparent density of the foam for a given amount of CFA added, the needed amount of epoxy resin (plus hardener) to mix was estimated as:

$$m_{resin} = 1.10 \times V_{core} \times \rho_{foam}(CFA\%) \qquad \text{Eq. 5-11}$$

An extra 10 wt% was added to account for the losses during the foam preparation. The density of the foam obtained with the addition of 5 wt% CFA was set to 0.4 g/cm^3, for practical use.

5.4.2 Larger batches

The preparation of the composite sandwich sample was very similar to the manufacturing of the foam batch. The main difference was that two GFRP small plates were added as outer facing. The dimensions were about 160×(100÷110) mm^2, supported at the frame of the PTFE mould itself and fixed by adhesive tape. The GFRP had unidirectional fibre reinforcement. The orientation of the fibres was always kept along the longer direction of the plate. This because the sandwich was then tested for its flexural performance, so the aim was to exploit the maximum stiffness the composite could offer. The width of the faces was always kept narrower compared to the mould cavity, in order to keep always a free gap at the sides for air and excess foam to spread out from the top gaps. The mould bottom was wrapped in the transpiring peel-ply, to contain the expanding foam, but letting the excess gas through.

When the pre-foam was ready, it was poured in the mould, where the lower face had already been placed (see Figure 5-19(b)). Then the top face was set in place while the foam gelling was ongoing (c). Once the foam had cured enough, it could proceed with the high-temperature post-cure (d). At this stage, the foam would

develop completely and fill the mould, bonding with the upper face. Once cooled down and removed from the mould (e), it was cut down to size with a diamond-coated circular saw, to get the required geometry for the mechanical specimens.

The main stages of the sandwich preparation are documented in the following pictures:

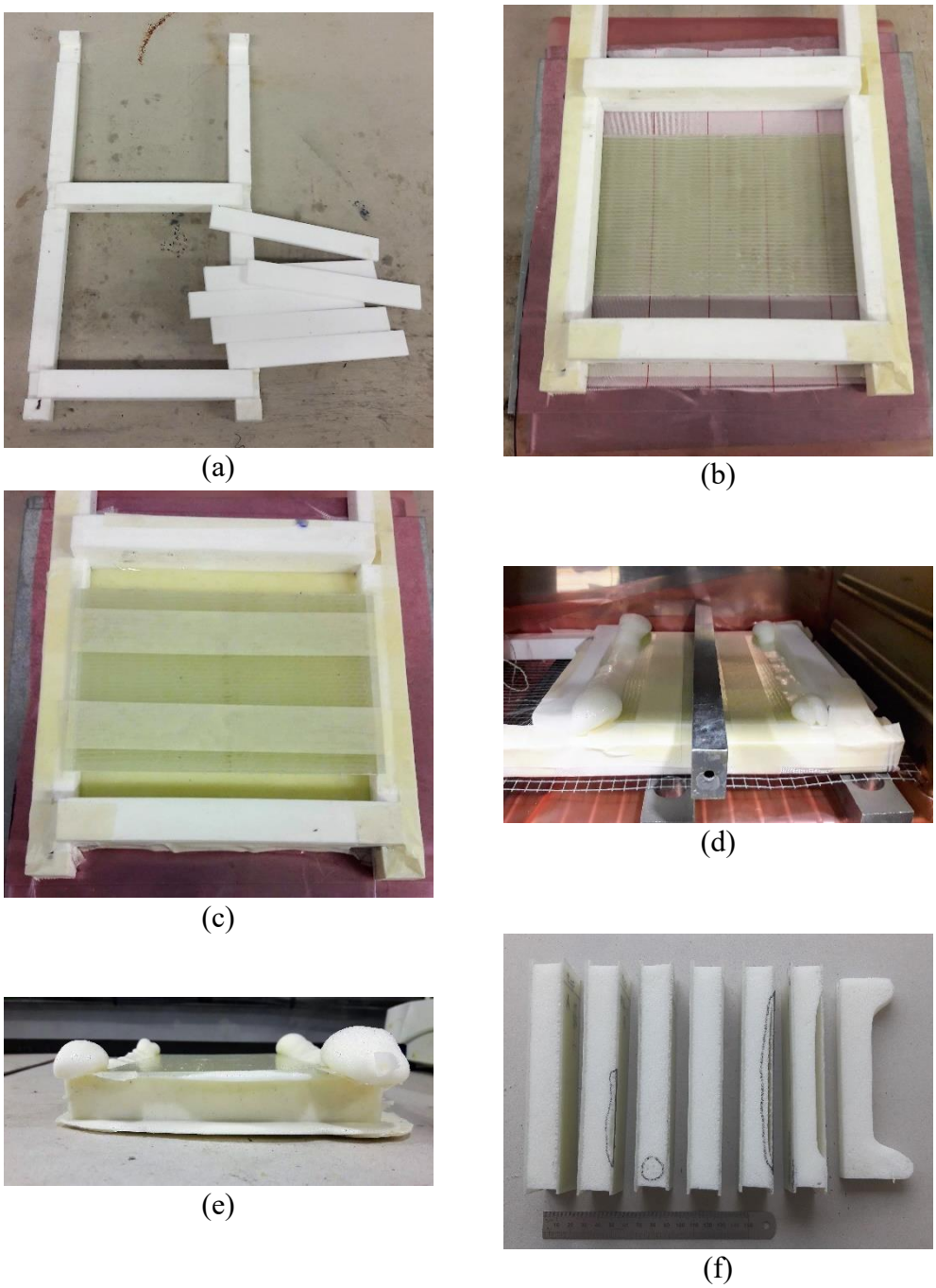

Figure 5-19: sandwich preparation sequence. (a) mould assembly; (b) setting of bottom face and peel-ply; (c) pouring of pre-foam and setting of the top face; (d) foaming and post-cure in the oven; (e) sandwich removed from the mould; (f) cut sandwich specimens, defects are highlighted.

5.5 Sandwich mechanical performance in bending

The mechanical properties of the sandwich were tested for their flexural performance, being the typical loading scenario for a sandwich structure. The dedicated standard followed was the ASTM C393-16, titled "Core Shear Properties of Sandwich Constructions by Beam Flexure" [107]. The aim indeed is to investigate the mechanical strength of the epoxy foam employed as the core of the sandwich. Also, the GFRP used for the facing was tested in bending on its own, for comparison.

5.5.1 Experimental setup

5.5.1.1 Specimen dimensioning

The set-up is similar to a three-point bending (3PB) test and consist of subjecting a beam to a bending moment laying in the plane of the sandwich but orthogonal to the beam longitudinal axes along the bending is taking place. The acceptable failure modes are those in which the core or the core-to-facings bond fails first.

We tried to follow the standard indications at the best of our possibilities, not always complying fully to the requirements. Support/loading cylinders with a diameter of 25 mm were needed, while we used 10 mm ones, le largest available. As the standard suggests, we tried to minimise the effect of stress concentrations, using 3 mm thick rubber pads This limited contact areas at the loading points could have contributed to a pair facing failures localised at the loading bar due to compressive fibre kinking. For the displacement measurement the crosshead travel was recorded, instead of the use of a deflectometer. The use of rubber pads might have altered the midspan displacement measurement, introducing some significant non-linearity due to the compressive response of the rubber.

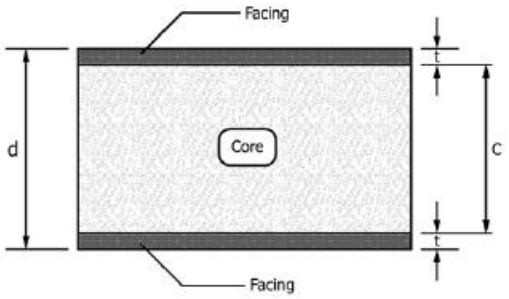

Figure 5-20: sandwich panel thickness dimensions [107]**.**

Performing the test using the standard specimen dimensions, with a length of 200 mm and a width of 75 mm, was not a viable option. The specimen was too long to be machined from the sandwich plated we manufactured. We opted to redesign the test specimen. The standard procedure prescribes some specimen dimensioning

limitations, in order to promote the failure to happen by shear in the core or at the core-facing interface:

a) The faces are identical and parallel;
b) The ratio between the core thickness and the face thickness is equal or bigger than 10;
c) The width should be at least twice the total thickness (but no more than 6 times). Also, it should be greater than three times the dimensions of the core cell: this way easily achieved as the pores' main dimension was in the order of tenths of a millimetre;
d) The support span should be sufficiently short that transverse shear forces are produced at applied forces low enough so that the allowable skin stresses will not be exceeded, i.e. failure will not happen at the skins first. The support span shall satisfy:

$$S \leq \frac{2k\sigma t}{F_s} \qquad \text{Eq. 5-12}$$

e) The core compression strength is:

$$F_c \geq \frac{2(c+t)\sigma t}{S l_{pad}} \qquad \text{Eq. 5-13}$$

Where:

- S: support span length [mm]
- σ: skin tensile strength [MPa]
- F_s: core shear strength [MPa]
- k: facing strength factor, recommended set at 0.75
- l_{pad}: length of the loading pads (direction of the bending span) [mm]
- F_c: core compression allowable stress [MPa]

The tensile strength for the composite skin is considered the UTS for the unaged GFRP in the longitudinal direction of the fibre reinforcement: σ = ~ 780 MPa (see § 4.3); a nominal face thickness of 2 mm was used. From the Eq. 5-12, it turns out:

$$S \times F_s \leq 2 \times 0.75 \times 780 \times 2 = 2340\ MPa \cdot mm \qquad \text{Eq. 5-14}$$

As a bending span of 140 mm was selected, the equation returns that:

$$F_s \leq 16.7\ MPa \qquad \text{Eq. 5-15}$$

Hence, the shear strength of the core should be lower than 16.7 MPa in order to promote its failure rather than a failure in the composite skin.

Considering that the foam compression strength is about 10 MPa, Eq. 5-13 would require a length of the loading pad in the longitudinal direction of the specimen of almost 50 mm.

$$l_{pad} \geq \frac{2 \times (20+2) \times 780 \times 2}{140 \times 10} \sim 49\ mm \qquad \text{Eq. 5-16}$$

This condition was not compatible with the test setup considering that the overall span is just 140 mm. In any case, the only loading bars available are in the format of cylinders: even considering the rubber pad deformability, the contact area

can add up to a few millimetres in length. This condition could not be met with the available test setup.

Considering the limitations due to the maximum sandwich plate dimensions and the available testing rig (which could not be modified due to a shortage of time), a reasonable compromise was found about the test specimen dimensions. The nominal dimensions were:

a) Core thickness: c = 19 mm
b) Skin thickness: t = 1.7 ÷ 1.9 mm
c) Width: w = 38 ÷ 40 mm
d) Length: l = 150 mm

The rate for the cross-head displacement was 6 mm/min.

5.5.1.2 Sandwich specimens

Three different sandwich batches were manufactured, namely batch #12, 13 and 14, from which specimens were machined out. A significant constructive difference characterised batch #13: the rougher bag-side of the GFRP substrates was facing outwards (hence not in contact with the foam core), contrarywise in the other two batches. While from a mechanical point of view, the GFRP had symmetrical properties, the roughness of the inner side can significantly affect the adhesion bond produced when the core is foamed. The manufactured sandwich specimens had the following dimensions:

Table 5-6: geometric dimensions of the prepared sandwich specimens.

Specimen	d (overall thickness)	t (faces thickness)		c (core thickness)	b (width)	l (length)
		top	bottom			
	mm	mm	mm	mm	mm	mm
A #12	24.05	1.62	1.63	20.80	46.70	150.65
B #12	24.82	1.69	1.63	21.50	46.58	150.72
A #13	22.21	1.61	1.77	18.84	40.47	151.08
B #13	21.45	1.68	1.78	17.98	37.82	151.16
A #14	23.62	1.89	1.80	19.94	40.75	152.05
B#14	23.60	1.96	1.79	19.85	40.59	152.21
C #14	23.12	1.82	1.76	19.54	37.35	152.26
D #14	23.83	1.74	1.92	20.17	40.52	152.22
F #14	22.52	1.71	1.86	18.95	39.56	152.11

Note that the GFRP facings were overhanging slightly longer than the foam core, due to the need to be fixed to the mould during the manufacturing. The length reported refers to the core dimension only.

From simple geometrical calculations and the weighing of the skins and final specimens, it was possible to estimate the apparent core density. To measure the weight of the core:

$$w_{core} = w_{specimen} - w_{skins} \quad \text{Eq. 5-17}$$

Moreover, to estimate the apparent core density:

$$\rho_{core} = \frac{w_{core}}{l \times b \times (d - t_{top} - t_{bottom})} \quad \text{Eq. 5-18}$$

The calculated core densities are reported in Table 5-7.

The values of the apparent density of the core of the sandwich appear to be in good agreement to the ones obtained for the foam alone with 5 wt% added CFA. This is further confirmation that the foaming process was good.

Table 5-7: estimated apparent core density for the sandwich specimens.

	Sandwich weight	**skins weight**	**core weight**	**core density**
	g	g	g	g/cm^3
A #12	98.75	44.44	54.31	0.37
B #12	103.50	45.28	58.21	0.39
A #13	85.02	45.47	39.55	0.34
B #13	77.48	43.62	33.86	0.33
A #14	82.82	43.68	39.15	0.32
B#14	86.52	44.29	42.23	0.34
C #14	74.40	38.82	35.58	0.32
D #14	83.89	43.15	40.74	0.33
F #14	77.86	39.20	38.66	0.34
Avg.				**0.36**
SD				0.02

5.5.1.3 Comparative 3PB on GFRP

To compare the results of the tests on the sandwich, three-point bending (3PB) runs were performed on the lone GFRP unidirectional laminate. The specimen's geometry was calculated accordingly. The dimensions and test parameters were:

a) Bending span: 64 mm
b) Specimen thickness: 1.7 ÷ 1.8 mm
c) Specimen width: 13 mm
d) Crosshead speed: 1 mm/min

The loading/support bars were fixed and had a radius of 5 mm. The specimens were manufactured in order to keep a span-to-thickness ratio of 32:1 or higher, as prescribed by ASTM D7264 [108]. This is a condition to ensure to minimise shear stress at the midspan and maximise the bending moment. The specimens were tested both placing the bag-side (rough-surface) and the tool side (smooth surface) in tension to evaluate if any difference occurs due to the different surface roughness. Five replicas for each surface orientations were tested.

5.5.2 Experimental results

5.5.2.1 Results of 3PB on GFRP

The results from the 3PB on the GFRP laminate only are presented in Table 5-8. The stress and strain were calculated with the same equations used for the neat foam bending test (see § 5.2.2). The data is presented as the average value plus-minus the sample standard deviation. The flexural modulus was calculated from the slope of the chord intersecting the stress-strain curve at 0.1 and 0.3 % strain. The strain data on the third column represents the strain applied at the maximum flexural strength.

Table 5-8: mechanical properties in bending for the unidirectional GFRP.

	Modulus E_{flex} [GPa]	*Strength σ_{flex} [MPa]*	*ε @ σ_{flex} [%]*
Bag-side in tension	31.26 ± 1.03	887.22 ± 22.25	3.83 ± 0.31
Tool-side in tension	30.54 ± 1.56	861.58 ± 43.89	3.56 ± 0.21

The results show the GFRP performs slightly better when the rougher bag-side is loaded in tension, but it has little statistical meaning as the average values are mostly within a single standard deviation range. Therefore, the flexural performance is independent of the bending direction in relation to the surface finish of the composite.

Compared to the quasi-static tensile test it appears that the flexural modulus is slightly lower than the tensile one, but the flexural strength is superior up to 100 MPa on average to the tensile (see § 4.3.5). This could be due to the more localised maximum stress state generated in the 3PB loading configuration, where only the midspan region of the specimen experiences the maximum degree of stress [109]. Hence, statistically it is less likely that the reinforcement fibres break due to the presence of a defect of critical size, compared to the tensile test, where the whole volume of the specimen experience (on average) the same loading condition and many more critical defects can be activated to cause the break.

5.5.2.2 Results of 3PB on the sandwich

The preparation of composite sandwich specimens was significantly more complex than the GFRP, so different factors could affect the result of the test. The larger dimensions of the test specimen and the smaller size of two of the manufactured sandwich batch led us with as little as 2 replicas for the test.

The test standard provides equations for the calculation of the shear stress in the core and the tensile stress in the facing in relation to the bending load [107]:

a) Core-shear ultimate stress:

$$F_s^{ult} = \frac{P_{max}}{(d+c)b} \qquad \text{Eq. 5-19}$$

b) Axial stress on the facings:

$$\sigma_{facing} = \frac{P_{max} \cdot S}{2t(d+c)b} \qquad \text{Eq. 5-20}$$

where P_{max} is the maximum load measured during the 3PB test.

From the force-displacement plots (see Figure 5-21) it can be seen how the loading curves are highly non-linear, with an extended leading toe which cannot be omitted. This can be due to the combined use of cylindrical loading bars and the rubber parts using at the contact point: the deformation of the rubber is likely to cause this apparent increase in the rigidity of the sandwich beam.

The test standard recommends that only failure happening first at the core or core-skin interface are to be considered valid for the purpose of the test.

The two specimens from batch #12 failed at very high value of the bending load (over 7 kN), but actually they failed first by fibre kinking in the upper skin due to local compressive stress at the loading bar [110]. The specimen kept some structural integrity by plastic deformation of the core until it failed completely at the core-skin interface (adhesive failure) for higher deformation. It is interesting how a typically brittle material gained some toughness in the sandwich configuration. If this was a repeatable behaviour, it could be interesting to develop a more crashworthy material. We observed such a response on this single foam batch, and it is not fully understood what determined it.

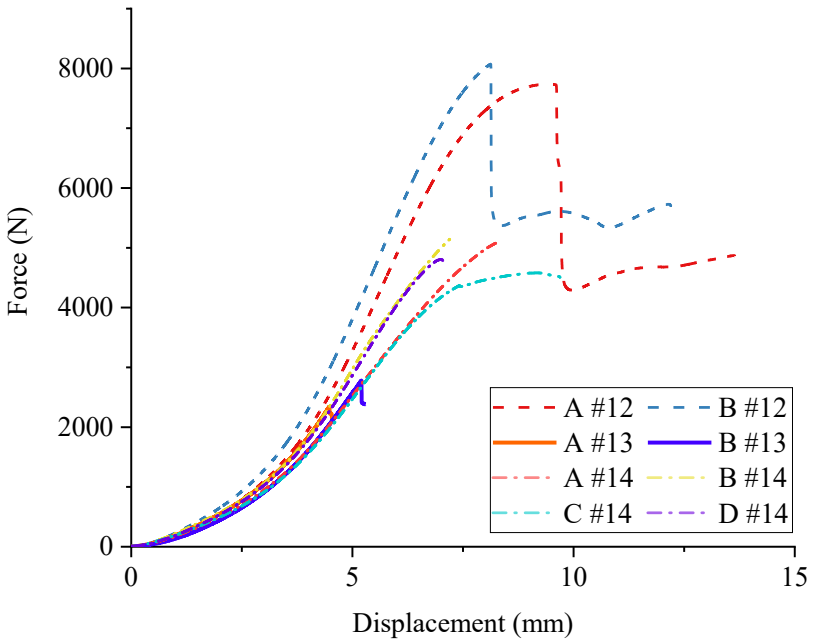

Figure 5-21: force-displacement plot for the 3PB test on the composite sandwich.

The two specimens obtained from batch #13 failed at relatively low loads (below 3 kN) by adhesive failure at the core-facing interface. The relative

smoothness of the tool-side of the composite limited the adhesive strength of the bond. It is critical to provide a substrate with adequate roughness to allow the core to bond properly to it. Some light sand-blasting can significantly improve bond strength.

The specimens from batch #14 showed a fairly repeatable behaviour. As required, the failure happens first at the core-facing interface to the bottom skin. The failure tends to climb across the core at an approximate 45° towards the midspan (see figure below), with a complete loss of structural integrity.

(a) (b)

Figure 5-22: 3PB broken sandwich specimens after unloading. (a) from batch #12, (b) from batch #14.

The test results calculated from Eq. 5-19 and Eq. 5-20 are summarised in the following table:

Table 5-9: 3PB test results on sandwich samples.

Specimen	P_{max}	$F_{s,ult}$	σ_{Skin}	P_{break}	$F_{s,break}$
	N	MPa	MPa	N	MPa
A #12	7739	>3.69	158.32	4847	2.31
B #12	8072	>3.74	160.35	5705	2.64
A #13	2341	1.41	55.85	N/A	N/A
B #13	2780	1.86	73.17	N/A	N/A
A #14	5077	2.86	111.41	N/A	N/A
B#14	5143	2.92	113.83	N/A	N/A
C #14	4578	2.87	114.07	N/A	N/A
D #14	4805	2.70	98.26	N/A	N/A

Given that the failures of the specimens from batch #12 are to be considered not in conformity to the test, it can be noticed that the apparent shear strength of there is core is higher than 3.7 MPa, much higher than the strength showed by samples from batch #14. If then we disregard, the first failure for those specimens, but then calculate the apparent core shear strength for the load at which the adhesive bond failure happens, we found values that are slightly lower than those returned by the regular break of samples from batch #14.

This difference in behaviour is not fully understood. There could be at least 3 possible explanations:

a) The test specimen was poorly dimensioned, not entirely promoting a shear failure at the core;
b) The foam adhesion and shear strength can vary substantially, although the processing was identical and the apparent density reasonably close. At the present stage, it is not possible to determine which variable or process condition altered the material properties.
c) The simplified solution for the calculation of the stresses generated in the specimen during the test is not fully applicable, and the numbers returned are not entirely reliable.

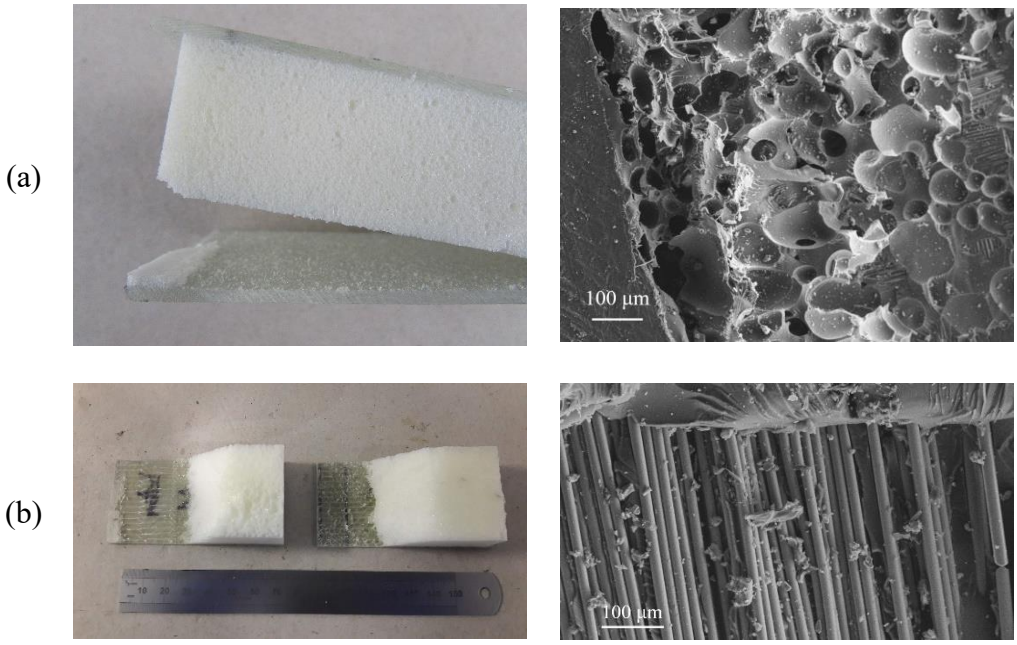

Figure 5-23: fracture surfaces in full view and SEM micrograph. (a) from batch #12 and (b) #14.

From SEM micrographs, there is evidence of a different way about the interface fracture propagation. For the sample from batch #12 (see Figure 5-23 (a)), the fracture seemed to be mostly cohesive, breaking in closest foam layer before the interface. On the other side, in the sample from #14 (see (b)), the failure appeared mostly adhesive, exposing a significant amount of glass fibres.

It is not clear how the bonding failure mode affects the adhesion strength. Also, there is no definitive answer about which variability in the sandwich manufacturing process causes the core-shear response to change in a significant way.

5.6 Conclusions

In this chapter, we presented the experimental activities related to the manufacturing and testing of an epoxy foam and a relative composite sandwich in which the same foam was also employed as a structural core.

The foam was prepared starting from the commercial Ampreg 26 epoxy resin and adding to it tetramethyl disiloxane as Chemical Foaming Agent. The foam underwent a thorough analysis of the thermal and mechanical performance.

The glass transition temperature of the foam was measured at 85 °C and seemed not to be significantly altered compared to the bulk epoxy. This shows that the CFA does not interfere with the polymerisation of the epoxy in a detrimental way. The foam can be employed in application up to such temperature for limited time and loads.

The thermal conductivity of the foam was characterised in function of the relative density and the environment temperature. We found a thermal conductivity as low as 0.07 W/(m·K), which is competitive with other insulating materials, and it is fairly constant in the whole operative range.

The 5 wt% CFA foam formulation was also tested for the mechanical performance: in flexure, it showed an elastic modulus of about 380 MPa and a strength of 12 MPa.

From the same epoxy foam, a polymer composite was manufactured by direct foaming the core within the GFRP composite facings. A good foam quality was obtained following the same curing process.

The adhesion strength of the core-to-facing strength was tested by a flexural test, and a value of shear strength up to 2.9 MPa was found, but it was not repeatable from batch to batch. Possible different bond failure modes were identified, but it was not possible to relate them to physical differences in the foam or the composite substrate. It might be that local differences in density could act as crack initiators and promote different modes of failure.

To further expand this work, rheology testing could be performed to gain a better understanding of the simultaneous curing and foaming process, which are critical to obtaining a proper foam morphology.

Moreover, this foaming technique is not chemically specific; it does work as long as an amine hardener is available. Alternative epoxy systems or foaming agent combinations could be investigated. It can be interesting to apply it to epoxy systems with higher glass transition temperatures, to possibly extend the operative range of this kind of materials.

From a manufacturing point of view, techniques such a combination of screw-mixing and extrusion could allow to gain better control in the pre-foaming if the process parameters are adequately controlled.

Chapter 6 Summary, conclusions and further work

Polymer Matrix Composites (PMCs) are growing in popularity for marine applications, from shipbuilding to renewable energy production. Oil & Gas industry is keen to benefit from the advanced mechanical properties and the corrosion resistance to manufacture hybrid- or fully-composite pipeline for deep-water production risers. PMCs are probably the only material that can enable economically viable exploitation of the rich offshore reservoirs that are located underneath oceanic seabed at 2000 m or more in-depth. The structural materials have to face a very harsh scenario, characterised by temperature up to 200 °C, extreme pressures and aggressive chemical species while carrying significant loads in both static and dynamic (e.g., depressurisations, sea currents and waves) conditions. On top of these, the structures are expected to last 25 years or longer with minimal maintenance.

Limited experience has been gained with composite materials in such specific applications, in particular for long term exposures. More refined ageing models and experimental data on material degradation are needed to accurately forecast how the polymer composite components will fare in such a demanding scenario.

In this PhD thesis are summarised the experimental work and the relevant results gathered along three years of research activities within the framework of the European project CoACH ETN (2015 – 2018) aimed at addressing some of those concerns.

The study focused mainly on the possibility of mapping the evolution of the physical and mechanical properties of a Glass Fibre Reinforced Polymer (GFRP) composite, in relation to the progress of the absorption of fluids. The performance of the material was monitored while it was exposed to a basic simulated offshore Oil & Gas environment. The ageing process due to exposure to seawater and oil was accelerated by using temperature as a leverage to boost both diffusion and degradation phenomena. The experimental trends show which exposure conditions the material is more affected by and provide insight into how the material will age at longer times.

In this project, we implemented standardised test methods, employed in composite material qualification for industrial application, in order to characterise it both from a physical and mechanical point of view. Differently from common studies [8,35,86], in this work, a parallel testing campaign was performed. It consisted of the gravimetric testing, Dynamic Mechanical Analysis (DMA) and mechanical testing on both epoxy matrix alone and GFRP.

Testing methodologies about accelerated exposures are widely discussed in literature [7,24,40,48,94]: being a relatively recent topic (the relevant literature is mostly dated since the ’00s) and due to the continued technological development on the PMC, there is no universal agreement on an optimised methodology to perform them; rather different approaches have been developed.

The aim was to characterise the materials at similar aged conditions, depending on the exposure temperature: the degree of ageing was estimated through the gravimetric absorption curves. From the experimental data obtained, some basic estimations on these properties outside the experimental range were calculated, like the relation of diffusion coefficient with temperature and the accelerating effect of exposure temperature on the mechanical degradation. In the future, thanks to parallel testing campaign as developed in this work, it will be possible to fully characterise the material properties in relation to ageing phenomena. Supporting this methodology, as a preliminary result, we found a relation between the loss of tensile strength and the amount of absorbed seawater.

For offshore pipelines, thermal insulation is critical for maintaining the fossil fuel flowing, as part of the *flow assurance* strategy [8], and improving the energy efficiency of the production system. An epoxy foam was successfully manufactured by means of a *Chemical Foaming Agent* (CFA): compared to the bulk epoxy, a significant reduction of the thermal conductivity was obtained. The foam also showed excellent adhesion properties and the possibility to manufacture a sandwich material, using it as a core. The possibility of adding a buoyant core to the pipeline structure, thanks to the foam’s low density, would significantly reduce the structural loads at the top of the riser due to the weight of the structure [91].

6.1 Fluid diffusion

An extensive accelerate fluid exposure campaign on an epoxy thermoset and an epoxy-based GFRP was the main subject of this research project, as presented in Chapter 4. The aim was to assess the evolution of their properties when exposed to a simulated marine environment, as for submarine application for the Oil & Gas industry. Three different temperatures were chosen (25, 55, and 80 °C), to compare the different rates at which the material properties would change, due to the increased physical/chemical kinetics.

The fluids we used to expose the materials specimens were synthetic seawater and an aromatic oil mixture, named Norsok oil, to resemble the exposure to the hydrocarbons.

The diffusion progress was monitored by gravimetric measurements. Seawater demonstrated to be an active diffusant. The gravimetric curves show that the behaviour is not completely Fickian (see § 4.1.2). There is evidence of some “Langmuir-like” diffusion, promoted at the higher temperatures, but unidirectional

Fick's solution was accurate enough to recover the diffusion coefficients. More complex is the description for the Norsok oil, due to anomalous behaviour, very dissimilar from the Fickian one: it seems that the oil almost does not interact with the materials at the lower temperatures and it appears to be absorbed by the material only at 80 °C (as shown at § 4.1.3).

In the case of the GFRP composite, its anisotropic nature influences the diffusion kinetics with increasing temperature, both due to the fibre presence and the changing conditions of the fibre-matrix interphase. Two different correction factors were used, and the one proposed by Starink et al. [37] provided more accurate results. Nevertheless, it is critical to use coupons with a width/length to thickness ratio of 50:1 or more (quasi-infinite plate) to reduce the effect of fluid diffusion through the edges.

Using an Arrhenius plot, the exponential relation between the diffusivity coefficient and the exposure temperature was verified and the diffusivity coefficient values for the materials at a temperature of 4 °C, typical of offshore operative scenarios, were estimated at 0.23 and 0.05 × 10^{-13} m^2/s for the neat Ampreg 26 and the composite, respectively.

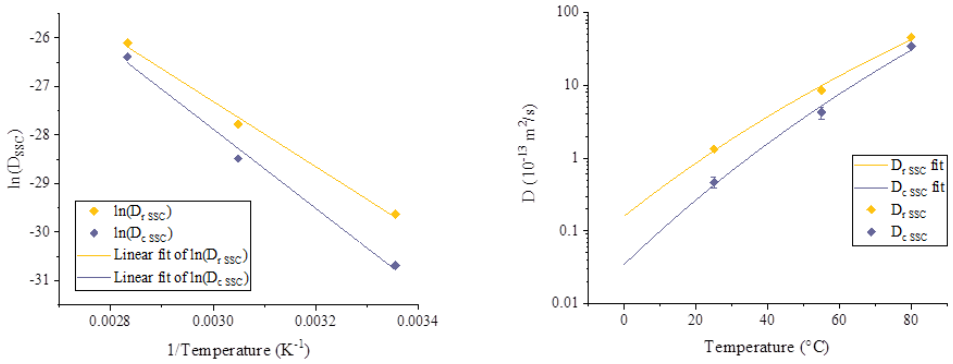

(a) (b)

Figure 6-1: (a) Arrhenius plot and (b) predicted diffusivities for the neat Ampreg 26 and GFRP materials.

The results confirm the feasibility of accelerating the diffusion of seawater in polymer and polymer composites as a reliable way to recover the diffusivity factors at different temperatures and to estimate them for temperatures well below the glass transition of the polymer.

The evaluation of the evolution of the *Glass Transition temperature* (Tg) is more complex due to the concurring mechanism which interacts with the polymer structure. Plasticisation was the immediate effect in seawater, which clearly showed in the drop of the Tg for all the exposure temperatures, and it progressed along with water absorption. However, the reduction in Tg is not proportional with such temperature: the 25 °C exposure exhibited the largest drop at saturation (as monitored by gravimetric testing, see § 4.2.1). In literature, this behaviour is justified by the formation of different kind of bonds of the diffusing molecules with the polymer network [92]. Once the material saturated in seawater, the Tg remained fairly stable. At a later stage, the samples soaked at 80 °C showed signs of

progressive ageing, with a further decrease in Tg. However, upon drying, the Tg was always recovered to the pristine material level, for all the exposure temperatures: the induced plasticisation was a completely reversible process.

The response of the samples exposed to Norsok oil was antisymmetric to the gravimetric test results for the same fluid exposure: only at the 80 °C, there was a consistent reduction of the Tg, which in this case was not reversible (see § 4.2.3). It is a further demonstration that the diffusion process depends highly on the chemical nature of the diffusing species, and the Fickian model is not sufficient to describe this kind of absorption phenomenon [21].

Due to the complex trends recorded in the DMA results, the technique cannot be employed on its own to monitor the diffusion or ageing process. The Tg is an important parameter for the characterisation of a GFRP, but it does not provide consistent metrics to evaluate the material' ageing. Increasing the number of sampling moments at progressive exposure time intervals will likely improve the understanding of the effect of adsorbed fluids on the visco-elastic properties of the epoxy matrix, in particular for the initial stage of absorption when the changes in Tg are more pronounced.

6.2 Ageing

In addition, tensile tests were performed on both materials to evaluate the evolution of mechanical performance with exposure to seawater. As a first result obtained through the parallel testing on the GFRP composite, a linear correlation between the tensile strength loss and the absorbed seawater weight fraction was found, regardless of the exposure temperature.

For illustration, Figure 6-2 presents the correlation found, (more information can be found at § 4.4).

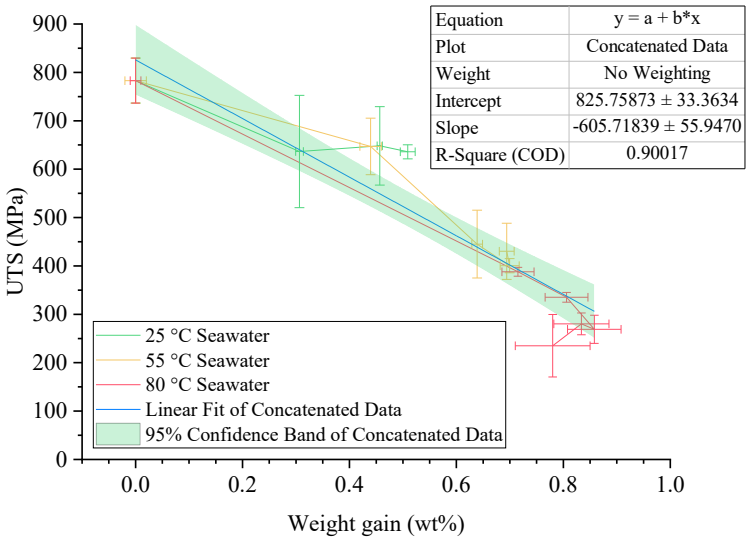

Figure 6-2: linear interpolation of the longitudinal UTS of the GFRP in relation to the weight uptake, with a 95% confidence interval.

In § 4.5, an estimation of Time-Shift factor was calculated, as proposed by Silva *et al.*[48]. It could be applied only to the transverse UTS for the GFRP. It turns out that exposure in seawater at 50 °C can accelerate the mechanical performance degradation up to 100 times than what experience by the material in operation at about 5 °C. As shown in the literature, this estimation is subject to the experimental error, and it highly depends on the function chosen to fit the experimental data. However, it offers a way to estimate the long-term ageing effect due to the exposure temperature. The evaluation of the TSF was successful for the tensile strength of the GFRP in the transverse direction; instead; it did not work for other mechanical properties because the trends were not decreasing in a proportional way or the impossibility to get a proper fitting of the experimental points.

The exposure to Norsok oil on the neat epoxy appeared to be much less demanding on the mechanical properties than the seawater. Only a slight decrease was recorded for the average material strength, and this is irrespective of the temperature exposure. This seems to be in partial agreement with the results from the gravimetric testing and highlights how the oil mixture has a significantly lesser ageing effect on the epoxy (see § 4.3.4).

A drawback of this testing methodology is that it is significantly time-consuming, without the possibility to foresee if the results are going to be meaningful in advance but only when the exposure test is at an advanced state. Also, most of the tests are destructive, so a relevant amount of material is needed to perform a campaign. To increase the accuracy of the method, more frequent test runs are necessary, even if this can quickly escalate the time required for the testing. It is advisable for the next generation of accelerated ageing test on composites to include more advanced analytical testing in order to reduce the resources needed to perform the material characterisation. Non-Destructive Testing (NDT) techniques such as ultrasounds or tomography (CT) scan would allow evaluating crack propagation [95]. Superficial techniques as ATR-FTIR and Raman spectroscopy can monitor the progress of the moisture distribution and chemical ageing, particularly for the composite material. Impedance spectroscopy is a technique which is increasingly investigated to measure the water diffusion, thanks to the very different dielectric properties compared to the polymer matrices [111]. Nuclear Magnetic Resonance (NMR) allows identifying water diffusing in a medium, even discerning the local chemical state, but returning a poor spatial definition [112].

A new monitoring technology can be provided by the introduction of active Optical Fibre Sensors (OFS), which are able to detect diffusing species without affecting the composite environment [62]. Moreover, with the Atomic Force Microscope or Nanoindentation, it would be possible to investigate the elastic state of the fibre-matrix interphase [41,43]. These techniques require sophisticated setup and are significantly time-consuming, in particular for a large number of sampling, but can provide much more detailed information about the micromechanics of the

ageing processes induced by the permeating species. The data treatment can greatly benefit from numerical modelling, in particular to account for anisotropic effect in composite geometries [57,71,113]. The application of statistical methods would allow describing more consistently the survival rate of the material during ageing, in particular as the majority of the failures from the test were of a brittle kind. However, the number of specimens tested will need to be significantly higher to achieve statistical validity [40,97].

6.3 Epoxy foam

An epoxy foam was successfully prepared following the synthesis route of adding a Chemical Foaming Agent (CFA) during the curing stage of an epoxy resin. This manufacturing approach can be competitive to other foaming processes (e.g., physical foaming, syntactic foams) as it does not involve the use of hazardous chemicals and requires to modify the resin curing routine slightly, yet it does rely on the sharp transition in the viscosity happening at the gel point. The foam samples obtained underwent a thorough characterisation regarding physical, mechanical and thermal properties, as shown in § 5.2.

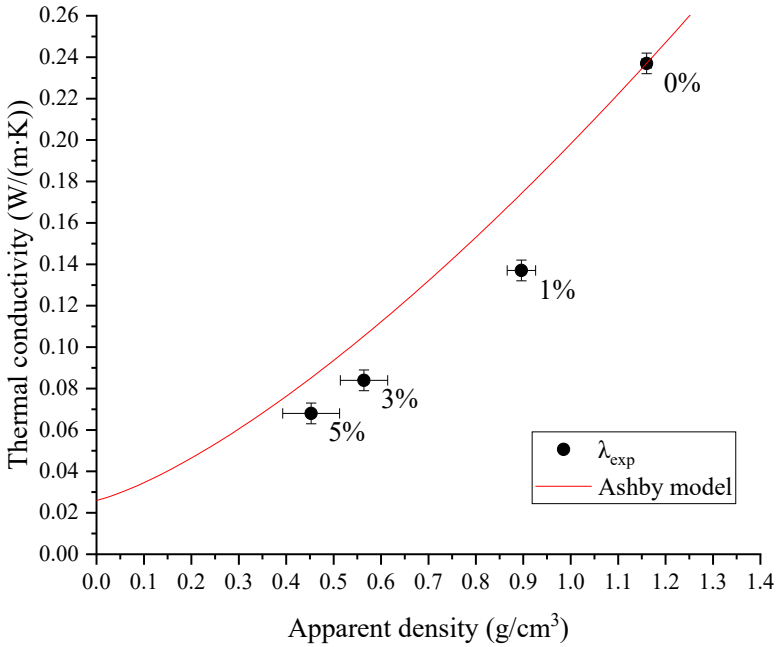

Figure 6-3: thermal conductivity of bulk epoxy and foams at 25 °C in relation to its apparent density. The percentages indicate the foaming agent wt% added to the relative foam formulation

The results show that a relevant decrease in the apparent density of the foam can be obtained by adding up to 5 wt % of CFA. Although the mechanical properties are inevitably affected by the foaming and made it not suitable for application at very high depth or structurally stressed areas, a notable reduction down to 30% of

the original value of the thermal conductivity can be achieved, while the glass transition temperature and the thermal stability of the material are unaffected. Conductivity in the order of 0.06÷0.07 W/(m·K) is competitive with other commercial insulation systems. The limitation of compression strength could be improved if the morphology of the porosities can be made more homogenous and decreasing the average pore section.

A composite sandwich was manufactured using the epoxy foam as a core and the unidirectional GFRP as facings (see § 5.4 and following). Microscopic investigation showed a continuous interface among the GFRP and the foamed layer. This confirms the compatibility of the foam with structural substrates, with an excellent interface and adhesion properties. The flexural test showed that the bond has a shear strength up to 2.9 MPa, but the foam morphology can significantly affect this value.

6.4 Future outlook

The data obtained by these accelerated exposures offer interesting insight into the ageing and degradation phenomena affecting the GFRP. However, the research activities could be further expanded, and the following threads can be worth exploring:

- Widen the investigation on different coupons geometry in the gravimetric test, in particular, to assess if it is possible to determine with precision the components of an anisotropic diffusivity tensor. It would be essential to determine if there are meaningful differences for the mass transport depending on the fibre orientation, in particular for numerical simulation purposes [70,71].
- Evaluate the effect of hydrostatic pressure on the ageing process, considering that the materials will operate at very high depths (over 2000 m), in combination with high mechanical loads. In these conditions, the polymer matrix can suffer from creep deformation.
- Exposing the materials to corrosive fluids, having high concentrations in CO_2 and H_2S, which are typically encountered in "sour" reservoir or Enhanced Oil Recovery (EOR) operations [14].
- Using the parallel testing campaign developed in this work, the ultimate goal will be to define an empirical model to describe the evolution of GFRP performance in relation to the ageing conditions of a simulated environment. A useful read about some basic approach to the issue of combining different parameters in a unique performance degradation model is offered by Maxwell and Broughton [94].

Appendix A

Table A1: Comparison of the results obtained at effective equilibrium for the gravimetric test of the neat Ampreg 26 using different equilibrium criteria. (Note: mean values of three coupons for each geometry are listed)

	Temperature		25 °C				55 °C				80 °C			
	Specimen		alpha	beta	gamma	delta	alpha	beta	gamma	delta	alpha	beta	gamma	delta
ASTM D5229M Eq. 1	Effective equilibrium	(days)[1]	131	145	117	113	70	63	76	55	40	22	35	9
	Moisture content	(%)	1.93	1.96	1.99	1.88	2.66	2.63	2.68	2.85	2.78	2.78	2.79	2.75
	Uptake rate[2]	(10^{-8}/s)	1.48	0.65	2.88	1.59	1.29	2.57	1.70	3.00	0.90	0.35	8.60	3.30
Criterion A as Eq. 2 (0.02, n=2)	Effective equilibrium	(days)	113	107	110	107	55	33	33	48	16	9	9	9
	Moisture content	(%)	1.94	1.90	2.01	1.91	2.69	2.60	2.63	2.91	2.77	2.77	2.79	2.73
	Uptake rate	(10^{-8}/s)	0.16	2.00	2.90	3.00	1.70	1.67	2.95	1.12	1.60	2.60	2.60	1.20
Criterion B as Eq. 2 (0.05, n=3)	Effective equilibrium	(days)	62	62	65	62	27	26	28	35	8	8	9	8
	Moisture content	(%)	1.63	1.59	1.75	1.62	2.52	2.49	2.57	2.76	2.69	2.73	2.75	2.75
	Uptake rate	(10^{-8}/s)	4.87	6.56	8.01	6.34	4.90	5.12	6.40	6.00	4.80	1.00	2.60	1.10

[1:] The time to effective equilibrium is round up to the next integer. [2:] The uptake rate is the average time ratio of the percent weight gain, i.e. a weight uptake "speed".

Appendix B - List of acronyms

3PB	Three-Point Bending flexural test
ASTM	American Society for Testing and Materials
CNC	Computer Numerical Controlled machine
DMA	or **DMTA:** Dynamic (Thermal) Mechanical Analysis
DSC	Differential Scanning Calorimetry
EOR	Enhanced Oil Recovery operations
FRP	Fibre Reinforced Polymers
FTIR	Fourier-Transform Infrared spectroscopy
GFRP	Glass Fibre Reinforced Polymer
GHP	Guarded Hot Plate
HFM	Heat Flow Meter
ISO	International Organization for Standardization
NDT	Non-Destructive Testing
RH	Relative Humidity
SEM	Scanning Electro-Microscope
tanδ	Tangent of the phase shift of the complex elastic modulus E^*
TGA	ThermoGravimetric Analysis
TSF	Time-Shift Factor

References

[1] M. Mrazova, Advanced composite materials of the future in aerospace industry, Incas Bull. 5 (2013) 139–150. doi:10.13111/2066-8201.2013.5.3.14.

[2] T.D. Ashwill, Materials and Innovations for Large Blade Structures: Research Opportunities in Wind Energy Technology, in: 50th AIAA Struct. Struct. Dyn. Mater. Conf., 2009. www.awea.org (accessed March 31, 2019).

[3] E.M. Fagan, Design of fibre-reinforced polymer composite blades for wind and tidal turbines, National University of Ireland, Galway, 2017.

[4] R. Martin, Composite Materials: An Enabling Material for Offshore Piping Systems, (2013). doi:10.4043/23925-ms.

[5] Andrei Costache, Anchoring FRP Composite Armor in Flexible Offshore Riser Systems, Technical University of Denmark, 2015.

[6] V. Jha, J. Latto, N. Dodds, T.A. Anderson, D. Finch, M. Vermilyea, Qualification of Flexible Fiber-Reinforced Pipe for 10,000-Foot Water Depths, in: Offshore Technol. Conf., Offshore Technology Conference, 2013: pp. 1–9. doi:10.4043/24160-MS.

[7] P. Davies, Y.D.S. Rajapakse, Durability of Composites in a Marine Environment, Springer, 2014. doi:10.1007/978-94-007-7417-9.

[8] P.-Y. Le Gac, P. Davies, D. Choqueuse, Evaluation of Long Term Behaviour of Polymers for Offshore Oil and Gas Applications, Oil Gas Sci. Technol. – Rev. d'IFP Energies Nouv. 70 (2014) 279–289. doi:10.2516/ogst/2013211.

[9] D. Choqueuse, P. Davies, Durability of Composite Materials for Underwater Applications, in: 2014: pp. 195–207. doi:10.1007/978-94-007-7417-9_10.

[10] P.M. Stefani, A.T. Barchi, J. Sabugal, A. Vazquez, T.A. Barchi, J. Sabugal, A. Vazquez, A.T. Barchi, J. Sabugal, A. Vazquez, Characterization of epoxy foams, J. Appl. Polym. Sci. 90 (2003) 2992–2996. doi:10.1002/app.13006.

[11] M. Roseman, R. Martin, G. Morgan, Composites in offshore oil and gas applications, in: Mar. Appl. Adv. Fibre-Reinforced Compos., Elsevier, 2015: pp. 233–257. doi:10.1016/B978-1-78242-250-1.00010-7.

[12] BP, Statistical Review of World Energy 2018, 2018. https://www.bp.com/content/dam/bp/business-sites/en/global/corporate/pdfs/energy-economics/statistical-review/bp-stats-review-2018-full-report.pdf (accessed March 13, 2019).

[13] US Energy Information Administration, International Energy Outlook 2013, 2013. www.eia.gov.

[14] V. Alvarado, E. Manrique, Enhanced oil recovery: An update review, Energies. 3 (2010) 1529–1575. doi:10.3390/en3091529.

[15] D.-C. Pham, N. Sridhar, X. Qian, A.J. Sobey, M. Achintha, A. Shenoi, A review on design, manufacture and mechanics of composite risers, Ocean Eng. 112 (2016) 82–96. doi:10.1016/J.OCEANENG.2015.12.004.

[16] U.S. Fernando, Challenges and Solutions in Developing Ultra-high Pressure Flexibles for Ultra-deep water Applications, in: MCEDD, 2015. http://mcedd.com/wp-content/uploads/2014/04/03_Upul-Fernando-GE-Oil-Gas.pdf (accessed March 13, 2019).

[17] L. Grace, Non-fickian three-dimensional moisture absorption in polymeric composites: development and validation of hindered diffusion model, University of Oklahoma, 2012.

[18] O.O. Ochoa, M.M. Salama, Offshore composites: Transition barriers to an enabling technology, Compos. Sci. Technol. 65 (2005) 2588–2596. doi:10.1016/j.compscitech.2005.05.019.

[19] P. Jukes, A. Eltaher, J. Sun, G. Harrison, Extra High-Pressure High-Temperature (XHPHT) Flowlines: Design Considerations and Challenges, in: 28th Int. Conf. Ocean. Offshore Arct. Eng., ASME, 2010: pp. 469–478. doi:10.1115/omae2009-79537.
[20] Y.J. Weitsman, Fluid Effects in Polymers and Polymeric Composites, Springer, 2012. doi:10.1007/978-1-4614-1059-1.
[21] D.A. Bond, P.A. Smith, Modeling the Transport of Low-Molecular-Weight Penetrants Within Polymer Matrix Composites, Appl. Mech. Rev. 59 (2006) 249. doi:10.1115/1.2202873.
[22] L.R. Grace, M.C. Altan, Characterization of anisotropic moisture absorption in polymeric composites using hindered diffusion model, Compos. Part A Appl. Sci. Manuf. 43 (2012) 1187–1196. doi:10.1016/j.compositesa.2012.03.016.
[23] R. Martin, Ageing of Composites, Woodhead Publishing, 2008.
[24] G. Mensitieri, M. Iannone, Modelling accelerated ageing in polymer composites, in: Ageing Compos., 2008: pp. 224–281. doi:10.1533/9781845694937.1.224.
[25] B.C. Ray, D. Rathore, Environmental Damage and Degradation of FRP Composites: A Review Report, Polym. Compos. 36 (2015) 410–423. doi:10.1002/pc.22967.
[26] J. El Yagoubi, G. Lubineau, F. Roger, J. Verdu, A fully coupled diffusion-reaction scheme for moisture sorption-desorption in an anhydride-cured epoxy resin, Polym. (United Kingdom). 53 (2012) 5582–5595. doi:10.1016/j.polymer.2012.09.037.
[27] J. Crank, The mathematics of diffusion, Oxford University Press, Oxford, 1979.
[28] P. Silva, P. Fernandes, J. Sena-Cruz, J. Xavier, F. Castro, D. Soares, V. Carneiro, Effects of different environmental conditions on the mechanical characteristics of a structural epoxy, Compos. Part B Eng. (2015). doi:http://dx.doi.org/10.1016/j.compositesb.2015.10.036.
[29] C.H. Shen, G.S. Springer, Moisture Absorption and Desorption of Composite Materials, J. Compos. Mater. 10 (1976) 2–20. doi:10.1177/002199837601000101.
[30] L.-R. Bao, A.F. Yee, Effect of temperature on moisture absorption in a bismaleimide resin and its carbon fiber composites, Polymer (Guildf). 43 (2002) 3987–3997. doi:10.1016/S0032-3861(02)00189-1.
[31] W.L. Cai, Y.J. Weitsman, Non-Fickian Moisture Diffusion in Polymeric Composites, J Compos Mater. 28 (1994) 130–154. doi:10.1177/002199839402800203.
[32] S. Roy, W.X. Xu, S.J. Park, K.M. Liechti, Anomalous Moisture Diffusion in Viscoelastic Polymers: Modeling and Testing, J Appl Mech. 67 (2000) 391. doi:10.1115/1.1304912.
[33] C. Maggana, P. Pissis, Water sorption and diffusion studies in an epoxy resin system, J. Polym. Sci. Part B Polym. Phys. 37 (1999) 1165–1182. doi:10.1002/(SICI)1099-0488(19990601)37:11<1165::AID-POLB11>3.0.CO;2-E.
[34] H.G. Carter, K.G. Kibler, Langmuir-Type Model for Anomalous Moisture Diffusion In Composite Resins, 12 (1978) 118–131. doi:10.1177/002199837801200201.
[35] L.R.R. Grace, M.C.C. Altan, Characterization of anisotropic moisture absorption in polymeric composites using hindered diffusion model, Compos. Part A Appl. Sci. Manuf. 43 (2012) 1187–1196. doi:10.1016/j.compositesa.2012.03.016.
[36] N. Burger, A. Laachachi, M. Ferriol, M. Lutz, V. Toniazzo, D. Ruch, Review of thermal conductivity in composites: Mechanisms, parameters and theory, Prog. Polym. Sci. 61 (2016) 1–28. doi:10.1016/j.progpolymsci.2016.05.001.
[37] M.J. Starink, L.M.P. Starink, A.R. Chambers, Moisture uptake in monolithic and composite materials: edge correction for rectanguloid samples, J. Mater. Sci. 37 (2002) 287–294. doi:10.1023/A:1013692026782.
[38] J.C.C. Arnold, S.M.M. Alston, F. Korkees, An assessment of methods to determine the directional moisture diffusion coefficients of composite materials, Compos. Part

A Appl. Sci. Manuf. 55 (2013) 120–128. doi:10.1016/j.compositesa.2013.08.012.
[39] L. Aktas, Y.K. Hamidi, C.M. Altan, Combined Edge and Anisotropy Effects on Fickian Mass Diffusion in Polymer Composites, J. Eng. Mater. Technol. 126 (n.d.) 427. doi:10.1115/1.1789959.
[40] E. Guzmán, J. Cugnoni, T. Gmür, Multi-factorial models of a carbon fibre/epoxy composite subjected to accelerated environmental ageing, Compos. Struct. 111 (2014) 179–192. doi:10.1016/j.compstruct.2013.12.028.
[41] Y. Joliff, W. Rekik, L. Belec, J.F. Chailan, Study of the moisture/stress effects on glass fibre/epoxy composite and the impact of the interphase area, 108 (2014) 876–885. doi:10.1016/j.compstruct.2013.10.001.
[42] T. Gates, The physical and chemical ageing of polymeric composites, in: Ageing Compos., 2008: pp. 3–33. doi:10.1533/9781845694937.1.3.
[43] A. Simar, M. Gigliotti, J.C. Grandidier, A.-K. I, I. Ammar-Khodja, A.-K. I, Evidence of thermo-oxidation phenomena occurring during hygrothermal aging of thermosetting resins for RTM composite applications, Compos. Part A Appl. Sci. Manuf. 66 (2014) 175–182. doi:10.1016/j.compositesa.2014.07.007.
[44] M.H. Han, J.A. Nairn, Hygrothermal aging of polyimide matrix composite laminates, Compos. Part A Appl. Sci. Manuf. 34 (2003) 979–986. doi:10.1016/S1359-835X(03)00154-4.
[45] S. Roy, Modeling of moisture diffusion in the presence of bi-axial damage in polymer matrix composite laminates, 38 (2001).
[46] B.G. Kumar, R.P. Singh, T. Nakamura, Degradation of carbon fiber-reinforced epoxy composites by ultraviolet radiation and condensation, J. Compos. Mater. 36 (2002) 2713–2733. doi:10.1177/002199802761675511.
[47] M. Kutz, Handbook of Environmental Degradation of Materials, 2018. doi:10.1016/c2016-0-02081-8.
[48] M.A.G. Silva, B. Sena da Fonseca, H. Biscaia, On estimates of durability of FRP based on accelerated tests, Compos. Struct. 116 (2014) 377–387. doi:10.1016/j.compstruct.2014.05.022.
[49] S. Deng, L. Djukic, R. Paton, L. Ye, Thermoplastic-epoxy interactions and their potential applications in joining composite structures - A review, Compos. Part A Appl. Sci. Manuf. 68 (2015) 121–132. doi:10.1016/j.compositesa.2014.09.027.
[50] E. Baumeister, S. Klaeger, Advanced New Lightweight Materials: Hollow-Sphere Composites (HSCs) for Mechanical Engineering Applications, Adv. Eng. Mater. 5 (2003) 673–677. doi:10.1002/adem.200320137.
[51] R. Rafiee, On the mechanical performance of glass-fibre-reinforced thermosetting-resin pipes: A review, Compos. Struct. 143 (2016) 151–164. doi:10.1016/j.compstruct.2016.02.037.
[52] D. Choqueuse, P. Davies, Ageing of composites in underwater applications, in: R.B.T.-A. of C. Martin (Ed.), Ageing Compos., Woodhead Publishing, 2008: pp. 467–498. doi:10.1533/9781845694937.3.467.
[53] M.V. V. Alonso, M.L.L. Auad, S. Nutt, Short-fiber-reinforced epoxy foams, Compos. Part A Appl. Sci. Manuf. 37 (2006) 1952–1960. doi:10.1016/j.compositesa.2005.12.011.
[54] O. Takiguchi, D. Ishikawa, M. Sugimoto, T. Taniguchi, K. Koyama, Effect of rheological behavior of epoxy during precuring on foaming, J. Appl. Polym. Sci. 110 (2008) 657–662. doi:10.1002/app.28727.
[55] K. Chen, C. Tian, A. Lu, Q. Zhou, X. Jia, J. Wang, Effect of SiO 2 on rheology, morphology, thermal, and mechanical properties of high thermal stable epoxy foam, J. Appl. Polym. Sci. 131 (2014) n/a-n/a. doi:10.1002/app.40068.
[56] K. Arjomandi, F. Taheri, Elastic buckling capacity of bonded and unbonded sandwich pipes under external hydrostatic pressure, J. Mech. Mater. Struct. 5 (2010) 391–408. doi:10.2140/jomms.2010.5.391.
[57] Y. Joliff, L. Belec, M.B. Heman, J.F. Chailan, Experimental, analytical and

numerical study of water diffusion in unidirectional composite materials – Interphase impact, Comput. Mater. Sci. 64 (2012) 141–145. doi:10.1016/j.commatsci.2012.05.029.
[58] Gurit (UK), Ampreg 26 epoxy laminating system, (n.d.) 1–8. http://www.gurit.com/sitecore/content/Old-Product-Pages/Other-Products/Laminating-Infusion-Systems/Ampreg-26.
[59] International Organization for Standardization, ISO 15166-2 Adhesives — Methods of preparing bulk specimens -- Elevated-temperature-curing one-part systems, (2000).
[60] L.F.M. Da Silva, S. Giannis, R.D. Adams, E. Nicoli, J.Y. Cognard, R. Cŕeac'hcadec, B.R.K. Blackman, H.K. Singh, C.E. Frazier, L. Sohier, B. Gineste, Manufacture of quality specimens, in: Test. Adhes. Joints, Best Pract., 2012: pp. 1–77. doi:10.1002/9783527647026.ch1.
[61] Henkel Corporation, Loctite Frekote 700NC, (2015). https://www.henkel-adhesives.com/us/en/product/mold-release-agents/loctite_frekote_700-nc.html (accessed April 17, 2017).
[62] C. Marro Bellot, M. Olivero, M. Sangermano, M. Salvo, Towards self-diagnosis composites: Detection of moisture diffusion through epoxy by embedded evanescent wave optical fibre sensors, Polym. Test. 71 (2018) 248–254. doi:10.1016/j.polymertesting.2018.09.019.
[63] C. Chen, R.S. Justice, D.W. Schaefer, J.W. Baur, Highly dispersed nanosilica–epoxy resins with enhanced mechanical properties, Polymer (Guildf). 49 (2008) 3805–3815. doi:10.1016/j.polymer.2008.06.023.
[64] S. Kalpakjian, S.R. Schmid, 19.13 Processing Polymer-matrix Composites, in: 7th ed., Pearson, n.d.
[65] International Organization for Standardization, BS EN ISO 1172:1999, Textile-glass-reinforced plastics - Prepregs, moulding compounds and laminates - Determination of the textile-glass and mineral-filler content - Calcination methods, 1999. https://www.iso.org/standard/5750.html.
[66] ASTM, D570 - Standard Test Method for Water Absorption of Plastics, 2010.
[67] ASTM, D5229 – Standard Test Method for Moisture Absorption Properties and Equilibrium Conditioning of Polymer Matrix Composite Materials, 2014. doi:10.1520/D5229.
[68] F. Pierron, Y. Poirette, A.V.-J. of Composite, U. 2002, A. Vautrin, A Novel Procedure for Identification of 3D Moisture Diffusion Parameters on Thick Composites: Theory, Validation and Experimental Results, J. Compos. Mater. 36 (2002) 2219. doi:10.1106/002199802027003.
[69] S.A. Grammatikos, M. Evernden, J. Mitchels, B. Zafari, J.T. Mottram, G.C. Papanicolaou, On the response to hygrothermal aging of pultruded FRPs used in the civil engineering sector, Mater. Des. 96 (2016) 283–295. doi:10.1016/j.matdes.2016.02.026.
[70] L.R.R. Grace, M.C.C. Altan, Non-fickian three-dimensional hindered moisture absorption in polymeric composites: Model development and validation, Polym. Compos. 34 (2013) 1144–1157. doi:10.1002/pc.22523.
[71] M. Beringhier, M. Gigliotti, A novel methodology for the rapid identification of the water diffusion coefficients of composite materials, Compos. Part A Appl. Sci. Manuf. 68 (2015) 212–218. doi:10.1016/j.compositesa.2014.09.026.
[72] ASTM D1141 - 98(2013) Standard Practice for the Preparation of Substitute Ocean Water, (n.d.). https://www.astm.org/Standards/D1141.htm (accessed October 22, 2016).
[73] M-710 Norsok Standard, Qualification of non-metallic sealing materials and manufactures, 2001. https://www.standard.no/en/sectors/energi-og-klima/petroleum/norsok-standard-categories/m-material/m-710/ (accessed November 10, 2017).

[74] Thermo Scientific, Labware Chemical Resistance Table, (2000) 7. http://tools.thermofisher.com/content/sfs/brochures/D20480~.pdf (accessed April 28, 2016).
[75] M. Ashby, Cellular Solids - Scaling of Properties, in: M. Scheffler, P. Colombo (Eds.), Cell. Ceram., WILEY-VCH Verlag GmbH, 2005.
[76] ASTM International, ASTM D7028 Standard Test Method for Glass Transition Temperature (DMA Tg) of Polymer Matrix Composites by Dynamic Mechanical Analysis (DMA), (2007) 1–14. doi:10.1520/D7028-07E01.2.
[77] ASTM International, E1640 Standard Test Method for Assignment of the Glass Transition Temperature By Dynamic Mechanical Analysis, ASTM Int. (2013) 1–6. doi:10.1520/E1640-13.2.
[78] ASTM International, ASTM C177-13: Standard Test Method for Steady-State Heat Flux Measurements and Thermal Transmission Properties by Means of the Guarded-Hot-Plate Apparatus, 2013. doi:10.1520/C0177-10.2.
[79] ASTM International, C518 - 17 Standard Test Method for Steady-State Thermal Transmission Properties by Means of the Heat Flow Meter Apparatus, (2017). https://www.astm.org/Standards/C518.htm (accessed March 22, 2019).
[80] B. Andrzej, T. Akhan, Effects of Interface Resistance on Measuremnet of Thermal Conductivity of Composites and Polymers, Proc. 30th Annu. Conf. Therm. Anal. Appl. (NATAS), K.J.Kociba, Ed. Pittsburgh B&K Publ. (2002) 512–517. https://www.tainstruments.com/pdf/literature/Effects of Interface Resistance NATAS2002.pdf (accessed March 28, 2019).
[81] ASTM International, ASTM D638 - 14 Standard Test Method for Tensile Properties of Plastics, (n.d.). https://www.astm.org/Standards/D638 (accessed January 17, 2018).
[82] J.K. Banerjee, Barreling of Solid Cylinders Under Axial Compression, J. Eng. Mater. Technol. 107 (1985) 138. doi:10.1115/1.3225789.
[83] M. Cavasin, M. Sangermano, B. Thomson, S. Giannis, M. Cavasin, M. Sangermano, B. Thomson, S. Giannis, Exposure of Glass Fiber Reinforced Polymer Composites in Seawater and the Effect on Their Physical Performance, Materials (Basel). 12 (2019) 807. doi:10.3390/ma12050807.
[84] S. Frost, Ageing of composites in oil and gas applications, in: R.B.T.-A. of C. Martin (Ed.), Ageing Compos., Woodhead Publishing, 2008: pp. 375–400. doi:http://dx.doi.org/10.1533/9781845694937.3.375.
[85] A. Toulitsis, M. Roseman, R. Martin, V. Kostopoulos, Experimental determinaion of ageing and degradation of glass fibre reinforced compositesmin petrochemical applications, in: ICCM19, 2013. http://confsys.encs.concordia.ca/ICCM19/AllPapers/FinalVersion/TOU81389.pdf (accessed March 13, 2019).
[86] S.A. Grammatikos, B. Zafari, M.C. Evernden, J.T. Mottram, J.M. Mitchels, Moisture uptake characteristics of a pultruded fibre reinforced polymer flat sheet subjected to hot/wet aging, Polym. Degrad. Stab. 121 (2015) 407–419. doi:10.1016/j.polymdegradstab.2015.10.001.
[87] S. Munch, G. Morgan, M. Roseman, B. Thomson, Laboratory Testing on Composites to Replicate Oil and Gas Service, in: springer, 2016. doi:10.1007/978-3-319-21762-8_37.
[88] D. Flore, K. Wegener, D. Seel, C.C. Oetting, T. Bublat, Investigation of chemical ageing and its effect on static and fatigue strength of continuous fibre reinforced plastics, Compos. Part A Appl. Sci. Manuf. 90 (2016) 359–370. doi:10.1016/j.compositesa.2016.08.001.
[89] Y. Chen, J.F. Davalos, I. Ray, Durability Prediction for GFRP Reinforcing Bars Using Short-Term Data of Accelerated Aging Tests, J. Compos. Constr. 10 (2006) 279–286. doi:10.1061/(asce)1090-0268(2006)10:4(279).
[90] G.D. Sims, S.J.P. Gnaniah, Improved procedures for the determination of Tg by

DMA, in: ICCM-17, 2009.
[91] X. Lefebvre, Sauvant-Moynot, D. Choqueuse, P. Chauchot, Durability of Syntactic Foams for Deep Offshore Insulation: Modelling of Water Uptake under Representative Ageing Conditions in Order to Predict the Evolution of Buoyancy and Thermal Conductivity, Oil Gas Sci. Technol. 64 (2009) 165–178. doi:10.2516/ogst/2008053.
[92] J. Zhou, J.P. Lucas, Hygrothermal effects of epoxy resin. Part II: variations of glass transition temperature, Polymer (Guildf). 40 (1999) 5513–5522. doi:10.1016/S0032-3861(98)00791-5.
[93] J. Zhou, J.P. Lucas, Hygrothermal effects of epoxy resin. Part I: the nature of water in epoxy, Polymer (Guildf). 40 (1999) 5505–5512. doi:10.1016/S0032-3861(98)00790-3.
[94] A.S. Maxwell, W.R. Broughton, Survey of Long-Term Durability Testing of Composites , Adhesives and Polymers, National Physical Laboratory, 2017.
[95] S.A. Grammatikos, R.G. Jones, M. Evernden, J.R. Correia, Thermal cycling effects on the durability of a pultruded GFRP material for off-shore civil engineering structures, Compos. Struct. 153 (2016) 297–310. doi:10.1016/j.compstruct.2016.05.085.
[96] S. Feih, K. Manatpon, Z. Mathys, A.G. Gibson, A.P. Mouritz, Strength degradation of glass fibers at high temperatures, J. Mater. Sci. 44 (2009) 392–400. doi:10.1007/s10853-008-3140-x.
[97] V. Pauchard, Application of a stress-corrosion-cracking model to an analysis of the durability of glass/epoxy composites in wet environments, (2002). doi:10.1016/S0266-3538(01)00139-7.
[98] J.O. Jansons, K. Glejbøl, J. Rytter, A.N. Aniskevich, Effect of water absoption, elevated temperatures and fatigue on the mechanical properties of carbon-fiber-reinforced epoxy composites for flexible risers, Mech. Compos. …. (2002).
[99] M. Cavasin, S. Giannis, M. Salvo, V. Casalegno, M. Sangermano, Mechanical and thermal characterization of an epoxy foam as thermal layer insulation for a glass fiber reinforced polymer, J. Appl. Polym. Sci. (2018) 7. doi:10.1002/app.46864.
[100] S.A. Song, H. Ju, B. Gi, S. Su, Novel foaming methods to fabricate activated carbon reinforced microcellular phenolic foams, Compos. Sci. Technol. 76 (2013) 45–51. doi:10.1016/j.compscitech.2012.12.018.
[101] E. Baumeister, S. Klaeger, A. Kaldos, Lightweight, hollow-sphere-composite (HSC) materials for mechanical engineering applications, J. Mater. Process. Technol. 155 (2004) 1839–1846. doi:10.1016/j.jmatprotec.2004.04.385.
[102] P.M. Stefani, V. Cyras, A. Tejeira Barchi, A. Vazquez, Mechanical properties and thermal stability of rice husk ash filled epoxy foams, J. Appl. Polym. Sci. 99 (2006) 2957–2965. doi:10.1002/app.23001.
[103] M. Ashby, Materials Selection in Mechanical Design, 4th ed., Butterworth-Heinemann, 2011.
[104] C. Forest, P. Chaumont, P. Cassagnau, B. Swoboda, P. Sonntag, Polymer nano-foams for insulating applications prepared from CO2foaming, Prog. Polym. Sci. 41 (2015) 122–145. doi:10.1016/j.progpolymsci.2014.07.001.
[105] ImageJ, (n.d.). https://imagej.nih.gov/ij/ (accessed February 26, 2018).
[106] M. Strozi Cilla, P. Colombo, M. Raymundo Morelli, Geopolymer foams by gelcasting, Ceram. Int. 40 (2014) 5723–5730. doi:10.1016/j.ceramint.2013.11.011.
[107] ASTM International, ASTM C393 / C393M - 16 Standard Test Method for Core Shear Properties of Sandwich Constructions by Beam Flexure, (2016). https://www.astm.org/Standards/C393.htm (accessed March 26, 2019).
[108] ASTM International, ASTM D7264 / D7264M - 15 Standard Test Method for Flexural Properties of Polymer Matrix Composite Materials, (2015). https://www.astm.org/Standards/D7264.htm (accessed March 27, 2019).
[109] Z. Rácz, L.M. Vas, Relationship between the flexural properties and specimen

aspect ratio in unidirectional composites, Compos. Interfaces. 12 (2005) 325–339. doi:10.1163/1568554053971551.

[110] N. Carbajal, F. Mujika, Determination of compressive strength of unidirectional composites by three-point bending tests, Polym. Test. 28 (2009) 150–156. doi:10.1016/j.polymertesting.2008.11.003.

[111] S.A. Grammatikos, R.J. Ball, M. Evernden, R.G. Jones, Impedance spectroscopy as a tool for moisture uptake monitoring in construction composites during service, Compos. Part A Appl. Sci. Manuf. 105 (2018) 108–117. doi:10.1016/j.compositesa.2017.11.006.

[112] S. Popineau, C. Rondeau-Mouro, C. Sulpice-Gaillet, M.E.R. Shanahan, R.-M. Corinne, S.-G. Christine, M.E.R. Shanahan, C. Rondeau-Mouro, C. Sulpice-Gaillet, M.E.R. Shanahan, R.-M. Corinne, S.-G. Christine, M.E.R. Shanahan, C. Rondeau-Mouro, C. Sulpice-Gaillet, M.E.R. Shanahan, Free/bound water absorption in an epoxy adhesive, Polymer (Guildf). 46 (2005) 10733–10740. doi:10.1016/j.polymer.2005.09.008.

[113] L.R. Grace, Projecting long-term non-Fickian diffusion behavior in polymeric composites based on short-term data: a 5-year validation study, J. Mater. Sci. 51 (2016) 845–853. doi:10.1007/s10853-015-9407-0.